From satellite pixels to fossil apes: targeting gaps in the hominid fossil record



João Pedro Valente de Oliveira Coelho

St. Catherine's College

University of Oxford

A thesis submitted for the degree of

Doctor of Philosophy

Michaelmas 2023

Acknowledgements

I express my heartfelt gratitude to my parents, my brother, and my family for their firm support throughout this journey. To my beloved Joana, I am profoundly grateful for your love and for you choosing to embark on, not only the years we've shared, but also the forthcoming ones in Gorongosa. You've helped in more ways than I can count. To all the friends in my hometown, Ansião, and those I've encountered in Coimbra, your enduring closeness throughout this period is truly appreciated. Thank you for all the laughs and hugs when I felt lost.

I extend my gratitude to all my colleagues and friends I met at Banbury Rd 64 in Oxford, with special thanks to those who welcomed me—Kat, Dan, Adam, Arran, Jacob, and Hristo. The memories shared with the cohort of students who embarked on this journey alongside me, Fig, Lynn, and Lucy, will be cherished always. My warmest appreciation to everyone who has been or is a member of the PrimoBevo Lab. Thank you for your guidance, support, and the enjoyable moments we've shared. As I write these words in a particularly cold winter, I find myself missing the mulled wine from The Rose & Crown, even though my initial encounter with its flavour was not a symphony for my taste buds. Here's a toast to these unforgettable moments at Oxford—may our memories also age well—Cheers!

In the lab at Oxford or amidst the landscapes of Kenya and Mozambique, I've had the pleasure of crossing paths with numerous researchers, students, field assistants, and *fiscais* who not only became cherished friends but also played a part in one way or another in bringing my research to fruition. I owe a special debt of gratitude to Dr. David R. Braun, co-director of the Koobi Fora field school, for his pivotal role in granting access to the field and offering an abundance of counsel and insights about East Turkana. His extensive involvement, from in-depth discussions on my research proposal to continuous support before, during, and after fieldwork is much appreciated. Special thanks also go to Frances Forrest, Silindokuhle Mavuso, and Sharon Kuo for making me feel like part of the Koobi Fora family.

Every person I encountered in Chitengo, Gorongosa, has been incredibly gracious and welcoming. This magical place *from the Montane to the Mangrove* truly works as an open lab and a field university. Marc Stalmans, Jason Denlinger, Tongai Castigo, and João Nhampoca provided crucial help with the logistics of field research and fossil surveying in the Miombo woodlands Gorongosa National Park. While there are many colleagues who have contributed to my delightful experience at Gorongosa, I want to highlight two particularly inspirational friends, Jacinto Mathe and Rassina Farassi. I wish to you both the very best as you continue to advance the fields of palaeoanthropology and primatology in Mozambique.

I'm deeply grateful for Dr. René Bobe's incredible generosity and guidance, which significantly shaped my dissertation by enriching both its depth and breadth. Learning anatomy and taxonomy under René's mentorship at the NMK in Nairobi was a priceless highlight of my life as a scientist. I also acknowledge Dr. Thomas Püschel key role as a senior research collaborator and field colleague, along with his contagious laughing and humour. Thank you, Thomas and Ara, for the friendship and sharing with me countless moments I'll forever treasure. Before arriving to Oxford, I would never expect that the best thing about the town would be all the "crazy" Chileans I've met there! I've learned a lot with all of you.

I am grateful to St Catherine's College and the School of Anthropology & Museum Ethnography for hosting me during my time at Oxford. Special thanks to FCT: *Fundação para a Ciência e Tecnologia* for its funding that supported my research and covered expenses throughout my DPhil. I also appreciate the generous support provided by The Boise Trust Fund, the Africa Oxford Initiative – AfOx, and the Centre for Functional Ecology. Their contributions were key in covering the expenses related to my fieldwork in the Rift, data collection at palaeontological museums, and participation in international conferences. This support proved indispensable for the success of my research endeavours over the past years.

Finally, I want to express my heartfelt appreciation for the invaluable feedback and mentorship provided by my supervisors. Prof Robert L. Anemone for all his steady support, sharp insights, and constructive feedback which have been instrumental for my growth as a researcher. The

initial moment I discovered Anemone's work online was bittersweet—first, I got a bit upset to learn I was not going to be the first person ever to uncover fossil sites from space using AI—but a split second after this sentiment was followed by immense joy as I realized I had found the best possible mentor for this project.

My most profound appreciation goes to Prof Susana Carvalho, who not only afforded me the opportunity to undertake this research under her guidance but also infused the journey with her boundless energy, unwavering dedication, and compassionate kindness. During these years many of my dreams have turned into reality due to her inspiring vision and superhuman work ethic. But the immense surprises during this wild learning experience were even greater than the dreams I had! I'm sincerely grateful for her consistent presence and support, especially during the moments when I needed it the most. I also want to acknowledge Prof Eugénia Cunha, who supervised my master's with great care, and played a pivotal role in connecting me with Prof Susana Carvalho for my DPhil in Anthropology, ultimately enabling me to pursue a career in Human Evolution. Their guidance has been instrumental in shaping my research journey, and I am profoundly grateful for their wisdom, support, and encouragement throughout this chapter of my life.

Abstract

Palaeoanthropological research encounters several limitations that impact our understanding of hominin origins. Fossil records are often incomplete and geographically biased, concentrating findings in specific regions. Temporal gaps and taphonomic biases lead to further uncertainties in evolutionary timelines. Nevertheless, ongoing interdisciplinary advancements shape and refine our understanding of human evolution. In Chapter 1, I contextualize these spatiotemporal gaps and propose potential solutions, including the implementation of remote fossil site detection methods. Chapter 2 offers a comprehensive review of the *Geospatial Palaeontology* literature, providing a thorough examination of existing research in this field.

The discoveries in each chapter carry significant implications for future research and practical applications. In Chapter 3, I introduce a new meta-analytical approach for dating time trees and test it on the *Pan-Homo* divergence event. This analysis indicates a high likelihood of the split occurring before 8 Ma. This method aids in fine-tuning our comprehension of *Pan* and hominin origins and directs efforts towards pinpointing fossil deposits with greater chronological precision. The breakthroughs presented in Chapter 4 regarding remote detection methods offer promising prospects for the efficient identification of fossil sites. This is especially relevant for regions characterized by limited sampling and challenging surveying environments like Gorongosa. We found new highly fossiliferous deposits that harbour Miocene apes and many other mammalian species using this approach. The incorporation of innovative tools for large-scale automated habitat predictions, as pioneered in Chapter 5, significantly enhances our ability to reconstruct ancient landscapes. This advancement provides valuable insights into the ecological context of hominins and, for the first time, enables the creation of a comprehensive palaeoenvironmental indicator for most of the Koobi Fora formation in East Turkana, spanning both spatial and temporal dimensions. In the concluding Chapter 6, I delve into the primary contributions, acknowledge limitations, and chart potential future directions for research. At its core, this thesis seamlessly integrates a diverse array of interdisciplinary methods and concepts from fields such as data science, geospatial learning, palaeobiogeography, and computational palaeontology. This fosters a holistic approach to fossil site exploration, opening new avenues for future research in this dynamic and ever-evolving field.

Table of Contents

1. Introduction 1
   1.1 Background 1
   1.2 Biogeography of Gorongosa 5
   1.3 Palaeobiogeography of Gorongosa 7
   1.4 Gorongosa for testing coastal models of hominin evolution 10
      1.4.1 "East African Ground Ape" hypothesis – Kingdon, 2003 10
      1.4.2 Coastal Refuge hypothesis – Joordens et al, 2019 13
      1.4.3 Adaptations and resource exploration in the littoral 15
      1.4.4 Alternative to coastal models 17
   1.5 Targeting the gaps – time beats timing 20
   1.6 Targeting the gaps – remote site detection 22
   1.7 Large-scale and automated palaeoecological reconstruction: a case-study in East Turkana 24
2. Literature Review 27
   2.1 Traditional discovery of fossil sites 27
   2.2 Searching localities from space 30
      2.2.1 The early years of archaeological predictive modelling 30
      2.2.2 Predictive modelling by means of environmental data in Palaeontology 33
      2.2.3 Other GIS applications in Palaeontology 35
      2.2.4 Geospatial fossil hunting for hominins 36
      2.2.5 Predictive modelling through remotely sensed imagery in Palaeontology 38
      2.2.6 New approaches: hybrid-datasets, continental-wide taxa-specific discovery, and individual fossil targeting 43
3. Parting ways: *Pan-Homo* Divergence Revisited 51
   3.1 Introduction 52
   3.2 Materials and Methods 56
      3.2.1 Pre-processing 56
      3.2.2 Fossil thresholds 57
      3.2.3 Regression analyses 59
      3.2.4 Meta-analyses 60
      3.2.5 Data and materials availability 61
   3.3. Results 61
      3.3.1 Dataset structure 61
      3.3.2 The 4.4 Ma threshold: The last Ardipithecus and the first Australopithecus 62
      3.3.3 The 6.2 Ma threshold: Orrorin tugenensis and Ardipithecus kadabba 63
      3.3.4 The 7.2 Ma threshold: Sahelanthropus tchadensis 64
      3.3.5 Regression analyses of molecular estimates from 1967–2023 65
      3.3.6 Bayesian meta-analyses 68
   3.4 Discussion 70
      3.4.1 Conclusions 74
   3.5 Supplementary Text 76
      3.5.1 S1: Dataset distribution 76
      3.5.2 S2: Bayesian meta-analysis: further details 77

3.5.3 Data S1. 84
4. Unsupervised learning of satellite images enhances discovery of late Miocene fossil sites in the Urema Rift, Gorongosa, Mozambique 85
4.1 Introduction 87
4.2 Materials & Methods 93
4.2.1 Applying the k-means algorithm to satellite images 95
4.2.2 Clusters as survey guides for fossil site discovery 96
4.3 Results 97
4.3.1 Digital validation 97
4.3.2 Ground-truthing 99
4.4 Discussion 103
4.4.1 Conclusions 105
5. Geospatial palaeoecology: estimating aquatic and terrestrial fossil abundance in East Lake Turkana 109
5.1 Introduction 111
5.1.1 Geospatial Learning: Supervised vs Unsupervised 111
5.1.2 Learning in the absence of counter-examples 114
5.1.3 Automated palaeoecological reconstructions: taking geospatial palaeontology a step further 115
5.2 Materials and Methods 117
5.2.1 Study area 117
5.2.2 Layered dataset 118
5.2.3 Data collection in the field: bone walks 122
5.2.4 BetaReg: Aquatic-to-terrestrial ratio 123
5.2.5 MaxEnt: Fossil distribution 124
5.2.6 PalaeoEnv: Filtered ensemble 125
5.3 Results 126
5.3.1 BetaReg results 126
5.3.2 MaxEnt results 128
5.3.3 BetaReg vs MaxEnt 130
5.3.4 Ileret 131
5.3.5 Karari 133
5.3.6 Koobi Fora 136
5.4. Discussion 138
5.4.1 Remote palaeoenvironmental reconstruction: spatiotemporal patterning 138
5.4.2 Short-wave infrared: soil content and moisture 143
5.4.3 Near-infrared: a “fossil band”? 145
5.4.4 The visible bands: RGB and ultrablue 146
5.4.5 Modern environmental and topographic contexts 147
5.4.6 Conclusion 149
5.5 Supporting Info 151
5.5.1 SF1. A leave-one-out cross-validation (LOOCV) procedure for the beta regression model 151
5.5.2 SF2. Calculating variable importance in Beta regression 153
5.5.3 SF3. Response curves for single variable MaxEnt independent models 155

5.5.4 SF4. Response curves of the final MaxEnt model for remote detection of fossiliferous deposits 156
6. Discussion 157
6.1 Summary 157
6.2 Key contributions 159
6.2.1 Through the hourglass: the double-helix and clocks 159
6.2.2 Filling gaps: the sands of time 161
6.2.3 The satellite's guide to Gorongosa's fossils 167
6.2.4 Searching for Kingdon's coastal ape 169
6.2.5 Do orbiting machines dream of ancient environments? 170
6.3 Future directions 173
6.3.1 Dating the tree of life 173
6.3.2 Gorongosa's unfinished symphony: a work of decades 174
6.3.3 Remote cave detection 177
6.3.4 Geospatial palaeoecology: an emerging new discipline 179
6.4 Conclusion 180
7. Works Cited 183
Appendix I 233
Appendix II 275
Appendix III 307

List of Figures

Figure 1.1 – **Chronological timeline of hominin species** and associated stratigraphic ranges, highlighting the emergence of the earliest known techno-complexes (adapted from Bobe & Reynolds, 2022). 3

Figure 1.2 – **Geological formations of the African Late Miocene**, including preliminary dates for Gorongosa sites (Bobe *et al.*, 2023). Notice the sparsity of deposits spanning the 9–7 Ma period within Africa (adapted from Bobe & Reynolds, 2022). 4

Figure 1.3 – **Gorongosa environments and the location of the southernmost fossil sites in the EARS**. Generated in R using the Leaflet package (Cheng, Karambelkar & Xie, 2021). ... 6

Figure 1.4 – **Palaeontological study area** currently being surveyed by the PPPG within the geological context of Gorongosa National Park. 7

Figure 1.5 – **Palaeogeographic reconstruction** and depositional environments indicate a Miocene Gorongosa by the sea (after Habermann *et al.*, 2019). 9

Figure 1.6 – **Sketch drawings of eastern Africa coastal apes** from Jonathan Kingdon's Lowly Origin (2003) overlapped to a photo of modern day estuarine coastal forest in Macaneta, Mozambique. 11

Figure 1.7 – **The role of orbitally-induced wet-dry cycles in the Pliocene CFEA**: A) Present day Indian Ocean coastal forests and Montane forests distribution. B) The humid-dry cycle oscillating between arid barriers and riverine corridors 5–2.5 Ma (after Joordens, 2011). 14

Figure 1.8 – **Primates foraging aquatic resources**: a) chacma baboon fishing in a desert waterhole (Hamilton & Tilson, 1985); b) chacma baboon eating shellfish in the littoral (Lewis & O'Riain, 2017); c) Japanese macaques are well known to explore coastal settings, but recently have also been found fishing salmon upstream (Takenaka *et al.*, 2022); d) bonobos bipedally wade when fishing for iodine-rich herbs (Hohmann *et al.*, 2019); e) chimpanzees forage for crabs in forest streams (Koops *et al.*, 2019); f) crab-eating macaques use stone tools to access marine invertebrates (Luncz *et al.*, 2017). 16

Figure 1.9 – **Polynomial regression showing the trend for hominin brain expansion** (dataset provided in Du *et al.*, 2018). 18

Figure 2.1 – **The two main approaches of data collection for geospatial predictive modelling.** Either using spectral bands (each band as a variable) or environmental variables as inputs. 31

Figure 2.2 – **Potential localities (red) in the Great Divide Basin, Wyoming** as estimated by an artificial neural network. Notice that prospecting the whole basin would take centuries even with large teams. This method severely reduces the area of prospection (after Emerson & Anemone, 2012). 40

Figure 2.3 – **Supervised and Unsupervised Learning** are the two main conceptual modes of thinking statistical problems within the machine learning paradigm. 42

Figure 2.4 – **Ensemble Learning approach to identify potential fossil areas with combined models** (after Block *et al.*, 2016). For a given taxon, the areas yield new fossils (red map) are those where the species used to live (brown map), where its fossils could be preserved (blue map), and where it is now possible to find its fossils (green map). 46

Figure 3.1 – **Molecular estimates histogram.** Dashed vertical lines represent fossil thresholds. Note that instead of following a normal distribution, studies seem to cluster in excess around important fossil discoveries, and there is an unexpected gap of mean-estimates at 9–9.5 Ma. 62

Figure 3.2 – **Interquartile range boxplots for divergence estimates filtered by different fossil thresholds.** The arithmetic means and the medians are represented by white diamonds and black bars, respectively. All boxplots fit within the late Miocene (11.6–5.3 Ma). 64

Figure 3.3 – **Trend of the "full-dataset model" fitting the sample of Panini/Hominini split estimates by date of publication.** The late Miocene period is shadowed and within the horizontal dotted black bars. Dotted error-bars are standard errors, presented when available (studies with confidence or credible intervals were transformed to SE). 65

Figure 3.4 – **Linear regressions for different types of source datasets.** A) Includes early phenetic studies (immunological, DNA-DNA hybridization, etc.), but also later studies with

virogenes and RNA; B) Mitochondrial datasets from early studies with selected sequences to later complete mitochondrial genome studies; C) Split estimates based on nuclear DNA sequences; and D) Large phylogenomic studies (also includes 'total evidence dating', i.e., integrative models).....67

Figure 3.5 – **Meta-analysis of the Pan/Homo phylogenomic divergence estimates.** Forest plot depicting the specific effect size and sampled posterior distribution of genome-based studies. 69

Figure 4.1 **– The great gaps of the African late Miocene.** a) Time gap**:** during this key period the African fossil record of primates is very incomplete (evaluated through species richness); but notice the split estimates from genomics; b) Spatial gap**:** virtually no fossils of this age are known in southeastern Africa, notice the strategic location of Gorongosa. Data extracted from palaeobiodb.org, map adapted from Bobe et al. (2018); c) study area for *k*-means within the geological context of Gorongosa, adapted from Habermann et al. (2019). 88

Figure 4.2 **– The miombo woodland and the challenges it presents to fossil prospecting: Gorongosa Palaeontological Location 1 (GPL-1).** a) GPL-1 outcrops, notice how the surrounding vegetation is far more dense and extensive than in typical fossil sites from the EARS; b) GPL-1 in high-resolution satellite image, extracted from bing.com, shows a reduction of vegetation, but outcrops are barely noticeable; c) GPL-1, in a black rectangle, appears brighter than surrounding areas, when being mapped by lower resolution Landsat 8 false colour (infrared) image, and the same happens with other fossil sites, suggesting the infrared bands might be a useful indicator of fossiliferous deposits. 90

Figure 4.3 **– Surveying for fossils in a densely vegetated context.** a) Despite the ground foliage and dense vegetation, in situ and surface evidence of fossils abound in the gully valley connecting GPL-12 to GPL-12B; b) Systematic mapping and collecting of surface fossil finds by students of the field school; c) Side gully (~3 m deep) exposure and shovel test pit at GPL-12. Photographs are from the Paleo-Primate Project Gorongosa archive.....91

Figure 4.4 **– Flowchart of the algorithmic pipeline used for remote fossil site detection:** 1) Example of one of the seven spectral bands satellite images used in this study; 2) false colour

map based on the infrared bands, after cropping to study area; 3) results of clustering using all seven spectral bands; 4) Binarize clusters for classification by selecting the cluster that contains most fossil sites as the target class ("walking back the cat") versus all other clusters combined into a single class. 95

Figure 4.5 – **Output from the *k*-means algorithm for data mining.** All geolocations "Vertebrates + Invertebrates" and "Invertebrates" recorded by the PalaeoPrimate Project Gorongosa team during 2016 and 2017 (Habermann et al., 2019) are plotted over the clusters, as well as the "Single vertebrate find" and "Fossilized wood" localities reported by Pickford (2012, 2013). You can see the cluster 1 (white) tends to be represented in locations with fossil vertebrates, indicating that it has some potential as a new feature/variable for finding new fossil sites. The map displays a 6 by 6 km square; axes scales are in meters. 98

Figure 4.6 – **Violin-boxplots comparing sample distribution of spectral bands between clusters.** Each spectral band is represented in its own cell, with nine bars comparing the range of spectral bands values at the geocoordinates of the fossil sites, plus the eight clusters generated by *k*-means. Notice how overall, cluster 1 tends to approximate better the true spectral range of known fossil sites in Gorongosa..... 100

Figure 4.7 – **Binarized classification plotting cluster 1 vs all other clusters.** New fossil sites GPL-10, 11, 12 and 12B are documented here for the first time. Trackways of surveys during 2018 are drawn in black. Clusters 2-8 are merged into a single cluster and compared against cluster 1 (predictive cluster). Total area = 36 km^2. One grid square = 1 km^2. One pixel-cell = 900 m^2. 101

Figure 4.8 – **Variable importance of spectral bands for clustering**. Bars represent relative importance of the spectral predictors for optimally classifying all clusters as calculated by a supervised random forest algorithm (Breiman, 2001). Specific variable importance for detecting cluster 1 is shown with open circles. 102

Figure 5.1 – **Study area geographic context**: a) East Turkana as depicted in a preview of scene ID = LC81690572018036LGN00, Landsat 8 image from 2018-Feb-5. The dashed rectangle was the cropped section used in all analyses. Notice the image has no clouds on the region of

interest; b) the raw satellite image overlaid on its larger geographic context, covering part of northern Kenya and southern Ethiopia. 119

Figure 5.2 – **All the layers of the stacked dataset used during training for predictive modelling**..... 121

Figure 5.3 – **Bonewalks raw data**: A) Geocoordinates of the points of interest (POI) over a map of the Paleontological Collection Areas (Brown and Feibel, 1990, revised by Bobe et al., 2022), also including the training extent of the models in a pink dashed rectangle, and three smaller rectangles with the Ileret (purple), Karari (teal), and Koobi Fora (yellow) sub-regions; B) Ratio of aquatic-to-terrestrial fauna sampled by systematic bone walks in each POI..... 124

Figure 5.4 – **Outputs of the main models for the East Turkana region**: A) aquatic-to-terrestrial ratio predictions; B) estimated distribution of fossils; C) Final paleoenvironmental reconstruction based on BetaReg's output filtered by MaxEnt. 127

Figure 5.5 – **A test of the MaxEnt model using 1903 georeferenced fossil presences extracted from the PaleoTurkana database** (Bobe et al., 2022); * - absences were generated by randomly selecting another set of 1903 xy points across the map..... 130

Figure 5.6 – **Comparison of variable importance metrics** for A) BetaReg and B) Maxent, as calculated by percent contribution, as defined in varImp() function from R (Liaw & Wiener, 2002). 131

Figure 5.7 – **Predictive modelling of Ileret**: A) BetaReg with raw output before masking; B) MaxEnt model predicting exposure of fossiliferous deposits; C) PaleoEnv model overlapped by the geological members of the Koobi Fora Fm (Gathogo, 2003; Gathogo & Brown, 2006). 132

Figure 5.8 – **Boxplot of PaleoEnv model outputs** (BetaReg predictions after MaxEnt masking). Each box width is relative to the total number of cells after filtering (i.e., total fossiliferous pixels). Fill colour is the ratio of cells remaining by the total cells in each area (i.e., fossiliferous density). Diamonds are average means; and boxes are interquartile of aquatic ratio (25%; median; and 75%). Boxes are ordered from BetaReg's median prediction of most terrestrial to most aquatic (after filtering by MaxEnt). 134

Figure 5.9 – **Predictive models of Karari's Area 105**. A) BetaReg output, before masking; B) MaxEnt model predicting exposure of fossiliferous deposits; C) PaleoEnv model with geological layers. 135

Figure 5.10 – **Predictive models of Koobi Fora's Area 103**. A) BetaReg with raw output, before masking; B) MaxEnt model predicting fossiliferous deposits; C) PaleoEnv with geological layers. 137

Figure 6.1 – **Preliminary temporal intervals for Gorongosa fossil sites** based on three-point estimates of $^{10}Be/^{9}Be$ dating using authigenic values based on different ecological assumptions (Appendix II), combined with the geological time scale from the Holocene to the Oligocene (GSA, 2022), and median divergence estimates of the literature, with respective confidence intervals, were obtained from timetree.org (Kumar *et al.*, 2022). 161

Figure 6.2 – **Challenges in deducing divergence times from the fossil record**. A) Primary obstacles in using palaeontological data to calibrate lineage splits: 1. Identifying and dating the clade's earliest known fossil (FAD); 2. Calculation of the temporal discrepancy ΔT_{Gap} between the FAD and the emergence of the lineage's initial fossilizable trait; 3. The interval $\Delta T_{Div\text{-}1stApo}$ between the clade's first fossilizable characteristics and the actual genetic point of divergence. The latter, $\Delta T_{Div\text{-}1stApo}$, cannot be known, as it pertains to a period for which the clade's fossils are indistinguishable and thus unidentifiable within the fossil record. B) The estimation of ΔT_{Gap} is complicated by the diminishing likelihood of fossil discovery near the lineage's origin, compounded by the inherently sporadic and fragmentary nature of fossils and stratigraphic records. Adapted from Marshall (2019) in order to illustrate the *Pan*/*Homo* split scenario. 166

Figure 6.3 – **BetaReg predictions on grid cells** known to contain A) *Homo* and *Paranthropus*; B) Antilopini and Bovini. Geocoordinates sampled from the PaleoTurkana Database (Bobe et al., 2022). 171

Figure 6.4 – **Morphospace for upper left first incisors**, a preliminary analysis to assess the phenetic affinities of the Gorongosa cf. Hominoidea UI1 PPG2022-P-091 to other Primates via PCA. 176

Figure 6.5 – **Karstic map of the Afro-Arabian continental landmass**. Vectorial dataset layer is the World Karst Aquifer Map (Goldscheider *et al.*, 2020), and the map was generated using the leaflet package for R (Cheng *et al.*, 2021). Zooming 10x: A) Total extension of cave systems in and around the Cradle of Humankind, South Africa; B) Gorongosa and associated limestone areas. 178

Authorship Statements

Collaborator Statement – Susana Carvalho

I hereby grant permission for the inclusion of the following chapters in the thesis submitted by João Pedro Valente de Oliveira Coelho to the University of Oxford for the degree of Doctor of Philosophy. I confirm that João Pedro Valente de Oliveira Coelho is the main author and contributor of these chapters including conceptualization, methodology, primary data collection and statistical analyses, as well as interpretation, data curation, visualization, and writing of the original manuscripts.

Chapter 3: Parting ways: *Pan-Homo* Divergence Revisited

Chapter 4: Unsupervised learning of satellite images enhances discovery of late Miocene fossil sites in the Urema Rift, Gorongosa, Mozambique

Chapter 5: Geospatial paleoecology: estimating aquatic and terrestrial fossil abundance in East Lake Turkana

Signature 

Name: Susana Cláudia Ribeiro Marques de Carvalho

Date: 15/12/2023

University: University of Oxford

Email: susana.carvalho@anthro.ox.ac.uk

Collaborator Statement – Robert L. Anemone

I hereby grant permission for the inclusion of the following chapters in the thesis submitted by João Pedro Valente de Oliveira Coelho to the University of Oxford for the degree of Doctor of Philosophy. I confirm that João Pedro Valente de Oliveira Coelho is the main author and contributor of these chapters including conceptualization, methodology, primary data collection and statistical analyses, as well as interpretation, data curation, visualization, and writing of the original manuscripts.

Chapter 3: Parting ways: *Pan-Homo* Divergence Revisited

Chapter 4: Unsupervised learning of satellite images enhances discovery of late Miocene fossil sites in the Urema Rift, Gorongosa, Mozambique

Chapter 5: Geospatial paleoecology: estimating aquatic and terrestrial fossil abundance in East Lake Turkana

Signature: 

Name: Robert L. Anemone

Date: Dec 17th, 2023

University: University of North Carolina at Greensboro

Email: Robert.anemone@uncg.edu

Collaborator Statement – René Bobe

I hereby grant permission for the inclusion of the following chapters in the thesis submitted by João Pedro Valente de Oliveira Coelho to the University of Oxford for the degree of Doctor of Philosophy. I confirm that João Pedro Valente de Oliveira Coelho is the main author and contributor of these chapters including conceptualization, methodology, primary data collection and statistical analyses, as well as interpretation, data curation, visualization, and writing of the original manuscripts.

Chapter 3: Parting ways: *Pan-Homo* Divergence Revisited

Chapter 5: Geospatial paleoecology: estimating aquatic and terrestrial fossil abundance in East Lake Turkana

Signature: 

Name: René Bobe

Date: 18-12-2023

University: Gorongosa National Park

Email: renebobe@gmail.com

Collaborator Statement – David R. Braun

I hereby grant permission for the inclusion of the following chapters in the thesis submitted by João Pedro Valente de Oliveira Coelho to the University of Oxford for the degree of Doctor of Philosophy. I confirm that João Pedro Valente de Oliveira Coelho is the main author and contributor of these chapters including conceptualization, methodology, primary data collection and statistical analyses, as well as interpretation, data curation, visualization, and writing of the original manuscripts.

Chapter 5: Geospatial paleoecology: estimating aquatic and terrestrial fossil abundance in East Lake Turkana

Signature: 

Name: David R. Braun

Date: December 19th 2023

University: George Washington University

Email: David_braun@gwu.edu

Covid Statement

Balancing the academic pressures, teaching and tutoring, personal commitments, fieldwork, scientific conferences, and the rigorous research required for a doctoral thesis, has occasionally overwhelmed me. But never in my wildest nightmares I thought I would also have to deal with a worldwide pandemic or the second and third-order effects it caused. My work was difficulted, interrupted, or delayed multiple times due to the Covid-19 pandemic and the prolonged government lockdowns. I was unable to access the laboratories or even an office space for about two years, which severely impacted my productivity. My scholarship also ended abruptly during this challenging period, and the extensions for Covid-impacted students were limited to a few months. The lack of social contact with my colleagues in real life, and the increased load of virtual events also impacted my stress levels. The fact that I had to alter multiple times and miss most of my final stages of field work plans were also very difficult to handle and interfered with my motivation and well-being. Adaptability and strategic planning played pivotal roles in this endeavour, and I hope that, despite the challenges, I managed to successfully craft a cohesive manuscript.

1

Introduction

1.1 Background

When and where did our ancestors, the earliest hominins, originate? The current and possible consensus from molecular and fossil evidence points to the late Miocene forests and woodlands of Africa (White *et al.*, 2015; Püschel *et al.*, 2021; Almécija *et al.*, 2021). Yet the late Miocene (11.6–5.3 Ma) is an extensive time period ranging over 6 million years, and Africa is a massive continent containing ~12.7% of the Earth's land (Kingdon, 1990, 2003, 2023). Regrettably the geographic distribution of African fossil sites during this key period is highly biased and the associated hominin fossil record is likewise sparse (Cote, 2004, 2018; Senut, 2015; Wood & Smith, 2022). Given the significant gaps and uncertainties in the hominin fossil record, it is pertinent to question the feasibility of achieving a more precise resolution regarding the window of time when hominins originated (Bobe & Wood, 2022). This thesis merges methods and techniques from data science, biogeography, and computational palaeontology to offer a novel contribution to understanding the contexts of hominin evolution. A set of goals is proposed to address the following outstanding issues: to define a more precise chronological range for the divergence event between the Hominini and Panini clades, so that we can target sediments of correct age (Chapter 3); to increase the accuracy of remote detection of fossil

sites, with a focus on under sampled temporal, geographic and palaeoecological settings (Chapter 4); and introduce new computational tools to remotely reconstruct palaeo-environmental features of the landscape (Chapter 5). Since geospatial palaeontology methods are used extensively throughout the thesis, a literature review to contextualize their role in augmenting the objectivity associated to the discovery process is also summarized in the following section (Chapter 2).

Finding hominins is a remarkably hard and serendipitous process and, as in any field of research, if the object of inquiry is of great rarity, small sample size inhibits robust data analysis and hypothesis testing (Smith, 2005; Marshall, 2008, 2017, 2019; Bobe & Wood, 2022; Wood & Smith, 2022). Yet, the collecting efforts of the last centuries resulted in a staggering number of described species, with possibly up to 30 hominins currently being recognized as valid taxa (Figure 1.1). Still the overall small and fragmentary samples are not always enough to understand the full range of morphological variability or distinguish two (or more) species from a single polytypic species (Haile-Selassie, Melillo & Su, 2016; Lahr, 2016; Rightmire, Margvelashvili & Lordkipanidze, 2019). Clearly, it is necessary to find more fossil evidence, and especially in those time periods and biogeographic areas for which we have little evidence or complete gaps in the record (Joordens *et al.*, 2019).

The lower Mazamba Formation in Gorongosa National Park (Mozambique) meets both those temporal and spatial criteria (Habermann *et al.*, 2019). There are major late Miocene chronological gaps from which very few fossils have been recorded. From all the known geological formations in Africa dating to the late Miocene, there are no known stratigraphic levels between 7.4 and 8 Ma, possibly a key period in earliest hominin evolution. Likewise, if C'horora Fm in Ethiopia is confirmed at 8 Ma (Suwa *et al.*, 2007; Katoh *et al.*, 2016), there is even a more staggering gap with no sites between 8 and 9 Ma, a key time period where important events like the Hominini-Panini divergence (Chapter 3) might have happened. Notice that C'horora is a formation standing alone in the African continent for the 7.4 to 9 Ma interval, and has yielded only ~200 fossils to date (Katoh *et al.*, 2016). Yet, this includes the first appearance datum (FAD) for Gorillini (Figure 1.2).

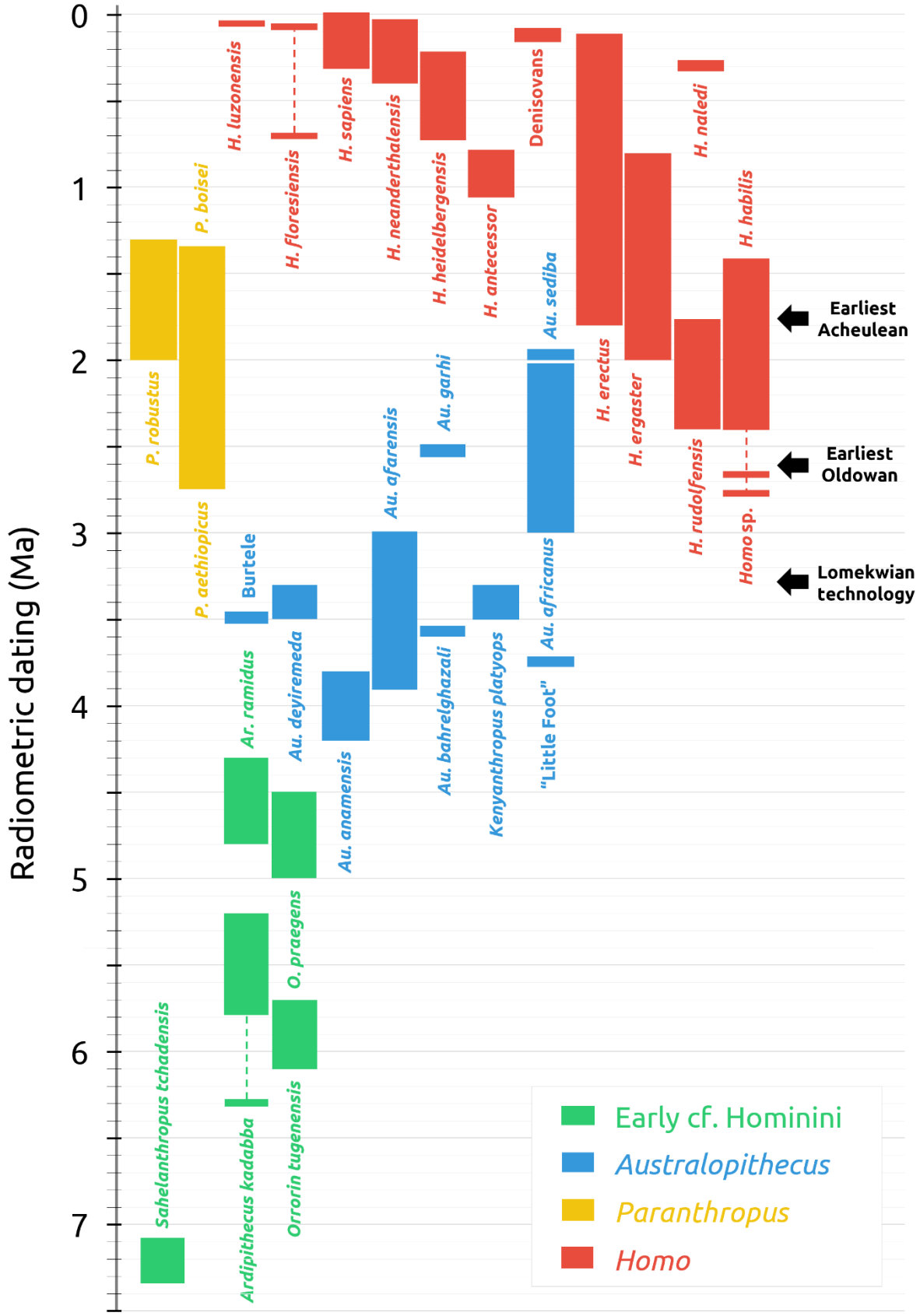


Figure 1.1 – **Chronological timeline of hominin species** and associated stratigraphic ranges, highlighting the emergence of the earliest known techno-complexes (adapted from Bobe & Reynolds, 2022).

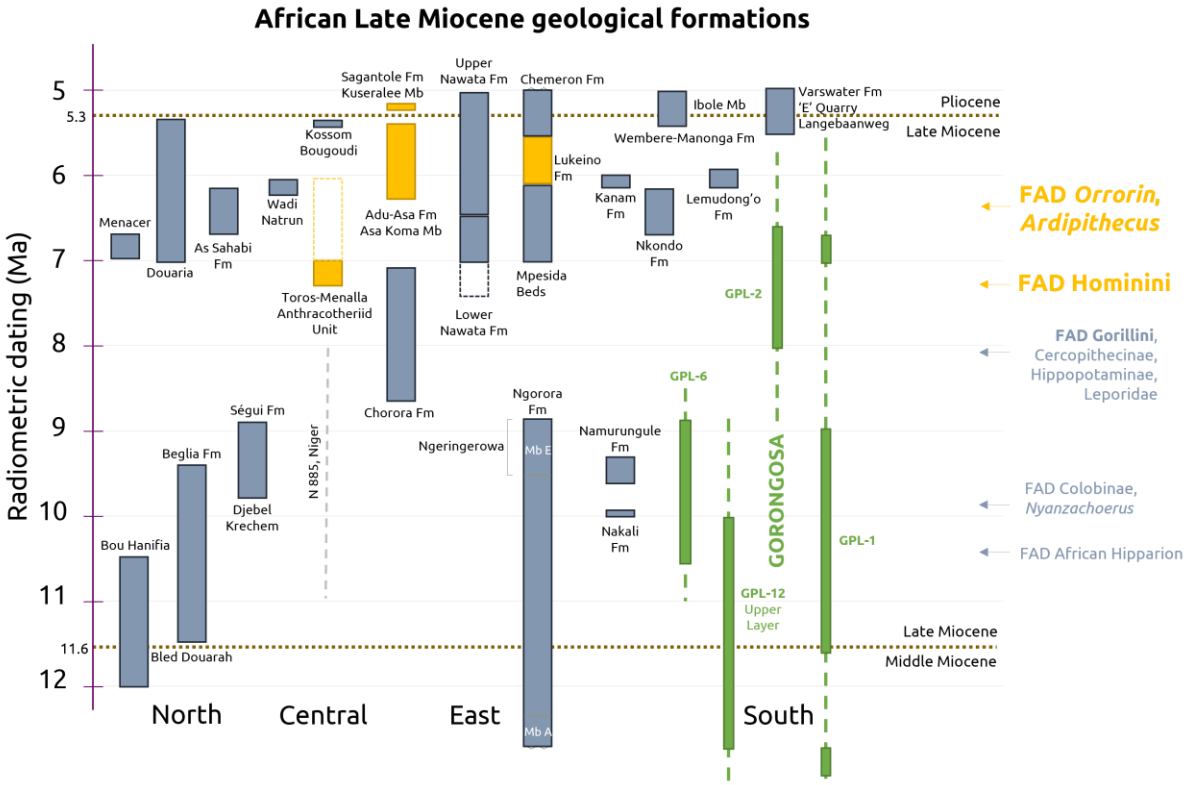


Figure 1.2 – **Geological formations of the African Late Miocene**, including preliminary dates for Gorongosa sites (Bobe *et al.*, 2023). Notice the sparsity of deposits spanning the 9–7 Ma period within Africa (adapted from Bobe & Reynolds, 2022).

The Palaeo-Primate Project Gorongosa (hereafter PPPG) has prospected sites and unearthed fossils in the lower Mazamba formation since 2016 (Habermann *et al.*, 2019). Preliminary cosmogenic dating for four different sites (GPL-1, 2, 6 and 12) indicates that multiple time periods within the 6.7 to 13.5 Ma range (Figure 1.2) are represented in the fossil deposits of Gorongosa (Bobe *et al.*, 2023). Therefore, this formation encompasses a crucial but poorly understood phase of hominin and ape evolution, namely the middle and late Miocene. Additionally, GPL-12 also contains a second (lower) layer, an extremely fossiliferous bonebed tentatively dated to 19.5–15.9 Ma. Thus, early Miocene (23.03–15.97 Ma) deposits are also abundant in Gorongosa, a period encompassing the first hominoid radiation, with twelve ape genera known in the African fossil record. As we move into the middle Miocene (15.97–11.6 Ma), a sub-epoch marked by warm conditions, significant hominoid diversification occurs across Africa and Eurasia (Harrison, 2010; Begun, 2010). The most recent total evidence

phylogenetic models suggest that the last common ancestor of all African apes (including humans) existed around the transition of the middle to the late Miocene (Püschel *et al.*, 2021). During the late Miocene (11.6–5.3 Ma) there was an expansion of grasslands due to prolonged climatic cooling and stronger aridity cycles (Kingdon, 2003; Schefuß & Dupont, 2020), associated with a decline of ape diversity in Africa (Cote, 2004), forest fragmentation (Cerling *et al.*, 2011), and biogeographic isolation of major African biomes (Joordens *et al.*, 2019), which might have led to the divergence of the last common ancestor (LCA) into the Panini (bonobos and chimpanzees) and Hominini (humans and bipedal apes) clades (Chapter 3).

Gorongosa is at the center of a major southeastern gap, with no other known Miocene fossil sites in all directions for over 1700 km (Chapter 4). Key questions in hominin origins pertain to the patterns of speciation and distribution and the palaeoenvironmental contexts associated with them. In the following sections I briefly discuss the unique ecological conditions of the fossil sites at Gorongosa, and how they enable testing for the first time a set of biogeographic hypotheses regarding the contexts of hominin origins (Kingdon, 2003; Wrangham, 2005; Joordens *et al.*, 2019; Bobe, Martínez & Carvalho, 2020b).

1.2 Biogeography of Gorongosa

Gorongosa National Park, in central Mozambique (18.96° S, 34.36° E), covers a ~4000 km^2 section of the East African Rift System (EARS) (Stalmans *et al.*, 2019). The park is characterized by heterogeneous environments in a young ~3 Ma rift valley (Macgregor, 2015), spanning montane woodland and rainforests, tall evergreen forests in limestone gorges, mixed woodland savannas, floodplain grasslands, swamps, rivers, and Lake Urema, a major hydrological feature of the landscape that expands and contracts seasonally (Tinley, 2020). These mosaic habitats with abundant fresh water and heterogeneous tree cover (Figure 1.3), provide a compelling case for Gorongosa as modern analogue for the evolution of early hominins (Wilson, 2014; Bobe *et al.*, 2020b; Lüdecke *et al.*, 2022), aligning with the

palaeoenvironmental reconstructions of *Orrorin tugenensis* (Pickford & Senut, 2001), and *Ardipithecus kadabba* (Su *et al.*, 2009).

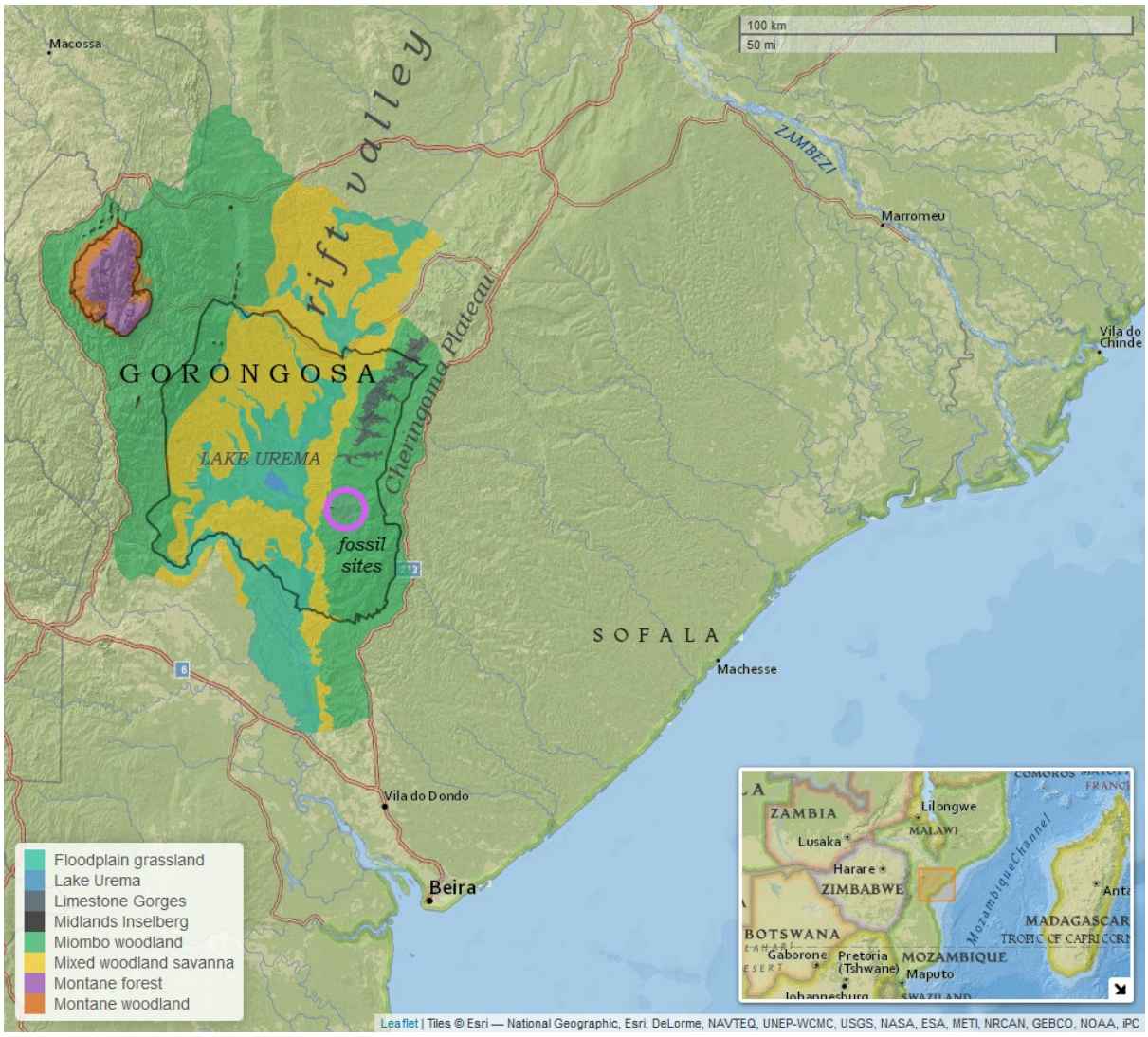


Figure 1.3 – **Gorongosa environments and the location of the southernmost fossil sites in the EARS**. Generated in R using the Leaflet package (Cheng, Karambelkar & Xie, 2021).

Additionally, present-day Gorongosa also has extensive miombo woodland, a type of habitat that has been argued to have the right features for the evolutionary emergence of upright posture and subsequently bipedal locomotion in early hominins (Senut *et al.*, 2018b). The park also has more than 220 troops of chacma baboons, *Papio ursinus* (Martinez *et al.*, 2019). Papionines have been proposed as a comparative species model for reconstructing hominin behaviour (Jolly, 1970, 2001), and Gorongosa allows to study primate adaptations and life history across dynamic mosaic environments (Bobe *et al.*, 2020b; Hammond *et al.*, 2022).

1.3 Palaeobiogeography of Gorongosa

Geological settings that are favourable for fossil preservation of mammals were first identified in the Gorongosa region by Pickford (2012, 2013). Most relevant for the study of hominin and ape evolution is the Mazamba formation, with clay and sandstones of Miocene age (Habermann *et al.*, 2019). It overlays the Cheringoma plateau (east of the Rift), that also contains the Cheringoma formation of Eocene limestone, which is rich in marine faunal remains (Figure 1.4). The Cheringoma plateau underwent extensive karstification during the Quaternary and thus it hosts many caves and rock shelters with speleothems and cave breccias. These caves are still under early stages of exploration, but a total of 89 have already been mapped in detail (Regala, Pinto & Paulo, 2023), and some of them show potential for palaeoanthropological and archaeological prospection (Laumanns, 2001; Mercader & Sillén, 2012, 2013; Gonçalves *et al.*, 2016; Regala *et al.*, 2022).

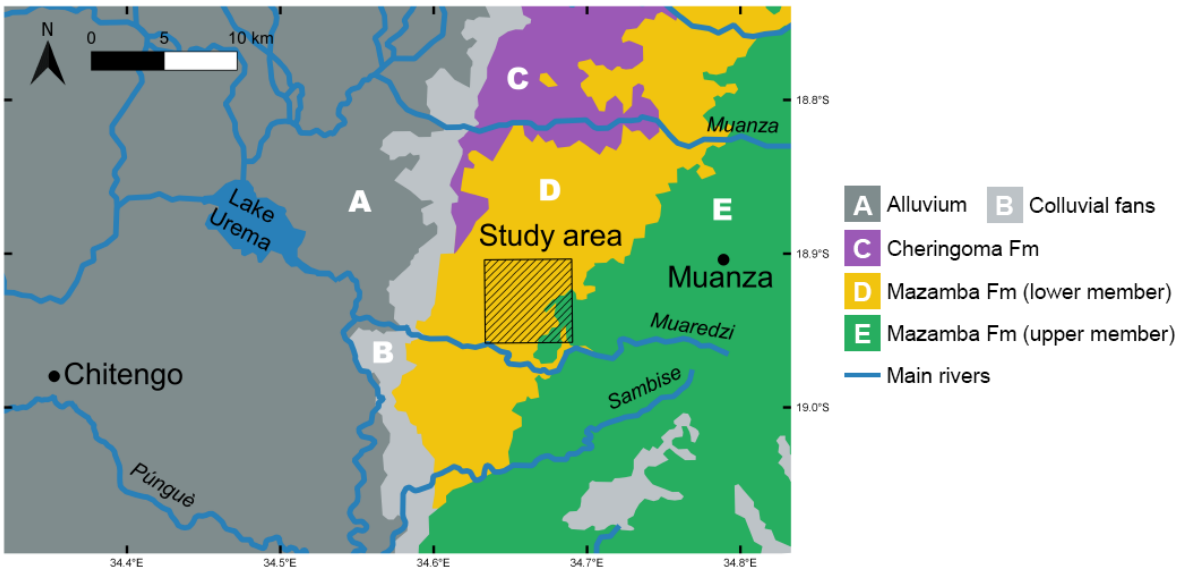


Figure 1.4 – **Palaeontological study area** currently being surveyed by the PPPG within the geological context of Gorongosa National Park.

During the 2016–2023 field seasons, the PPPG recovered and documented over 1800 fossil specimens from multiple novel fossil localities. Fossil wood and preliminary stable carbon and oxygen isotope analysis from carbonate nodules retrieved in these fossil sites indicated a

woodland/shrubland ecosystem, dominated by C_3 vegetation, and only moderately influenced by evaporation (Appendix II). The fossil specimens were associated with continental sediments consisting of river-dominated coastal plain, with estuaries and deltaic deposits (Habermann *et al.*, 2019). The faunal assemblages comprise many types of land mammals such as chalicotheres, anthracotheres, sivatheres, suids, proboscideans, hyracoids, and primates (d'Oliveira Coelho, 2023), as well as fossil remains of dugongs, turtles, crocodiles, catfish, sharks, and batoids. Invertebrate remains abound in many of the localities, including crustaceans, bivalves, gastropods, oysters, among others (Habermann *et al.*, 2019; d'Oliveira Coelho *et al.*, 2023; Bobe *et al.*, 2023).

Early hominin occupation of humid and watered habitats such as riparian woodlands next to lake margins is well-documented in East African fossil sites (Reed, 1997; Egeland, Nicholson & Gasparian, 2010; Foley & Lahr, 2014; Foley, 2018; Barboni *et al.*, 2019; Bobe & Reynolds, 2022). But Gorongosa is the first of its kind, a rift valley estuarine and littoral site, partially covered by marine deposits (Figure 1.5) (Habermann *et al.*, 2019).

Studying extinct populations within all their palaeoenvironmental and climatic contexts puts palaeontology in a position to fully understand not only the modalities of hominin and ape emergence and evolution, but also the factors that might have affected adaptations. As of 2023 we have identified five primate fossils from Gorongosa (GPL-12), showing strong affinities to Hominoidea (d'Oliveira Coelho *et al.*, 2023), and potentially aligning with Gorillini (see Chapter 6.2.4). Together with the palaeoecological reconstruction of the region and the current geochronological estimations, suggests that Gorongosa can play an important role in testing biogeographic hypotheses of hominin origins in Miocene coastal forests (Kingdon, 2003; Joordens *et al.*, 2019) or deltaic settings (Wrangham, 2005) (see Chapter 1.4, below).

There are limits to test such hypotheses since coastal forests are not yet represented in the fossil record associated with the earliest stem hominins. *Sahelanthropus tchadensis* habited a gallery forest bordering a lake, with some open grassland and swamps, including freshwater habitats (Le Fur *et al.*, 2009). *Orrorin tugenensis* is associated with fluvial and shallow lake deposits with open woodlands on a floodplain (Pickford & Senut, 2001). The habitat of *Ardipithecus*

kadabba was reconstructed as riparian woodlands and floodplain grassland along water margins (Su *et al.*, 2009). These reconstructions fit relatively well within the 'hand-assisted arboreal bipedalism' hypothesis (Thorpe, Holder & Crompton, 2007; Thorpe, McClymont & Crompton, 2014), which states bipedalism evolved within a tree-dwelling context, based mostly on behavioural observation of extant apes. This hypothesis also found support on skeletal remains of *Ar. ramidus* and some orthograde Eurasian and African Miocene apes (Crompton, Sellers & Thorpe, 2010; Böhme *et al.*, 2019). While this scenario does not require coastal settings, it also positions hominin origins within forest to woodland paleoenvironmental contexts (Drummond-Clarke *et al.*, 2022).

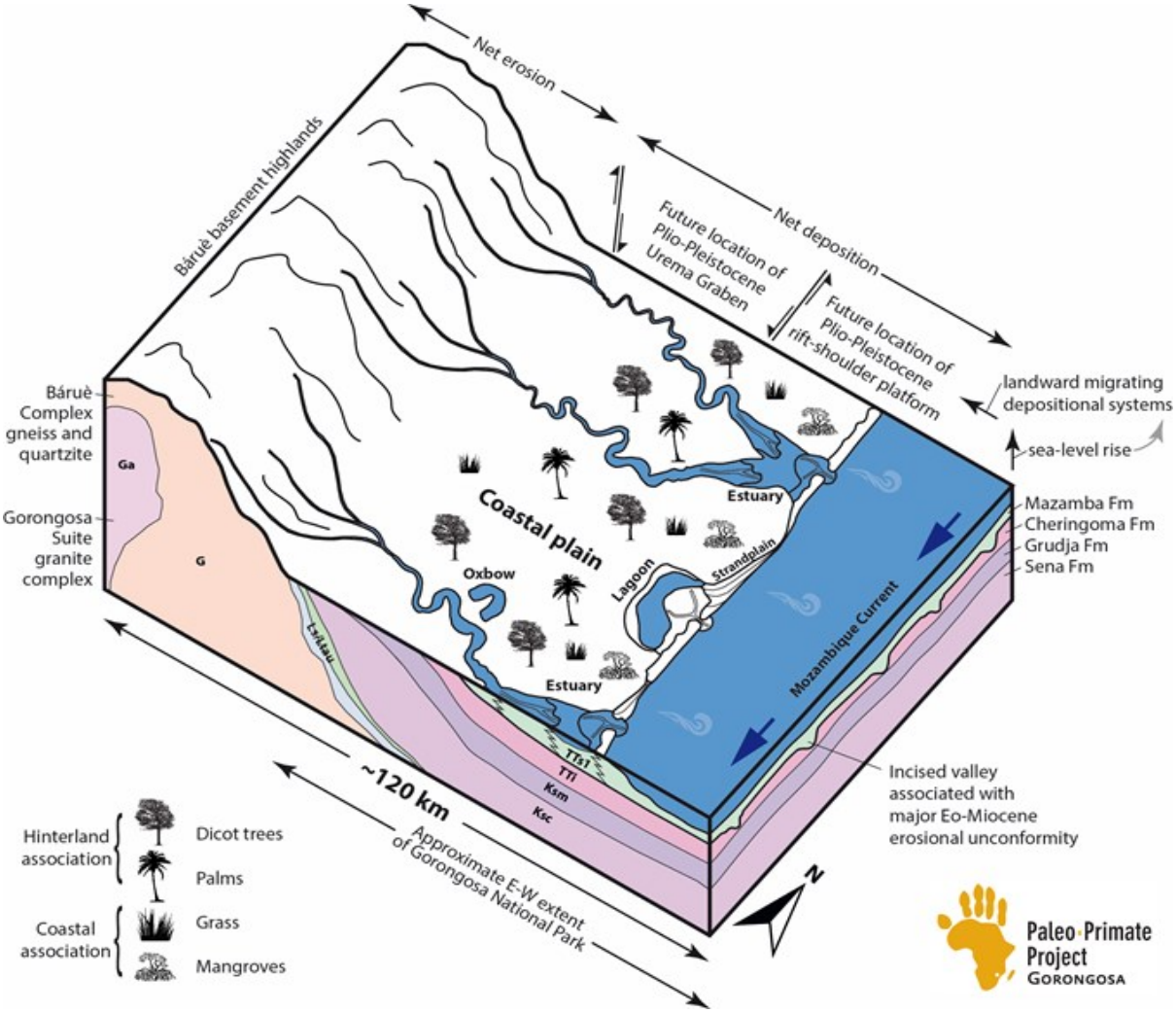


Figure 1.5 – **Palaeogeographic reconstruction** and depositional environments indicate a Miocene Gorongosa by the sea (after Habermann *et al.*, 2019).

1.4 Gorongosa for testing coastal models of hominin evolution

1.4.1 "East African Ground Ape" hypothesis – Kingdon, 2003

Lowly Origin (Kingdon, 2003) offers a biogeographic overview of hominin evolution, with original insights for what may have happened during and after the split of *Pan-Homo* lineages. Thus, it has a strong focus on explaining the functional origins of bipedalism and other traits among the very first hominins. Kingdon's ideas are inspired by the terrestrial squat-feeding hypothesis (Jolly, 1970). In this earlier model, delicate foraging for seeds from grasses, as geladas and savannah baboons do today, allowed for a more upright posture while squatting was favoured as an early precursor behaviour for bipedal walking (Jolly, 2001). Kingdon proposed a change of scenario from grassland to forest, and expanded seeds to a variety of other nutritional resources, including crustaceans, small vertebrates, various kinds of vegetation, and low-hanging fruits that would be readily available on the Indian Ocean coastal forests (Figure 1.6) extending continuously from Somalia all the way to South Africa. This hypothetical event might have occurred as African ape lineages become geographically isolated because of aridity cycles starting at 10.5 Ma, with maximum dry peaks at 7.8 and 6.2 Ma (Kingdon, 2003), due to the impact of the Indian plate with Asia at about 11 to 10 Ma, that disrupted global climatic cycles (Griffin, 2002; Schefuß & Dupont, 2020; Steinthorsdottir *et al.*, 2021). This accelerated dramatically the rift-induced split of the greater African tropical forests into a large western-central forest with its core at Congo Basin, and an eastern coastal forest, by forming an arid corridor associated with the EARS (Bobe *et al.*, 2023).

Throughout *Lowly Origin* many details are provided for when, where and how this may have happened, but the overall thematic focus is on changes in daily foraging range and foraging strategies due to a coastal forest biogeographic setting. These are considered to be significant because "quadrupedalism would never have been abandoned if substantial distances had to be covered, especially if such journeys involved exposure to predators" (Kingdom, 2003: 125). One can summarize the anatomical descriptions of this conjectural ground ape, with a special

focus on those that would be detectable in fossilized material. These can be referred to as Kingdon's osteological hypotheses for a coastal ground ape:

1. Anterior placement of *foramen magnum* before major pelvic specializations.
2. Orthograde posture predating obligate bipedalism (spine anatomy).
3. Lumbar vertebrae expanding in relative size.
4. Shortening of the hip bones, giving more freedom to thoracic movement.
5. Sacrum co-adapting to maintain balance and a supportive pelvic griddle.
6. Foot bones structured as a platform instead of claspers.



Figure 1.6 – **Sketch drawings of eastern Africa coastal apes** from Jonathan Kingdon's Lowly Origin (2003) overlapped to a photo of modern day estuarine coastal forest in Macaneta, Mozambique.

The cranial fragments associated with *Orrorin* (6.1–5.7 Ma) and *Ardipithecus kadabba* (6.3–5.4 Ma) are too incomplete to even address the topic of basal cranium anatomy without resorting to speculation (Senut *et al.*, 2001; Haile-Selassie, Suwa & White, 2004). However, a later form of *Ardipithecus* (4.8–4.3 Ma), *Ar. ramidus* has almost half of its *foramen magnum* preserved, and Suwa et al. (2009) suggested an anterior positioning based on a micro-CT reconstruction that would match osteological hypothesis 1. The placement of the *foramen magnum* in the occipital of *S. tchadensis* (7.34–7.1 Ma) is highly controversial. The original publication infers a more human-like positioning, meaning this species would be a potential ground ape (Brunet *et al.*, 2002). However, many researchers have criticized the conclusions of Brunet and his team on the basis of the inherent subjectivity of the angle-method applied, plus the wide variability in this measure within modern chimpanzees. The fractures and deformations of the cranial base in this specimen also make it extremely difficult to ascertain if the *foramen magnum* was less posteriorly positioned than in quadrupedal apes (Wolpoff *et al.*, 2002, 2006).

Unfortunately, the orientation of the vertebral column, the length of the lumbar region, and the anatomy of the sacrum are not known from the early hominin fossil record, since the spinal region is poorly represented in *Ar. kadabba*, *Orrorin* or *Sahelanthropus* (Senut *et al.*, 2001; Haile-Selassie, 2001; Brunet *et al.*, 2002). Again, the early Pliocene *Ar. ramidus* gives some better insights as its pelvic structure indicates that it retained a primitive spine, and the preserved illiacs are still long (Lovejoy *et al.*, 2009b). In this case, it is ambiguous, as osteological hypothesis 3 cannot currently be addressed, while 4 can be rejected, but 1 implies that 4 might happen later and 1 might be true as seen in the previous paragraph. Currently, hypothesis 2 is supported by various older Miocene apes, including: *Morotopithecus bishopi* (18–22 Ma) from eastern Africa, plus *Pierolapithecus catalaunicus* (12 Ma), *Danuvius guggenmosi* (11.6 Ma), and *Hispanopithecus laietanus* (10 Ma) from Europe (Thorpe *et al.*, 2014; Böhme *et al.*, 2019).

In the three earliest genera of hominin, we can only test hypothesis 6 with *Ar. ramidus*, for whom we have a very complete left foot of an individual. While it still looks very ape-like with

a divergent hallux, it has been argued that it maintains archaic anatomic characteristics from other Miocene apes that would enable it to maintain a rigid foot while walking, a characteristic that was lost in non-human African apes (Lovejoy *et al.*, 2009a). This matches Kingdon's conjectural ground ape to some extent. Still, none of the earliest hominins were found in the same ecological and geographic settings described by Kingdon (2003) due to the absence of fossil sites in the EARS that sample estuarine/coastal contexts—all the current fossil evidence comes from fluvial and lacustrine contexts (Le Fur *et al.*, 2009; Su *et al.*, 2009). Thus, the current fossil record is potentially sampling a later phase of hominin evolution, after migrations inland during wet periods (Joordens *et al.*, 2019; Kingdon, 2023). Finding hominin cranial, vertebral, pelvic or foot remains in Gorongosa would provide a more direct comparison to test Kingdon's model for a coastal east African ground ape.

1.4.2 Coastal Refuge hypothesis – Joordens et al, 2019

The Coastal Refuge hypothesis aims to test the biogeographic conditions for the "East African Ground Ape" model, by studying patterns in the fossil record while also predicting locations of new fossil research areas. To undertake her hypothesis testing, Joordens (2011; Joordens *et al.*, 2019) establishes the Afar basin as a proxy for the Indian Ocean coastal forests, potentially fully connected to these forests during the period between 5 to 3 Ma (Figure 1.7). It then uses palaeoclimatological data (Zachos *et al.*, 2001) to evaluate when exactly the astronomically-driven humid-arid cycles (Trauth *et al.*, 2005; Joordens *et al.*, 2011; Maslin *et al.*, 2014; Nutz *et al.*, 2017; Yost *et al.*, 2021) were occurring. This is very important to understand the mechanics of her model, since the coastal forest, including the Afar basin, would remain a refuge offering optimal conditions for living even during the peak of dry cycles, unlike Turkana (Villaseñor, Bobe & Behrensmeyer, 2020) or Laetoli (Su & Harrison, 2008), where such favourable conditions did not endure. These cyclical climatological patterns lasted until the rain forests underwent an abrupt retreat to an area approximately equivalent to their current extent, a consequence of the intensification of the Northern Hemisphere Glaciation event around 2.7 Ma (Hayashi *et al.*, 2020).

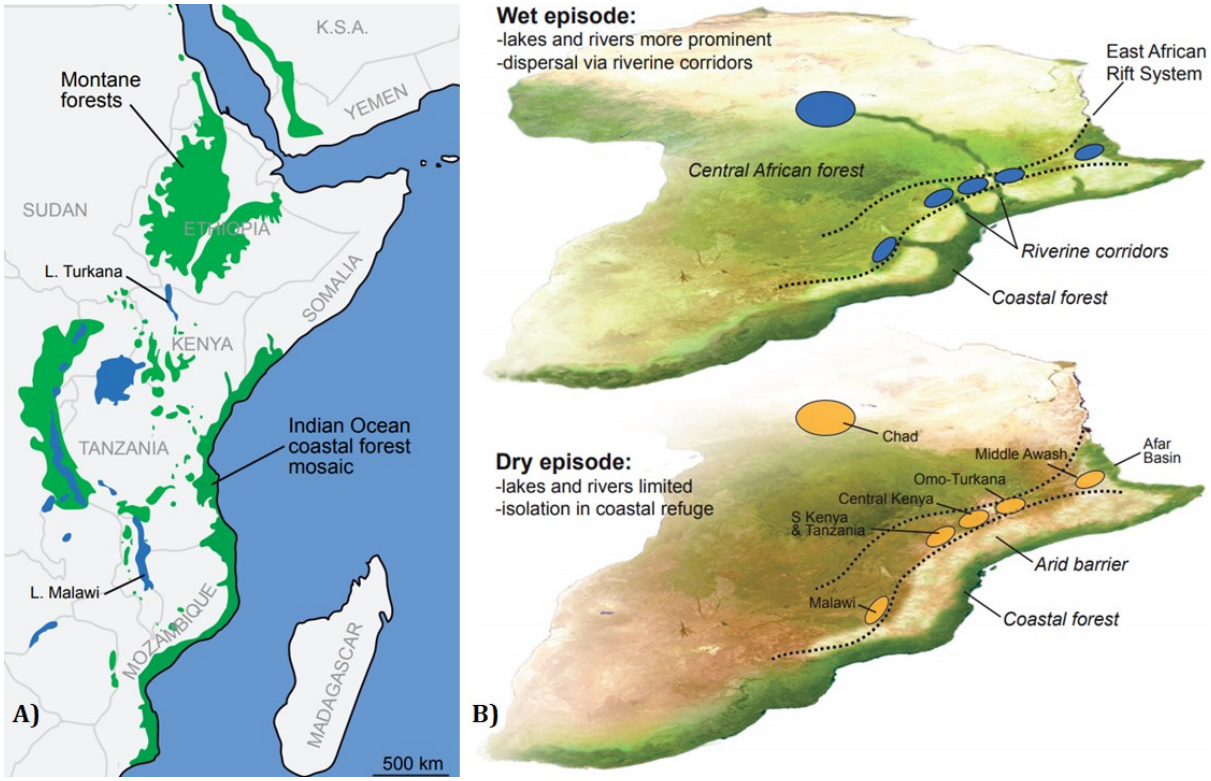


Figure 1.7 – **The role of orbitally-induced wet-dry cycles in the Pliocene CFEA**: A) Present day Indian Ocean coastal forests and Montane forests distribution. B) The humid-dry cycle oscillating between arid barriers and riverine corridors 5–2.5 Ma (after Joordens, 2011).

When more humid conditions returned, hominins could disperse and occupy eastern basins such as Turkana, Baringo, Laetoli or Malawi, and even the more westerly remote Chad basin. Following Joordens' palaeoclimate assumptions, all the analysed basins would be connected by rivers to the Indian Ocean coastal forests during these optimal periods. Hominin populations would be isolated in or even disappear from the basins during arid episodes (but see also Blumenthal *et al.*, 2017 for an alternative view). Meanwhile species would keep evolving in the Indian Ocean coastal mosaic forests, then dispersing and repopulating the basins again in humid periods. All the analysed fossil evidence from the selected basins seems to fit, to different extents, the general expectations of Joordens' model. Interestingly, this analysis makes a strong argument for *Ardipithecus ramidus* as a very likely Kingdon's "East African Ground Ape". Lastly, the model predicts the coasts of Kenya, Tanzania, and Mozambique as the core areas for early hominin occupation. Hence, the Mazamba formation at Gorongosa,

known to contain estuarine deposits of Miocene to Pliocene age, is a strategic field site for testing and potentially validating this model (Joordens *et al.*, 2019).

1.4.3 Adaptations and resource exploration in the littoral

Accelerated hominin brain evolution after ~2 Ma might not be possible without direct intake from the aquatic food resources (Crawford, 2002; Cunnane *et al.*, 2007). Docosahexaenoic, a specific brain fatty-acid seems particularly essential, and it can only be continuously exploited in littoral ecosystems (Joordens *et al.*, 2014). Some trace elements such as iodine and selenium that are critical for proper brain development are also very abundant in marine resources but rare in land-based food (Crawford & Broadhurst, 2012; Cunnane & Crawford, 2014). Several modern primates are known to explore and forage in littoral settings (Kempf, 2009; Habermann *et al.*, 2019), as well as inland aquatic resources (Figure 1.8). There are communities of chimpanzees (Nowak & Coles, 2019), gorillas (Head, Healy & Nowak, 2019), and orangutans (Matsuda *et al.*, 2019) exploring coastal forests and mangroves. Orangutans are also able to engage in tool-assisted fish catching (Russon *et al.*, 2014).

Despite *Homo* having some clearly important adaptations to arid environments (Bobe, 2006; Blumenthal *et al.*, 2017; Pontzer *et al.*, 2021), hominins are water-dependent mammals (Foley & Lahr, 2014) that preferred wooded mesic habitats (Rowan & Reed, 2015; Forrest, Plummer & Raaum, 2018) and ranged into shallow-water habitats and other types of wetland refugia (Joordens *et al.*, 2009; Wrangham *et al.*, 2009; Stewart, 2010, 2014). It is also likely that some of the main dispersal routes in later hominins were via the coast (Bailey, 2004; Field, Petraglia & Lahr, 2007), but also through complex inland waterways and riverine green corridors (Lahr, 2010; Drake *et al.*, 2011). Wrangham and colleagues (2009) propose that underwater buried tubers would be targeted as fall-back resources. The authors also propose that wading while foraging in shallow water may be a precondition for triggering selection of bipedal locomotion, an hypothesis that found support in energetic cost studies (Halsey, Tyler & Kuliukas, 2014). All living apes and many other primates wade occasionally when dealing with similar flooded contexts (Gross, 2005; Nowak, Barnett & Matsuda, 2019). These ideas were also discussed

within the delta hypothesis for hominin evolution (Wrangham, 2005), that explores the Okavango delta as a model for early hominin evolution. Likewise, coastal regions would also support varied resources such as fish, molluscs, gastropods and crustaceans that could also be explored by early hominins or hypothetical eastern coastal apes, particularly at the Miocene forests and woodlands with deltaic and estuarine features of Gorongosa (Bobe *et al.*, 2020b).

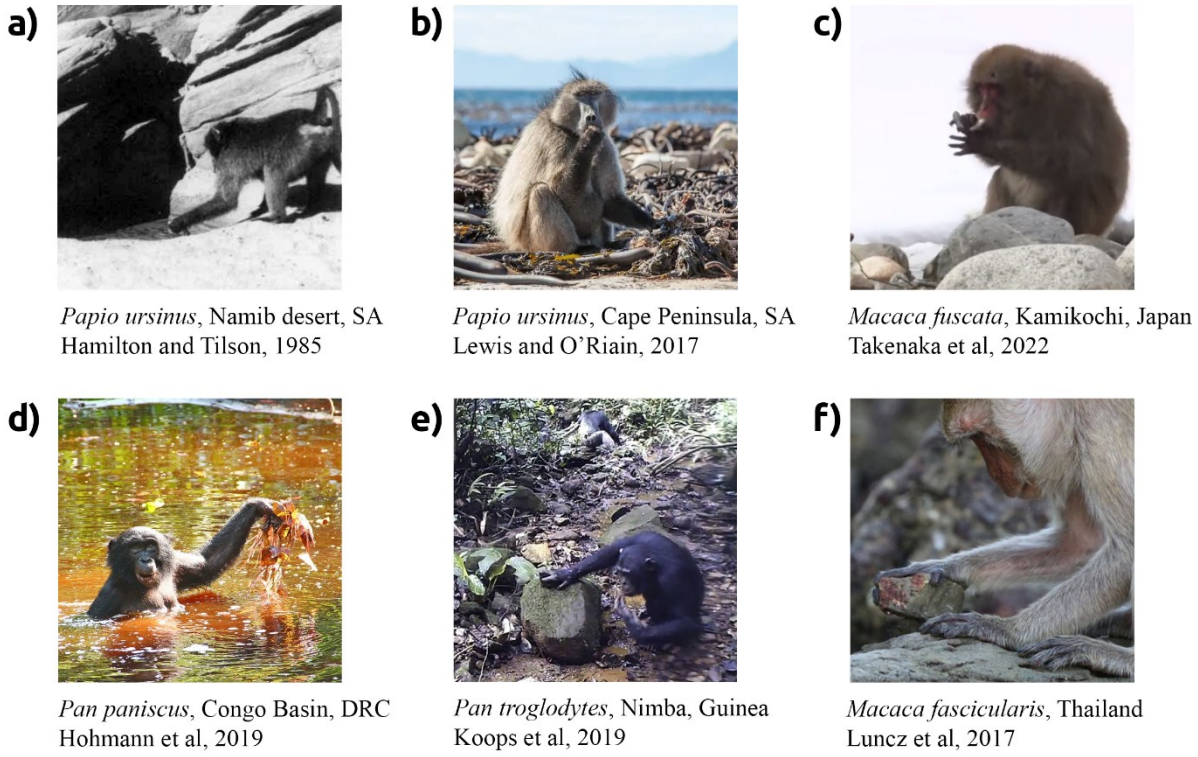


Figure 1.8 – **Primates foraging aquatic resources**: a) chacma baboon fishing in a desert waterhole (Hamilton & Tilson, 1985); b) chacma baboon eating shellfish in the littoral (Lewis & O'Riain, 2017); c) Japanese macaques are well known to explore coastal settings, but recently have also been found fishing salmon upstream (Takenaka *et al.*, 2022); d) bonobos bipedally wade when fishing for iodine-rich herbs (Hohmann *et al.*, 2019); e) chimpanzees forage for crabs in forest streams (Koops *et al.*, 2019); f) crab-eating macaques use stone tools to access marine invertebrates (Luncz *et al.*, 2017).

In the fossil record there is very limited evidence of primates in littoral settings, with the Oligocene of Fayum being the notable exception (Bown *et al.*, 1982). Another possible exception is *Oreopithecus*, a Miocene ape of uncertain phylogenetic standing, that inhabited the Tuscany region at a time when it was an archipelago separated from the mainland (9–7 Ma). Sedimentary, palynological, and faunal evidence suggest that *Oreopithecus* lived in a generally moist and warm mesophytic forest (Harrison & Harrison, 1989). While there is

debate about its locomotion (Hammond *et al.*, 2020), some argue that *Oreopithecus* was a bipedal wader adapted to swampy environments (Rook *et al.*, 1999), possibly consuming freshwater invertebrates and plants with pad-to-pad precision grip (Moyà-Solà, Köhler & Rook, 2005). However, other authors lean toward some unique form of suspensory locomotion (Russo & Shapiro, 2013) with an emphasis on ape-like power grasping (Susman, 2004). Regardless, *Oreopithecus*' association with wet and wooded insular environments remains unquestioned (Sponheimer, Loudon & Howells, 2019). There is also an Hominoidea indet. molar from the ~16 Ma coastal forests of Namaqualand (Pickford & Senut, 1997).

While there are no fossils sustaining the diet-based hypotheses at the earliest stages of hominin evolution, intake of resources at seashore has been well established in later periods with obligate bipeds. The most striking example might be the findings associated with *H. neanderthalensis* incorporating dolphins, seals, molluscs and fish into its diet during the Upper Palaeolithic (Stringer *et al.*, 2008). In *H. sapiens*, the evidence for marine food consumptions goes back as early as 164 ± 12 Ka (Marean, 2014). It is also highly probable that *H. habilis* and *H. erectus* were exploiting fish at Olduvai during the Early Pleistocene (Stewart, 1994), but there is a stronger case for *H. erectus* consuming marine resources at Trinil around 1.5 Ma (Joordens *et al.*, 2009, 2015). There is also well-documented fossil evidence for consumption of turtles, crocodiles, and fish by tool-using hominins from Koobi Fora at 1.95 Ma (Braun *et al.*, 2010). It could be speculated that as Kingdon's ground ape became an obligate biped, already living close by the shoreline, it began to increasingly explore opportunistically such environments around 4.5–2.5 Ma just before rapid increase in cranial capacity starts to manifest in the fossil record (Figure 1.9). An event that would overlap the origins of the genus *Homo* estimated to have occurred between 4.30 and 2.56 Ma (Püschel *et al.*, 2021).

1.4.4 Alternative to coastal models

The significance of wetlands and littoral biomes on later phases of hominin evolution—from about 2 Ma to the present—is uncontroversial (Braun *et al.*, 2010; Colonese *et al.*, 2011; Cortés-Sánchez *et al.*, 2011; Archer *et al.*, 2014; Joordens *et al.*, 2015; Petraglia, Breeze &

Groucutt, 2019). However, the role of eastern coastal forests and woodlands as hominin refugia during the Pliocene dry pulses (Joordens *et al.*, 2019), or for hominin origins in the late Miocene (Kingdon, 2003) is yet to be supported by direct fossil evidence. Therefore, these should be seen as speculative for now.

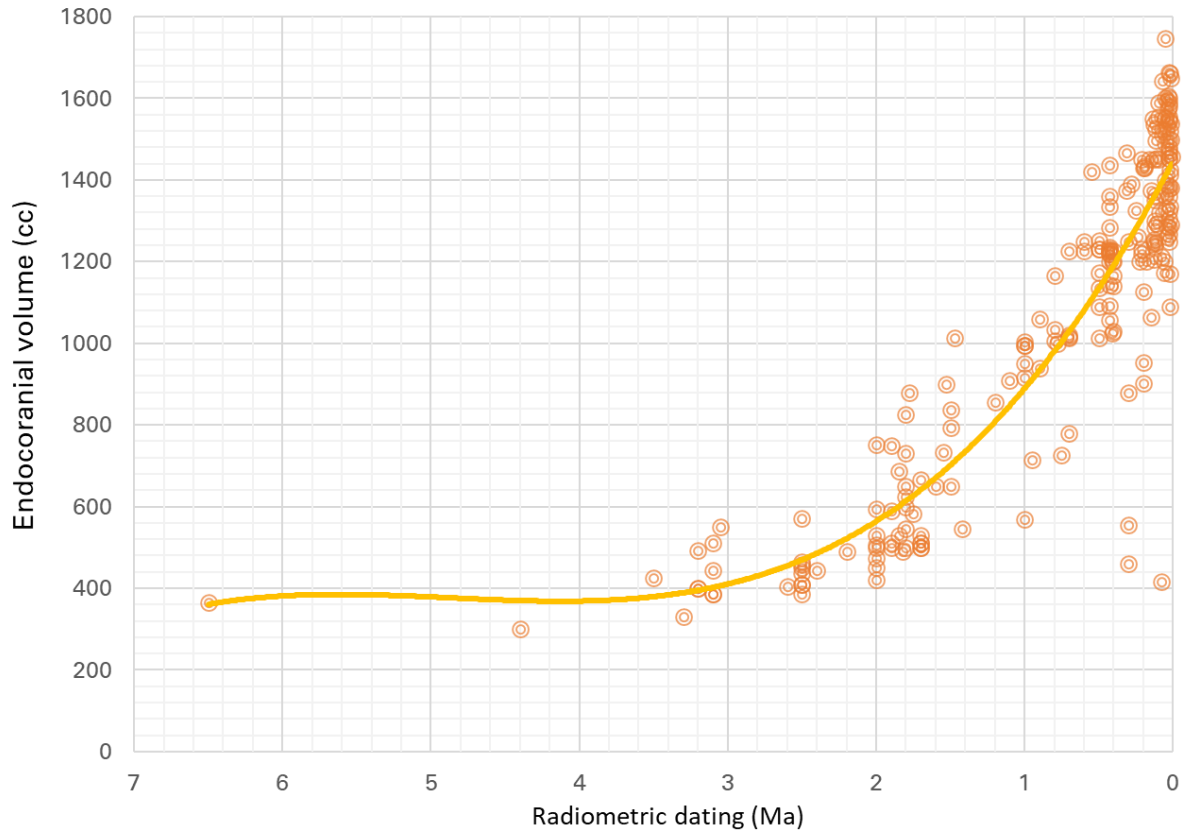


Figure 1.9 – **Polynomial regression showing the trend for hominin brain expansion** (dataset provided in Du *et al.*, 2018).

There are many alternative hypotheses to a coastal origin for the Hominini clade. The savannah hypothesis (Darwin, 1871; Dart, 1925) proposes that the transition from forest to more arid environments in Africa led to bipedalism and other key adaptations in early hominins. However, all putative early hominins and their paleoenvironmental reconstructions reject the savannah hypothesis, and instead show they inhabited mesic woodlands and forests (Pickford & Senut, 2001; Vignaud *et al.*, 2002; Thorpe *et al.*, 2007, 2014; Le Fur *et al.*, 2009; Su *et al.*, 2009; Crompton *et al.*, 2010). There is, however, a drying and cooling trend starting in the late Miocene that expands grasslands and other savannah-like environments across eastern and

southern Africa (Zachos *et al.*, 2001; Steinthorsdottir *et al.*, 2021). Notwithstanding, the dry corridor running northeast to southwest from Somalia to Namibia emerging in the late Miocene (Morley & Kingdon, 2013; Bobe *et al.*, 2023) most likely acted as biogeographic barrier between the earliest Panini and Hominin populations (Kingdon, 2023), instead of being the core ecosystem for the development of hominin traits, as the proponents of the savannah hypothesis popularized (Robinson, 1963; Wheeler, 1984).

Sahelanthropus tchadensis inhabited gallery forests bordering Mega-Chad Lake ~7.2 Ma, featuring extensive freshwater habitats and swampy, well-vegetated areas (Vignaud *et al.*, 2002; Le Fur *et al.*, 2009). *Ardipithecus kadabba*, thrived in riparian woodlands and floodplain grasslands along water margins between 6.3 and 5.2 Ma (Haile-Selassie, 2001; WoldeGabriel *et al.*, 2001; Su *et al.*, 2009). *Orrorin tugenensis* (6.1 to 5.8 Ma), likely inhabited floodplains with open woodlands, potentially fringing lake margins and streams draining into the lake, as suggested by Pickford & Senut (2001). These reconstructions provided fertile ground for the arboreal hypotheses of hominin origins (Thorpe *et al.*, 2007, 2014; Crompton *et al.*, 2010). The presence of wooded areas and abundant water sources in these environments supports the idea that early hominins utilized trees for shelter, foraging, and protection from predators, before eventually transitioning to more terrestrial lifestyles.

The arboreal hypotheses have now gained favourable consensus, and they do not directly contradict any coastal woodland or forest models, since they do not specify a particular subtype of arboreal ecosystem or a geographic location. However, there is a Miombo woodland hypothesis for hominin and bipedalism origins (Senut *et al.*, 2018b) that fits within the broad category of 'arboreal hypotheses' but makes more specific regional predictions, as it points to the Miombo ecosystems extending primarily throughout the Zambezi basin but also as far as Tanzania and all the way to the Atlantic coast in Angola. In its eastern extent the Miombo, also known as '*Brachystegia* woodland', is considered part of the gradient of vegetations and biomes that characterize the modern coastal forests of eastern Africa together with mangrove forests, rainforest, *Cynometra* thicket, swamps, seasonal ponds, among others (Joordens *et al.*, 2019; Tinley, 2020).

While the current large distribution of Miombo woodlands in southern Africa might at a first glance seem to contradict, at least partially, the coastal models, it should be noted that from a paleobiogeographic perspective the Miombo could only have expanded after the rainforests contracted, during the late Miocene global cooling event (Kaya *et al.*, 2018). This is confirmed by recent phylogenomic studies that place Miombo origins at about 8.6–2.8 Ma. Moreover, the divergence between western and eastern species of *Brachystegia* at 3.7–1.2 Ma shows that their major expansion westwards probably only occurred at the Plio-Pleistocene transition (Boom *et al.*, 2021). Therefore, it is likely that the initial Mio-Pliocene core of the Miombo woodlands would be restricted to the transition of eastern Africa coastal forests to more open inland habitats, which overlaps extensively with the region predicted by coastal models.

Ultimately, we could also argue for a scenario where the LCA populations lived across multiple African basins, similar to what Scerri et al. (2018) proposes for later phases of hominin evolution (i.e., *Homo sapiens*). Although this presents a plausible anti-thesis to the coastal models, it remains essential to acknowledge that at some point, some form of barrier—whether ecological or behavioural—must have precipitated the divergence between *Pan* and *Homo.*

1.5 Targeting the gaps – time beats timing

When did the earliest hominins first appear? There is currently a bias towards assuming that hominin origins occurred around the transition period of the late Miocene to the early Pliocene (~5.33 Ma) with suggested intervals at 7–5 or 6–4 Ma (Chapter 3). However, this assumption is likely due to the scarcity of fossil deposits corresponding to crucial time periods of the late Miocene. For example, as previously stated, the crucial period ranging from 9 to 7 Ma in Africa is represented by a single geological formation and locality with ~200 vertebrate fossils (Chorora Fm, Ethiopia; Katoh et al., 2016).

What is the age of fossil deposits that should be surveyed to find our earliest hominin ancestors? A possible approach to answer this question is to understand the current consensus in molecular divergence estimates (Besenbacher *et al.*, 2019). This can be examined by curating the

molecular estimates available in the literature for the split event between the Panini and Hominini clades and evaluate the range of estimated values by comparing it to the geological dating of the earliest known hominins in the fossil record. Exploring the trends of split estimates using Bayesian meta-analysis and polynomial regressions of all data points, as well as exploring subsets of data selected using FAD-based thresholds of important fossil evidence, should clarify to palaeoanthropologists the most likely specific age of deposits to target. Thus, the findings of such approach would be very valuable to consider increasing sampling efforts at specific intervals of the late Miocene of Africa.

Chapter 3 introduces a novel meta-analytic approach to study divergence dates, using ~200 molecular split estimates gathered from the literature published between 1967 and 2021. Measuring branch lengths is the quintessential way to estimate molecular dates of divergence since most recent common ancestors. However, molecular clock models rely on many assumptions that can strongly bias the results (Bromham, 2019). Historically, some molecular studies have attempted to reject the hominin status of some species based on their models (e.g. Sarich, 1971; Hasegawa, Kishino & Yano, 1985). Instead, I propose to consider the high variance of results in molecular clock models, and use the palaeontological discoveries, and geological work done in the late Miocene of Africa as statistical 'filters' (for a detailed explanation, see Chapter 3.2.2) to better understand which of the many available molecular models are compatible with the current palaeontological evidence.

The resulting meta-analysis suggests that contrary to widespread belief, a very recent (after 8 Ma) scenario for hominin origins is highly unlikely. All reported estimates ever published modelled through a polynomial regression and its 95% confidence interval are trending towards an interval of 7.5 to 9.5 Ma. Using a variety of data sets filtered by fossil evidence the results indicate that the split must have happened quite early within the late Miocene, most likely before 8.5 Ma, with stricter models (assuming *S. tchadensis* as a hominin) suggesting it might have happened as early as between 9 and 11 Ma. These findings indicate that more fossil deposits with ages older than 7 Ma should be discovered and targeted in Africa in order to test these estimations.

These results obtained in Chapter 3 suggest that Gorongosa could be a key region to concentrate surveying efforts. Preliminary Beryllium dates suggest that it might contain fossil deposits of critical age for targeting the earliest hominins (Figure 1.2), with some sites potentially covering some intervals poorly represented elsewhere in the continent, especially GPL-2 (8.9 to 5.7 Ma) and GPL-6 (10.9 to 8.5 Ma). Moreover, some sites could also be relevant for the LCA chronology (which predates for some unknown extent of time the divergence event), including the GPL-1 middle fossiliferous layer (12.4 to 6.8 Ma), and GPL-12 upper fossiliferous layer (13.1 to 8.8 Ma). All these sediment date estimates are preliminary, with high variance, and need further work and refinement, as well as validation through complementary methods, such as uranium series, palaeomagnetism, and biochronology, in order to be properly constrained (Bobe *et al.*, 2023). Yet they suggest that Gorongosa holds the potential to fill some of the major temporal gaps in the fossil record of African Hominoidea (Begun & Nargolwalla, 2004; Begun, 2018), particularly within the *Pan-Homo* branches (Chapter 3).

1.6 Targeting the gaps – remote site detection

The Coastal Forest of Eastern Africa (hereafter CFEA) stands as a distinctive ecological niche that potentially played a pivotal role in primate evolutionary history. In the Miocene epoch, the CFEA spanned a much larger territory, stretching continuously from Somalia to South Africa (Joordens *et al.*, 2019). It is reasonable to surmise that the expansion of the northeast-southwest arid corridor traversing Africa (Morley & Kingdon, 2013; Bobe *et al.*, 2023) led to the complete isolation of ancestral ape populations inhabiting the western and central rainforests of Africa from the ones inhabiting the CFEA (see Figure 1 *in* Appendix II). Kingdon (2003) postulated the existence of a "Ground Ape" residing within this eastern coastal forest and that it evolved into the earliest hominins as aridity cycles intensified during the late Miocene (Griffin, 2002; Zhang *et al.*, 2014). Despite Kingdon's intriguing hypothesis, concrete fossil evidence has remained elusive in support of this conjectural coastal ape.

If the fossil sites at Gorongosa harbour "ground apes", they have the conditions to test the coastal and deltaic hypotheses of hominin origins detailed in Chapter 1.4. However, the total surveying area for the lower Mazamba formation has several thousands of square kilometres (Real, 1966; Tinley, 1977; Laumanns, 2001; Habermann *et al.*, 2019), so how will the prospection area for novel fossiliferous localities be restricted to the most optimal places? Without thoughtful quantitative analysis, the endeavours of searching for new fossil-bearing localities will remain mostly a matter of luck (Anemone, Conroy & Emerson, 2011a). Even though palaeontologists have been using geographic information systems (GIS) regularly in their search for vertebrate fossils, much of the prior work has involved laborious visual inspection of satellite images and geologic maps that only guided later ground surveys (Nigro *et al.*, 2003; Haile-Selassie *et al.*, 2007; Njau & Hlusko, 2010).

Geospatial palaeontology is a new discipline that uses machine learning (ML) algorithms for automating this process (Anemone & Conroy, 2018). To teach these algorithms to "see" where unknown fossil localities are hiding, researchers have sampled coordinates of previously known localities, with associated geo-environmental variables (Oheim, 2007; Block *et al.*, 2016; Wills, Choiniere & Barrett, 2018), satellite spectral bands (Malakhov, Dyke & King, 2009; Anemone, Emerson & Conroy, 2011b; Conroy *et al.*, 2012; Emerson & Anemone, 2012), or both (Emerson *et al.*, 2015). This probabilistic approach maps new potential hotspots for productive localities, that can later be systematically probed. Despite the incredible advances achieved during the last decade (Chapter 2), these approaches have not yet been applied to the search for hominin fossils in the EARS. In Chapter 4, I demonstrate the first successful application of automated remote fossil detection in the EARS, at its southernmost section, in the Miocene deposits of Gorongosa.

Our recent fossil discoveries of hominoid teeth in Gorongosa (Chapter 6) offer an invaluable opportunity to evaluate the east African ground ape hypothesis (Kingdon, 2003) and extend the dataset of Miocene African apes (Pugh, 2022; Urciuoli & Alba, 2023). The research of Chapter 4 underscores the efficacy of computer-aided methodologies in identifying fossil-rich deposits and offers the possibility of testing for the first time some theories related to primate evolution.

Due to the rarity of Miocene coastal woodlands and forests in the fossil record, ongoing investigations and expeditions to Gorongosa will remain pivotal in advancing our comprehension of palaeoecological aspects concerning both the evolution of apes and other coastal fauna, and potentially of the earliest hominins (Bobe *et al.*, 2020b, 2023; d'Oliveira Coelho, Anemone & Carvalho, 2021).

1.7 Large-scale and automated palaeoecological reconstruction: a case-study in East Turkana

The use of satellite data to remotely detect fossil sites (d'Oliveira Coelho *et al.*, 2021), and the search for hominin and ape fossils in previously understudied palaeoenvironments (Habermann *et al.*, 2019) has led to a third research question: can we automate palaeoecological reconstruction using similar geospatial approaches? However, to explore this avenue, we require a larger volume of data and a site where palaeoenvironmental interpretations are widely accessible and have been conducted for decades using multidisciplinary methods (Appendix I). Only then could the estimates of a large scale satellite-based palaeoecological model be properly validated (Dorans *et al.*, 2020).

Researchers working in the Koobi Fora formation of northern Kenya have long inquired about the geographic patterning of extinct fauna and their respective palaeoenvironments (e.g., Behrensmeyer, 1975a; Isaac & Behrensmeyer, 1997). During fossilization it is expected that different taphonomic and ecological conditions will result in different sediments, with specific spectral signatures (Wills *et al.*, 2018). To investigate differential preservation of aquatic and terrestrial habitats, we introduce the first attempt at predicting regional palaeoecological patterns by means of geospatial analysis of topographical, ecological, and spectral variables that may distinguish between aquatic and terrestrial contexts in the palaeoenvironments across the Koobi Fora Formation.

Chapter 5 presents a novel approach for predicting the ratio of terrestrial to aquatic conditions across a large territory, and this was tested on East Turkana, Kenya. To achieve this goal, we

present a method that can be generalized to other fossil regions of the EARS (and elsewhere) rich in surface finds, as it only requires as the outcome variable the proportions of aquatic to terrestrial fauna obtained during bone walks. The aquatic-ratio layer guides the machine learning training when stacked over a set of other georeferenced variables.

This innovative method extends the existing paradigm of geospatial palaeontology, which has traditionally focused exclusively on remote detection of fossil deposits, as extensively reviewed in the following section (Chapter 2). Therefore, Chapter 5 extends geospatial palaeontology by pioneering a new sub- or sister- discipline "geospatial palaeoecology", that aims to enhance our understanding of the past ecological context in which fossils were deposited by integrating machine learning techniques with satellite and field palaeoecological data. The application is demonstrated in estimating aquatic to terrestrial conditions across the Koobi Fora Formation (Chapter 5), and rigorously validated in a fossil-rich basin with decades of palaeoecological evidence (Appendix I). However, the protocol's adaptability is suggested for reconstructing various other palaeoecological features, such as vegetation habitat gradients or habitat cover categories, using geolocations of fossil bovids and their known habitat preferences across time (Chapter 6.3.4).

2

Literature Review

2.1 Traditional discovery of fossil sites

Traditional fossil discovery has been the result of educated guesswork, followed by systematic probing of a terrain. Before going to the field, researchers might resort to literature to investigate historical palaeontological findings and generic descriptions of a region. In barely studied areas such information might be scarce, so a more appropriate method is to collect and optically scrutinise aerial photos and military or geological maps. On arrival, local contacts and explorers are important to gather tacit information and insights about the field site (Oheim, 2007; Njau & Hlusko, 2010; Wills *et al.*, 2018).

However, it is in previously unidentified sites that most novel finds tend to occur (d'Oliveira Coelho, Anemone & Carvalho, 2020). Yet recognising potential new fossil assemblages over vast areas is a technical challenge using aforementioned approaches (Block *et al.*, 2016). Therefore, methods that can save time and money in the search for new fossil localities while also increasing the rate of success, are in urgent need of being developed, validated, and adopted by field palaeontologists (Dorans *et al.*, 2020). Before offering any solution, it is

important to understand the historical development of palaeoanthropological fieldwork in Africa.

The first explorers of hominin origins in Africa have been trained as archaeologists or medical doctors and they were responsible for the emergence of palaeoanthropology as a discipline. The earliest fieldwork started in South Africa, and it was usually carried out by individuals or small teams. Such efforts gave rise to the first discoveries of *Australopithecus*, Taung 1 and MLD1 (Dart, 1925, 1948) as well as Sts 5, Sts 14 and Sts 71 (Broom, Robinson & Schepers, 1950); *Paranthropus*, notably TM 1517 and SK 46 (Broom, 1938, 1949); and the SK 15 mandible as well as the SK 847 cranial composite might represent early *Homo* (Broom & Robinson, 1949; Clarke & Howell, 1972). Fossil sites were haphazardly identified as surveying was mostly done in association with mining operations often involving the use of explosives, which resulted in fragmentation of specimens. Most early publications did not rely on analyses from experts of other disciplines, and most interpretations of evolutionary relationships were solely based on anatomic comparison with extant species of primates (Anemone *et al.*, 2011a). During the 1950s and 60s, the Leakey family and their teams of local collectors started working in similar fashion at Olduvai Gorge, Tanzania (Leakey, 1958, 1969). Amongst dozens of hominin individuals recovered from this region, some are particularly significant, including OH 5 and OH 7, the holotypes of *Paranthropus boisei* and *Homo habilis*; OH 9, a *H. erectus* cranial vault; and OH 62, a partial skeleton of *H. habilis* (Leakey, 1959, 1960, 1961; Johanson *et al.*, 1987).

Leakey's luck with Olduvai Gorge is associated with the perhaps apocryphal story of the accidental discovery of the Gorge itself. The story is that in 1911 an entomologist was chasing a rare butterfly and fell down a ravine, and realized he was surrounded by fossil beds of great anthropological significance. However, this is most likely not true, but rather a myth perpetuated in the literature, since the person in question, William Kattwinkel, was a neurologist and a member of the *Bayerische Palaeontologische Staatssammlung* of Munich, researching sleep sickness in the region at that time. Still the point on the chance factor is still valid, with a medical doctor with a parallel interest in palaeontology who ended up stumbling

upon on what would later be considered one of the most important palaeoanthropological sites in the world (Maier, 2003; Henke, 2015).

The Leakeys would increasingly collaborate with anatomists and geologists, setting the stage for multidisciplinary team fieldwork (Leakey, Evernden & Curtis, 1961; Leakey, Tobias & Napier, 1964; Leakey & Hay, 1979). During the 1970s and 80s this practice would spread and become the standard for prospection, data analysis and publication in palaeoanthropology. Meanwhile new exposures and deposits were being explored within the Omo-Turkana basin and the Awash Triangle. Howell led excavations at Omo and is generally recognized as the most important promoter of integrative and collaborative approaches within African palaeoanthropology (Anemone *et al.*, 2011a). He gathered together in the field specialists in palaeontology, geology, osteology, archaeology, radiometric dating, palynology, and other disciplines (Howell, Haesaerts & de Heinzelin, 1987).

Another example of a serendipitous but hugely important find is the recognition of Middle Awash as fossiliferous during exploratory work by geologists, first Gortani and Bianchi in the 1930s, and more systematically by Maurice Taieb in the 60s (Kalb *et al.*, 1980). Much later, in a team effort, excavations were undertaken, radiometric dates were determined and the first Pliocene hominins were recovered (Clark *et al.*, 1984). To this date it remains the area with the biggest output of *Australopithecus afarensis* (over 400 specimens), including perhaps the most famous hominin partial skeleton, AL 288-1 ‘‘Lucy’’ (Johanson & Taieb, 1976).

Of course, sometimes trained palaeoanthropologists also identified unexplored sites that later proved of major importance, as is the case of Koobi Fora being recognized by Richard Leakey from a small airplane, when he was flying back to Nairobi from Ethiopia on a detour to avoid a storm (Gibbons, 2006). Also in West Turkana Plio-Pleistocene sediments were confirmed through reconnaissance work and aerial photographs in 1983 (Leakey & Walker, 1985).

Over the last two decades, most palaeoanthropological inquiry in East and South Africa has relied on well-established teams with very diverse academic backgrounds and utilizing a variety of recent scientific and technological tools and methods (e.g. Hawks *et al.*, 2017). These include 3D laser scanning, photogrammetry, and X-Ray computed tomography for virtual

fossil reconstructions, and geometric morphometrics and finite element analysis for advanced quantitative analysis (Williams *et al.*, 2017).

During this time the use of aerial photography, of remote sensing (RS) data and GIS to optically recognise suitable fossil exposures become far more widespread (Njau & Hlusko, 2010). More recently, potential fossil sites have been identified by modelling remote sensing images through machine learning algorithms (Conroy, 2014; Emerson *et al.*, 2015). ML algorithms can classify the pixels of a satellite image to identify the spectral properties of fossil sites and infer potential site locations at fine resolutions (~15-30m). Besides satellite images, now unpiloted aerial vehicles (UAVs) or drones, not only carrying photographic cameras but also miniaturized LiDAR scanners, thermal cameras, or multispectral scanners have been used to collect data for the purpose of automating fossil site discovery (Emerson & Anemone, 2018). Despite all these innovations becoming increasingly more accessible, computer-assisted remote fossil prospection has not yet been applied to areas that could have been inhabited by early hominids.

2.2 Searching localities from space

2.2.1 The early years of archaeological predictive modelling

In archaeology, predictive modelling has been used since the 70s to discover new productive localities, using artefact or site distribution data (Stringer & Cook, 1974; Lyons & Avery, 1977). Yet decades before, it was noticed that site location was non-random and certain topological features could be used to guide prospection (Willey, 1953; Williams, 1956). When modelling, each data instance of a locality is recorded with positional coordinates, in the form of points, lines or polygons. Then, any variable that might be useful to describe a locality pattern is also recorded. The early studies used slope, aspect, soil type, vegetation cover and distance to water, as ecological proxies (Kvamme, 1983; Kohler & Parker, 1986; Kvamme & Jochim, 1989). Occasionally, some studies also used economic or sociocultural variables as human behaviour proxies, to better model site distribution (Kohler & Parker, 1986; Verhagen *et al.*, 2012). Most predictive modelling in archaeology uses GIS data with ecological variables,

without relying on any satellite imagery (Figure 2.1), but there are some early notable studies that used spectral bands for modelling (e.g., Stringer & Cook, 1974; Custer, Eveleigh & Klemas, 1983; Custer *et al.*, 1986).

On 23rd July 1972, NASA launched the first satellite in a series that transformed the way of doing archaeological prospection. This remote sensing program, nowadays known as Landsat, has launched nine different satellites to this date (Masek *et al.*, 2020). Access to all past archive and current data collected by the orbiting satellites is free and managed by the USGS EROS Data Center. This multi-spectral data has been widely used by archaeologists in a variety of applications, including remote site prospection (Giardino, 2011).

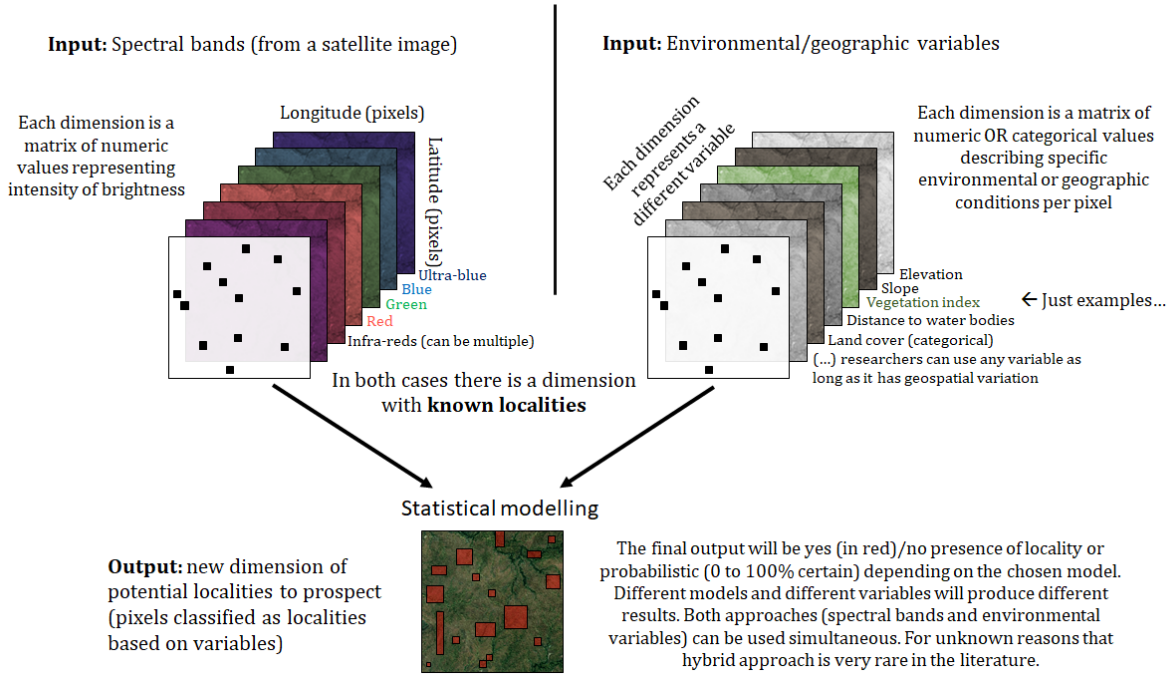


Figure 2.1 – **The two main approaches of data collection for geospatial predictive modelling.** Either using spectral bands (each band as a variable) or environmental variables as inputs.

The potential of Landsat imagery to detect archaeological sites was first noticed by van Liere (1973 in Limp, 1989), who optically identified the large site of Angkor Wat on a Landsat 1 (active from 1972-78) scene. Cook and Stringer (1974) pioneered the use of quantitative procedures that to some extent correspond to the automated methods for archaeological site discovery used today. They studied a region in Alaska by analysing multispectral data from Landsat 1 with a parallel-piped classifier. This model discriminated areas based on their

spectral signature, and those that matched signatures from known archaeological examples were flagged as new potential sites. Custer et al. (1983, 1986) also followed a similar approach but using logistic regression models instead. Besides classifying the study area into 16 different classes, this had the advantage of developing a probability surface covering the whole studied area. These early studies indicated that human occupation leaves characteristic spectral signatures detectable from space imagery.

Predictive modelling for remote reconnaissance interested archaeologists for reasons of cost and efficiency associated with prospection of large areas. Foremost, it provides a quantitative estimation for the likelihood of sites in an area, prior to surveying (Kohler & Parker, 1986). It is also an important planning tool for cultural resource managers to support their decisions to prioritize specific areas deemed more sensitive or at risk. Some warned that predictive modelling was inherently tied to a return to environmental determinism (e.g. Gaffney & van Leusen, 1995), but in point of fact archaeological predictive modelling has been moving towards using more historical and sociocultural data (Verhagen *et al.*, 2012; Achino & Barceló, 2019) while still maintaining that environmental features are important for site distribution. Archaeological predictive modelling is ultimately a probabilistic tool striving for finding patterns. Like in many scientific areas this motivation comes from ‘‘recognizing order in the chaos of the natural world by formulating generalizations or rules (laws, principles) of increasing specificity’’ (Kvamme, 2005, p. 3). Therefore, predictive modelling should work as a decision support system during surveying, a guide benefitting researchers that will still rely on their expert knowledge to make anthropological interpretations and spatial decisions based on outputs of probabilistic models (Field *et al.*, 2007; McCoy & Ladefoged, 2009).

The main criticisms of predictive modelling for archaeological sites have been framed in terms of environmental determinism and a shift from theory to method, or from analytical thinking to computer-based research. But critics also argued there is not much theoretical thought regarding processes of site formation and human behaviour behind the statistical modelling techniques employed by researchers (Ebert, 1999). Other questionable assumptions relate to the usefulness of variables collected over present-day environments since values would differ

in the past, including the location of important water and edible resources. Other problems reflect archaeological sample bias: we cannot model what is still buried; much archived data is not shared; many known sites (mainly pre-GPS) are inaccurately recorded; sites may not represent discrete units; neither different types of sites should be clumped; and interesting sites are unique and therefore will not fit patterns. Some other more technical critiques about GIS features, imagery resolution and statistical problems of working with this kind of data can be also be found in the literature (Gaffney & van Leusen, 1995; Ebert, 1999; Wheatley, 2004; Kvamme, 2005). However, theoretical concerns regarding thoughtless use of spatial data are very important because they lead the scientific community to reevaluate their protocols, what kind of data to collect, or algorithms to choose and other details that eventually result in more robust approaches (Ebert & Singer, 2004; Kvamme, 2005; Verhagen *et al.*, 2012).

Predictive spatial modelling does not attempt to be an end in itself and prospection will always depend on image interpretation by humans and ground-truthing if we are to acquire reliable metrics of accuracy and improve future iterations of statistical models (Kvamme, 2005). It should be noted these modelling techniques have been used not only to find new sites for the sake of purely academic purposes but also to identify areas requiring protection from poaching, urban development or natural threats (Verhagen *et al.*, 2012). Moreover it is a technique that has been proven valuable on multiple occasions for rescuing artefacts, remains and data that otherwise might have disappeared forever (Perakis & Moysiadis, 2011; Balla *et al.*, 2014).

2.2.2 Predictive modelling by means of environmental data in Palaeontology

We have seen previously that as early as the 1970s archaeologists started experimenting with the idea of using spatial data and statistical modelling for predicting new sites (Stringer & Cook, 1974; Kvamme, 1983, 1999). Sophisticated uses of GIS and RS in the literature of vertebrate palaeontology are far more recent and sparse (Anemone *et al.*, 2011a). The first analogous study in palaeontology was Oheim's (2007) attempt to identify areas with high density of dinosaur bearing deposits in the Two Medicine Formation. By means of site suitability analysis (SSA), the following variables were selected: geological cover, elevation,

vegetation cover, and distance to roads, then these were normalized into scores (ranging from 0 to 4) according to criteria of "suitability" for site discovery. Ground-testing of the model was fulfilled by systematically surveying areas of both high and low probability. Results demonstrated strong correlation (R^2 = 0.905, Oheim, 2007, p. 363) between predicted likelihood of finding fossils and fossil density per square kilometre observed at the field.

Egeland et al. (2010) also experimented SSA with the following geographic or environmental variables: slope, aspect, elevation, land cover and proximity to rivers, using scores from 0 to 100. The authors were interested in showing evidence of hominins using northern Armenia as one of the routes during out-of-Africa migrations. The methodological twist here was to use GIS techniques to calculate a least cost exit path from Africa to Dmanisi (Georgia), and to model the areas surrounding this computationally projected path. As typical in SSA the output implied plotting the "Unsuitable", "Suitable", and "Very Suitable" regions on a raster map of the region. The results indicated that the highest suitability scores were associated with areas located near rivers with low slope and cropland vegetation. During a field season in 2009, a total of 25 new sites throughout the estimated path were identified. Of these, 2 sites preserved Oldowan-type chopper forms, possibly associated with Plio-Pleistocene hominin occupation (Egeland *et al.*, 2010).

Recently, Wills et al. (2018) applied a supervised learning model for remote fossil site identification on the Elliot Formation (Upper Triassic to Lower Jurassic) of South Africa. Here, six environmental features were selected: land cover, vegetation cover, elevation, slope, aspect and drainage density. A matrix containing all variables and a dataset of 81 known palaeontological localities was pre-processed by multidimensional scaling (MDS) and the resulting scores were then modelled by a linear discriminant analysis (LDA). A split test set containing 20% of the fossil site occurrences was evaluated by the model, which correctly estimated 95% of the localities. No other performance metrics were provided, so it is not certain if the overall accuracy was inflated by fossil locality overestimation. Nonetheless, two new productive localities are reported as being discovered as a direct result of a recent field expedition guided by the LDA's output (Wills *et al.*, 2018).

2.2.3 Other GIS applications in Palaeontology

While not specifically about locality prediction, general research with applied uses of GIS abounds in the palaeontological literature. The earliest implementations started with the development of geospatial databases of species occurrences (Graham *et al.*, 1996; Ferguson *et al.*, 2000; Graham, 2000; DeBlieux *et al.*, 2003). GIS techniques have also been used to reconstruct the habitat ranges and distribution of extinct species (Rode & Lieberman, 2004, 2005; Stigall-Rode, 2005; Stigall & Lieberman, 2006; Ghaffar, 2010; Jurestovsky & Joyner, 2017), correlate fossil taxa over geographical and temporal extents for biostratigraphic dating (Rayfield *et al.*, 2005; Viglietti *et al.*, 2016; Parker & Martz, 2017), for studying differential taphonomic effects on sampled material (Jennings & Hasiotis, 2006; Chew & Oheim, 2009), as well as for spatial analyses of fossil deposits in three-dimensional reconstructions (Nigro *et al.*, 2003; Jennings & Hasiotis, 2006) or even for 3D morphometric and topographic analyses of tooth morphology and microwear (Zuccotti *et al.*, 1998; Ungar, 2004; Scott *et al.*, 2005). Likewise, the effects of large-scale geological events have been approached with RS. For instance, Bailey and colleagues (2011) used Landsat 7 Enhanced Thematic Mapper (ETM+) and Shuttle Radar Topographic Mission (SRTM-3) imagery covering southern Africa to explore the role of active volcanism for habitat choice of hominins during the Plio-Pleistocene. Conroy (2006) argues for the importance of using GIS in palaeontological studies for a variety of purposes: access to interactive maps of the study area; ability to update and visualize your database at any time; ability to query the catalogued fossil finds through attribute tables. This last aspect is particularly useful in survey work since it can be used to examine specific distribution patterns. Another relevant feature is the ability to share spatial data, do open research and collaborate at a distance (Conroy *et al.*, 2008; Emerson & Anemone, 2018). While using handheld GPS in the field has become a common practice, the way this data is distributed across the scientific community is not yet entirely satisfactory or uniform. Converting geospatial databases to the Keyhole Markup Language (KML) file format, allows researchers and others to visualize very complex datasets even in free software like Google Earth. Conroy,

Anemone, Van Regenmorter and Addison (2008) were among the first to provide their palaeontological database in KML, containing data collected in the field such as GPS coordinates of fossil sites, associated along with other important variables such as elevation (from DEM, 30-meter resolution), slope, and geology. Alas, it is hard to find others following this example, with the great exception being the Turkana Database. The Turkana Database was created and is maintained by René Bobe, earlier versions are freely available online and it contains very complete information for 70000 fossil occurrences (at this date); however older records on the database are not geolocated yet (Bobe *et al.*, 2011).

Using GIS in biostratigraphy is particularly interesting, since quantitative data can be used to test if species proposed to be land vertebrate faunachrons (LVF) really do fit the criteria of being (1) temporally restricted, (2) numerically abundant and (3) spatially widespread. LVFs can be used as a dating technique based on the evolutionary trajectories of certain extinct species commonly found on fossil assemblages. Rayfield et al. (2005) found that some proposed LVFs did not fit all the criteria. Taphonomic bias can also be quantitatively analysed with greater scrutiny using GIS techniques (Jennings & Hasiotis, 2006). One example is Chew and Oheim's (2009) analysis of palaeontological data within a geospatial framework to investigate the impact of two taphonomic variables (variation in sampling area and rate of sediment accumulation) on species richness and relative body size in vertebrate fossil assemblages. Their results suggested that sampling area added significant bias to calculations of species richness at the level of individual localities as well as throughout the whole basin.

Although the applications presented here are very diverse, the use of GIS in the fields of palaeontology and biological anthropology is still emerging and many possibilities are yet be explored (Conroy, 2006; Conroy *et al.*, 2008; Chew & Oheim, 2009; Anemone *et al.*, 2011a; Anemone & Conroy, 2018).

2.2.4 Geospatial fossil hunting for hominins

A critical project that demonstrated the potential of satellite imagery for searching hominin fossils was the *Palaeoanthropological Inventory of Ethiopia* (Asfaw *et al.*, 1990). This pioneer

endeavour started in 1988, in somewhat unexplored regions of the Main Ethiopian Rift and the Afar Depression. Its main objective was to discover geological formations with the potential to harbour fossils using remotely sensed imagery. False colour images were created from Landsat data in order to visually compare the lithologies of known fossil localities with those of the analysed areas. This intuitive visual inspection method allowed the researchers to pinpoint locations with promising fossil deposits. Later field work guided by this work was then performed at Fejej and Kesem-Kebena (Asfaw *et al.*, 1991; Wood, 1992). The first location contained a diverse faunal assemblage including the 4 Ma dental remains associated to *Australopithecus anamensis* (Ward, 2014), the second contained several Pliocene vertebrates and an Acheulean lithic assemblage (WoldeGabriel *et al.*, 1992).

Once again in the Afar region of Ethiopia, we have more evidence of the symbiotic link between visual inspection of aerial imagery and palaeoanthropological research. Navigation through the field site was guided by 1:60000 to 1:25000 scale aerial photographs and satellite imagery of the area of interest. The authors reported an astounding discovery of 77 novel fossil sites, with over 1000 discrete remains recovered during the field seasons of 2002-2006. Among these, over 20 craniodental and postcranial remains of Pliocene hominins, including one partial skeleton corresponding to an important transition period (3.5–3.8 Ma) from the *Australopithecus anamensis* to *Au. afarensis* lineages (Haile-Selassie *et al.*, 2007).

There are even completely new species, such as *Australopithecus sediba* and *Homo naledi*, being discovered as a direct consequence of geospatial digital surveys. In the Cradle of Humankind (South Africa), an area that has been extensively and continuously explored by hundreds of palaeoanthropologists and other researchers since the 1920s (Dart, 1925), up until 2008 there were only 130 identified caves. Of these, around 20 were fossil sites. Using nothing but Google Earth and his own eyes, Lee Berger discovered over 700 new palaeocaves, from which at least 80 have confirmed fossiliferous deposits (Berger *et al.*, 2010, 2015; Dirks *et al.*, 2010; Dirks & Berger, 2013; Berger, 2020).

Njau and Hlusko (2010), also used Google Earth in such fashion, but they complemented their visual inspection with imagery from IKONOS, a commercial high-resolution (as close as 1

meter per pixel) satellite company, that improved their chances of finding smaller outcrops (< 10 km^2). A finding from this paper that has repercussions for other field sites is how high spectral brightness is a good predictor of sedimentary rock outcrops. These high reflectance pixels were later ground surveyed during three short field expeditions (2006–2008), which led to the discovery of 28 new fossil-bearing and/or archaeological localities (Njau & Hlusko, 2010). As a side note, the same holds true for Gorongosa, where the first sites with fossils of mammals were described as "white patches" visible from Google Earth images by Martin Pickford (2013).

Together those 4 distinct projects (Asfaw *et al.*, 1990; Haile-Selassie *et al.*, 2007; Njau & Hlusko, 2010; Berger, 2020) established a ''proof-of-principle'' for using satellite imagery as a tool for locating palaeoanthropological deposits. Inspired by this foundational work, a very important series of papers attempting to automate these principles in important open-air sites at the Great Divide Basin (Wyoming) and the Uinta Basin (Utah) started to emerge in the literature.

2.2.5 Predictive modelling through remotely sensed imagery in Palaeontology

The shift for using images collected by satellites as the main data input for the predictive models is rather recent in palaeontology. The first study using such approach was by Malakhov, Dyke and King (2009) and incorporated Landsat ETM+ imagery to perform a computational search for Late Cretaceous sediments potentially harbouring fossil vertebrate fauna in Kazakhstan. Using Spectral Angle Mapper, an image classification algorithm, the authors classified the studied area into: (1) yellow Late Cretaceous Clays; (2) red Late Cretaceous clays; (3) overlying Neogene and Palaeogene sediments; (4) Quaternary clay beds; and (5) dried bottom of temporary lake. Then, the areas containing Late Cretaceous clays were prospected and according to Malakhov et al. (2009, p. 7) fieldwork "yielded almost perfect results" and was superior to "more traditional surface prospecting of sediments of the correct age where our teams found fossil material much less frequently". But no statistical metrics or number of new fossil sites discovered is provided, making it impossible to draw any

comparisons with other studies. It should be noted that this approach outputs spectral classes that can be used for extrapolation of prospective fossiliferous sites by virtue of having the correct age and lithology, rather than directly indicating where potential fossiliferous areas may occur.

One of the main stages for the development of geospatial palaeontology during the last decade has been the Great Divide Basin of southwestern Wyoming. In the earliest contribution (Anemone *et al.*, 2011b; Emerson & Anemone, 2012), a supervised image classification model was trained with spectral signatures of previously known localities, aiming to find novel fossil deposits. Remotely sensed imagery from Landsat 7 ETM+ from August and September 2002, were selected because they were cloud-free and captured previously to one of the sensor's collapse in 2003. In a pre-processing step, the spatial resolution of these satellite scenes was improved from 28.5 to 14.25 m using principal component analysis (Anemone *et al.*, 2011b). The pipeline used an artificial neural network (ANN) to mine the numeric patterns of the spectral data. The ANN architecture was composed by an input layer with 6 nodes, two hidden layers and an output layer with 10 nodes. The ANN's 6 input nodes correspond to the 6 spectral bands of visible and infrared light extracted from the Landsat 7 scenes.

Since the learning is supervised, the authors had to manually label representative pixels of each output class (in this case: localities, white soil, dark soil, red soil, grassland, sagebrush, cropland, mixed scrub, forest, herbaceous wetland) in order to teach the algorithm to recognize the spectral signature corresponding to each of these classes. Localities were defined using GPS coordinates from 110 fossil sites assessed during several field seasons spanning 1994 to 2010 (Emerson & Anemone, 2012). The identified pixels were split into a training (75%) and a test set (25%) in order to obtain reliable accuracy metrics. Over the test set pixels, the model correctly classified 84.21% of landcover classes. Of the 5589 pixels predicted as localities, 5525 were true localities, which translates to a positive predictive value (or precision) of 98.85%, but the model is slightly overfitting since it only had a true predictive rate (or sensitivity) of 79.03%.

When generating a digital map based on the model's output prediction of localities, only pixels classified with over 95% probability of belonging to the locality class and on a slope of more than 5% were accepted for generating the final visual layer (Figure 2.2). These steps further enhanced the robustness of the results and reduced the total surveying area. The output's spectral signature for the localities was described as a "complex mix of brightness values that result from the sunlit and shadow areas of the outcrops, the eroded mudstone and sand at the base of the outcrops, and any other materials that may be found within the roughly 203 m^2 area (14.25 m squared) corresponding to a training pixel" (Anemone *et al.*, 2011b, p. 172). Finally, as a conservative validation test of the ANN model, researchers attempted to classify a separated area from the Bison basin and the ANN was able to identify its 3 most productive fossiliferous deposits, despite the model being trained without any localities from that region (Anemone *et al.*, 2011b).

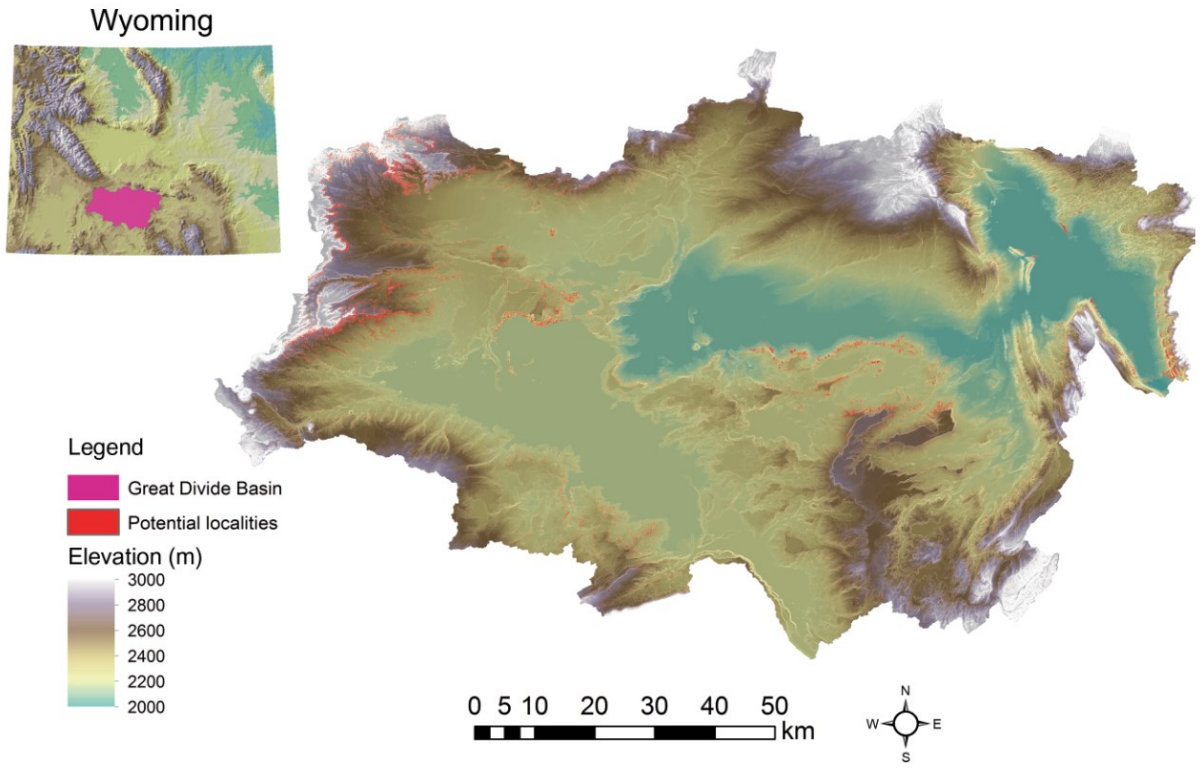


Figure 2.2 – **Potential localities (red) in the Great Divide Basin, Wyoming** as estimated by an artificial neural network. Notice that prospecting the whole basin would take centuries even with large teams. This method severely reduces the area of prospection (after Emerson & Anemone, 2012).

Following this, further research within the theoretical frame of computer-assisted remote fossil prospecting was developed by Conroy et al. (2012) for the Uinta Basin, Utah. Landsat 7 ETM+ satellite data was acquired from July 2002 covering the region of interest. A maximum likelihood classification model was trained to identify the following classes: 1) fossil localities; 2) oil/gas field infrastructure; 3) water; 4) agricultural land; 5) scrub/tree cover; 6) steep slopes. All the fossil sites used in the dataset for training the model were known previously to 2005, while the sites discovered after were not. Instead, the latter were kept separated for an independent validity assessment of the model. For constructing a final plot of the predictions, two filters were imposed: only accept pixels classified with over 98% probability of detecting localities and belonging to the Eocene period. All of the 17 new fossil localities that had been found from 2005 onwards matched areas predicted by the algorithm to be fossiliferous. While we cannot speak of accuracy in a technical statistical sense this *post hoc* validation was an excellent indicator of this approach ability for finding productive spots in the area.

All the studies mentioned here (Malakhov *et al.*, 2009; Anemone *et al.*, 2011b; Conroy *et al.*, 2012; Emerson & Anemone, 2012) used supervised learning, meaning that the authors had to manually define landcover classes (including "fossil localities") so that the algorithms could learn how to distinguish spectral patterns amongst them. An alternative approach, of particular interest when there is no *a priori* knowledge or labels of the landcovers one might encounter in a survey area is unsupervised learning (Figure 2.3).

A notable example is Conroy's *Walking Back the Cat* (2014) which provides a step-by-step protocol for using the iso-cluster algorithm to segregate the map pixels into different clusters, depending on the similarities of their spectral signatures. The field site was again the Uinta Basin, and the input data were the bands of Landsat 7 ETM+ pansharpened imagery covering an eastern portion of the basin containing Eocene beds. Since this is a blind approach (i.e., the model has no information of what each cluster represents), two random fossil localities were chosen to select which clusters were representing regions to prospect for fossil localities. This step reduced total remote prospecting area (1899540 pixels) to ~5% (91861 pixels) that "should reflect the areas in the satellite coverage area having the highest probability of including other

fossiliferous outcrops" (Conroy, 2014, p. 176). To validate if the clusters were indeed predictive of fossil sites, all known GPS coordinates of localities were dropped onto a map of the basin overlain by the predictive cluster, and indeed all fell on top of it or "very near".

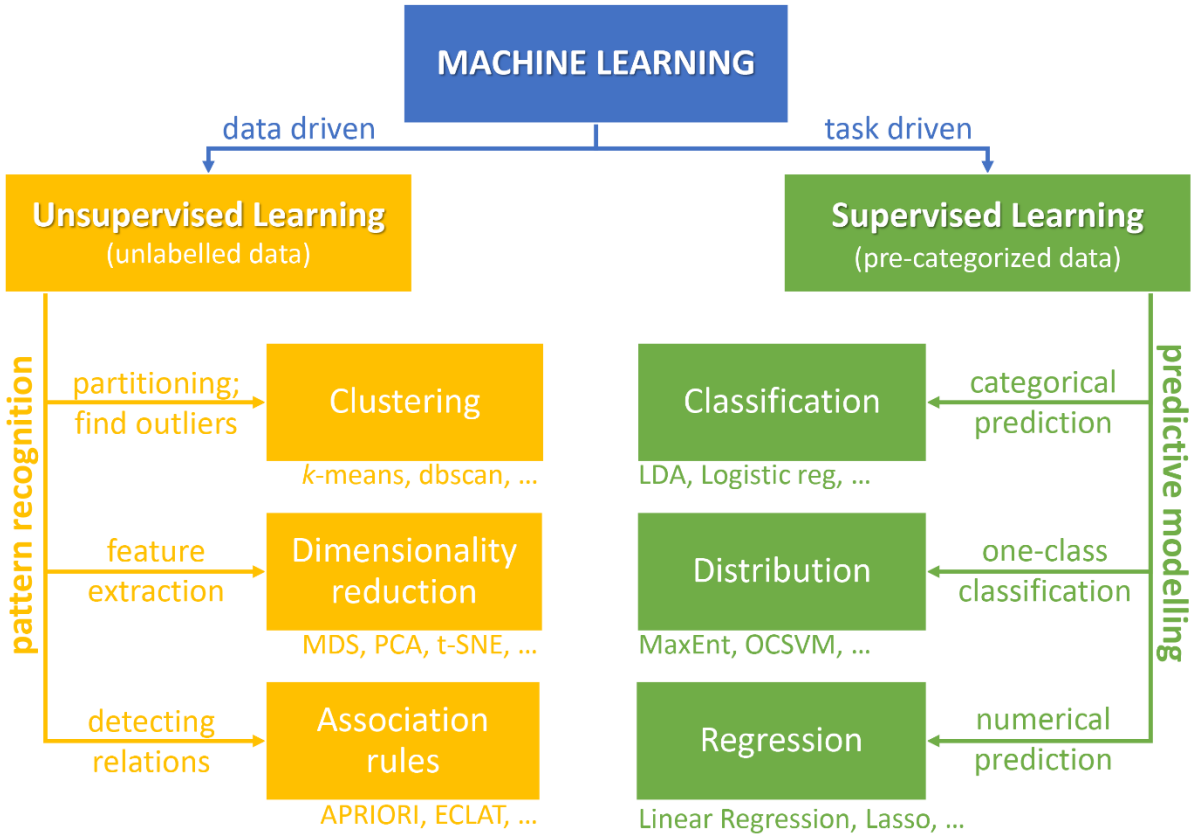


Figure 2.3 – **Supervised and Unsupervised Learning** are the two main conceptual modes of thinking statistical problems within the machine learning paradigm.

Unfortunately, no exact numbers or metrics are provided on the manuscript, but from the plot provided we can see this corresponds to around 40 localities. Thus, the greatest advantage of unsupervised approaches with spectral data is that they work even in the absence of any *a priori* information of landscape cover on the field site. But the most important insight to take from this study, is that in order to deduce the location of other promising areas for future fossil prospecting, it is enough to know only one or two fossil localities, since that was adequate to define a cluster to generate the predictive map in this study (Conroy, 2014).

Recently, Conroy and colleagues (2018) have provided two case-studies of unsupervised learning in regions documenting important past episodes of major global warming, the Early

Eocene Climatic Optimum (EECO) in the Bighorn Basin, and the Palaeocene/Eocene Thermal Maximum (PETM) in the Great Divide Basin. The iso-cluster tool was applied to pan-sharpened Landsat 8 datasets consisting of 11 spectral bands, and it allowed the team to efficiently select areas to be targeted for fossil prospecting, while discarding the areas that would most likely be a waste of resources and time. In the first case-study, the model generated 50 different clusters, and six of them overlapped productive EECO sites Then, the model was tested on the field and most new fossil sites found matched the predictive class created by combining the six clusters of interest. The second case-study focused on a single fossil site (Tim's Confession—a very productive locality) to select one cluster. For a digital validation of the model, all sites known in the Great Divide Basin were plotted on top of the cluster analysis, 40% of them overlapped the predictive cluster perfectly, and the remaining 60% were within a 30 meters buffer of the predictive cluster. Contrary to the first case-study, no ground-truthing was described for the second case-study. While both case-studies are very important contributions to the discipline of geospatial palaeontology and demonstrate the usefulness of unsupervised learning for remotely-guided surveying, they do not provide any statistical performance metrics of the models, making it harder to compare them to the remaining literature.

2.2.6 New approaches: hybrid-datasets, continental-wide taxa-specific discovery, and individual fossil targeting

While some previous work used exclusively geolocated environmental variables as input for modelling (Oheim, 2007; Egeland *et al.*, 2010; Wills *et al.*, 2018), the above mentioned palaeontological remote prospection projects employed only spectral images (Malakhov *et al.*, 2009; Anemone *et al.*, 2011b; Conroy *et al.*, 2012; Emerson & Anemone, 2012; Conroy, 2014). The first to combine these two types of data input for predictive modelling in a palaeontological context are Emerson and collaborators (2015). Besides, instead of doing a classic raster analysis (i.e., operating on a per-pixel basis), they analysed groups of homogeneous pixels representing

image objects. This paradigm has been described in the literature as geographic object-based image analysis (GEOBIA), and the image objects correspond to real-world phenomena (Hay & Castilla, 2008) such as a highly productive fossil locality. Emerson et al. (2015) acquired commercial high-resolution imagery from QuickBird satellites (pan-sharpened to 0.6 m). A 25 km^2 image of an exceedingly prolific area containing several fossil sites in the southern part of the Great Divide Basin was used to train the model. For a field season in 2013, a 160 km^2 QuickBird image from 2009 was analysed, representing a section in the northwest part of the Great Divide Basin that was deemed high priority for exploration by Anemone et al. (2011b). Subsequently, during a 2014 field season, a Landsat 8 OLI scene from 2013, pan-sharpened to a spatial resolution of 15 m, was analysed to spread the predictive model to other regions of the basin. Besides the matrix of spectral bands extracted from the satellite imagery, other variables included in the model were: elevation, geological cover, road presence, and watershed boundaries. Two other variables were used as a logical threshold to select areas, slope (> 6%) and normalized difference vegetation index (NDVI < 16%), since the authors know from experience that flat and/or heavily vegetated areas do not tend to be productive (Emerson *et al.*, 2015).

After hierarchical segmentation, the QuickBird-based model, the Landsat8-based model and an ANN model (as in Emerson & Anemone, 2012) were validated with 12 known fossil localities of the 25 km^2 training area. In this case, the first two models detected 11 out of 12 localities (within a radius of 100 m), beating the ANN approach that only detected 10. After computational validation, a map was layered with polygons of areas that met all criteria for being potentially fossiliferous, plus the road network of the basin was also added to enhance accessibility to high priority sites during the expeditions. During the 2013 field season a total of 26 sites (17 predicted to be fossiliferous, and 9 non-localities) were surveyed. As a result, 18 new fossil localities have been found (14 of these matching the predictions), while the other 8 negative sites were sandstone outcrops or mudstone areas where fossils have not been found during reconnaissance. Despite the overall accuracy (73.1%) of the best model (QuickBird), considering that 4 of the new sites were not supposed to be found (as estimated by the model

to represent non-localities), the model had a particularly low false omission rate (56%), meaning it is not effective at recognising areas unlikely to contain fossils. For the 2014 field season, southeast of Dugout Draw, 14 sites were surveyed (a balanced sample, as only 7 were predicted to be localities), a similar overall accuracy was reached (71.4%) for both the Landsat8-based model and the ANN model. However, the ANN model overestimated fossil sites, as it only detected 40% of false positives correctly (Emerson *et al.*, 2015).

Block and colleagues (2016) have implemented ensemble learning in order to find extinct fauna in Australia. While not using spectral imagery, this study stands out for two reasons: it is the first palaeontological remote survey to be carried out on a continental scale and is also the first taxa-specific approach with remote surveying. Inspired by GIS applications commonly used in ecological studies to examine species distribution (Guisan & Thuiller, 2005; Varela, Lobo & Hortal, 2011), they demonstrated how their method informed by species spatio-temporal variation could be used to find new potential fossils of five genera of Late Pleistocene megafauna in Australia: *Diprotodon*, *Genyornis*, *Protemnodon*, *Thylacoleo*, and *Zygomaturus*. For this to work, 3 different models had to be made, each able to estimate suitable: 1) climatic conditions for the taxon to inhabit over the last 120 Ka; 2) geological conditions for fossilization; and 3) present-day environmental conditions for fossil detection. Data regarding fossil occurrences were obtained from the FosSahul database and all models had 5-fold cross-validation schemes (Figure 2.4).

First, the palaeoclimate suitability models were taxa-specific and built using simulation data for absolute values of mean annual temperature and total annual precipitation from the last 120 Ka years. Second, the geological preservation model was a logistic regression with 3 input variables (suitable-rock cover, lake cover, and cave presence), in this case, all fossil records despite taxonomy and age quality were indiscriminately used, since the mere presence of a fossil demonstrates that zone can harbour fossilized remains. Third, suitability of the present-day environment for fossil discovery model used bare soil, rain intensity, and mean slope as proxy variables for understanding erosion, since erosion is the main driving force exposing

fossils and thus enhancing chances of discovering them. After internal validation, predictions were better than random (mean Kolmogorov-Smirnov statistic = 0.53; Block *et al.*, 2016, p. 8). However, no field expeditions were done to ground truth the predictive abilities of the final model, which was the 3 models combined using the mean of their respective outputs. This is due to this approach's main problem: it has incredibly low resolution—with a grid cell resolution of 1 × 1°, Australia is represented by only 849 grid cells—that is of no practical use in informing palaeontologists on how to prospect a particular area, since each cell has dozens of thousands of squared kilometres. However, the authors argue it can work as an initial exploration filter for identifying potential hot spots. Then it could be complemented with finer-resolution remote sensing approaches (e.g. Conroy *et al.*, 2012; Emerson *et al.*, 2015) or expert knowledge to obtain finer detail at more appropriate scales (Block *et al.*, 2016). A summary of this, and all other studies is available in Table 2.1.

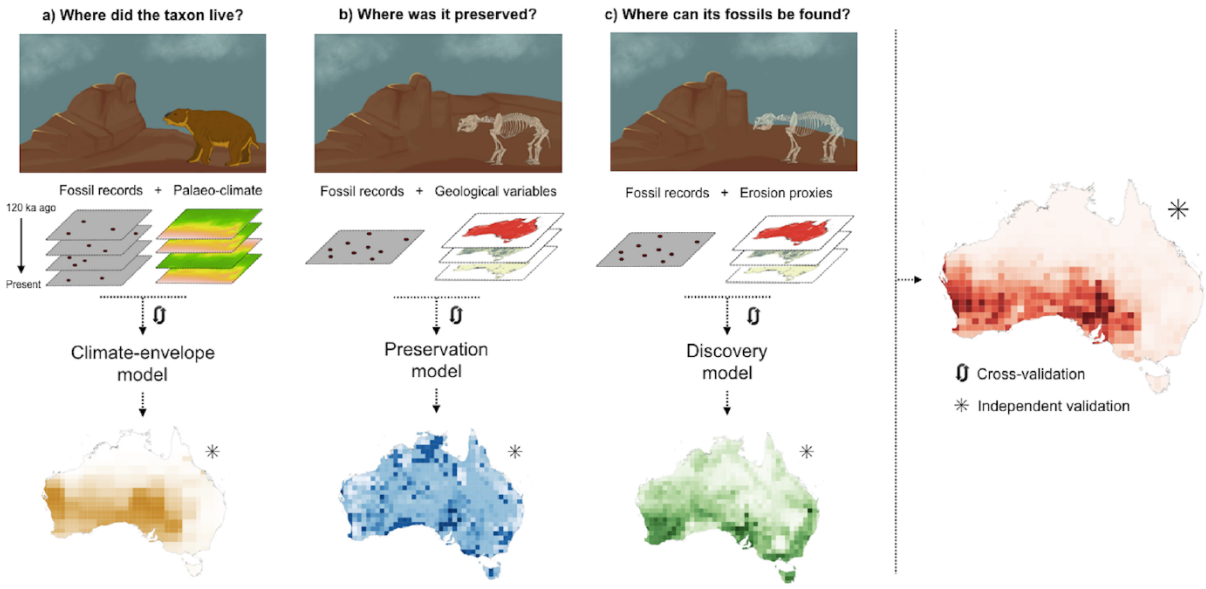


Figure 2.4 – **Ensemble Learning approach to identify potential fossil areas with combined models** (after Block *et al.*, 2016). For a given taxon, the areas yield new fossils (red map) are those where the species used to live (brown map), where its fossils could be preserved (blue map), and where it is now possible to find its fossils (green map).

In their recent study, Ghezzo, Massironi and Davis (2022) introduced a remote sensing method for detecting individual fossils, rather than just fossil sites. The dataset is a high-resolution satellite imagery (2 m pixels, adjusted to 50 cm with the panchromatic band) and the method

was tested to detect the fossilized wood logs in the upper Triassic of the Petrified Forest National Park in Arizona, USA. This article presents a classic remote sensing workflow using multispectral satellite imagery and supervised classification algorithms, but novel in the sense that it is applied for detecting individual fossils (very large fossil trees). The steps of this workflow include satellite acquisition, image pre-processing and segmentation, clustering analysis (ISODATA algorithm) for feature extraction, classification algorithms, namely Maximum Likelihood (ML) and Spectral Angle Mapper (SAM), and finally an accuracy assessment via confusion matrices. The approach demonstrated high specificity in detecting true negatives, but it was found to underfit the data and produced an excessive number of false positives, resulting in low sensitivity values ranging from 0.03 to 0.22. The fossil logs are sparsely distributed in a large area with mixed lithologies and Ghezzo et al. (2023) successfully detected individual fossils exposed on the surface using this approach with very high resolution satellite data. Future research could explore potential applications of this workflow in other fossil sites around the world known to be rich in very large fossils, such as Cenozoic sites with articulated skeletons of whales, or Mesozoic sites rich in surface finds of dinosaurs. The high resolution of the satellite imagery used in this study (50 cm) is a significant limitation for the practical applicability of the approach. Most satellite imagery freely available to researchers and practitioners has a much lower resolution (15-30 meters or more), which may not be sufficient for detecting individual fossils. Furthermore, the study focused on detecting petrified tree trunks, which are among the largest types of surface fossils, and are relatively easy to detect across the landscape without the assistance of sophisticated technology. However, most types of fossils are much smaller than petrified tree logs and will likely not be visible at standard or even very high satellite resolutions. Therefore, while the approach presented in this study is promising for detecting very large individual fossils using remote sensing, its practical applicability may be limited by the availability and cost of high-resolution satellite imagery and its effectiveness for detecting smaller or less distinct fossils.

Table 2.1 – All literature of remote fossil site discovery summarized by main features of the study, including data analysis and method of validation. In more recent studies, authors started using free and reproducible software, and implemented more wide-ranging approaches.

Study	**Premise**	**Location**	**Software**	**Input**
(Oheim, 2007)	Find new sites through suitability	TM Fm, Alberta, USA	ESRI ArcGIS 8.3 & 9.1	Ecological variables
(Malakhov et al.*, 2009)*	Remotely identify ideal outcrops	Syrdarya, southern Kazakhstan	RSI ENVI 4.2	Landsat 7 (spectral bands)
(Egeland et al.*, 2010)*	Searches new sites along least-cost path	Northern Armenia	ESRI ArcMap	Ecological variables
(Anemone et al.*, 2011b; Emerson & Anemone, 2012)*	Supervised classification for fossil localities	Great Divide Basin (GDB), Wyoming, USA	ENVI Image Analysis	Landsat 7 (spectral bands)
(Conroy et al.*, 2012)*	Supervised classification for fossil localities	Uinta Basin, Utah, USA	ESRI ArcGIS 10	Landsat 7 (spectral bands)
(Conroy, 2014)	Unsupervised clustering	Uinta Basin, Utah, USA	ESRI ArcGIS 10	Landsat 7 (spectral bands)
(Emerson et al.*, 2015)*	Supervised classification for fossil localities	GDB, Wyoming, USA	eCognition + ESRI ArcPad	QuickBird (spec. bands) + Ecological variables
(Block et al.*, 2016)*	Supervised classification for A, B and C specific problems	Australia *Note*: largest study in terms of covered space.	R statistical language. *Note*: all code is available on GitHub.	palaeoclimate (A); taphonomic (B); and erosion (C) variables
	Ensemble learning for fossil sites			A, B and C outputs
(Wills et al.*, 2018)*	Supervised classification for fossil localities	Elliot Fm, South Africa	R statistical language 3.3.2 + ESRI ArcGIS 10.3.1	Ecological variables (some mined from spectral)
(Conroy et al.*, 2018)*	Unsupervised clustering	Big Horn; and GDB, Wyoming, USA	ESRI ArcGIS 10	Landsat 8 (spectral bands)
(Ghezzo et al.*, 2023)*	Unsupervised and supervised detection of individual fossils	Petrified Forest National Park, Arizona, USA	”Remote sensing platforms”	WorldView-2 (multispectral)

(Continuation from Table 2.1, see previous page).

Pipeline	Output	Field testing	Key benefits	Criticism
Site Suitability Analysis	3 ranked classes of suitability	Yes. 90% accuracy.	Optimal for estimating fossil density.	Prospecting area remains very large.
Spectral Angle Mapper	5 geological classes of sediments	Yes. But no statistical evaluation.	No need of knowing sites beforehand.	Finds rock outcrops, not fossil sites.
Site Suitability Analysis	3 ranked classes of suitability	Yes. 25 new localities identified.	Also found 2 lithic sites.	No statistical evaluation of models.
Neural Networks >95% prob. + >5% slope filter	10 classes of landscape (including fossil sites)	Yes. Hold-out 84.21% accuracy; valid on 3 new sites.	Generalizable to other areas (e.g. Bison basin).	Seems to be overfitting for fossil site class.
Maximum likelihood classification > 98% prob.	6 classes of landscape (including fossil sites)	Yes. Validated by 17 new localities found.	Can be filtered for geological epoch of interest.	Only *post hoc* validation provided.
Iso-cluster classification (k = 10)	10 clusters. 2 matched fossil sites	No. Hold-out validation, but no metrics.	95% area reduction for prospection.	Internal validation is not explicit.
GEOBIA binary classifier + slope > 5% + NDVI < 16%	Identified object is fossil site? (yes/no)	Yes. On ground 73.1% accuracy. And 18 new sites.	Identifies user-defined objects (groups of pixels).	Training is slow and very reliant on user.
Bioclim, MaxEnt, GLM (A); Logistic regressions (B and C)	species range (A); preservation (B); and discovery (C) probabilities	No. Though, some recent literature found fossils on proposed areas (e.g. Miller *et al.*, 2016).	All R code is available. So, this approach is fully reproducible. Taxa-specific; Continental-wide.	Selected variables are hard to find for higher resolutions.
Arithmetic mean of A, B, C	Odds of fossil presence (%)			Low-res. No ground-truthing.
MDS → LDA	Fossil locality present? (yes/no)	Yes. Hold-out 95% accuracy. Also, 2 new sites found.	Generalizable to all types of variables, easy to implement.	Only uses RS for feature extraction, not for modelling.
Iso-cluster classification (k = 50; 9)	Sub-set of predictive clusters	No. Hold-out validation, but no metrics.	No need of manual labelling.	No statistical evaluation of models.
ISODATA, SAM and Maximum Likelihood (ML)	Sub-set of predictive clusters. Fossil present (yes/no)-ML	Mixed field + Google Earth. But there are no splits of test or validation sets.	Targets individual large fossils for the first time.	Paid high-res satellite data. Not applicable for detecting smaller fossils.

3

Parting ways: *Pan-Homo* Divergence Revisited

Submitted to *Biological Reviews* on September 29th 2023

Parting ways: *Pan-Homo* divergence revisited

João d'Oliveira Coelho[1,2], Robert L. Anemone[3], René Bobe[1,4,5], Susana Carvalho[1,2,4,5]

[1] Primate Models for Behavioural Evolution Lab, Institute of Human Sciences, School of Anthropology, University of Oxford, Oxford, UK
[2] Centre for Functional Ecology (CFE), Universidade de Coimbra, Coimbra, Portugal
[3] Department of Anthropology, University of North Carolina at Greensboro, Greensboro, NC, USA
[4] Interdisciplinary Centre for Archaeology and Evolution of Human Behaviour (ICArEHB), Universidade do Algarve, Faro, Portugal
[5] Gorongosa National Park, Sofala, Mozambique

Abstract

The timing of divergence between hominins and the bonobo-chimpanzee clade has been at the core of palaeoanthropological debate for over a century. The earliest molecular studies indicated divergence times ranging from 5 Ma (Sarich and Wilson, 1967) to as recently as 1.3 Ma (Goodman, 1981). Such recent divergence estimates put into question the hominin status of Australopithecus species known to be of Pliocene age. This study critically reviews the trends of time estimates published between 1967 and 2023, and analyses how these are supported or rejected by the current molecular and fossil records. We compiled 202 divergence estimates and generated three distinct thresholds based on fossil evidence at 4.4 Ma (*Au. anamensis* and *Ardipithecus ramidus*), 6.2 Ma (*Orrorin tugenensis* and *Ar. kadabba*), and 7.2 Ma (*Sahelanthropus tchadensis*). We then used these thresholds to filter out molecular estimates that are too young to fit the fossil record. This approach provides a novel way to integrate molecular and fossil data. Overall, the data suggests a divergence event within the late Miocene, with each threshold pushing it further back, 8.63–6.38, 10.33–7.81, and 10.95–8.81 Ma, respectively. We use a quadratic regression to demonstrate that estimates have been slowly shifting from ~6 Ma to ~8.5 Ma over the past 56 years. A Bayesian meta-analysis of genomic estimates filtered by our most consensual and conservative threshold (i.e., assuming *Australopithecus* belongs to Hominini) indicates that the split must have occurred early in the late Miocene, most likely before 7 Ma (~99.8% probability) with a pooled effect of 8.59–7.40 Ma. We conclude that, despite an initial bias towards younger estimates, the divergence timing for the last common ancestor (LCA) of *Pan-Homo* has been progressively approaching the intervals suggested by the current fossil record.

3.1 Introduction

Huxley (1863) and Darwin (1871) proposed that humans and African apes form a clade on the basis of morphological and biogeographic evidence. This hypothesis gained wide support after it was empirically demonstrated by the immunochemistry studies of Goodman in the 1960s (1961, 1963). In the same decade, Sarich and Wilson (1967) used immunological data to estimate that the divergence between humans and the African apes had occurred at around 5

Ma by assuming a calibration point of 30 Ma for the split between Hominoidea and Cercopithecoidea. This was based on the assumption that some genetic changes arose at nearly constant rates, and so there "may thus exist a molecular evolutionary clock" (Zuckerkandl & Pauling, 1965, p. 148). Later, by defining a split calibration of 75 Ma between Perissodactyla and Primates, the divergence of humans and other apes was readjusted by Wilson and Sarich (1969) to between 5 and 4 Ma. In the following decades, some molecular biologists have estimated even more recent times for this evolutionary event, such as 1.3 Ma (Goodman, 1981), or 2.8–0.3 Ma (Ruvolo, 1997), which would challenge the hominin status attributed not just to *Australopithecus* but also to *Paranthropus* as well as multiple species of *Homo*.

The hypothesis of a very recent divergence event between humans and African apes sharply contrasts with the much older dates proposed by palaeontologists prior to the advent of molecular techniques. For example, Keith (Keith, 1920, p. 507) argued that humans diverged from other apes before the Miocene, while Simpson (1959) proposed a divergence event at ~32 Ma. Later, and with access to more fossil evidence, Pilbeam (1967) suggested that the hominin clade could have originated at any time between 35 to 20 Ma. However, by the early 1970s, when the phylogenetic issues of the *Gorilla–Pan–Homo* trichotomy were yet to be fully resolved, Vincent Sarich asserted that the field of molecular biology had decisively won the debate: "[t]o put it as bluntly as possible, I now feel that the body of molecular evidence on the *Homo-Pan* relationship is sufficiently extensive so that one no longer has the option of considering a fossil specimen older than about eight million years a hominid no matter what it looks like" (1971, p. 76).

Indeed, it was not uncommon to cast doubt on the fossil evidence due to molecular models, e.g.: "this dating [2.68 Ma] may pose a problem for the widely believed hypothesis that the bipedal creature *Australopithecus afarensis* […] was ancestral to man and evolved after the human-ape splitting." (Hasegawa *et al.*, 1985, p. 160). Nevertheless, consilience between molecular clocks and the fossil record after decades of disagreement can happen, as demonstrated by the case of the origin of placental mammals (Goswami, 2012). With the acceptance of molecular clock techniques, the scenario of a human–ape divergence happening

near the Oligocene–Miocene transition, defended by palaeontologists up to the 1960s, rapidly lost supporters. It's worth noting however that such scenario developed when the fossil evidence available was substantially more limited than the record available today. Likewise, the earliest molecular studies were also carried with access to far less data quantity and quality than available now and with simpler techniques. Thus, many palaeontologists remained sceptical of early molecular studies suggesting the divergence must have happened during the Pliocene. As it tends to happen with conflicting views stemming from different methodological paradigms (Wilson, 1998), some expected that the evidence of both disciplines would eventually coalesce at some intermediate time, in the Miocene (Senut, 2010, 2015).

The main problem introduced by the Pliocene and the 6–4 Ma divergence narratives is that they are in direct conflict with most early hominin fossil discoveries of recent decades. There are now several likely candidates for early hominin status spanning from 5.4 Ma to possibly 7.4 Ma, such as *Ardipithecus kadabba* (Haile-Selassie, 2001), *Orrorin tugenensis* (Senut & Pickford, 2001) and *Sahelanthropus tchadensis* (Brunet *et al.*, 2002). There are also late Miocene fossils from Africa that are likely to belong to the Gorillini clade, e.g. the 8 Ma remains of *Chororapithecus abyssinicus* (Suwa *et al.*, 2007), a 6–5 Ma canine from Nkondo, Uganda (Pickford *et al.*, 1988), and the 5.9–5.8 Ma dental finds attributed to the Kapsomin large ape (Senut, 2010, 2015). *Nakalipithecus nakayamai*, dated to 9.9–9.8 Ma (Kunimatsu *et al.*, 2007), has also recently been proposed to be a member of the tribe Gorillini (Katoh *et al.*, 2016). Additional findings showing strong affinities with the Panini tribe include the 6.1 Ma "Cheboit ape" molar (Senut, 2010), and possibly the BAR 91'99 lower molar from the 12.5 Ma Ngorora Formation (Pickford & Senut, 2005). The latter would be very difficult to fit with current divergence estimates if it is indeed a member of the Panini. Other late Miocene African apes that have not been ascribed to either Hominini, Panini or Gorillini include a second hominid (indet.) from Nakali (Kunimatsu *et al.*, 2016), as well as *Samburupithecus kiptalami* from the 9.5 Ma Samburu Hills of Kenya (Ishida & Pickford, 1997). It should be noted, however, that the primate fossil record is, overall, relatively scarce, with only 7% of fossil

record preservation at the species level (Tavaré *et al.*, 2002). Furthermore, this record is particularly thin in the late Miocene of Africa (d'Oliveira Coelho *et al.*, 2021).

Molecular studies for the *Pan*/*Homo* divergence over the past 55 years have produced a disparity of results ranging from as recent as 1.3 Ma (Goodman, 1981) to as early as 14 Ma (Romero-Herrera *et al.*, 1973). Yet there is no formal meta-analysis of the trend of estimates over time and how well they are supported by the current fossil record and novel molecular techniques (Jensen-Seaman & Hooper-Boyd, 2008; but see Bradley, 2008). We address this gap by combining the current state of the art of both molecular and fossil data. In the past, molecular studies attempted to reject fossil evidence based on their models, but this proved unsuccessful. Likewise, the best approach would not be to reject molecular models using palaeontology or vice-versa. Instead, we allow for, and assess, multiple scenarios based on different subsets of the molecular data defined by palaeontological criteria (see *Fossil thresholds* section in Methods) following the rule: if a given species *X* is part of the hominin clade, any divergence time estimate that is more recent and thus excludes *X* is not compatible with *X* being a hominin. Thus, a palaeontological threshold has the function of a minimum hard bound, as supported by specific fossil evidence. Allowing for multiple scenarios is crucial given the lack of taxonomic consensus around some of the earliest proposed hominins. As an example, by using the first threshold at 4.4 Ma (supported by *Au. anamensis* + *Ar. ramidus*) we are assuming that all molecular clock models inferring that the *Pan*/*Homo* divergence happened more recently than 4.4 Ma are invalid if either *Au. anamensis* or *Ar. ramidus* are more closely related to the *Homo* than to the *Pan* lineage. The same logic applies to the second (*O. tugenensis* + *Ar. kadabba*) and third thresholds (*S. tchadensis*) but using the respective dating and taxa and associated with each specific threshold.

To account for the fossil evidence when analysing the trend of molecular divergence estimates, we propose using the palaeontological thresholds as cut-off points or minimum age bounds grounded on the fossil data. Unfortunately, the true temporal range of any fossil species is hard to assess as it is extremely unlikely to sample a first appearance datum (FAD) that matches the actual speciation event, considering that the first detectable skeletal apomorphies in any taxon

can take several million years to evolve (Marshall, 2008, 2017, 2019). This study aims to evaluate: 1) the historical trend of *Pan*/*Homo* divergence models and how they stood the test of time; 2) if the fossil discoveries of recent decades have had any impact or influence on molecular estimates of the *Pan*/*Homo* divergence; 3) which estimates may be the most parsimonious when considering both the current fossil record and the molecular evidence.

3.2 Materials and Methods

3.2.1 Pre-processing

To understand what the consensus in molecular biology is regarding the time of divergence for the *Pan–Homo* pair, we created a new database documenting the published estimates of this splitting event. As a starting point, we downloaded a dataset containing molecular time estimates available at http://timetree.org (TimeTree 5) (Kumar *et al.*, 2017, 2022). This dataset contains five variables (Time, Title, Reference, Year, Data) and 81 entries published between 1985 and 2020. We reorganized and increased the number of variables, ending up with the following features for data analysis: Reference, Title, Year, Month, Max, Estimate, Min, Material, ErrorMetric, and Notes. The first four variables are identifiers, and the Max-Estimate-Min triplet represents the corresponding range of values estimating the *Pan*/*Homo* split. Material is a variable that identifies what was analysed (e.g., mtDNA, genome, etc). ErrorMetric is a binary Bayes/SE variable to record if the interval of estimates was calculated with a 95% Credible Interval (Bayesian), or a Standard Error (frequentist). SE also includes studies that only presented a 95% Confidence Interval (CI). During database imputation, frequentist CI was transformed into SE by the following operation: $SE = (upperCI - lowerCI)/3.92$, in order to achieve standardization of frequentist errors. While Bayesian 95% Credible Intervals (BCI) were kept in the database without transformations. Finally, the Notes column contains general observations and remarks about the articles.

After scanning the studies collected at timetree.org to confirm the data and extract new variables, we also corrected several entries containing mistakes (e.g. mismatches in estimate

values) in the original dataset (documented in Notes), and removed one entry from the timetree.org set that was considered an outlier—a paper focused on Archaean lifeforms (David & Alm, 2011) that contains an estimate of the *Pan*/*Homo* divergence at 139.7 Ma. To expand our dataset, we added new entries cited in these same papers and acquired further novel entries by searching Google Scholar using combinations of "divergence", "homo", "pan", "hominin", "molecular", and "split". When papers had multiple models, we recorded them as multiple entries (1 per model/output), unless models had extremely similar outputs and could straightforwardly be grouped and averaged by similar sets of techniques. To enhance reproducibility, our final database is publicly available at GitHub and can be used and updated by others interested in maintaining the project or working on future iterations of it (https://github.com/Delvis/Pan-Homo). Currently, it has a total of 12 variables and 202 entries, each corresponding to an individual molecular time estimate for the *Pan*/*Homo* divergence published between 1967 and 2023.

3.2.2 Fossil thresholds

For the data analysis, we defined three different palaeontological thresholds based on the fossil and stratigraphic evidence. The first is a 4.4 Ma threshold supported primarily by *Australopithecus anamensis* (estimated origination = 4.37 Ma) (Du *et al.*, 2020), a widely accepted hominin. But notice that *Ardipithecus ramidus* was also found at 4.493–4.3 Ma deposits (Simpson *et al.*, 2019) giving further support to a 4.4 Ma minimum bound. The second is a 6.2 Ma threshold based on *Orrorin tugenensis* first appearance datum (FAD = 6.1 Ma) (Roche *et al.*, 2013) and *Ardipithecus kadabba* (FAD = 6.3 Ma) (Simpson *et al.*, 2015). The third is a 7.2 Ma threshold for *Sahelanthropus tchadensis,* known from 7.34–7.10 Ma deposits (Lebatard *et al.*, 2010) that have been suggested to possibly reach 7.4 Ma (McDougall & Feibel, 2003). We rely on each species FAD, since they can be used as an absolute minimum estimate for the divergence of two distinct taxa (Marshall, 2008). Yet, given that all FADs underestimate the divergence times they are estimating (Marshall, 1990), all the palaeontological thresholds we provide might be too conservative.

The 4.4 Ma threshold: By the mid-1990s *Australopithecus anamensis* (Leakey *et al.*, 1995) and *Ardipithecus ramidus* (White, Suwa & Asfaw, 1994) had been described as new species of hominins older than 4 Ma. More precisely, the FAD of *Au. anamensis* is ~ 4.2 Ma (Ward, Plavcan & Manthi, 2020) while *Ar. ramidus* is known from 4.51–4.32 Ma (White *et al.*, 2009). However, recent work has suggested that the origination date of *Au. anamensis* may be 4.37 Ma (Du *et al.*, 2020), or even reach 4.6 Ma (Bobe *et al.*, 2020a), and new fossil discoveries push the FAD of *Ar. ramidus* to 4.8 Ma (Simpson *et al.*, 2019). Recent phylogenetic studies further confirm the consensus regarding the classification of both species as hominins (Mongle, Strait & Grine, 2019). Moreover, KNM-LT 329 (Lothagam mandible) and KNM-TH 13150 (Tabarin mandible) are specimens expected to be in the ranges of 4.9–4.4 Ma and are likely to belong to either taxon (Kissel & Hawks, 2015).

The 6.2 Ma threshold: In 2001, discoveries in Kenya and Ethiopia of late Miocene hominins described as *Ardipithecus kadabba* (Haile-Selassie, 2001) and *Orrorin tugenensis* (Senut & Pickford, 2001) challenged many traditionally held views about human evolution, such as the savanna-based models of hominin origins (Crompton *et al.*, 2010). If we accept either of these species as hominin, with FADs around 5.8 and 6.1 Ma, respectively, we must accept that the *Pan/Homo* divergence happened some time before 6 Ma. Furthermore, it should be noted that now there is also 6.3 Ma material from Gona, Ethiopia, attributed to cf. *Ar. kadabba* (Simpson *et al.*, 2015). Consequently, this threshold was defined at 6.2 Ma.

The 7.2 Ma threshold: The discovery of *Sahelanthropus tchadensis* (Brunet *et al.*, 2002), found between two strata dated to 7.34±0.12 and 7.10±0.14 Ma (Lebatard *et al.*, 2010), challenged recent split estimates. Despite its controversial status as a hominin (Wolpoff *et al.*, 2002, 2006; Pickford, 2005; Macchiarelli *et al.*, 2020; Meyer *et al.*, 2023), *Sahelanthropus*' known morphology seems to share some derived features with hominins such as the reduction of the canine that may be correlated with a non-honing C-P3 complex, and a more anteriorly positioned *foramen magnum,* likely related to an incipient form of bipedal locomotion (Zollikofer *et al.*, 2005). Moreover, two recently described antimeric ulnae and one left femur share more morphological traits with *Ardipithecus*, *Orrorin*, *Australopithecus*, *Paranthropus*

and *Homo* than with extant and Miocene apes (Daver *et al.*, 2022). Therefore, we regard *S. tchadensis* as the oldest record of a plausible hominin. Notice that even if *S. tchadensis* belonged to the Panini tribe rather than Hominini (Meyer *et al.*, 2023), the logic to support this fossil threshold would still apply. This is because any fossil from both lineages would contribute to establishing the minimum age boundary of their split.

If we consider that Cenozoic mammal species have an average duration of 2.3–1.6 Ma (Marshall, 2017), together with the patchiness of the early Pliocene and late Miocene of Africa (virtually no hominin evidence older than 7.2, or at 7.1–6.3 and 5.2–4.8 Ma), we can further argue that the values chosen for thresholds are conservative. This is mostly due to the unlikelihood of the sampled FAD matching the true origination date in species known from few localities and individuals (Marshall, 2019; Du *et al.*, 2020; Bobe *et al.*, 2020a). This is further complicated by the fact that the period ranging from 9 to 7.2 Ma in Africa is represented by a single geological formation (Chorora Fm, Ethiopia) and locality with only ca. 200 vertebrate fossils (Katoh *et al.*, 2016). In a recent study, Bobe and Wood (2022) used confidence intervals to calculate the origin of taxa, and estimated *Sahelanthropus* speciation at 9 Ma while *Orrorin* and *Ardipithecus* origins were placed at 8 Ma. Under that scenario the fossil thresholds defined above can be seen as practical but conservative minimum age bounds. Since, ultimately, we use the palaeontological thresholds to filter out estimates that do not match the hypotheses of specific extinct taxa being hominins.

3.2.3 Regression analyses

After curating the new database of split dates, we performed several regression analyses using the divergence estimates as the outcome variable, with year-and-month of publication as its covariate. In this study, publication date can be seen as a general proxy variable for technological, statistical, and theoretical advancements on phylogenetical inference and divergence estimation models. This allows us to understand if any specific trends exist that support the common intervals cited in human evolution textbooks that usually consider the *Pan*/*Homo* split to have occurred at 6–4 or at 7–5 Ma (e.g. Boyd & Silk, 2009; Larsen, 2009;

Foley & Lewin, 2013). To better grasp the nuances of the dataset, five different regression models were built: Ω) full-dataset model; A) miscellaneous; B) mitochondrial; C) nuclear DNA; D) genome. The first regression analysis includes all data points available. Reg-A combines the phenetic estimates (immunological and DNA-DNA hybridization) with RNA estimates. Reg-B is focused on mitochondrial derived studies, while Reg-C is based on sequences of nuclear DNA. The last regression model only includes studies of divergence using genomic data—these were only possible after the genome of *Pan troglodytes* had become publicly available in 2005 (Gunter & Dhand, 2005). Approaching the dataset from different perspectives is crucial in order to have an unbiased estimate of the divergence event between the Hominini and Panini tribes.

3.2.4 Meta-analyses

Additionally, we interpreted the dataset and the subsets filtered by the different thresholds using a Bayesian multilevel regression for meta-analysis as implemented in the brms package (version 2.16.3) for R (Bürkner, 2017, 2018). We are not aware of other meta-analyses of molecular divergence studies in the literature (Supplementary Methods, S2. Bayesian meta-analysis: further details). The different divergence time estimates in the literature, have been built using different assumptions. Consequently, they have different types of clock models, material sampled (DNA, mtDNA, etc.), datasets used and partitioning schemes, generation times, mutation rates, min-max bounds, priors used, among other variables. The point could be made that they cannot be directly comparable. However, following Cumming's definition of an effect size as anything we might be interested in measuring across studies, including "a mean, a difference between means, a percentage, a median, or a correlation […] standardized value, such as Cohen's d [...] or a regression coefficient, path coefficient, odds ratio, or percentage of variance explained" (Cumming, 2013, p. 38) we *assume* that any molecular divergence estimate obtained from the literature can be used as a proxy to calculate effect size, since despite being obtained through different methods they are all estimating the same phenomenon (in this case, divergence between *Pan* and *Homo*) in the same units of

measurement (Ma). Furthermore, our primary meta-analysis exclusively incorporates genome-derived divergence estimates from 2005 onwards (i.e., same as Reg-D). Contrary to previous studies, these estimates share several methodological similarities and exhibit a more cohesive and comparable initial set of assumptions. In our meta-analysis both studies with frequentist standard errors (SE) or Bayesian Credible Intervals (BCI) were included. Assuming a Gaussian shape of the posterior distribution, the formula $SE = (upperBCI - lowerBCI)/3.92$ can be applied to convert Bayesian 95% Credible Intervals into SE, similarly to what is usually done to transform frequentist confidence intervals into standard errors (but in the frequentist scenario, the assumption here enounced is not required).

3.2.5 Data and materials availability

The raw data HomoPanDivergences.csv contains published divergence estimates of *Pan*/*Homo* for replicating the data analyses presented in this manuscript in a fully reproducible manner. It is available for download at https://github.com/Delvis/Pan-Homo as a legacy version. The code used for generating all analyses, figures, and tables is also publicly available at the same GitHub repository.

3.3. Results

3.3.1 Dataset structure

The dataset contains 203 molecular divergence estimates for the *Pan*/*Homo* pair, ranging from 1.3 to 14 Ma, with a mean estimate of 6.79±0.16 Ma and a standard deviation of 2.2 Ma (Table 3.1). With standard deviation allowing for a divergence as recent as 4.59 Ma, all the early putative hominins (*Ardipithecus*, *Orrorin*, *Sahelanthropus*) appear to be incompatible with the central tendencies observed in the dataset. Moreover, the data is positively skewed (skewness = 0.66) which indicates that most values are concentrated on the left side of the distribution (i.e., skew towards younger dates), as well as slightly leptokurtic, entailing that there are more estimates than expected around the mean, a possible indicator of systematic reporting bias.

Overall, the molecular estimates tend to cluster at points in time coinciding with the palaeontological thresholds we defined. These thresholds match FAD dates established for the major early hominin fossil discoveries, and form statistically anomalous peaks in the histogram likely due to underestimation combined with calibration issues shifting the estimates to the fossil-informed minimum (Figure 3.1).

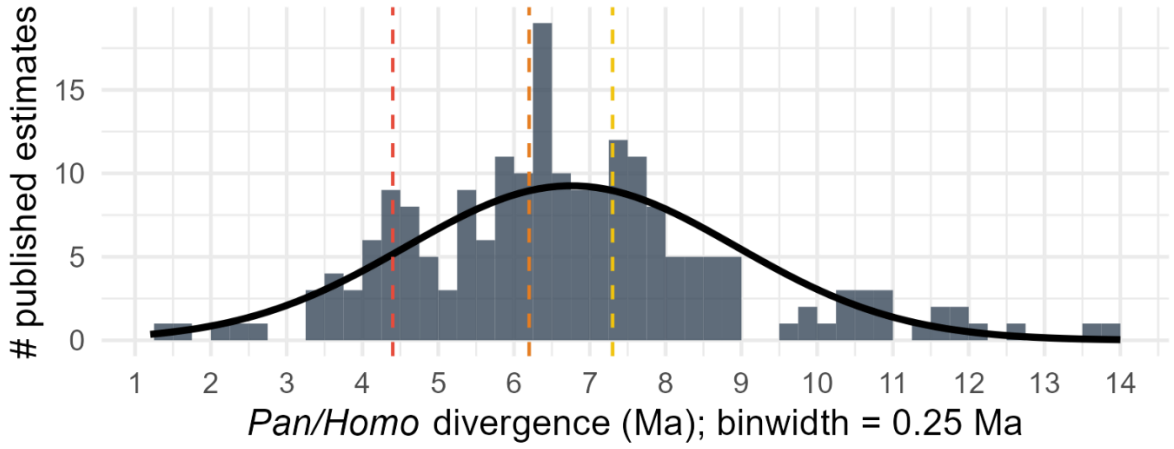


Figure 3.1 – **Molecular estimates histogram.** Dashed vertical lines represent fossil thresholds. Note that instead of following a normal distribution, studies seem to cluster in excess around important fossil discoveries, and there is an unexpected gap of mean-estimates at 9–9.5 Ma.

3.3.2 The 4.4 Ma threshold: The last Ardipithecus *and the first* Australopithecus

Using the most consensual of the palaeontological thresholds at 4.4 Ma, we discovered that a total of 25 divergence estimates in the dataset of *Pan*/*Homo* split dates fall outside of this bound (Table 3.1). Surprisingly, 14 of these were published after the fossil material of *Ardipithecus ramidus* and *Australopithecus anamensis* was described in 1994–95 (White *et al.*, 1994; Leakey *et al.*, 1995). This suggests that there is sometimes a noticeable lag between genetic divergence studies and the incorporation of new palaeontological findings into their model assumptions. Some of these divergence estimates are younger than 2.8 Ma and could even be rejected based solely on the fossil record of *Paranthropus* or early *Homo*, long recognized as hominins. Excluding molecular models that do not meet the 4.4 Ma threshold would result in an interval of 8.63–6.37 Ma for the *Pan*/*Homo* divergence. Note how strikingly this deviates

from the more commonly cited interval of 6–4 Ma popularized in introductory text books of human evolution and biological anthropology (e.g., Hoffecker, 2017, p. 126), and in the first molecular studies (e.g., Wilson & Sarich, 1969).

Table 3.1 – Descriptive statistics of the *Pan*/*Homo* divergence estimates. Includes the distributions for the full dataset, and for the three subsets using hominin fossil thresholds used in meta-analyses, as well as the distributions of the subsets used in regression.

Filtered by threshold											
Subset	*n*	*mean*	*sd*	*median*	*mad*	*min*	*max*	*range*	*skew*	*kurtosis*	*se*
Full	202	6.76	2.18	6.52	1.77	1.3	14	12.7	0.61	0.84	0.15
4.4 Ma	177	7.21	1.91	6.9	1.48	4.5	14	9.5	1.12	1.26	0.14
6.2 Ma	120	8.06	1.72	7.56	1.28	6.29	14	7.71	1.38	1.34	0.16
7.3 Ma	73	8.95	1.68	8.3	1.05	7.3	14	6.7	1.16	0.4	0.2
Subsets for regression analyses											
Reg-A	24	6.41	2.92	5.88	2.38	1.3	14	12.7	0.75	0.3	0.6
Reg-B	62	6.62	2.26	6.46	1.3	2.5	13.7	11.2	0.88	0.9	0.29
Reg-C	65	6.22	1.65	6.29	1.47	1.55	11.75	10.2	0.3	1.25	0.21
Reg-D	51	7.76	1.98	7.74	1.28	3.69	12.71	9.02	0.21	-0.01	0.28

3.3.3 The 6.2 Ma threshold: Orrorin tugenensis *and* Ardipithecus kadabba

The average minimum age for the *Pan*/*Homo* split is at 5.62 Ma for our full dataset of molecular divergences (Table 3.1; Fig. 3.S1), a date too recent to be supported by the fossil evidence assuming that either the *Orrorin* or the *Ardipithecus* lineages represent early hominins. After applying a 6.2 Ma threshold to the estimates in order to reduce potential bias towards young values, we obtain instead an interval of 10.30–7.77 Ma for the hominin split. This result is very close to the interval of 10–7 Ma that White and colleagues (2009) proposed based solely on palaeontological and stratigraphic evidence from the African late Miocene. Nevertheless, this threshold is likely not strict enough as the majority of published estimates cluster just after it (Figure 3.1). In fact, there are over twice as many estimates at 6.25–6.5 Ma as would be expected by a normal distribution curve. This suggests that some molecular studies may be inclined towards reporting estimates at the particular intervals occurring just before the occurrence of landmark extinct species rather than at any other random interval.

3.3.4 The 7.2 Ma threshold: Sahelanthropus tchadensis

When we set 7.2 Ma as an absolute minimum for the divergence of hominins, we find that 130 out of the 202 molecular clock estimations pose challenges. If we filter by the available minimum estimates instead (i.e., lower estimate of the confidence interval), 86.11% of the observed divergence estimates for *Pan*/*Homo* are incompatible with this threshold. The exclusion of these estimates would increase the arithmetic mean estimate of all *Pan*/*Homo* divergence models from 6.79 (7.91–5.62) Ma to 9.88 (10.95–8.81) Ma, aligning more closely with the current palaeontological data (Marshall, 2019). Figure 3.2 provides boxplots summarizing the results of all threshold analyses. The arithmetic means consistently indicating older temporal ranges than the respective medians is a behaviour typical of log-normal distributions (Supplementary Text, 3.5.1 S1: Dataset distribution) and can thus be interpreted as evidence of a skew towards recent divergences (Figure 3.2).

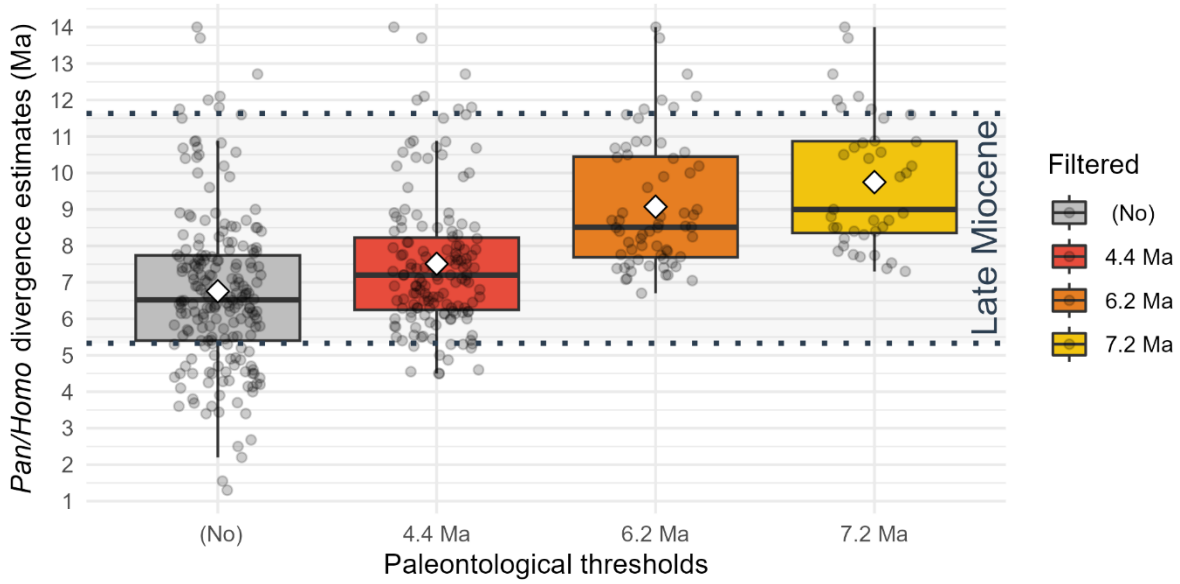


Figure 3.2 – **Interquartile range boxplots for divergence estimates filtered by different fossil thresholds.** The arithmetic means and the medians are represented by white diamonds and black bars, respectively. All boxplots fit within the late Miocene (11.6–5.3 Ma).

3.3.5 Regression analyses of molecular estimates from 1967–2023

Regression models with 95% confidence intervals show patterns within the divergence estimates over a 56-year period (Figure 3.3; Table 3.2 Ω). In the "full-dataset model" polynomial regression we have an early stage with much uncertainty associated (1960-1980s) due to the large disparity of values and scarcity of studies. For this period, the regression curve suggests a divergence date around 6 Ma. After 1990, the lower limit of the confidence interval reaches and remains within the boundaries of the late Miocene. Following the discovery of the earliest hominins at the turn of the century (Senut & Pickford, 2001; Haile-Selassie, 2001; Brunet *et al.*, 2002), plus the first phylogenomic studies after the chimpanzee genome was published (Gunter & Dhand, 2005), and the renewed interest in the hominoid slowdown hypothesis (Steiper, Young & Sukarna, 2004; Elango *et al.*, 2006), the trend towards older divergence estimates accelerated significantly, and as of 2023 it suggests 8.4 (9.4–7.4) Ma.

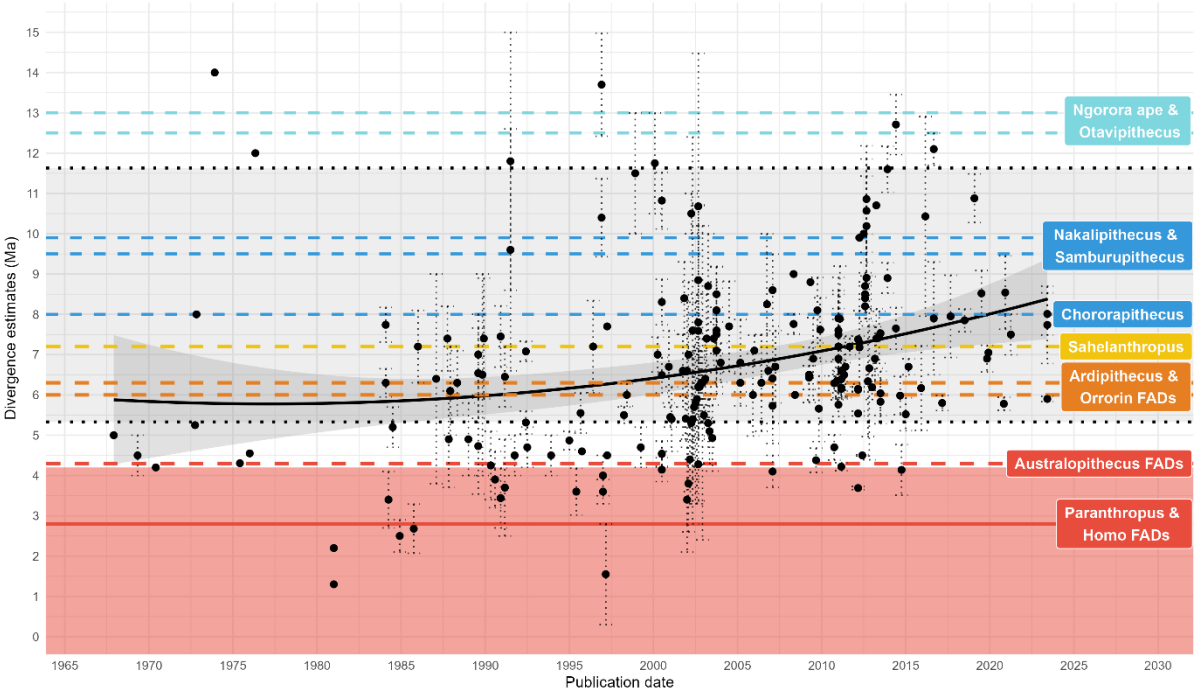


Figure 3.3 – **Trend of the "full-dataset model" fitting the sample of Panini/Hominini split estimates by date of publication.** The late Miocene period is shadowed and within the horizontal dotted black bars. Dotted error-bars are standard errors, presented when available (studies with confidence or credible intervals were transformed to SE).

Table 3.2 – **Summary statistics for the regression analyses.** (Ω) full-dataset model; (A) miscellaneous model; (B) mitochondrial model; (C) nuclear DNA model; and (D) phylogenomic model.

(Ω) DIVERGENCE ESTIMATES of the full dataset

Predictors	β	CI	p
(Intercept)	6.76	6.47–7.05	**<0.001**
date [1st degree]	8.36	4.23–12.49	**<0.001**
date [2nd degree]	2.98	-1.15–7.11	0.157
Observations			202
R^2 / R^2 adjusted			0.083 / 0.073

(A) DIVERGENCE ESTIMATES

Predictors	β	CI	p
(Intercept)	-82.1	-283.29–119.02	0.406
date	0.04	-0.06–0.15	0.371
Observations			24
R^2 / R^2 adjusted			0.037 / -0.007

(B) DIVERGENCE ESTIMATES

Predictors	β	CI	p
(Intercept)	-70.89	-202.1–60.3	0.284
date	0.04	-0.03–0.10	0.242
Observations			62
R^2 / R^2 adjusted			0.023 / 0.006

(C) DIVERGENCE ESTIMATES

Predictors	β	CI	p
(Intercept)	-94.48	-217.8–28.8	0.131
date	0.05	-0.01–0.11	0.108
Observations			65
R^2 / R^2 adjusted			0.041 / 0.025

(D) DIVERGENCE ESTIMATES

Predictors	β	CI	p
(Intercept)	-173.00	-427.81–81.8	0.179
date	0.09	-0.04–0.222	0.160
Observations			51
R^2 / R^2 adjusted			0.040 / 0.020

Considering the different type of genetic material used across studies (nuclear vs mitochondrial), or the resolution of the datasets (selected sequences vs genome-wide analysis), and the fact that the early immunological studies are phenetic instead of phylogenetic (i.e., they cannot distinguish between derived and plesiomorphic similarity), we provide results to different sets of regressions focusing on different source material (Figure 3.4). While all sub-regressions Reg-A, Reg-B, Reg-C and Reg-D showed positive slopes, with divergence estimates suggesting older intervals of the late Miocene as date of publication progresses, none seems to exhibit a significant relation between date of publication and estimate. Summary statistics for each model are available on Table 3.2 A-D.



Figure 3.4 – **Linear regressions for different types of source datasets.** A) Includes early phenetic studies (immunological, DNA-DNA hybridization, etc.), but also later studies with virogenes and RNA; B) Mitochondrial datasets from early studies with selected sequences to later complete mitochondrial genome studies; C) Split estimates based on nuclear DNA sequences; and D) Large phylogenomic studies (also includes 'total evidence dating', i.e., integrative models).

The first sub-model is based on the early immunological and DNA-DNA hybridization techniques of the 1960-1980s, as well as some later RNA-based studies. It has the smallest signal-to-noise ratio of the four sub-models, including a negative adjusted R^2, smallest n = 24. The second model and third models based on mitochondrial and nuclear DNA divergence studies have similar outputs, showing gentle positive slopes that are not significant.

Finally, the "genomics-specific model" uses a linear regression to analyse the estimation trend of every genomic data point in the database. It has the highest positive slope of all regression analyses, increasing quickly from 7.1 (8.2–5.9) Ma since the publication of the chimpanzee genome (Gunter & Dhand, 2005) towards 8.6 (9.9–7.3) Ma as of 2023. The regression formula obtained for genomic-only datasets indicates divergence estimates published between 2005 to 2023 have been getting older on average by 90 Ka per year (Table 3.2 D).

3.3.6 Bayesian meta-analyses

To combine evidence from multiple studies, we performed a meta-analysis of the literature under the framework that a meta-analysis is a special case of Bayesian multilevel regression modeling (Supplementary Text, 3.5.2S2: Bayesian meta-analysis: further details). Using the 4.4 Ma, the 6.2 Ma, and the 7.2 Ma thresholds we obtained meta-estimates ranging from 7.22–6.61 Ma (Fig. 3.S2, Table 3.S1), 8.03–7.40 Ma (Fig. 3.S3, Table 3.S2), and 9.11–8.22 Ma (Fig. 3.S4, Table 3.S3), respectively. Notice that even the last would be supported by some of the most recently published divergence studies e.g., 8.52 (9.81–7.58) Ma (dos Reis & Yang, 2019). After sub-setting the dataset to only include phylogenomic studies (i.e., same as Reg-D) and also older than 4.4 Ma (the most conservative threshold) in order to exclude studies that reject both *Australopithecus anamensis* and *Ardipithecus ramidus* status as hominins, we obtained a meta-estimate of 8.0 Ma with a distribution of the pooled effect ranging from 8.59 to 7.40 Ma (Figure 3.5; Table 3.3).

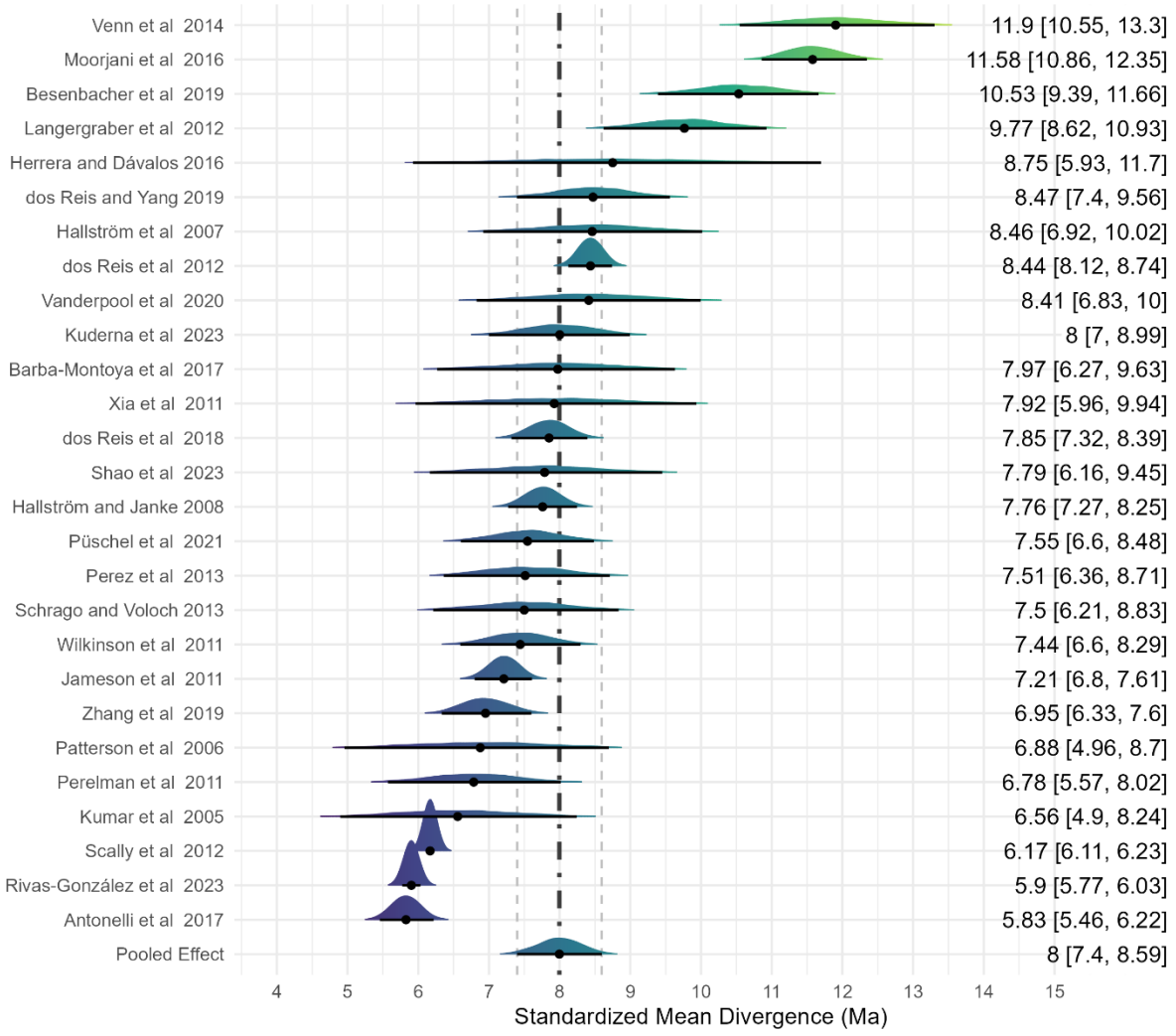


Figure 3.5 – **Meta-analysis of the Pan/Homo phylogenomic divergence estimates.** Forest plot depicting the specific effect size and sampled posterior distribution of genome-based studies.

According to the phylogenomic meta-model there is only a 0.125% chance that hominins originated later than 7.0 Ma, and a 6.9% chance at 7.5 Ma or later. In this type of approach, the effect sizes and credible intervals displayed in the forest plot (Figure 3.5) do not represent the observed effect sizes (i.e., reported in the original studies), but the posterior effect size of each study estimated by the Bayesian model. For example, Venn et al. (2014), estimated the *Pan*/*Homo* divergence at 12.71 (14.18–11.25) Ma, but this was readjusted to 11.9 (13.3–10.5) Ma through the Bayesian method.

Table 3.3 – Summary statistics for the Bayesian meta-analysis for the phylogenomic studies.

7.3 Ma threshold	*Divergence | SE ~ 1 + (1 | Study)*	
Predictors	Estimates	CI (95%)
Intercept	8.0	7.40 – 8-59
Std. Dev.	1.33	0.97 – 1.79
Random Effects		
$\tau_{00\ Study}$	2.83	
ICC	0.75	
$N_{\ Study}$	27	
Observations	41	
Conditional R^2	0.748	

3.4 Discussion

In 1982 there was a meeting organized at the Vatican that "led to a consensus between palaeontologists and molecularists: the divergence occurred at around 7 Ma" (Senut, 2015, p. 2050) for the *Pan/Homo* pair. However, the majority of molecular studies still indicate divergence dates more recent than 7 Ma (median = 6.52 Ma; Table 3.1). Conversely, in light of the new fossil and molecular evidence, palaeoanthropologists have significantly updated their views. Split estimates based on the improved stratigraphic and fossil record of the late Miocene of Africa include intervals of 12.8–10.1 Ma (Marshall, 2019); ca. 12 Ma (Senut & Pickford, 2004); 10–7 Ma (White *et al.*, 2009); 9.5–7.5 Ma (Haile-Selassie, Suwa & White, 2009); and 10–6.5 Ma (Benton & Donoghue, 2007). Taken together these palaeontological estimates average 9.48 Ma. Considering this difference of roughly 2.96 million years between the average estimates of molecular biologists and palaeoanthropologists, it is evident that although a complete consensus remains elusive, there is a noticeable trend toward greater convergence between the two fields.

The idea that hominins must have diverged at around 6–4 Ma has prevailed for many decades, even though hundreds of molecular clock estimates have been published after Sarich and Wilson (1967) with increasingly sophisticated methods and higher resolution datasets. Despite

computational and data improvements, there are still many methodological issues in divergence estimations that can greatly impact the models. Bromham (2019) discusses six problematic assumptions of molecular dating approaches that are often violated in studies: 1) alignments always represent homology; 2) molecular change is straightforwardly measurable; 3) rate variation of molecular evolution can be captured; 4) sequences have been sampled randomly; 5) rates of speciation and extinction are constant; 6) data is more important for the model than the priors, or calibration points, or min-max bounds. The use of constants in molecular clock models, that was the dominant paradigm for over four decades, was equally problematic, i.e., estimates of substitution rates have been shown to not be constant, but instead to be affected by body size, population fluctuations, generation times, overlapping generations, and other ecological and life history factors that can have very different properties and dynamics over the course of millions of years (Steiper *et al.*, 2004; Elango *et al.*, 2006; Bromham, 2011). Some of these problems have become exacerbated with the advent of genomics and the increase in data quantity that can directly translate into a larger noise-to-signal ratio in models. The great improvement of sequence data availability brought by genomics must be accompanied by a similar increase of quality in modelling assumptions and techniques (Kuderna *et al.*, 2023; Rivas-González *et al.*, 2023; Shao *et al.*, 2023).

The primary determinant affecting substitution rates is most likely the generation time (Steiper & Seiffert, 2012). Specifically, due to the longer generation times observed in hominoids compared to other primates (Steiper *et al.*, 2004), this effect is exacerbated in human generation times which are even longer when contrasted with other apes, and this reflects on substitution rates (Steiper & Young, 2006). Consequently, molecular divergence dates in hominoids are easily prone to underestimation, especially if not adjusted through calibration of the *Pan*/*Homo* split and through the utilization of a relaxed molecular clock model capable of accommodating variations in substitution rates across the evolutionary tree (Schrago & Voloch, 2013; dos Reis *et al.*, 2018). This variability in substitution rates was largely overlooked until the early 2000s, coinciding with the advent of genomics, which furnished compelling evidence supporting the 'hominoid slowdown hypothesis' (Goodman, 1961). This paradigm shift suggests that

conventional methodologies, assuming a uniform rate of evolution across species, most certainly inadequately grasped the intricacies of hominin evolutionary dynamics (Yi, 2013).

Minimum age constraints should be established using the oldest fossil evidence of the extant clades. As for the clade's maximum age, it can be estimated by probabilistic methods using a suite of fossil occurrences, together with palaeobiogeographic and taphonomic data (Tavaré *et al.*, 2002; Marshall, 2019; Du *et al.*, 2020). However, it is far more difficult to determine a maximum bound, because the dependency on fossil-based phylogenies (in contrast to genetic-based), as well as the uncertainty associated to taxonomic assignments tend to increase, the further back we go into deep time (Marshall, 1990). The value defined for minimum calibration should always consider improved geological dating of the material. For example, most divergence studies that took *S. tchadensis* into consideration selected 6 or 6.5 Ma as the respective min-calibration value, even though the dating of the fossil material attributed to this species has been pushed to 7.2–6.8 Ma (Lebatard *et al.*, 2008) and then again with substantial methodological improvements to 7.34–7.1 Ma (Lebatard *et al.*, 2010). Accordingly, *Sahelanthropus'* associated fauna (Anthracotheriid Unit, Chad) shows similarities with the faunal record from the lower Nawata Formation from Kenya which may be as old as 7.4 Ma (McDougall & Feibel, 2003; dos Reis & Yang, 2019). Since calibration points can establish a hard-coded minimum, selecting underfitting values will impact the distribution of results and bias the overall trend towards younger estimates (Steiper *et al.*, 2004; Marshall, 2008). It should be noted, however, since not all specimens have fossilized or been discovered, that there also exists always uncertainty associated with minimum bonds, and that this uncertainty should be accounted for in the models used for time estimations of species divergence (Yang & Rannala, 2006).

All the results suggest that there is indeed a bias towards younger estimates that sometimes directly contradicts the palaeontological evidence. In our database there is a complete gap of mean divergence estimates for *Pan*/*Homo* between 9 and 9.5 Ma, even though under a normal distribution we would expect to find around ten reported studies within that interval. Interestingly the Bayesian meta-analysis using the most restrict threshold (7.2 Ma), resulted in

8.66 Ma which is in better agreement with the regression of the full-dataset model (8.4 Ma, when x= 2023) than with any of the other regressions. Yet, we recommend the meta-phylogenomic analysis as a less controversial approach, and this resulted in 8.0 Ma instead. However, due to studies with lower numerical estimates being more likely to have smaller SE than studies with higher estimates, there is a high likelihood that any meta-analysis of divergence estimates will always be biased towards more recent values, since the weight given to each study is inversely proportional to the size of its SE. Therefore, by design, the standard algorithms of meta-analytical models might not be ideal to tackle the molecular clock divergence literature, as they will have a tendency to take into more consideration the younger estimates than the older ones by virtue of how the weights are calculated. This will influence not just the final pooled estimate of the model but also the posterior distribution and effect size of each study. In this study, the dataset was analysed using multiple statistical approaches to make up for the current shortcomings of meta-regressions with this type of data.

As for the validity of the fossil thresholds selected to work as minimum bounds, they depend on the taxonomic and geological dating rigour associated with each taxon (Püschel *et al.*, 2021). Apomorphies that would fossilize and be detectable require some time to evolve after the divergence happened (Marshall, 2008, 2017), and these may not be readily sampled given the fragmentary nature of the fossil record (Tavaré *et al.*, 2002; Wilkinson *et al.*, 2011). Therefore, some authors argue that estimates between 8–7 Ma are too recent and unlikely to be compatible with *Sahelanthropus*, *Orrorin* or *Ardipithecus* being hominins (Marshall, 2019; Bobe & Wood, 2022). Yet these multiple lines of fossil evidence, which some researchers suggest might represent a single genus (White *et al.*, 2009), did not have much effect on reconsidering the assumptions and establishment of min-max bounds, despite their profound implications for the outcomes of molecular models. This is clearly evidenced by the majority of estimations published after 2002 (58.78%) still indicating divergence estimates more recent than the dates associated to the fossil material that might represent the earliest Hominini or Panini (Macchiarelli *et al.*, 2020; Daver *et al.*, 2022; Meyer *et al.*, 2023).

Historically some studies have attempted to reject the hominin status of some fossil taxa based on molecular models. Instead, we need to consider the high variance associated with reported molecular estimates, and use the palaeontological record and geological work done in the late Miocene of Africa as tools to understand which of these models are compatible with the fossil evidence (Moorjani *et al.*, 2016; Barba-Montoya, dos Reis & Yang, 2017). All regression models suggest that molecular divergence estimates have been slowly, but progressively, trending toward values that are in better agreement with the palaeontological data.

Overall, all analyses indicated that the late Miocene is the most likely geological period for the hominin divergence from the other African apes. However, this represents a large period spanning 6.3 million years, which is in fact more time than has passed since the end of the Miocene up to the present. Our study indicates that there is a structure to the published molecular data that can be used to increase the accuracy and precision of our estimates of when the hominin lineage first emerged. The Bayesian meta-model employing only genomic data suggested that the split must have happened quite early in the late Miocene, most likely before 7 Ma (99.875% credible interval). These findings have significant implications for our understanding of hominin divergence and call for the need to target more fossil deposits covering the reported intervals to test and validate these estimations. Notably, the current absence of fossil sites with 9 to 8 Ma and 8 to 7.4 Ma deposits in the late Miocene of Africa represents a critical research gap that warrants thorough investigation and attention.

3.4.1 Conclusions

(1) Despite historical discrepancies, there is a trend toward greater convergence between molecular biology and palaeoanthropology in estimating *Pan-Homo* divergence.

(2) Considering the patchiness of the fossil record, establishing accurate minimum age constraints for calibration points is crucial for improving divergence estimates.

(3) Molecular models should incorporate up-to-date palaeontological record and geological data to align with the full spectra of scientific evidence.

(4) All analyses suggest a late Miocene divergence, most likely before 7.5 Ma, but we are yet to find sites with 9 to 8 Ma fossils in Africa.

Acknowledgments

J d'O C would like to thank Matti Vuorre, Richard McElreath, David Navega, Thomas Püschel, José G. Almeida, and Solomon Kurz, for insightful discussions concerning statistical details of Bayesian meta-analysis. The authors would like to thank Katarina Almeida-Warren and anonymous reviewers for suggestions that improved the overall quality of the manuscript. Jd'OC was supported by the Portuguese Foundation for Science and Technology (FCT)—Grant SFRH/BD/122306/2016.

3.5 Supplementary Text

3.5.1 S1: Dataset distribution

Is the database generally biased toward values that are too recent in geological time to be possible? We would expect that the density curves of estimations (Fig. 3.S1) would approximate a normal distribution and that their left tail should start close to the levels of the fossil thresholds (4.4 to 7.2 Ma). Moreover, they should center on some larger value and then mirror to some extent this pattern at the right tail i.e., normality. Instead, we obtained displaced (starting at ~1.3 Ma) and right-skewed density curves, especially for the Min range values. Overall, these statistical artefacts are strong evidence of a bias towards underestimation of time passed since the *Pan/Homo* divergence. As expected, the Max estimations are platykurtic—revealing uncertainty—since deriving a maximum bound from the fossil record is more problematic as it must rely on negative evidence (i.e., the absence of a palaeo-taxon in a stratigraphic horizon or time interval) (Marshall, 1990).

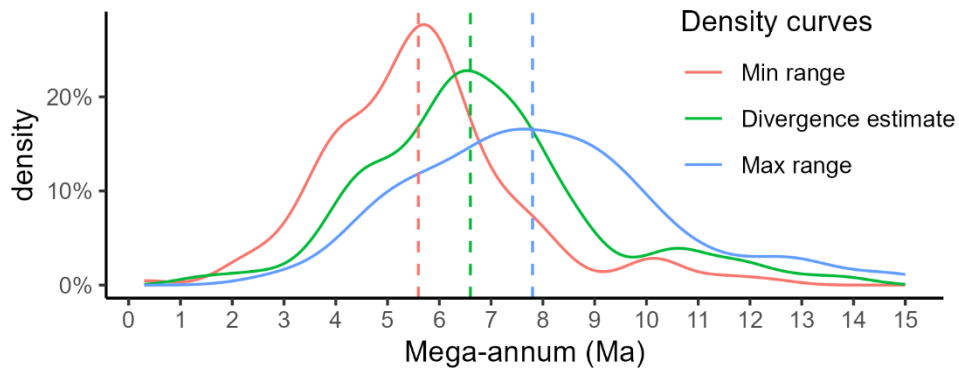


Fig. 3.S1.

Density curves for the min-estimate-max triplets sampled from the literature. Dashed vertical bars represent median values for each density curve.

3.5.2 S2: Bayesian meta-analysis: further details

A Bayesian meta-analysis can be seen as a special case of a Bayesian multilevel regression (Higgins, Thompson & Spiegelhalter, 2009; Bürkner, 2018; McElreath, 2020; Röver, 2020). By definition, a meta-analysis is structured hierarchically, i.e., it has an inherent multilevel architecture (Cumming, 2013). In our case, the first level includes the individual estimates of divergence dates for the *Pan*/*Homo* pair. In a meta-analysis, data on this level is generally described as the calculated effect sizes y_i of each study i. Since some studies include multiple model outputs with different divergence estimates, we assume that estimates are nested within studies on the second level. Thus, the true effect sizes θ_i of different studies in the second level of our meta-analysis follow their own distribution with a pooled effect μ and a variance τ^2 (between-study heterogeneity).

To formalize our Bayesian multilevel model, it follows that

$$y_i \sim Normal(\theta_i, \sigma_i^2)$$
$$\theta_i \sim Normal(\mu, \tau^2) \qquad \text{(eq. 1)}$$

where we assumed that our effect sizes y_i were sampled from a population of i studies. This population can be estimated as having a distribution with mean θ_i (i.e., the "true" effect of each divergence estimate), and a variance σ^2. The pooled effect size, that is, what we want to estimate in a meta-analysis, is defined as the mean μ of the distribution of true effect sizes. The study-specific true effects θ_i will deviate from the population-mean μ, because the second-level distribution has a variance τ^2.

The objective of a Bayesian meta-analysis is to estimate a single pooled true effect from observed effect sizes available in the literature. Thus, it shares the same objective of any conventional meta-analysis (Röver, 2020). However, there are clear advantages of using Bayesian approaches. The main one is that domain knowledge—in this case,

palaeoanthropological expertise, and specifically, the dates provided by the fossil record—can be easily incorporated into our models, by assigning prior distributions on the population-level parameters μ and τ^2. Prior distributions are used to account for the uncertainty in the parameter values.

We rely on weakly informative priors, instead of the more commonly used non-informative or uniform priors (i.e., all effect sizes are equally credible). Weakly informative priors are more sophisticated, as they allow models to consider that some estimates are more credible than others (Williams, Rast & Bürkner, 2018; Röver *et al.*, 2021). Assuming a normal distribution, we can thus define our μ prior as having a mean u and variance v. Our τ prior should always be non-negative, and thus will follow a Half-Cauchy distribution (Williams *et al.*, 2018; Wołodźko, 2020) with a peak around 0, and a scaling parameter around 0.1 to avoid a flat tail and spread distribution:

$$\mu \sim Normal(u, v)$$
$$\tau \sim \mathcal{HC}(0, 0.1) \quad \text{(eq. 2)}$$

In our case, we directly calculated the prior beliefs from our dataset after pruning it by applying the estimating averages and standard deviations of each sub-set under analysis.

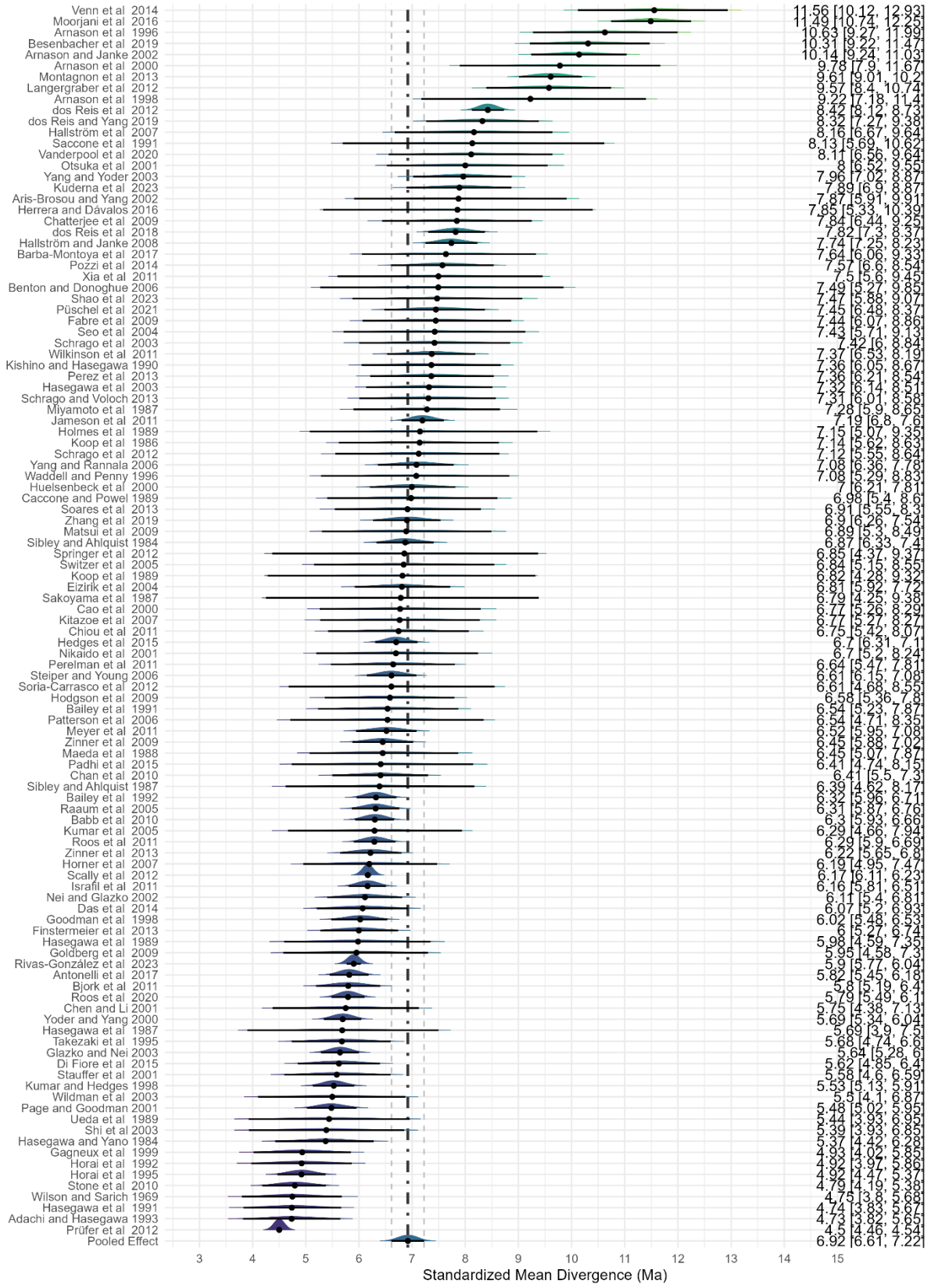


Fig. 3.S2.

Forest plot depicting the specific effect size and sampled posterior distribution of each study after applying the 4.4 Ma threshold.

Table 3.S1.

Summary statistics for the Bayesian meta-analysis for the 4.4 Ma threshold.

4.4 Ma threshold	Divergence | SE ~ 1 + (1 | Study)	
Predictors	Estimates	CI (95%)
Intercept	6.92	6.61 – 7.22
Std. Dev.	1.51	1.30 – 1.77
Random Effects		
$\tau_{00\ Study}$	2.29	
ICC	0.70	
$N_{\ Study}$	111	
Observations	159	
Conditional R^2	0.651	

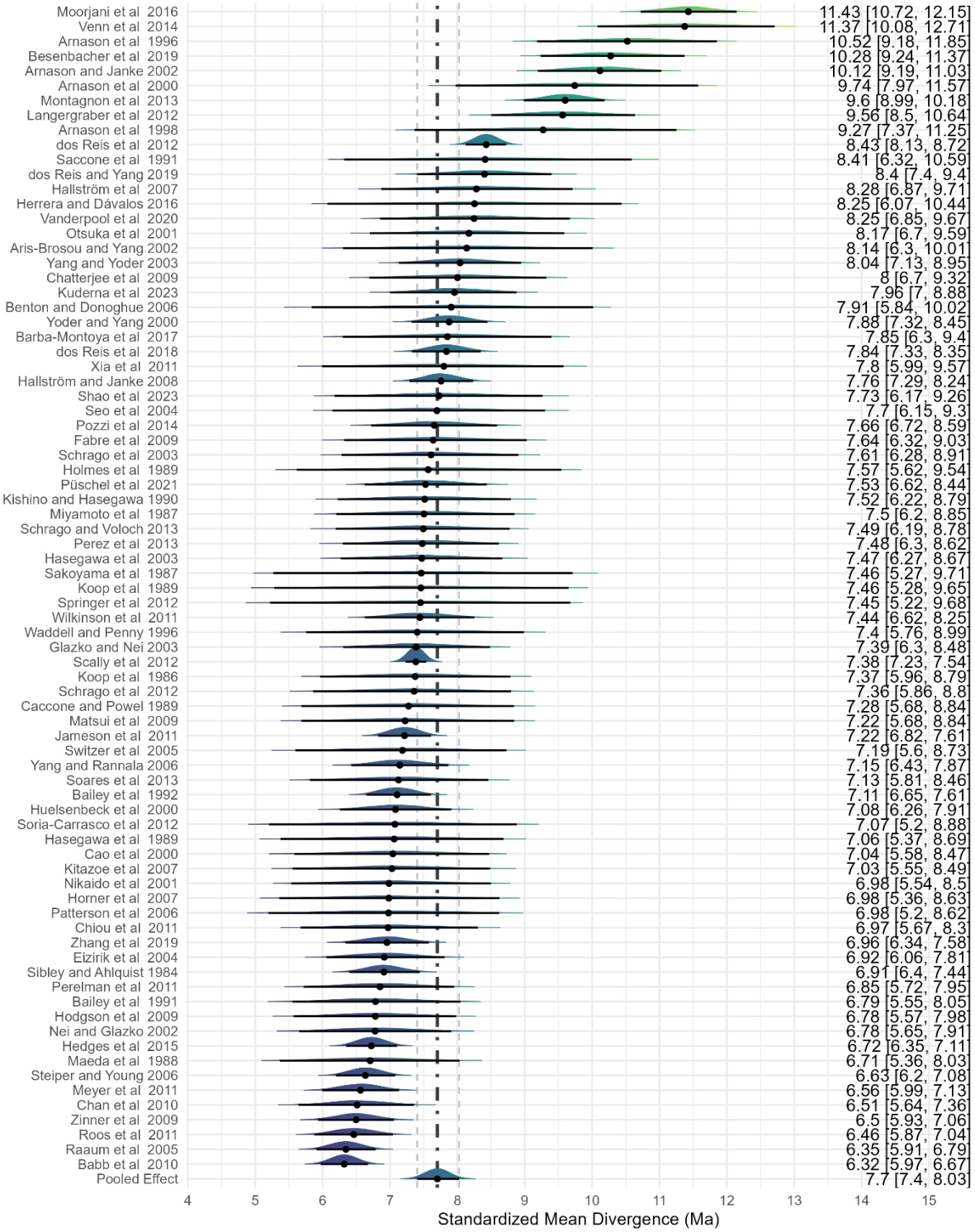


Fig. 3.S3.

Forest plot depicting the specific effect size and sampled posterior distribution of each study after applying the 6.2 Ma threshold.

Table 3.S2.

Summary statistics for the Bayesian meta-analysis for the 6.2 Ma threshold.

6.2 Ma threshold	Divergence | SE ~ 1 + (1 | Study)	
Predictors	Estimates	CI (95%)
Intercept	7.71	7.40 – 8.03
Std. Dev.	1.26	1.02 – 1.54
Random Effects		
$\tau_{00\ Study}$	1.59	
ICC	0.61	
$N_{\ Study}$	79	
Observations	108	
Conditional R^2	0.558	

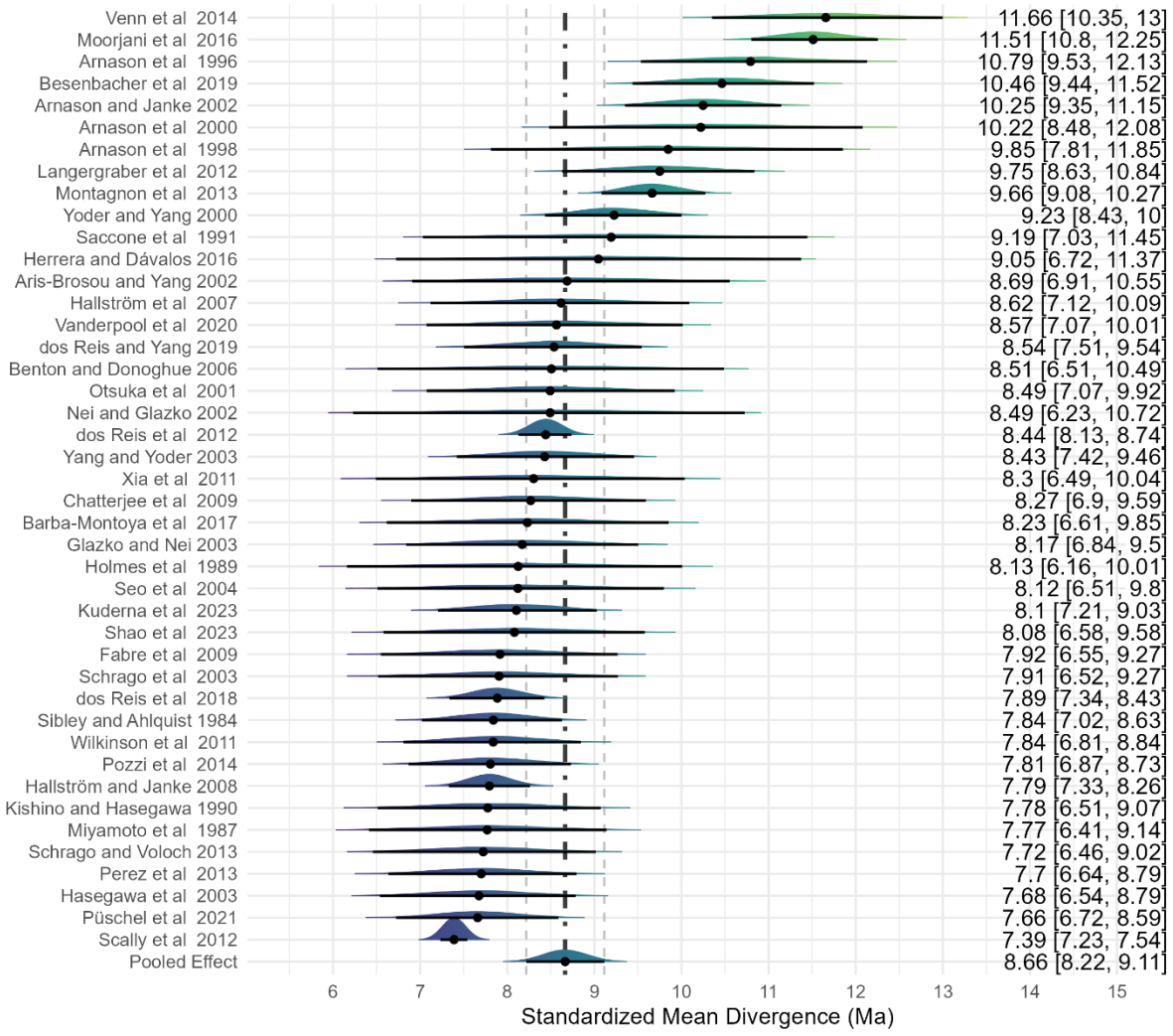


Fig. 3.S4.

Forest plot depicting the specific effect size and sampled posterior distribution of each study after applying the 7.2 Ma threshold.

Table 3.S3.

Summary statistics for the Bayesian meta-analysis for the 7.2 Ma threshold.

7.2 Ma threshold	*Divergence | SE ~ 1 + (1 | Study)*	
Predictors	Estimates	CI (95%)
Intercept	8.66	8.22 – 9.11
Std. Dev.	1.28	0.95 – 1.70
Random Effects		
$\tau_{00\ Study}$	1.65	
ICC	0.64	
$N_{\ Study}$	40	
Observations	62	
Conditional R^2	0.527	

3.5.3 Data S1.

Maintained and Available on GitHub: https://github.com/Delvis/Pan-Homo

4

Unsupervised learning of satellite images enhances discovery of late Miocene fossil sites in the Urema Rift, Gorongosa, Mozambique

Published in *PeerJ,* 10.7717/peerj.11573

Unsupervised learning of satellite images enhances discovery of late Miocene fossil sites in the Urema Rift, Gorongosa, Mozambique

João d'Oliveira Coelho[1,2], Robert L. Anemone[3], Susana Carvalho[1,2,4,5]

[1] Primate Models for Behavioural Evolution Lab, Institute of Human Sciences, University of Oxford, Oxford, UK
[2] Centre for Functional Ecology (CFE), Universidade de Coimbra, Coimbra, Portugal
[3] Department of Anthropology, University of North Carolina at Greensboro, Greensboro, NC, USA
[4] Interdisciplinary Centre for Archaeology and Evolution of Human Behaviour (ICArEHB), Universidade do Algarve, Faro, Portugal
[5] Gorongosa National Park, Sofala, Mozambique

Abstract

Background: Palaeoanthropological research focus still devotes most resources to areas generally known to be fossil rich instead of a strategy that first maps and identifies possible fossil sites in a given region. This leads to the paradoxical task of planning paleontological campaigns without knowing the true extent and likely potential of each fossil site and, hence, how to optimize the investment of time and resources. Yet to answer key questions in hominin evolution, paleoanthropologists must engage in fieldwork that targets substantial temporal and geographical gaps in the fossil record. How can the risk of potentially unsuccessful surveys be minimized, while maximizing the potential for successful surveys?

Methods: Here we present a simple and effective solution for finding fossil sites based on clustering by unsupervised learning of satellite images with the k-means algorithm and pioneer its testing in the Urema Rift, the southern termination of the East African Rift System (EARS). We focus on a relatively unknown time period critical for understanding African apes and early hominin evolution, the early part of the late Miocene, in an overlooked area of southeastern Africa, in Gorongosa National Park, Mozambique. This clustering approach highlighted priority targets for prospecting that represented only 4.49% of the total area analysed.

Results: Applying this method, four new fossil sites were discovered in the area, and results show an 85% accuracy in a binary classification. This indicates the high potential of a remote sensing tool for exploratory paleontological surveys by enhancing the discovery of productive fossiliferous deposits. The relative importance of spectral bands for clustering was also determined using the random forest algorithm, and near-infrared was the most important variable for fossil site detection, followed by other infrared variables. Bands in the visible spectrum performed the worst and are not likely indicators of fossil sites.

Discussion: We show that unsupervised learning is a useful tool for locating new fossil sites in relatively unexplored regions. Additionally, it can be used to target specific gaps in the fossil record and to increase the sample of fossil sites. In Gorongosa, the discovery of the first estuarine coastal forests of the EARS fills an important palaeobiogeographic gap of Africa. These new sites will be key for testing hypotheses of primate evolution in such environmental settings.

4.1 Introduction

Palaeontological and molecular evidence indicate that *Homo* shared a most recent common ancestor (MRCA) with the *Pan* lineage during the late Miocene (11.6-5.3 Ma) in Africa (Montagnon, 2013; Moorjani *et al.*, 2016; Barba-Montoya *et al.*, 2017; dos Reis & Yang, 2019). This makes this period critical to understand the origins of our clade, and yet the geographic distribution of African fossil sites during this time is surprisingly sparse and strongly biased (Figure 4.1a, b). Currently only three regions contain lithostratigraphic units that have yielded possible early hominins from the late Miocene: Djourab Desert, Chad (*Sahelanthropus tchadensis* Brunet *et al.*, 2002); Tugen Hills, Kenya (*Orrorin tugenensis* Senut *et al.*, 2001); Middle Awash, Ethiopia (*Ardipithecus kadabba* Haile-Selassie, 2001).

If we expand this sample to include fossils of the African great apes during the same time period, the record is likewise sparse (Andrews, 2019), being limited to the gorilla-like *Chororapithecus abyssinicus* from Ethiopia (Suwa *et al.*, 2007), *Samburupithecus kiptalami* (Ishida & Pickford, 1997) and the basal hominid *Nakalipithecus nakayamai* (Kunimatsu *et al.*, 2007) from Kenya, plus some taxonomically uncertain dental and mandibular finds from Kenya and Niger (Table 4.1). Furthermore, there is still no consensus regarding the phylogenetic relationships among late Miocene African hominids or how they relate to the MRCA (Senut, 2010, 2015; Kunimatsu *et al.*, 2016). Even less understood are the biogeographic distributions and temporal spans of these taxa that existed within or around the estimated time range for the *Pan/Homo* divergence event. For the great apes, clear fossil evidence only reappears much more recently, in the Pleistocene, demonstrating the temporal extension of these gaps in the fossil record (McBrearty & Jablonski, 2005).

Fundamentally, many of these uncertainties originate from significant gaps in the fossil record. As a discipline, palaeoanthropology seeks to answer key questions regarding origins and adaptations of our and other related lineages, but the available data are often too sparse to provide satisfactory answers. Overcoming these limitations may depend largely on developing

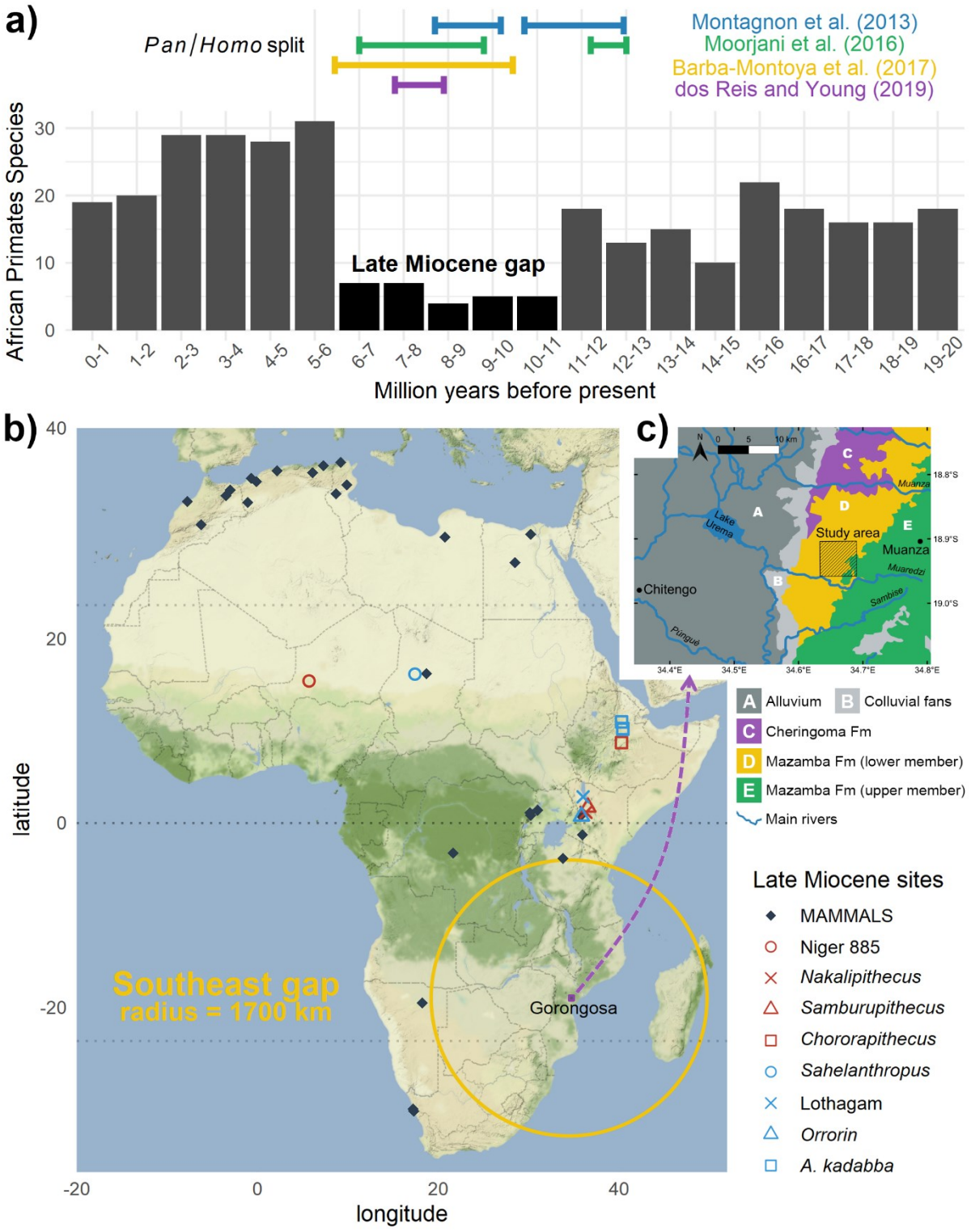


Figure 4.1 – **The great gaps of the African late Miocene.** a) Time gap**:** during this key period the African fossil record of primates is very incomplete (evaluated through species richness); but notice the split estimates from genomics; b) Spatial gap**:** virtually no fossils of this age are known in southeastern Africa, notice the strategic location of Gorongosa. Data extracted from palaeobiodb.org, map adapted from Bobe et al. (2018); c) study area for *k*-means within the geological context of Gorongosa, adapted from Habermann et al. (2019).

new strategies for field work, targeting areas and time periods that are undersampled and poorly understood. This may involve considerable risk for palaeoanthropological campaigns that most field workers and funding institutions might not be willing to take (Emerson & Anemone, 2012). Moreover, finding hominins is not a straightforward endeavour. For instance, it took the Leakeys 33 years of work at Olduvai Gorge to find their first hominin, the holotype skull of *Paranthropus boisei* (Leakey, 1959). Therefore, innovative risk-aversion methods that can maximize information and improve current surveying approaches are urgently needed (Njau & Hlusko, 2010; Anemone *et al.*, 2011b).

Table 4.1 – All hominids described for Africa during the Late Miocene (11.6–5.3 Ma).

Age (Ma)	Fossil site(s)		Taxon	Reference(s)
ca. 5.4	ESC2;3;8, Gona, Ethiopia		*Ardipithecus kadabba*	(Simpson *et al.*, 2015)
5.6–5.2*	Amba East, Ethiopia		*Ardipithecus* cf. *kadabba*	(Haile-Selassie, 2001; Haile-Selassie *et al.*, 2004)
5.77–5.54	ALA; ASK; DID; STD †		*Ardipithecus kadabba*	
5.8–5.7	Tugen Hills, Kenya	Kapcheberek	*Orrorin tugenensis*	(Senut *et al.*, 2001; Senut, Pickford & Gommery, 2018a; Sawada *et al.*, 2002; Pickford & Senut, 2005; Senut, 2010, 2015)
5.9–5.8		Kapsomin	*Orrorin tugenensis*	
			Incertae sedis (*Gorilla*?)	
ca. 6.1		Cheboit	*Orrorin tugenensis*	
			Incertae sedis (early *Pan*?)	
		Aragai	*Orrorin tugenensis*	
6–5	Nkondo, Uganda		cf. *Gorillini*	(Pickford *et al.*, 1988)
6.3	ABD1, Gona, Ethiopia		cf. *Ardipithecus kadabba*	(Simpson *et al.*, 2015)
6.5–5‡	Lothagam, Kenya		Homininae indet.	(Leakey & Walker, 2003)
7.34-7.1§	Toros-Menalla, Chad		*Sahelanthropus tchadensis*	(Brunet *et al.*, 2002, 2005)
8.0	Ch'orora, Ethiopia		*Chororapithecus abyssinicus*	(Suwa *et al.*, 2007)
9.5	Samburu Hills, Kenya		*Samburupithecus kiptalami*	(Ishida & Pickford, 1997)
9.9–9.8	NA39, Nakali, Kenya		*Nakalipithecus nakayamai*	(Kunimatsu *et al.*, 2007)
			Hominidae indet.	(Kunimatsu *et al.*, 2016)
11–8¶	N 885, Niger		*Incertae sedis* (early *Pan*?)	(Pickford *et al.*, 2008, 2009)

* Probably closer to 5.2 Ma than 5.6, but the Kuserale Mb of the Sagantole Fm is bracketed as in Renne et al (1999).
† Fossiliferous localities in the Asa Koma Mb of the Adu Asa Fm (Middle Awash, Ethiopia). ALA = Alayla (ALA-VP-2), ASK = Asa Koma (ASK-VP-3), DID = Digiba Dora (DID-VP-1); STD = Saitune Dora (STD-VP-2).
‡ Not the KNM-LT 329 mandible, but two teeth (KNM-LT 22930 M3; KNM-LT 25935 I1) from older deposits (Upper Nawata).
§ Cosmogenic nuclide dating (Lebatard et al., 2010).
¶ Only biostratigraphic dating available, a more conservative range would be 11.6–5.3 Ma (Late Miocene).

How do we know where to look for fossils in unexplored and remote regions? When an area has been extensively surveyed, we can focus on previous work to guide our efforts. If that is not the case, we can use the geology and topography to enhance surveying efforts (Asfaw *et al.*, 1990). However, that is not always possible if the modern topographic and ecological conditions for looking for fossil are not ideal. In places like the miombo woodlands of Gorongosa (Figure 4.2), where nine late Miocene paleontological localities have recently been described, the surrounding dense vegetation cover can make reading the landscape for clues to fossiliferous deposits extremely difficult (Habermann *et al.*, 2019). The fossil sites are found just north of the Muaredzi river and east of Lake Urema, between the villages of Chitengo and Muanza (Figure 4.1c).



Figure 4.2 – **The miombo woodland and the challenges it presents to fossil prospecting: Gorongosa Palaeontological Location 1 (GPL-1).** a) GPL-1 outcrops, notice how the surrounding vegetation is far more dense and extensive than in typical fossil sites from the EARS; b) GPL-1 in high-resolution satellite image, extracted from bing.com, shows a reduction of vegetation, but outcrops are barely noticeable; c) GPL-1, in a black rectangle, appears brighter than surrounding areas, when being mapped by lower resolution Landsat 8 false colour (infrared) image, and the same happens with other fossil sites, suggesting the infrared bands might be a useful indicator of fossiliferous deposits.

The terrain of the study area can be described as flat to slightly undulating, with active incision and upstream erosion of stream sources. Topographic relief is also dotted by island thickets on

termitaria hills. The vegetation in the study area is dominated by closed canopy *Brachystegia* (miombo) woodlands, with riverine forests occurring along the drainage network (Figure 4.3). The grass layer density can vary greatly spatially and across the seasons, from widely spaced grass tufts in sandier substrates, to medium and tall (>2 m height) grass layers that are subject to regular, typically annual, fires (Tinley, 1977).



Figure 4.3 – **Surveying for fossils in a densely vegetated context.** a) Despite the ground foliage and dense vegetation, in situ and surface evidence of fossils abound in the gully valley connecting GPL-12 to GPL-12B; b) Systematic mapping and collecting of surface fossil finds by students of the field school; c) Side gully (~3 m deep) exposure and shovel test pit at GPL-12. Photographs are from the Paleo-Primate Project Gorongosa archive.

Modern geospatial technologies such as remote sensing, handheld GPS devices and geographic information systems (GIS) software have been applied to different paleoanthropological research questions with spatial components (Conroy, 2006; Egeland *et al.*, 2010; Anemone & Conroy, 2018). Surveys aimed at discovering new fossil assemblages with hominins have also been guided by military, geological and topographic maps, aerial photography and satellite images (Asfaw *et al.*, 1990; Malakhov *et al.*, 2009; Hlusko, 2018; Habermann *et al.*, 2019). With recent advances in artificial intelligence, cheaply available computer power, and free access to satellite imagery of reasonable resolution, paleoanthropologists and GIS technicians have been implementing machine learning techniques to automate the demanding visual analysis of remote fossil site detection (e.g., Anemone *et al.*, 2011b; Conroy *et al.*, 2012, 2018; Conroy, 2014; Emerson *et al.*, 2015; Block *et al.*, 2016; Wills *et al.*, 2018).

Here, we pioneer the application of such automated computational approaches for remote fossil site detection within the EARS (East African Rift System), specifically at its youngest and southernmost subsection, the Urema Rift (where rifting initiated at ~3 ± 1 Ma), in Gorongosa National Park, Mozambique (Böhme *et al.*, 2006; Steinbruch, 2010; Fonseca *et al.*, 2014; Macgregor, 2015). The southern part of the EARS is far less explored than its northern counterpart, which is rich in lacustrine and fluvial palaeontological settings (Bobe *et al.*, 2020b). The first fossil sites of the Urema Rift and their geological features have been recently described by Habermann et al. (2019). All the sites described are part of the lower member of the Mazamba Formation which has been attributed to a Miocene or Mio-Pliocene age (Real, 1966; Grantham *et al.*, 2011; Pickford, 2013; Habermann *et al.*, 2019). Preliminary authigenic $^{10}Be/^{9}Be$ dating suggests the fossil sites fit into the earliest part of the late Miocene interval (Bobe *et al.*, 2023). The lower Mazamba successions record coastal nearshore conditions that formed in a shallow ramp setting by marine transgression that occurred prior to rifting. North-eastern sites tend to be richer in fossils of marine fauna and are dominated by sand, while the southern sites are dominated by basal conglomeratic and sandy units overlain by clayey sandstones and sandy marl- and claystone facies (Habermann et al., 2019). The Miocene palaeoenvironments of Gorongosa were reconstructed as estuarine coastal forests and woodlands (Habermann *et al.*, 2019)—a unique context in the EARS—that is both promising for the presence of primates (Nowak *et al.*, 2019) and crucial for testing biogeographic hypothesis of early hominin evolution in estuarine or deltaic wetlands (Wrangham, 2005) and in coastal forest biomes of eastern Africa (Kingdon, 2003; Joordens *et al.*, 2009, 2019; Bobe *et al.*, 2020b).

In order to find new fossil sites in Gorongosa, a decision support system based on unsupervised learning of satellite images was created to guide prospecting during the 2018 field season. This was achieved by applying a simple clustering algorithm to satellite images of the field area. There are only two other examples in the literature that applied unsupervised clustering for detecting fossil sites, one in the Uinta Basin, Utah (Conroy, 2014) and the other in the Bighorn and Great Divide Basins, Wyoming (Conroy *et al.*, 2018). Cluster analysis does not use

categories that tag objects with prior identifiers (class labels). The absence of categorical information distinguishes data clustering (unsupervised learning) from classification or discriminant analysis (supervised learning). The aim of clustering is to find structure in data and it is therefore exploratory in nature (MacQueen, 1967). One of the most popular and simple clustering algorithms, *k*-means, was first conceptualized in the 1950s (Steinhaus, 1956) and while thousands of different clustering algorithms have been published since then, *k*-means is still widely used because of its effectiveness, speed and simple implementation (Bock, 2008). While *k*-means is a standard technique for many remote sensing applications, it has never been used for fossil site detection. Here, for the first time, this algorithm has been adopted for the purpose of finding fossil sites using satellite imagery.

The goal of this pilot study was to determine if *k*-means, a simple unsupervised computer vision technique for processing satellite images, could improve our ability to identify fossil sites in a limited region of interest in Gorongosa with no *a priori* knowledge of the geology, stratigraphy, topography and land cover. In addition, we sought to characterize the lower Mazamba Formation (see Habermann *et al.*, 2019) through extensive ground surveys to catalogue the presence and distribution of palaeontological resources. These new fossil discoveries will help us to better understand an ancient ecosystem that existed during a crucial period of African great ape diversification and hominin origins. The insights gained from our fieldwork, in combination with the analyses of satellite imagery, allow us to gauge the accuracy of our model and to refine future iterations of these statistical modelling approaches for fossil site detection.

4.2 Materials & Methods

Field experiments were approved by Dr Marc Stalmans, Director of the Department of Scientific Services of Gorongosa National Park in Mozambique (project number: PNG/DSCi/C019/2018). The code for the complete protocol and input files are available in an open access repository at https://github.com/Delvis/kmeansGorongosa/. The dataset

consists of a freely available atmospherically corrected scene with 30×30 m resolution of Landsat 8 OLI (Roy *et al.*, 2014) from July 28th, 2017 (id: LC08_L1TP_167073_20170628_20170714_01_T1), covering a portion of central Mozambique. Spectral data from Landsat and other medium-resolution satellites is updated daily and can be accessed at the USGS Earth Explorer website (https://earthexplorer.usgs.gov/). After downloading the satellite image, we applied a cropping filter to restrict it to an area of interest known to contain late Miocene to early Pliocene deposits (Real, 1966; Grantham *et al.*, 2011), corresponding to approximately 36 km^2, in the lower Mazamba Formation within Gorongosa National Park (Figure 4.1c). A multidimensional matrix containing the brightness values for 7 spectral bands (2 short-wave infrared, 1 near-infrared, 3 visible 'RGB', and 1 ultrablue) of Landsat 8 in UTM/WGS 84 coordinate system was processed through *k*-means, an unsupervised learning algorithm that can split the satellite image into different *k* clusters based on the spectral pattern of each pixel (a 30×30 m point in space). The clusters were then compared to geocoordinates of known late Miocene fossil sites in Gorongosa (available in Habermann *et al.*, 2019) in order to determine whether there was a consistent visual pattern matching cluster(s) with fossil sites, as in Conroy's (2014) 'walking back the cat' approach. In other words, to algorithmically retrace our steps to identify other potential fossiliferous outcrops. This is achieved by generating clusters in an unsupervised manner, and then selecting the cluster(s) containing most fossil sites as the target cluster(s) for the field season (Figure 4.4). The advantages of such approach is that it works: a) when we only have very few fossil sites known in the region; b) in the absence of any prior knowledge of landscape cover over the proposed survey area; and c) without pre-processing or training any landcover classes (Conroy, 2014; Conroy *et al.*, 2018). For data analysis purposes, we define "fossil site" as the 30x30 m pixel in the Landsat grid that includes the geographic centroid corresponding to a locality in the landscape with exposed outcrops containing either fossilized vertebrates, invertebrates and/or wood reported in the study area (Pickford, 2012, 2013; Habermann *et al.*, 2019).

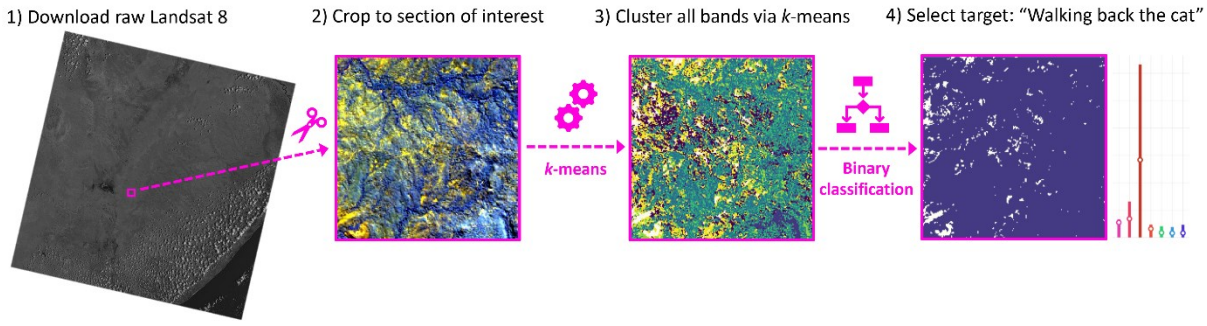


Figure 4.4 – **Flowchart of the algorithmic pipeline used for remote fossil site detection:** 1) Example of one of the seven spectral bands satellite images used in this study; 2) false colour map based on the infrared bands, after cropping to study area; 3) results of clustering using all seven spectral bands; 4) Binarize clusters for classification by selecting the cluster that contains most fossil sites as the target class ("walking back the cat") versus all other clusters combined into a single class.

4.2.1 Applying the k-means algorithm to satellite images

Partitional clustering is a family of unsupervised learning techniques for grouping a set of data points (instances) into k disjoint groups, better known as clusters. The goal is to increase intra-cluster similarity (in this case, Euclidean distance between grouped instances) while decreasing inter-cluster similarity. More specifically, the k-means algorithm approximates the best division of n data points in k groups, so that the total distance between each grouped instance $x_i,\ i \in \{1, \dots, n\}$ and its corresponding centroid $\mu_j,\ j \in \{1, \dots, k\}$ is minimized. Formally, this partition occurs through minimization of the within-cluster sum of squares ($WCSS$), defined as

$$WCSS = \sum_{j=1}^{k} \sum_{i=1}^{n} \left\| x_i^j - \mu_j \right\|^2 \qquad \text{(Eq. 1)}$$

where $\left\| x_i^j - \mu_j \right\|$ calculates the distance between an instance and a cluster's centroid.

With a rich history starting in the 1950s, the k-means algorithm was independently discovered in various scientific fields (Steinhaus, 1956; Ball & Hall, 1965; Forgy, 1965; MacQueen, 1967; Lloyd, 1982). Its most standard implementation can be broken down into two stages: initialization, where k cluster centroids $(\mu_1, \dots \mu_k)$ are randomly selected (Forgy, 1965); and a second, iterative or repeat stage, following Lloyd's algorithm (Lloyd, 1982). Lloyd's iterative refinement technique can be further broken down into the assignment and update steps: first,

each instance is assigned to the cluster with the closest centroid μ_j; then the set of centroids is updated, by recalculating each centroid with the new instances attached to the clusters. This repetition should run iteratively until cluster membership for the entities converges to a stable solution. Computationally, if C and C' are the set of centroids obtained at consecutive Lloyd's iterations, then the algorithm stops when

$$|WCSS(C) - WCSS(C')| \leq \varepsilon, \text{for a fixed threshold } \varepsilon \ll 1 \qquad \text{(Eq. 2)}$$

The greatest advantage of k-means is scalability, as only the centroid coordinates are stored in memory, it can deal with very large datasets. Moreover, every step can be parallelized, which increases computation performance (Wu *et al.*, 2008; Zhao, Ma & He, 2009). Nevertheless, it can be slow to compute, since each instance might be processed many times throughout the iterations. Another limitation is that the results are dependent on the initial random allocation of the centroids (Äyrämö & Kärkkäinen, 2006).

In the specific case of satellite images, each instance is a geolocated point/pixel (30×30 m) with associated brightness values for all the seven spectral bands. Therefore, by applying the k-means algorithm to such data, each instance is assigned to one of the k clusters, and instances with similar spectral characteristics will cluster together. Thus k-means has many uses, including the ability to: a) explore and mine hidden patterns in the satellite data; b) partition a dataset into different groups that might correspond to real types of land cover; and c) feature learning(a data science technique for encoding new features from raw data), since the output clusters can be used as new variables for subsequent modelling approaches (Jain, 2010).

4.2.2 Clusters as survey guides for fossil site discovery

If we allow a specific cluster, say cluster 1, to be a predictor for fossil sites, after applying a k-means where k = 8, we can consider from a statistical classification paradigm: True Positives (TP) = fossil sites on cluster 1; False Positives (FP) = non-localities on cluster 1; False Negatives (FN) = fossil sites on clusters 2 to 8; True Negatives (TN) = non-localities on clusters

2 to 8. The clustering results were validated digitally using geolocated coordinates for fossil sites and non-localities collected through ground surveys during the 2016 and 17 field seasons. Then, the region was revisited during the first two weeks of August 2018 to survey unexplored areas on foot and ground-truth the model. Localities that could not be thoroughly observed due to obstacles such as high vegetation density, dry foliage, difficult access, or other factors, were recorded as NA (not applicable) and were removed from the current analysis. All other surveyed localities were evaluated as either TP, FP, FN, or TN and analysed through measures of statistical performance to assess the efficiency of the implemented approach.

To clarify the mechanisms responsible for generating different clusters, a supervised random forest algorithm for classification (Breiman, 2001) was built on top of the new learned features (cluster 1 to 8). Variable importance metrics, like the permuted mean square-error (%IncMSE), can be extracted from the random forest model. Calculating %IncMSE is achieved by internal out-of-bag estimates of error rate, and then verified by reruns excluding each predictor variable (i.e., permutation). For all the trees in the model, the difference between error rates is averaged, and normalized by the standard deviation of the differences, thus calculating a metric of variable importance (Liaw & Wiener, 2002).

4.3 Results

4.3.1 Digital validation

A plot with the clustering results of the satellite image was rendered and superimposed with a layer representing all the nine known Gorongosa Palaeontological Localities (GPL) at the time, provided by Habermann et al. (2019), and two possible vertebrate sites with single-fossil finds of large mammals, plus two sites with fossil wood from earlier work by Pickford (2012, 2013). Additionally, all areas previously surveyed in 2016 and 2017 but without any fossiliferous material discovered ('non-localities') were also mapped. Clusters resulting from the k-means analysis can thus be compared with all the coordinates to uncover the patterns in the satellite

images, such as any combination of spectral wavelength values having more likelihood of remotely detecting the fossil sites (Figure 4.5).

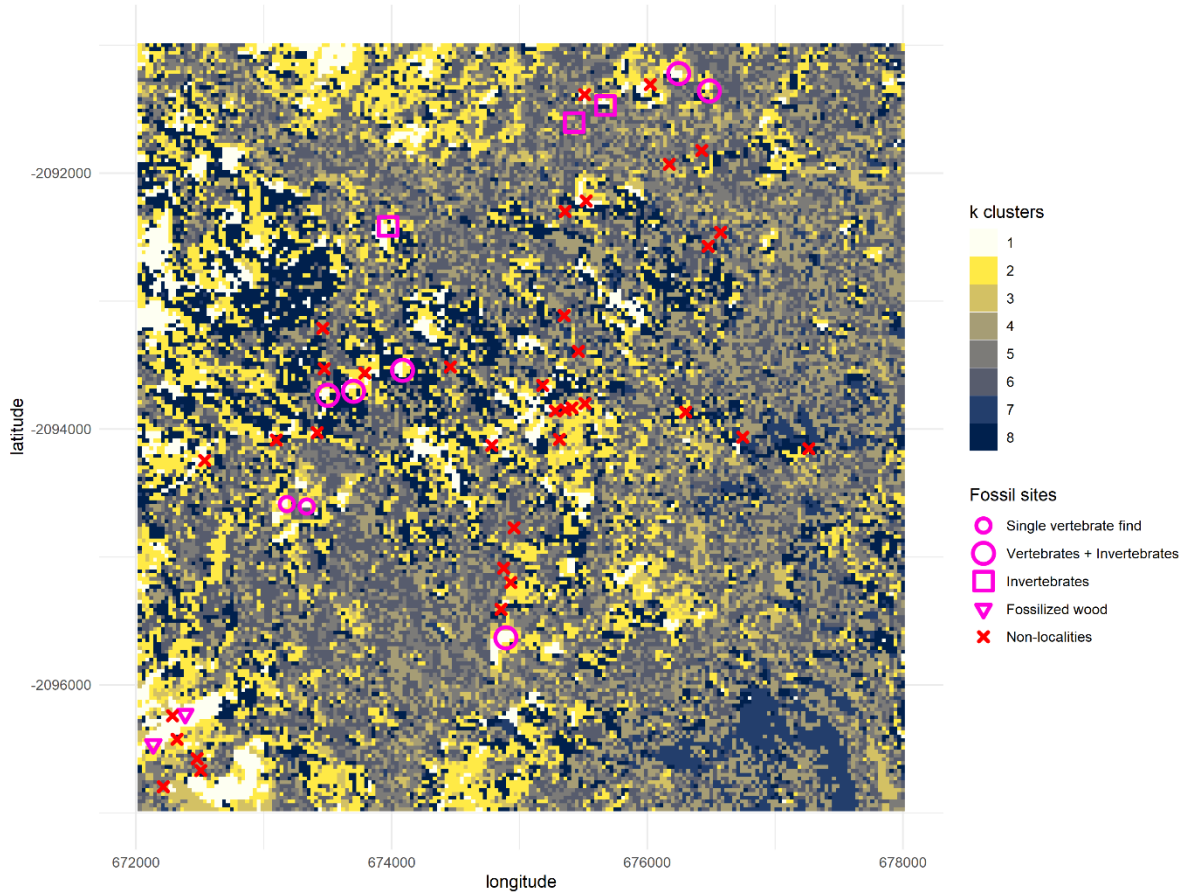


Figure 4.5 – **Output from the *k*-means algorithm for data mining.** All geolocations "Vertebrates + Invertebrates" and "Invertebrates" recorded by the PalaeoPrimate Project Gorongosa team during 2016 and 2017 (Habermann et al., 2019) are plotted over the clusters, as well as the "Single vertebrate find" and "Fossilized wood" localities reported by Pickford (2012, 2013). You can see the cluster 1 (white) tends to be represented in locations with fossil vertebrates, indicating that it has some potential as a new feature/variable for finding new fossil sites. The map displays a 6 by 6 km square; axes scales are in meters.

All fossil sites containing vertebrate remains recorded in the area overlapped cluster 1 (Figure 4.5), as well as the fossil wood sites and two out of three invertebrate sites (only GPL-9 did not match the pattern). However, the non-fossiliferous localities spread randomly over all clusters. Consequently, we decided to consider cluster 1 as a statistical classifier (i.e., predictive cluster) of potential new fossil sites to guide us during survey and thus increase the likelihood of finding sites. As a statistical classifier, cluster 1 cells that do not overlap with a fossil site are considered FP, which is required information to evaluate accuracy and other performance metrics. It

should be noted that before being targeted a considerable range of this same cluster remained mostly unexplored, representing only 4.49% of the total area of the cropped image analysed (1795 pixels out of 40000). This severe reduction in total space to prospect – from 36 km^2 to roughly 1.6 km^2 – is one of the main advantages of geospatial palaeontology approaches. Prior work has demonstrated that the likelihood of success in locating fossil localities can be greatly increased by highlighting priority targets for prospecting (Oheim, 2007; Egeland *et al.*, 2010; Anemone *et al.*, 2011b; Conroy *et al.*, 2018). The spectral range of each cluster generated by *k*-means was also compared with the spectral range of the fossil sites. This again shows us very clearly that cluster 1 matches best the pattern exhibited by the fossiliferous deposits at the lower Mazamba Fm, especially in the NIR, SWIR1, and SWIR2 wavelength regions of the spectral band (Figure 4.6).

4.3.2 Ground-truthing

During the 2018 season, four new fossil localities were discovered (GPL-10, 11, 12 and 12B), 3 out of 4 completely overlapped with cluster 1, the cluster identified as more likely to enable fossil discovery (Figure 4.7). However, the only "miss" (GPL-12, a false negative, since it was not detected by the algorithm), was less than 90 m from a high concentration of white pixels (cluster 1), and thus it was highly likely to be detected following this survey protocol, since it was in the same gully system as GPL-12B—which is detected by *k*-means, and thus was extensively surveyed. Therefore, it can be argued that all the new sites were ultimately discovered by using the *k*-means surveying workflow, including the only one that does not meet the stricter criteria to be considered a true positive, since its discovery was a by-product of surveying guided by the algorithm to that particular area containing a high density of white pixels in proximity, where GPL-12B, was found. There are two possible interpretations, either 1) the buffer areas around a high concentration of cluster 1 pixels might also be more likely to be fossiliferous or 2) the algorithm simply failed to detect this site as the spectral signature differed from other fossil sites. Considering the expressly dense canopy at GPL-12 (Figure 4.3), the second is likely the most parsimonious explanation. To be explicit, GPL-9 and -12

were considered false negatives (Table 4.2a) since cluster 1 of the *k*-means algorithm was defined as the predictive cluster, and it fails to detect them.

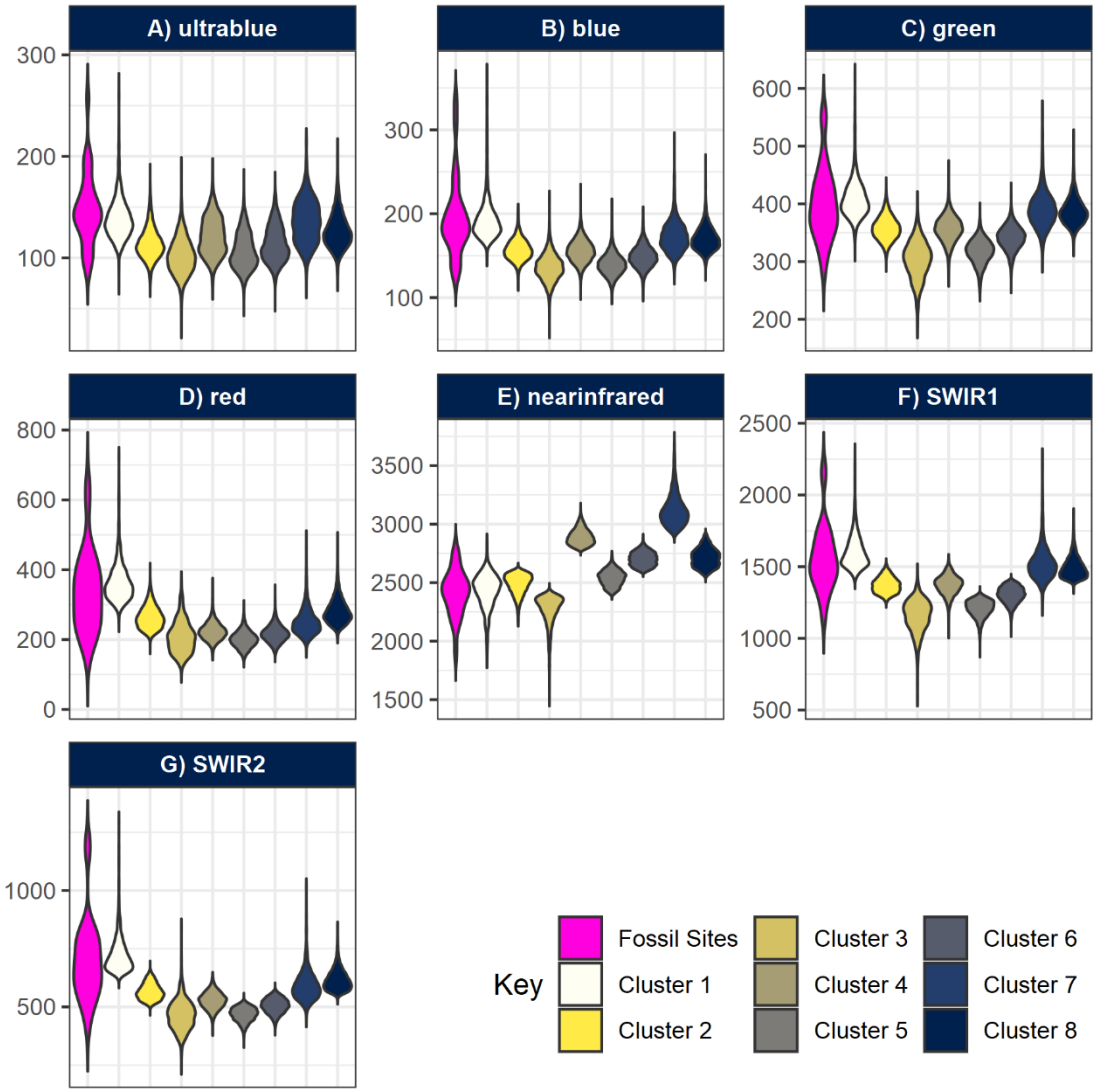


Figure 4.6 – **Violin-boxplots comparing sample distribution of spectral bands between clusters.** Each spectral band is represented in its own cell, with nine bars comparing the range of spectral bands values at the geocoordinates of the fossil sites, plus the eight clusters generated by *k*-means. Notice how overall, cluster 1 tends to approximate better the true spectral range of known fossil sites in Gorongosa.

Table 4.2 – Model goodness-of-fit a) confusion matrix; b) performance metrics.

a)

	Real +	**Real -**
Predicted +	TP=15	FP=12
Predicted -	FN=2	TN=62

b)

Measure	**Derivations**	**Value**
Sensitivity	TPR = TP / (TP + FN)	0.8824
Specificity	SPC = TN / (FP + TN)	0.8378
Precision	PPV = TP / (TP + FP)	0.5556
NPV	NPV = TN / (TN + FN)	0.9688
Accuracy	ACC = (TP + TN) / (P + N)	0.8462

The new outcrops GPL-10 and GPL-11 were located at two river cut-banks (ca. 500 m apart) exposing a series of sandstone beds and they are both rich in invertebrate remains, but vertebrates were also found at the latter. They have been interpreted as representing a coastal delta-plain and fluvio-deltaic to marginal marine conditions, respectively. GPL-12 and GPL-12B are two sites in a gully system that might be continuously exposing fossiliferous sediments from at least three different sandstone layers for more than 100 m (from north to south). These localities yield a remarkably well-preserved fossil record, including *in situ* and surface finds. Hundreds of identifiable fossil mammals, as well as crocodiles, turtles, and fish, have been recovered from this new area, and it has been tentatively inferred to be a river-dominated estuarine context (Bobe & Carvalho, 2019a, 2020; Bobe *et al.*, 2020b).

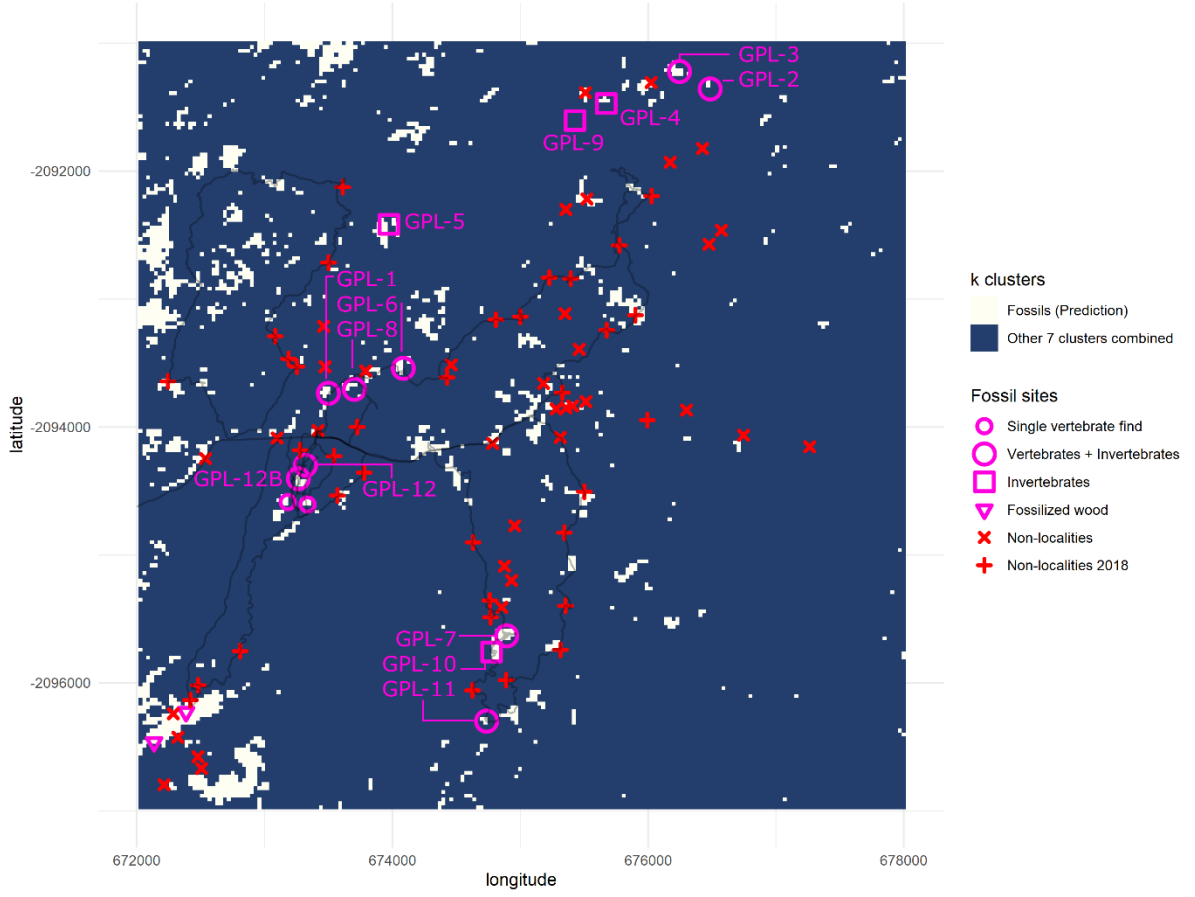


Figure 4.7 – **Binarized classification plotting cluster 1 vs all other clusters.** New fossil sites GPL-10, 11, 12 and 12B are documented here for the first time. Trackways of surveys during 2018 are drawn in black. Clusters 2-8 are merged into a single cluster and compared against cluster 1 (predictive cluster). Total area = 36 km^2. One grid square = 1 km^2. One pixel-cell = 900 m^2.

Our approach had a high overall accuracy of 84.6%. Statistical measures of performance for model evaluation (defined in Table 4.2b) such as the negative predictive value (NPV = 96.88%) indicate that the model was able to detect almost perfectly the vast majority of TN 'non-localities'. In contrast, a low 55.56% precision shows the model overestimated false positives. On the other hand, the model demonstrated a high level of sensitivity (88.24%), because of the very low number of false negatives generated, since only two fossil sites from the database did not match cluster 1 (see Figure 4.7). Other metrics like specificity performed well, albeit slightly lower than sensitivity (83.78%), again due to the high number of FP detections, and this performance metric fared much better than the precision metric because it takes into account the model's ability to correctly detect TN (see Table 4.2).

The supervised random forest model (Breiman, 2001; Liaw & Wiener, 2002) was built to assess the relative importance (%IncMSE) of spectral variables in the clustering analysis (Figure 4.8). It can thus be demonstrated that for this region of the lower Mazamba Formation the bands in the visible spectrum (0.45–0.67 μm) are the worst predictors of different clusters, while the near-infrared (NIR) is the variable that most contributed to the clustering.

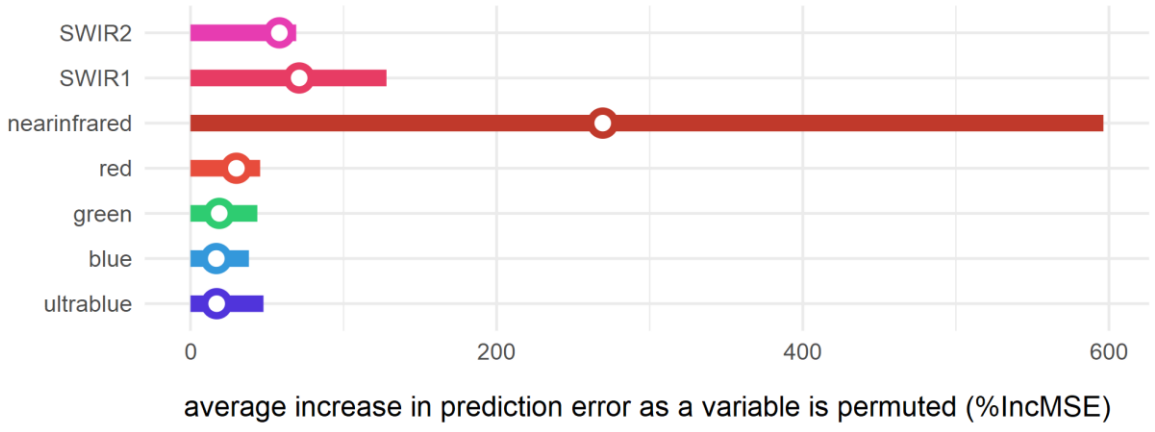


Figure 4.8 – **Variable importance of spectral bands for clustering**. Bars represent relative importance of the spectral predictors for optimally classifying all clusters as calculated by a supervised random forest algorithm (Breiman, 2001). Specific variable importance for detecting cluster 1 is shown with open circles.

This suggests that visual inspection of satellite images (usually depicted in RGB bands) is far from being ideal for this particular task (finding fossil sites). In addition, the bands sampling longer wavelengths in the electromagnetic spectrum (0.85–2.29 μm), from NIR to short-wave infrared 2 (SWIR 2), are notably important at improving detection of cluster 1, and thus are also likely indicators of fossil sites (Figure 4.8).

4.4 Discussion

Four new fossil sites from the late Miocene of southerneast Africa have been discovered by remote unsupervised learning. This analysis has also succeeded in pointing out the highest priority regions for future fossil prospecting in the lower Mazamba Formation of Gorongosa. In terms of overall accuracy, our unsupervised approach yielded similar results (84.6%) when compared with other implementations for remote fossil site detection, using supervised neural networks (84.21% with an hold-out sample in Anemone *et al.*, 2011b; Emerson & Anemone, 2012) and object-based binary classifier (73.1% with an hold-out sample in Emerson *et al.*, 2015). Notice that in an unsupervised pipeline like *k*-means, by definition, all the sample is hold-out as it has not been used to train the algorithm. However, overestimation of false positives (precision = 55.56%) needs to be improved, this can be done in future iterations using different model architectures that also learn from data collected in this campaign. The non-localities are particularly helpful as they can be used as negative weights in models to improve precision.

A limitation of unsupervised methods is that the results are not dependent on any target, since a cluster might not fully match a true cover class. Therefore, a cluster is a subjective entity whose significance and interpretation requires domain knowledge, in this case, the field researchers comparing the different areas targeted by the cluster of interest to understand what they have in common (Jain, 2010). By visually inspecting satellite imagery of higher resolution and having visited multiple points of interest, we suggest that cluster 1 is detecting outcrops with soil erosion, or slightly less vegetated areas that occasionally contain sediment exposures

(sometimes hidden under forest canopy). In Gorongosa, the sediment exposures are usually along river valleys or gullies subject to fluvial incision, and the most productive palaeontological localities were found at the upstream terminations of tributary channels. In a modern miombo woodland context, like much of Gorongosa, knowing before-hand where to go and find such rare contexts might be sufficient to increase considerably the chances of finding fossiliferous material, simply as a consequence of improved visibility for surveying in the points highlighted remotely through machine learning approaches.

Our variable importance analysis using the random forest algorithm (Breiman, 2001; Liaw & Wiener, 2002) showed the key importance of longer wavelengths for detecting these promising spots within a forest to woodland setting. Infrared reflectance has been used for more than a century to analyse rocks and minerals (e.g. Coblentz, 1906) and its applications in geology are well established (Lyon & Burns, 1963). More recently, near-infrared remote sensing has been applied in soil sciences for multiple purposes, including: mapping proportions of sand, silt, and clay content (Saleh, Belal & Arafat, 2013; Silva *et al.*, 2016); determination of soil salinity (Feyziyev *et al.*, 2016); monitoring soil moisture and capacity of water absorption (Ben-Dor *et al.*, 2002; Whiting, Li & Ustin, 2004); estimate organic carbon content (Hu, Chau & Si, 2015; Viscarra Rossel & Hicks, 2015); differentiate types of clay minerals (Surech, Sreenivas & Sivasamy, 2014); and assessing soil contamination and detection of heavy metals (Mohamed *et al.*, 2016, 2018). Yet, until now, machine learning approaches in geospatial palaeontology tended to achieve good results but as "black-boxes" that did not reveal how exactly they were interpreting a "fossiliferous signal", and thus the relative importance of specific spectral bands for remote fossil site detection has not previously been demonstrated. Here, we show another application of NIR in remote sensing: increasing probability of finding fossils by clustering spectral reflectance values (a proxy for soil properties) that are likely to enhance fossil discovery. While the specific properties are hard to discern at this level of resolution (both spatial and spectral) the most likely candidates are reduced biomass (low foliage and vegetation, are proxies for visibility), and detection by clustering of similar soil types and mineral contents (Mohamed *et al.*, 2018). SWIR1 and SWIR2 variables were also important

for the model and higher values are associated with higher soil moisture, and thus are a proxy for water erosion of the soils. This result makes sense considering that most fossil sites in Gorongosa are close to the upstream terminations of the modern drainage system of the region. Erosion proxies have been used before in remote sensing models for fossil site discovery (e.g. Block *et al.*, 2016; Wills *et al.*, 2018). This suggests that the predictive cluster is remotely identifying the same environmental features that Habermann and colleagues observed in the field regarding the "rock exposures most commonly provided by incised gullies at head regions of small tributary channels or by channel flanks, are highly localized due to dense ground vegetation" (2019:727).

Our approach is likely reliable and replicable in other areas of dense vegetation, but it might have limited potential when applied in other areas of the Rift that are drier and have much less vegetation cover and consequently, more exposure. However, previous implementations of unsupervised clustering approaches in modern deserts of North America have been successful at finding Eocene deposits with early primate fauna (Conroy, 2014; Conroy *et al.*, 2018), thus indicating that similar approaches are likely to be useful throughout the EARS. One last issue with *k*-means is that it creates equiprobable clusters, and thus might fail to properly represent the spectral signatures of the landcovers in certain surveying areas, so other unsupervised learning models without this characteristic might also improve the current results (Schubert *et al.*, 2017).

4.4.1 Conclusions

The *k*-means approach performed well with high overall accuracy, contributing to the discovery of four new fossil sites, albeit with some limitations (see precision metric). To address this constraint, in future field seasons a set of different modelling approaches will be implemented using different architectures and other features besides the spectral bands, such as geo-ecological variables (elevation, slope, aspect, vegetation index, etc.). Importantly, the 2018 field season yielded several new sites as well as numerous negative coordinates (non-localities), and these data are vital to implement supervised approaches, which are more robust

and may achieve better results than the method presented here. Considering NIR is usually interpreted as a proxy to biomass content in the soils (Hu *et al.*, 2015; Viscarra Rossel & Hicks, 2015), ground-truthing future implementations of different machine learning models should be done in the peak of the dry season in Gorongosa and/or after the wildfires, to further enhance visibility of topographic features, outcrops, and exposures of sedimentary rock. It is still too soon to fully understand how much remote sensing and unsupervised learning methods can be generalized to the problem of remote fossil site detection, but with an accuracy of 84.6% and new fossil sites detected the potential is clear.

What we do know, and what we can know about evolutionary processes is constrained by the fossil record. Indeed, palaeontological inference is dependent – as are all historical disciplines – on the contexts that produce the data. The way to avoid biased inferences is thus to find more contexts to sample, so that our data do not increase only in quantity but also in representativeness of the natural and historic processes intricately linked to evolution. Early hominin occupation of humid and watered habitats such as riparian woodlands next to lake margins is well-documented across the basins of the EARS (Cerling *et al.*, 2011; Behrensmeyer & Reed, 2013). But Gorongosa is the first of its kind, a rift valley estuarine and littoral site, partially covered by marine deposits (Habermann *et al.*, 2019). Finding new fossil sites in under-studied African palaeo-biomes of the late Miocene, such as coastal forests in estuaries, is crucial in order to test critical hypotheses related to early hominin evolution in such contexts (Kingdon, 2003; Wrangham, 2005; Joordens *et al.*, 2019). Future studies should use unsupervised learning algorithms coupled with ground-truthing as these are likely to become key tools to identify areas worth prospecting, leading to the discovery of fossil-bearing localities. As these and other computer vision approaches improve, they will directly tackle some of the main limiting factors for palaeontological studies: sample size, geographic gaps, and temporal biases, and thereby allowing substantial progress in the pace and content of palaeontological and palaeoanthropological discoveries.

Acknowledgements

The Palaeo-Primate Project Gorongosa would like to thank the Gorongosa Restoration Project, the National Geographic Society, the John Fell Fund Oxford, and the Leverhulme Trust, for generous support with this interdisciplinary endeavour. We want to thank Dr. René Bobe and Dr. Thomas Püschel for insightful comments on early drafts of the manuscript. We are very grateful to the reviewers, Dr. Anna Behrensmeyer and Dr. Jonah Choiniere, for their insightful comments which helped greatly improve this article. Jd'OC thanks the Portuguese Foundation for Science and Technology (FCT)—Grant SFRH/BD/122306/2016—for supporting his doctoral project, Dr. Jörg Habermann and Nhampoca for all the incredible help during the 2018 field season, and The Boise Trust Fund for supporting the field work in Mozambique. Our work is only possible due to the visionary approach of Greg Carr and the dedicated staff from Gorongosa National Park, guided by Dr. Mateus Mutemba and Pedro Muagara. We are very grateful to all the park rangers, our students, and colleagues across all our institutions who have been very enthusiastic about this project.

5

Geospatial palaeoecology: estimating aquatic and terrestrial fossil abundance in East Lake Turkana

Submitted to *Journal of Human Evolution* on December 27th 2023

Geospatial palaeoecology: estimating aquatic and terrestrial fossil abundance in East Lake Turkana

João d'Oliveira Coelho[1,2], Robert L. Anemone[3], René Bobe[1,4,5], David R. Braun[6], and Susana Carvalho[1,2,4,5]

[1]Primate Models for Behavioural Evolution Lab, Institute of Human Sciences, University of Oxford, Oxford, UK

[2]Centre for Functional Ecology, Universidade de Coimbra, Coimbra, Portugal

[3]Department of Anthropology, University of North Carolina Greensboro, USA

[4]Interdisciplinary Center for Archaeology and Evolution of Human Behaviour (ICArEHB), Universidade do Algarve, Portugal

[5]Gorongosa National Park, Sofala, Mozambique

[6]Center for the Advanced Study of Human Palaeobiology, Department of Anthropology, George Washington University, USA

Abstract

Background: Geospatial palaeontology is a new paradigm combining remote sensing imagery with data mining techniques to increase the likelihood of finding fossiliferous deposits. Despite previous successful attempts, such techniques have yet to be applied to the hominin-bearing fossil sites of Africa. Researchers working in the Koobi Fora Formation of northern Kenya have long interrogated about the geographic patterning of extinct fauna and their respective palaeoenvironments. Here, we attempt to use machine learning techniques to capture palaeoecological patterns through satellite data that may be predictive of palaeoenvironments in the Koobi Fora Formation.

Methods: LANDSAT and SRTM satellite images covering East Turkana were used to obtain spectral, environmental, and topographical variables of interest. We carried out fossil bone walks to sample fossils and measure the relative abundance of aquatic fauna within specific points of interest that match cells in the satellite's grid. These fossil faunal input data were used to construct a Beta regression model predicting past aquatic conditions based on the remote sensing data. The same coordinates were also used to generate a MaxEnt model to predict fossil distribution.

Results: Median predictive error of BetaReg using leave-one-out cross-validation was 11.3%, indicating this approach to be robust at accurately estimating the percentage of aquatic fauna we would find at a random bone walk. MaxEnt obtained an AUC of 90% using an independent test set. Combining BetaReg and MaxEnt outputs leads to an interpretable palaeoenvironmental model. This approach stands out from previous work in the geospatial palaeontology literature because instead of predicting optimal places for surveying, it goes a step further by generating problem-specific palaeoecological reconstruction maps.

Discussion: The high predictive power of data from satellite imagery supports the application of geospatial and machine learning techniques to enhance traditional fieldwork methods in the exploration of fossil localities. The preliminary results of this study encourage future extensions of these methods to address specific palaeontological research questions, such as the use of faunal abundance data to predict the distribution of specific palaeoenvironments.

5.1 Introduction

Geospatial palaeontology is an emergent discipline that uses remote sensing data, GIS and statistical algorithms to model the probability of finding new fossiliferous deposits (Anemone & Conroy, 2018). By utilising the advantages of both satellite imagery and on-site fieldwork, researchers can gain a more comprehensive understanding of the palaeontological sites and the context in which fossils are found (Asfaw *et al.*, 1990; Njau & Hlusko, 2010; Anemone *et al.*, 2011a; Hlusko, 2018). A palaeontological or fossil site, is a locality where a set of fossil occurrences (of any concentration or type) are present and co-located geographically and temporally (DeMiguel *et al.*, 2021). For instance, satellite imagery can be used to identify potential fossil sites and then during fieldwork, researchers can confirm the findings and collect samples to improve the satellite-based models (Emerson & Anemone, 2018). This results in a more efficient use of resources and allows researchers to cover a larger area in a shorter amount of time (Dorans *et al.*, 2020). Geospatial palaeontology research has been applied in Utah and Wyoming to identify new Eocene deposits containing, among other vertebrates, early primates (Conroy, 2014; Emerson et al., 2015). Researchers also applied these techniques to the Pleistocene of Australia (Block *et al.*, 2016), the Triassic and Jurassic of South Africa (Wills *et al.*, 2018), and to the Miocene coastal forests of Mozambique (d'Oliveira Coelho *et al.*, 2021). However, such approaches have yet to be applied to regions known to be rich in hominin-bearing fossil deposits, such as the Omo-Turkana basin.

5.1.1 Geospatial Learning: Supervised vs Unsupervised

In recent years, geospatial techniques have been developed to improve the chances of discovering fossil-bearing deposits (Wills *et al.*, 2018; d'Oliveira Coelho *et al.*, 2021; Ghezzo

et al., 2023). These approaches use satellite imagery (e.g., Conroy *et al.*, 2012), or environmental and topographic variables (e.g., Egeland *et al.*, 2010), or both combined (e.g., Emerson *et al.*, 2015), to train machine learning algorithms to identify patterns associated with fossil-rich outcrops across a region (Oheim, 2007; Malakhov *et al.*, 2009). Machine learning algorithms operate by analysing numerical structures from data (Navega *et al.*, 2015). They iteratively process information, identify underlying patterns, and use these insights to make predictions or decisions (Calder *et al.*, 2022). The learning process allows algorithms to improve their performance, adapting to new data and optimising their ability to solve specific tasks (d'Oliveira Coelho & Curate, 2019), such as identifying fossil-rich deposits in geospatial palaeontology (Emerson & Anemone, 2012). In this paradigm it is optimal to randomly split the dataset into three parts: a training set for model fitting, a validation set for estimating prediction error and model selection, and a test set (i.e., held-out through the entire process) for assessing the generalisation error and overfitting of the final chosen model (Hastie, Tibshirani & Friedman, 2009). This practice ensures robustness and predictive accuracy, marking a key distinction from traditional predictive modelling approaches (James *et al.*, 2013). Two main statistical paradigms are commonly used in geospatial palaeontology: supervised learning and unsupervised learning (Anemone & Conroy, 2018).

Supervised learning uses labelled landcover classes like grassland, wetland, shrubland, forest, roads, cropland, rivers, lakes, and fossil-bearing deposits to train the model (Emerson & Anemone, 2012). Landcover class denotes a distinctive category of observable bio-physical surface features, crucial for classifying Earth's landscapes using remote sensing data (Horning *et al.*, 2010; Wulder *et al.*, 2018; Talukdar *et al.*, 2020). Thus, this approach requires a significant amount of manual pre-processing of the satellite data to label the pixels (e.g., Anemone *et al.*, 2011b) or image objects (e.g., Emerson *et al.*, 2015) with context-dependent landcover classes. This labour-intensive process can be time-consuming and costly, making it challenging to automate or apply to large datasets or projects with limited resources. Moreover, researchers will often have databases of precise GPS coordinates for mapped fossiliferous deposits (e.g., Conroy *et al.*, 2008; Anemone *et al.*, 2011a; Reed *et al.*, 2015; Reed, Barr &

Kappelman, 2018; Bobe & Carvalho, 2019b), but no efficient way of correctly labelling all the other landcover classes. Another limitation of supervised learning is when there are either no known fossil sites in the study area or only a limited number, making it difficult to create an accurate target class with which to train the model (Conroy, 2014). Despite these limitations, supervised learning has been found to be effective in identifying conditions ideal for preservation, exposure, and discovery of fossils in a wide range of geographic and chronological contexts (Oheim, 2007; Block *et al.*, 2016; Ghezzo *et al.*, 2023). One of its main advantages is that it allows for the direct mapping of landcover classes, which can be useful for understanding the distribution of different habitats in the study area and how they may have influenced the preservation and exposure of fossils (Malakhov *et al.*, 2009; Wills *et al.*, 2018). Overall, while supervised learning may be more time-consuming and costly than unsupervised learning, it offers the advantage of being able to directly map multiple landcover classes and incorporate expert knowledge, which might increase accuracy, thus making it a valuable tool in geospatial palaeontology (Anemone & Conroy, 2018).

On the other hand, unsupervised learning groups unlabelled spectral patterns into clusters, without the need for user-defined labels (Conroy *et al.*, 2018). The enhanced generalisation in unsupervised learning is primarily attributed to its independence from predefined landcover classes. These classes often exhibit context-specific characteristics and require extensive knowledge of the study area (Enderle & Weih, 2005). By obviating the requirement for human-guided annotated data and manual feature engineering, unsupervised learning facilitates the development of more adaptable, generalizable, and automated (i.e., computer-guided) protocols for data analysis (Romero, Gatta & Camps-Valls, 2016). One limitation of unsupervised learning is the lack of certainty that any specific cluster generated by the model is actually associated with fossil-bearing deposits, without further validation through fieldwork (e.g. d'Oliveira Coelho *et al.*, 2021) or by testing the model on a different area with known fossil sites, which can be achieved by applying the model to a region where it has not been trained and using that other area as an independent validation set (e.g. Conroy, 2014). Furthermore, it can be challenging to assign meaning to the other clusters that are generated,

and to determine if they are truly representative of underlying patterns in the data (Alloghani *et al.*, 2020). Despite these limitations, unsupervised learning can be a useful tool in the early stages of palaeontological surveying when there are few fossil sites known in the region, since it can identify potential points of interest, as opposed to supervised learning which requires a significant number of labelled examples of the target class (i.e., fossil sites) to train an efficient and accurate model (Conroy *et al.*, 2018; d'Oliveira Coelho *et al.*, 2021).

5.1.2 Learning in the absence of counter-examples

One-class classification (OCC, Moya, Koch & Hostetler, 1993) models provide a third and semi-supervised solution for geospatial fossil prospection. These models only require the coordinates of known fossil-bearing deposits as training data and assume that all unlabelled data comes from a mixed set of locations that may or may not contain fossils. Also known as "concept learning" (Japkowicz, 1999; Tax, 2001), this approach addresses the major difficulty of manual labelling in supervised approaches, while also addressing the lack of explicit targets to detect in unsupervised approaches (Tax & Duin, 2001). Here, we present a novel application of one-class classification models in the field of geospatial palaeontology, which has not been previously explored.

The purpose of a one-class classifier is similar to that of a supervised binary classifier, where new data is classified as belonging to one of two classes based on a model trained from labelled samples (Khan & Madden, 2010). However, the key difference is that the training data of a one-class classifier only contains labelled samples from the class of interest (Seliya, Abdollah Zadeh & Khoshgoftaar, 2021), also known as the positive class, presences or target class which, in this case, are the fossil sites. Collecting a representative training set for the negative class can be costly and time-consuming, making one-class classifiers particularly useful when only the positive class needs to be mapped and when the acquisition of representative labelled data for the negative class is expensive or not possible (Mack & Waske, 2017). In geospatial contexts, this issue is exacerbated by the fact that we often deal with multiclass classification problems, rather than binary ones, which requires labelling a wide range of "negative classes"

that represent a plethora of dynamic and complex landcover types (Conroy, 2014). These might also change across time, making the models difficult to generalise, even for the same region. One-class models are more flexible and thus offer a potential solution to that problem.

5.1.3 Automated palaeoecological reconstructions: taking geospatial palaeontology a step further

Palaeoecologists use various methods to determine what kinds of environments existed in the past (Behrensmeyer, 2006; Andrews, Reynolds & Bobe, 2022). One of the most common methods involves analysing fossil assemblages to identify the types of organisms present, as distinct environments tend to have different types of animals and plants, therefore fossils can act as proxy variables for past environmental conditions (Behrensmeyer, 1975a; Reed, 1997; Bobe, Alemseged & Behrensmeyer, 2007a; Bobe & Leakey, 2009; Fortelius *et al.*, 2016; Baumgartner & Peppe, 2021). Taphonomy is also vital for the reconstruction of past habitats as it explains the underlying processes that shape the preservation of organic remains (Brain, 1974; Behrensmeyer, 1975b, 1978, 1982, 1992; Alemseged, 2003; Patterson *et al.*, 2014). This understanding enables palaeoecologists to interpret biases in fossil assemblages, refining reconstructions for more accurate depictions of ancient environments and landscapes (Brain, Behrensmeyer & Hill, 1980; Behrensmeyer, Gordon & Yanagi, 1986; Behrensmeyer & Reed, 2013; Tappen *et al.*, 2022). Another component of palaeoecological reconstruction involves sediment analysis. Depositional conditions influence a myriad of factors such as presence of particular minerals as well as grain size, sorting, and fabric (Trauth *et al.*, 2005; Habermann *et al.*, 2019). All these factors impact the preservation of materials that are used to reconstruct ancient environments. Pollen and diatom analysis can also be used, as their type and abundance in sediments can help identify the types of plants and algae present, respectively (Bonnefille *et al.*, 2004; Trauth *et al.*, 2007; Owen *et al.*, 2008, 2009, 2011; Westover *et al.*, 2021, p. 20221; Sanchez Goñi, 2024). Additionally, stable isotopes can also assist in reconstructing past environments and the behavioural ecology of organisms that inhabited them (Schoeninger,

Reeser & Hallin, 2003; Cerling, Harris & Passey, 2003; Cerling *et al.*, 2013, 2015; Sponheimer *et al.*, 2013; Roche *et al.*, 2013; Negash *et al.*, 2015, 2020; Patterson *et al.*, 2019; Manthi *et al.*, 2020; Wynn *et al.*, 2020; Lüdecke *et al.*, 2022; Fillion & Harrison, 2023). The ability to estimate water availability in ancient habitats across large regions has significant implications for hominin palaeobiology (Cerling, Bowman & O'Neil, 1988; Levin *et al.*, 2011; Blumenthal *et al.*, 2014, 2017; Barboni *et al.*, 2019; Pontzer *et al.*, 2021), particularly in multi-method studies trying to reconstruct the evolution of basins and associated landscapes (Quinn *et al.*, 2013; Levin, 2015; Patterson *et al.*, 2017b, 2017a; Bobe *et al.*, 2020a; Dumouchel *et al.*, 2021; Villaseñor *et al.*, 2023). Although these methods offer valuable insights at a high resolution for the localities under analysis, they share a common limitation in that they are logistically challenging to implement for large-scale palaeoenvironmental reconstructions.

In this study, we propose a new geospatial approach to determine relative abundance of extinct aquatic and terrestrial species, involving the use of geolocated ratios of aquatic/terrestrial fauna, remote sensed data, and machine learning algorithms. Systematic documentation of faunal composition in a geolocated fossil site provides a comprehensive record of the distribution and relative abundance of different animals (Roach *et al.*, 2016; Bobe *et al.*, 2022). This data can be combined with satellite images and machine learning algorithms as a proxy to identify the relative water availability of past environments based on multispectral reflectance of the soils and topographic variables (Egeland *et al.*, 2010). This approach has the potential to streamline the identification of palaeoenvironments, allowing palaeoecologists to analyse large data sets more efficiently and gain new insights into ancient ecosystems, not just in East Turkana, but also in fossiliferous contexts around the world.

The ability to automatically estimate how well-watered ancient habitats were, across large regions, has important implications for palaeoecological research (Holden *et al.*, 2019; Kutzbach *et al.*, 2020) and human evolution (Joordens *et al.*, 2009, 2011, 2015, 2019; Pontzer *et al.*, 2021). By enabling the rapid analysis of large datasets, our method allows for a more comprehensive understanding of palaeoecological patterns across East Turkana (see also

'FARUBO' in Bobe *et al.*, 2022) (Appendix I). It contributes to the larger field of palaeoanthropology by introducing a new technique to spatially evaluate hydrological conditions of ancient ecosystems and their evolution over time. Overall, our study presents a significant step forward in the automation of palaeontological research via state-of-the-art remote sensing and artificial intelligence technologies. By pioneering this interdisciplinary framework, we establish the field of "geospatial palaeoecology" which unlocks exciting new avenues for exploration and scientific discovery.

5.2 Materials and Methods

5.2.1 Study area

The Koobi Fora Formation (Fm) is present throughout the eastern part of Lake Turkana in northern Kenya (approximate geographic extent: 36.16°W, 3.52°S, 36.53°E, 4.46°N) and includes extensive deposits from the Plio-Pleistocene period (4.3–0.7 Ma) that contain a wide variety of fossilized fauna (Bobe *et al.*, 2022), including hominins (Wood, 1991; Wood & Leakey, 2011), as well as fossilized flora (Bamford, 2017). Presently, East Turkana is a hot and dry region with historic mean annual temperature of 30°C and 200 mm precipitation (Yost *et al.*, 2021). Vegetation is moderately sparse in a region that could be generally characterised as a dry tropical dwarf shrubland. *Commiphora*, *Salvadora,* and *Vachellia* trees and shrubs dominate, along with grasslands that become more abundant in proximity to the margins of Lake Turkana (Bamford, 2017). Riparian woodlands and forests are also present, but are very localized, representing <0.5% of the region (Mbaluka & Brown, 2016).

The Koobi Fora Fm consist of different types of depositional environments, including fluvial, lacustrine, and deltaic palaeoenvironments, with intermittent tuffaceous episodes (Feibel, Brown & McDougall, 1989; Feibel, Harris & Brown, 1990; Feibel, 2011). The fossil-rich parts of the Koobi Fora Fm were mostly lake margins and fluvial areas formed by the palaeo-Omo river during periods when the lake was absent or limited to certain parts of the rift basin (Isaac & Behrensmeyer, 1997). The palaeo-Omo river originated in the Ethiopian highlands and was

likely perennial. Other rivers forming dynamic riverine networks also flowed into the Turkana basin from different directions. Throughout the basin evolution, these fluvial sequences were interrupted by lakes of varying size and duration (Feibel, 1993, 1999). The Koobi Fora Formation's individual members are identified through the underlying tuff layers, which serve as the basis for their nomenclature, e.g., Tulu Bor tuff underlies Tulu Bor Mb (Brown & Feibel, 1986). For our data collection we only targeted exposures of erosional deflated surfaces rich in fossils and belonging to either the Upper Burgi (1.98–1.87 Ma), KBS (1.87–1.56 Ma) or Okote (1.56–1.38 Ma) members of the Koobi Fora Fm, as these have a particularly abundant fossil record (Bobe, 2011) and document an important period in the evolution of *Homo* and *Paranthropus* (Patterson *et al.*, 2017a). Spatially, we focused on the Ileret, Karari, and Koobi Fora regions (Brown & Feibel, 1990) (Appendix I). Our analyses excluded the outlying exposures in the Loiyangalani region, situated south of the contiguous core area of Koobi Fora Fm exposures (Gathogo, Brown & McDougall, 2008).

5.2.2 Layered dataset

All data was cleaned and processed with R version 4.2.1 (R Core Team, 2023). A Landsat 8 image of a northeast section of Turkana with scene ID "LC81690572018036LGN00" dated February 5th, 2018, was downloaded from the USGS Earth Explorer website (https://earthexplorer.usgs.gov/). Due to the large size of the raw satellite data, a rectangular extent that encompasses the majority of East Turkana was cropped (Figure 5.1) to a raster object containing 2362500 cells (resolution: 30×30 m) per layer, within a 2625 km^2 area. This satellite image contains seven electromagnetic bands: ultrablue, blue, green, red, near-infrared (NIR), shortwave infrared 1 (SWIR1), and shortwave infrared 2 (SWIR2). Each of these bands corresponds to a different wavelength of light, and each data point in each band is a 30×30 m geolocated pixel representing the amount of energy reflected or emitted at that wavelength (Roy *et al.*, 2014).

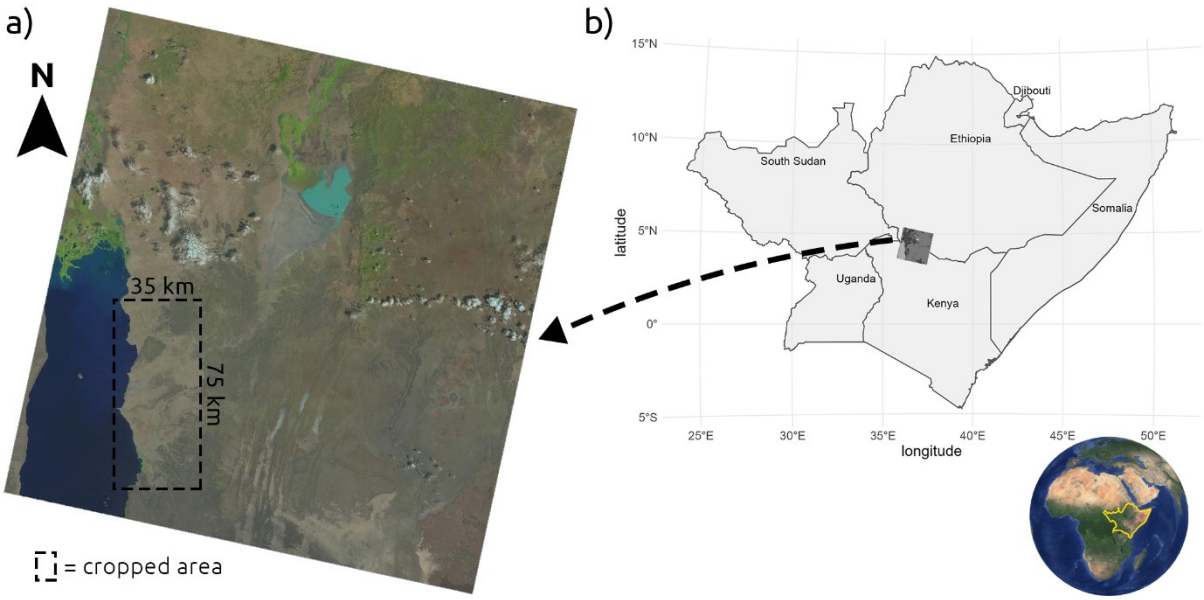


Figure 5.1 – **Study area geographic context**: a) East Turkana as depicted in a preview of scene ID = LC81690572018036LGN00, Landsat 8 image from 2018-Feb-5. The dashed rectangle was the cropped section used in all analyses. Notice the image has no clouds on the region of interest; b) the raw satellite image overlaid on its larger geographic context, covering part of northern Kenya and southern Ethiopia.

Using the Landsat variables, we calculated a normalised difference vegetation index (NDVI) for East Turkana. The NDVI is a proxy measurement for concentrations of green leaf vegetation, and with Landsat 8 images it is calculated as $NDVI = (Band\ 5 - Band\ 4)/(Band\ 5 + Band\ 4)$, where the spectral values of bands 4 and 5 represent the reflectiveness of the red and near-infrared spectra, respectively. This index results in values ranging from -1 to 1, with negative values indicating no vegetation (e.g., water bodies or barren land), values close to zero indicating sparse or stressed vegetation, and values close to 1 indicating healthy vegetation with a high photosynthetic activity (Tucker, 1979; Huang *et al.*, 2021).

Shuttle Radar Topography Mission (SRTM) data (scene ID: n03_e036_1arc_v3) was also downloaded from the USGS Earth Explorer portal (https://earthexplorer.usgs.gov/). Although the SRTM data is primarily a digital elevation model (OpenTopography, 2013), slope and aspect can be calculated from it with the terrain() function from the 'terra' package for R (Hijmans, 2023). Slope is a measure of the steepness of the land surface, which is calculated by measuring the rate of change in elevation between neighbouring points on the landscape (Fleming & Hoffer, 1979; Jones, 1998). It is usually expressed as an angle in degrees, and it

can range from 0 (flat terrain) to 90 degrees (vertical cliff). Aspect, on the other hand, is a measure of the direction that a slope is facing, which is usually expressed as a compass direction or in degrees from 0 to 360 (Ritter, 1987; Malaperdas & Panagiotidis, 2018). In our case, aspect was calculated in radians and further decomposed into two variables, northness or $cos(aspect)$, and eastness or $sin(aspect)$. For predictive modelling purposes, northness and eastness are preferable over aspect, because aspect is really a direction vector in two dimensions, and it presents serious problems as a continuous variable. Aspect is circular and does not follow patterns in a similar way as other continuous variables. As an example 359 degrees is actually closer to 1 degree than 359 is to 356 degrees, however the model will not interpret it in this way (Ilich *et al.*, 2023). Moreover, there is a convention in 'terra' for calculating this variable that makes water and any other flat cells as always facing eastwards by default (i.e., if slope = 0, aspect is set to 0.5*pi radians, or 90 degrees) (Hijmans, 2023). To address this calculation convention and eliminate eastward biases, all instances where $slope = 0$ were readjusted to have corresponding values of 0 in both northness and eastness. Therefore, we obtained two linear continuous variables ranging from -1 to 1, or from south to north in "northness", and from west to east in "eastness". After extracting the four SRTM-derived topographic features (elevation, slope, northness and eastness), these were combined into a raster stack object. The projectRaster() function from the 'raster' package (Hijmans, 2022) was used to project Landsat's coordinate reference system onto the SRTM stack. Then, the SRTM topographic data was aligned to the cropped Landsat 8 stack using the resample() function with the predefined bilinear interpolation parameter from the 'terra' package (Hijmans, 2023).

The final processing step was to join the Landsat 8 stack, the NDVI variable, and the SRTM stack into a unified raster stack object. This multilayer object is equivalent to the independent variables in a classic statistical analysis (Figure 5.2). To summarise, the dataset is composed of a layered raster object of 2625 km^2 with a pixel resolution of 30×30 m, cropped from the Landsat 8 and SRTM open-access libraries of satellite imagery. These images capture a total of twelve spectral, environmental, and topographical variables for the East Turkana region.

From these satellite resources we obtained the following variables: seven bands from the electromagnetic spectrum, vegetation (NDVI), and topography (elevation, slope, northness and eastness). The 12-layered raster stack is projected in metres to the WGS 84 / UTM zone 37N (EPSG: 32637) coordinate reference system, with an extent of xmin: 185000; xmax: 220000; ymin: 405000; ymax: 480000 metres, representing the W, E, S, and N limits, respectively.

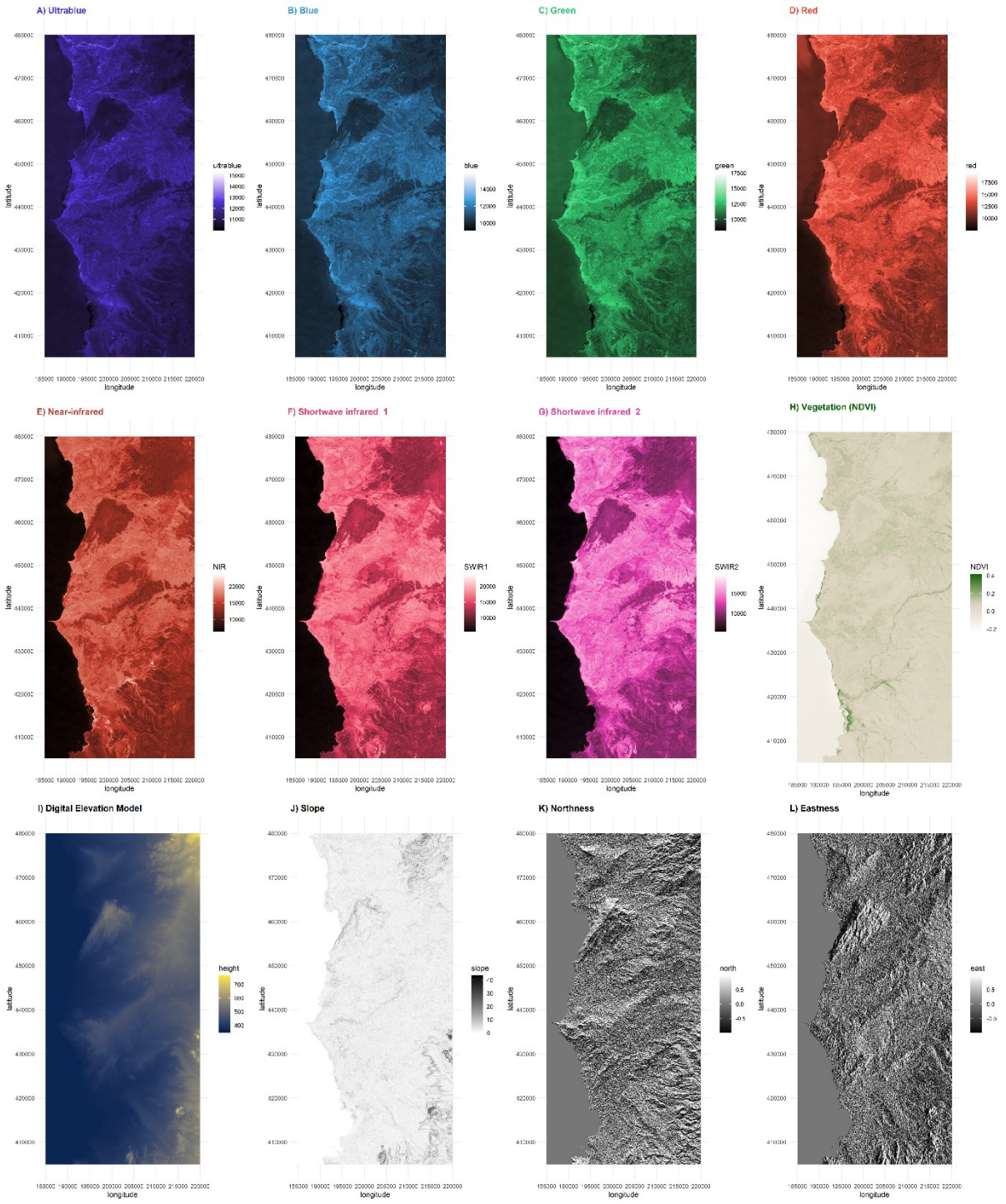


Figure 5.2 – **All the layers of the stacked dataset used during training for predictive modelling**.

5.2.3 Data collection in the field: bone walks

During July 2019, multiple surface surveys were conducted in three subregions of East Turkana, namely Ileret (Areas 1, 1A, 8A, and 8B), Karari (Area 105), and Koobi Fora (Area 103). The "Palaeontological Collecting Areas" are discrete geographic units at East Turkana (Brown & Feibel, 1990), and are numbered from 1 to 263 (see Appendix *in* Bobe et al 2022, for a detailed description). Geographic coordinates of each point of interest (POI) were recorded with a handheld Bad Elf GPS Pro. A POI was any cell of the satellite grid that had fossil occurrences, indicating optimal conditions for a systematic fossil survey. These conditions included the absence of stratigraphic boundaries along the survey transect, which was verified using previously published geological maps. Fossil surveys used a total collection method, known informally as "bone walks" in which all identifiable fossilised invertebrates and vertebrate bones and teeth observed on the ground surface were recorded (Behrensmeyer, 1985). Researchers conducted a bone walk to sample faunal abundance within the boundaries of each POI's survey area (30×30 m cell). Each bone walk included four to eight researchers standing at arms' length apart from one another and moving in a straight line across the sampling area while scanning for fossils. Topographic context is selected to minimise contamination from other stratigraphic layers. We relied on geological maps and the expertise of senior colleagues and field geologists from the Koobi Fora Field School (KFFS) to guarantee each bone walk was limited to a single sedimentary deposit. We also verified and confirmed each time that we did not leave a cell during a bone walk by inspecting a tablet with the grid of the Landsat 8 cells superimposed onto high resolution satellite images of East Turkana, connected to a 1-m-accurate GPS device, the Bad Elf GPS Pro, via Bluetooth.

Identifiable fossils were classified into one of the following categories: terrestrial mammal, Hippopotamidae, 'reptile' (crocodiles or turtles), fish, or invertebrate. Hippopotamidae have their own class because they are a semi-aquatic mammal (Behrensmeyer, 1975a; Kingdon, 2019). Recording every single fossil reduces preferential collecting bias (e.g., targeting primates), and leads to a more complete picture of the faunal composition, which is vital for

obtaining palaeoecological accurate data (Roach *et al.*, 2016; Bobe *et al.*, 2020a). Since fossilised skeletal remains found during a bone walk may include fragments from a single individual, we minimise this potential bias by counting skeletal elements that refit as one entry (i.e., the minimum number of elements or MNE) in the tally (Behrensmeyer & Barry, 2005), but all other fragments were tallied individually. For each POI sampled in the bone walks, aquatic fossil counts were summed and divided by total fossil counts to yield a percent value of aquatic fauna per point of interest (Figure 5.3). After stacking these data points obtained in the field with the multispectral, ecological, and topographic features extracted from satellite images, we attained a final dataset totalling 13 variables. It is possible that some POIs may have been sampled previously, and in certain cases, specimens may have been selectively collected, which could impact the accuracy of the results. To reduce this sampling bias we avoided the grid cells that contained previously recorded coordinates from the PaleoTurkana (Bobe & Carvalho, 2019b; Bobe *et al.*, 2022) or the KFRTP (Patterson *et al.*, 2019) databases.

5.2.4 BetaReg: Aquatic-to-terrestrial ratio

The aquatic-ratio based on relative faunal abundance data was selected as the target variable to train a Beta regression model (Ferrari & Cribari-Neto, 2004) predicting the distribution of aquatic and terrestrial palaeoenvironments using multispectral reflectance of the soils, and modern environmental and topographic data. Beta regression (BetaReg) is a statistical method used to model continuous variables that are bounded between zero and one (or 0% and 100%), such as rates, proportions, or percentages. The beta distribution via maximum likelihood is used to model the dependent variable y, and the model includes predictors and parameters that estimate the mean and variance of the outcome variable (Grün, Kosmidis & Zeileis, 2012). We employed the betareg() function available in the 'betareg' R package (Cribari-Neto & Zeileis, 2010), which implements the beta regression as proposed by Ferrari and Cribari-Neto (2004) with extensions by Simas et al (2010). Model accuracy was evaluated using a standard technique for out-of-sample testing (Stone, 1974).

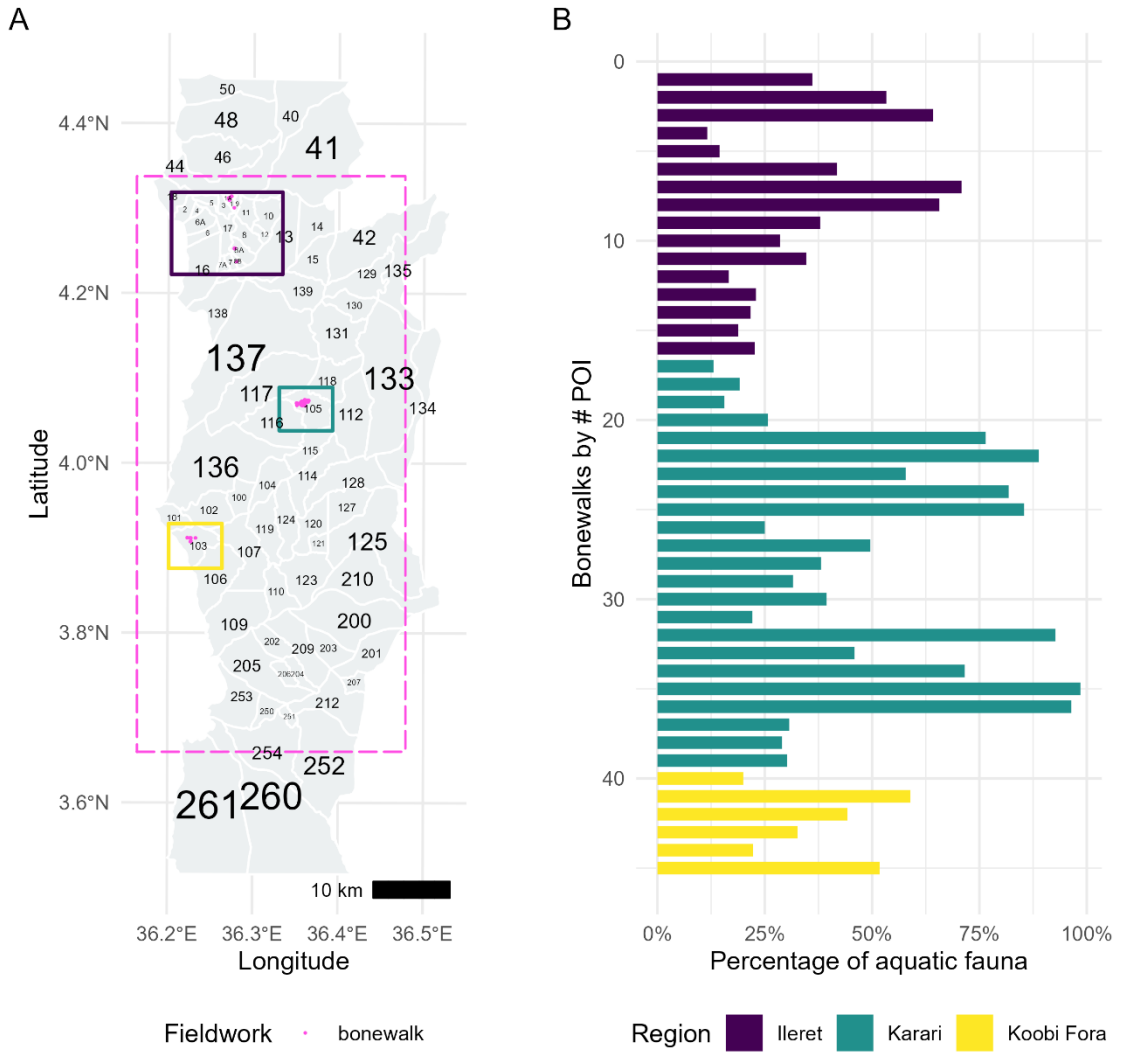


Figure 5.3 – **Bonewalks raw data**: A) Geocoordinates of the points of interest (POI) over a map of the Paleontological Collection Areas (Brown and Feibel, 1990, revised by Bobe et al., 2022), also including the training extent of the models in a pink dashed rectangle, and three smaller rectangles with the Ileret (purple), Karari (teal), and Koobi Fora (yellow) sub-regions; B) Ratio of aquatic-to-terrestrial fauna sampled by systematic bone walks in each POI.

5.2.5 MaxEnt: Fossil distribution

Using the same coordinates of the points of interest used in the previous model, an OCC MaxEnt model (Li & Guo, 2010) was then constructed to identify sites with spectral, environmental, and topographical features like those observed during sampling efforts (bone walk data), thus targeting sites with ideal conditions for fossil deposition, preservation, and exposure. MaxEnt is a popular machine learning algorithm, mainly used by ecologists to model species niches and distributions using occurrence data (Elith *et al.*, 2011). For the target class,

instead of using the aquatic ratio values, we used only the coordinates of the bonewalks. Therefore, in this model, cells represent the locations where bone walks were conducted, or in other words, where high fossil density was observed and recorded. MaxEnt (Phillips, Dudík & Schapire, 2004; Phillips, Anderson & Schapire, 2006; Phillips *et al.*, 2009, 2017) can be used to build a model of the potential distribution of high fossil density based on the environmental variables in the presence and background cells. The model uses a machine learning algorithm to identify the relationship between the satellite-derived variables and high fossil density. We used the popular dismo::maxent() implementation of the algorithm coded by Steven Phillips and Robert J. Hijmans that is available in the 'dismo' package for R (Hijmans *et al.*, 2022).

To evaluate model performance, we used an independent dataset that was not part of model training or parameterization. In this case, the PaleoTurkana database (PTdb) was employed for external validation (Bobe *et al.*, 2022). The PTdb contains presence points for a set of georeferenced fossils, which were utilised to validate a MaxEnt model developed with satellite-data and bone walk coordinates. The predicted probabilities were then compared to the observed presence of fossils in the database plus an equal number of randomly generated absences, and model performance was assessed using various evaluation metrics such as confusion matrices, area under the receiver operating characteristic curve (AUC), true positive rate (TPR), negative predictive value (NPV), and others (Hastie *et al.*, 2009). The evaluation metrics provide an estimate of the accuracy of the MaxEnt model and its ability to predict fossil distribution. The use of independent validation data helps to assess the generalizability of the model and its potential for making reliable predictions in the future and in less explored areas of the region (James *et al.*, 2013).

5.2.6 PalaeoEnv: Filtered ensemble

The final "PalaeoEnv" model is a combination of the Beta regression and maximum entropy models, which predicted aquatic-to-terrestrial environmental ratio and high fossil density, respectively. To limit the palaeoecological reconstruction of BetaReg to the fossiliferous areas,

the model excluded all pixels with a fossil-yielding likelihood of 25% or lower, as determined by the MaxEnt model. This threshold of 25% was selected because it was found to be the optimal threshold between the performance metrics of sensitivity and specificity during the model training. Sensitivity refers to the proportion of true positives (fossils present) that are correctly identified by the model, while specificity refers to the proportion of true negatives (background cells) that are correctly identified by the model (Hastie *et al.*, 2009; Powers, 2011). The equal training sensitivity and specificity cumulative threshold is determined by calculating the sensitivity and specificity for all possible threshold values and identifying the threshold value that maximizes the cumulative sum of sensitivity and specificity (Elith *et al.*, 2011). This approach eliminated BetaReg outputs that were unlikely to contain fossils or were of limited interest for palaeoecological reconstruction, such as thickly vegetated shrublands, modern water bodies, Holocene exposures, clay pans, alluvial deposits and lagas (ephemeral streams), among others. This helped to ensure that only the exposed fossiliferous sediments of interest were included in the final reconstruction. This step played a critical role in enhancing both the accuracy and interpretability of the algorithmically generated palaeoecological outputs.

5.3 Results

5.3.1 BetaReg results

The Beta regression model (Figure 5.4 A) was fitted to predict the aquatic ratio (outcome variable) using eleven satellite-derived predictor variables. The model used a logit link function for the mean model and an identity link function for the precision model (Grün *et al.*, 2012). The standardised weighted residuals ranged from -2.0713 to 2.4650 with a median of -0.1070, indicating that the model has not under- or over-predicted the outcome variable (Ferrari & Cribari-Neto, 2004). The type of estimator used in the model was maximum likelihood, and the log-likelihood was 30.78 with 14 degrees of freedom, indicating a good fit. The pseudo-R-squared value was 70.23%, indicating that the model explained a significant amount of the

variance in the outcome variable (Hastie *et al.*, 2009). The model was iterated 1364 times using the BFGS algorithm and 16 times using the Fisher scoring algorithm to find the parameter estimates that maximise the likelihood function (Broyden, 1970; Goldfarb, 1970; Shanno, 1970; Fletcher, 1970). The φ-coefficient in the precision model had a positive estimate of 10.927 ($p < 0.001$), indicating that the model accounts for overdispersion in the data (Cribari-Neto & Zeileis, 2010).

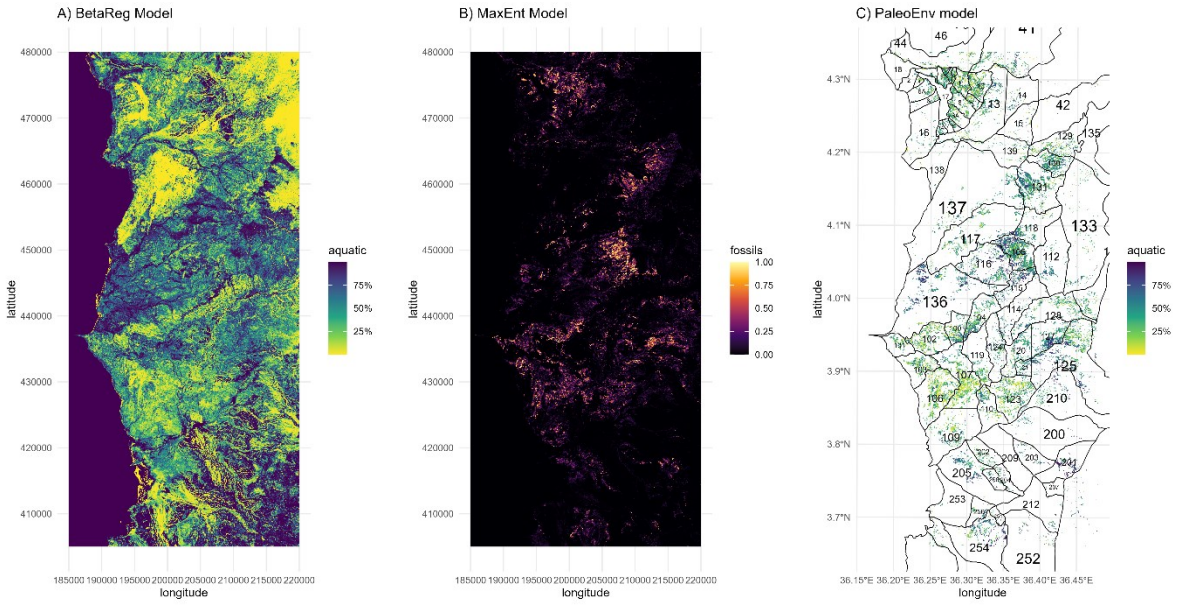


Figure 5.4 – **Outputs of the main models for the East Turkana region**: A) aquatic-to-terrestrial ratio predictions; B) estimated distribution of fossils; C) Final paleoenvironmental reconstruction based on BetaReg's output filtered by MaxEnt.

The coefficients of the mean model (intercept and predictors) indicate the effect of each predictor on the outcome variable after controlling for the other predictors (Table 5.1). The intercept had a positive estimate of 0.72 ($p < 0.001$), which represents the expected aquatic ratio when all the predictive raster layers are equal to zero (i.e., if in a hypothetical cell, all variables = 0, such a cell would be classified as 72% aquatic). The predictor variables that had a statistically significant effect on the aquatic ratio were blue ($p = 0.0011$), green ($p = 0.0025$), red ($p = 0.0036$), near-infrared ($p = 0.0021$), SWIR1 ($p = 0.0002$), SWIR2 ($p = 0.0073$), vegetation index ($p = 0.0027$), and slope ($p = 0.0008$). Ultrablue, elevation, northness and eastness did not have a statistically significant effect when estimating aquatic ratio.

Table 5.1 – BetaReg table of coefficients and goodness-of-fit metrics.

Variables	**Estimate**	**Std. Error**	**z value**	**Pr(>|z|)**
(Intercept)	71.50524	20.55396	3.4789	0.00001
ultrablue	0.00208	0.00356	0.58332	0.55968
blue	-0.00916	0.0028	-3.26792	0.00108
green	0.00839	0.00278	3.01902	0.00254
red	-0.03684	0.01267	-2.9085	0.00363
NIR	0.0316	0.01027	3.07773	0.00209
SWIR1	-0.00361	0.00096	-3.76549	0.00017
SWIR2	0.00246	0.00092	2.68318	0.00729
vegetation	-908.9769	303.7735	-2.99228	0.00277
elevation	0.00231	0.00763	0.30321	0.76173
slope	0.2381	0.07126	3.3413	0.00083
northness	-0.2026	0.22436	-0.90302	0.36652
eastness	0.03824	0.19623	0.19488	0.84549
Precision				
φ (phi)	10.92677	2.23777	4.88288	0.000001

To evaluate the accuracy of the model, we conducted leave-one-out cross-validation (LOOCV) by iteratively testing each observation against the model (Molinaro, Simon & Pfeiffer, 2005; Hastie *et al.*, 2009). The resulting LOOCV median error for estimating aquatic ratios was 11.30% (IQR: 6.03–25.01%) across the entire range of possible errors (0–100%). This level of percent agreement ($1 - error$ = 89.70%) under cross-validation is indicative of a precise and reliable model that can be confidently applied for further analyses and predictions (Extended Data Fig. S1).

5.3.2 MaxEnt results

The MaxEnt model identified the most suitable locations to survey for fossils across East Turkana (Figure 5.4 B). This model achieved a training AUC (Area Under the Curve) of 98.91%, which indicates a highly accurate predictive performance (Phillips *et al.*, 2017). The most important geospatial variables for predicting fossil distribution across East Turkana were near-infrared (contributing 33.95%), SWIR2 (27.14%), ultrablue (23.37%), and elevation (6.82%). The permutation importance of the variables showed similar results, with near-infrared (27.96%), SWIR2 (37.54%), ultrablue (27.58%), and elevation (4.53%) contributing the most towards optimal modelling of fossil hot-spots. Algorithmic run terminated after 500

iterations and had a high regularised training gain of 2.7186 and an unregularized training gain of 3.3472, suggesting the model is able to accurately capture the relationships between the predictor variables and the presence of fossil sites. Finally, the model provided different threshold values for presence probability, with a minimum training presence cumulative threshold of 21.01, a 10% percentile training presence cumulative threshold of 33.34, and an equal training sensitivity and specificity cumulative threshold of 23.96. Within an OCC framework, these thresholds are set to the values that provide an equal balance between correctly identifying sites as present or absent, while minimising the number of errors (Li & Guo, 2010). These values can be useful for setting a threshold in a practical application of the model. Response curves display the impact of individual variables on MaxEnt predictions, with each curve representing a MaxEnt model using a single variable (Extended Data Fig. S2), but they can also show its effect on predicted suitability while accounting for dependencies with other variables in the final model (Extended Data Fig. S3).

The testing of MaxEnt predictions against an independent dataset is important for assessing the accuracy and reliability of the model in predicting the distribution of fossils. When evaluating the performance of MaxEnt predictions using the PaleoTurkana database (Bobe & Carvalho, 2019b) for an hold-out test of the model, we obtained a testing AUC of 90.60%, sensitivity of 85.97% and an NPV of 85.22% (Figure 5.5). In the context of OCC models, where there is only presence data available, sensitivity and negative predictive value (NPV) are the preferred metrics to compare models (Fitzgibbon, Pisut & Fleisher, 2022). This is because they are the only two metrics that do not rely on false positives estimates, a misleading metric considering absence data was randomly generated. Sensitivity, also known as true positive rate (TPR), measures the proportion of true presences that are correctly classified by the model, while NPV measures the proportion of true absences that are correctly classified. These metrics provide valuable insights into the performance of the model and help to ensure that the predictions are robust and reliable for use in further research and analysis of the ecological and evolutionary processes that have shaped the Turkana Basin over time.

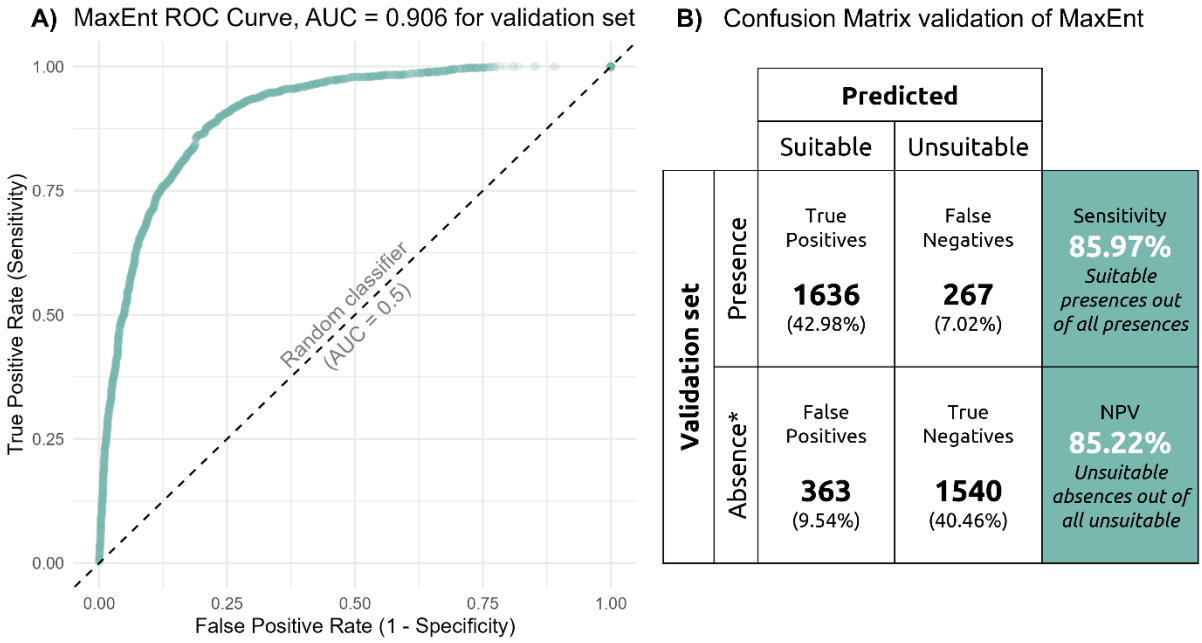


Figure 5.5 – **A test of the MaxEnt model using 1903 georeferenced fossil presences extracted from the PaleoTurkana database** (Bobe et al., 2022); * - absences were generated by randomly selecting another set of 1903 xy points across the map.

5.3.3 BetaReg vs MaxEnt

Using two different models for addressing two different palaeontological questions, such as Beta regression for estimating the percentage of aquatic fauna and maximum entropy for detecting fossil-rich areas, has yielded an important new insight. It has been observed that the most relevant geospatial variables for each problem are markedly different (Figure 5.6). On one hand, spectral bands SWIR1 and blue, as well as slope, contributed the most to generate the BetaReg model and estimate aquatic ratios (Figure 5.6 A). On the other hand, the variables that contributed the most to the MaxEnt model and therefore, finding fossils, were spectral bands near-infrared, SWIR2 and ultrablue, followed by elevation (Figure 5.6 B). While in the BetaReg model the red-green-blue (RGB) or visible bands contributed considerably (R = 11.66%, G = 11.22%, B = 12.27%), in MaxEnt's fossil-detection these were almost completely discarded by the likelihood estimators (combined 0.3% contribution). Similarly, the vegetation index was an important feature for habitat reconstruction (12.21%), but it was not informative at all for fossil distribution prediction. However, this is likely due to the dominance of NIR in the MaxEnt model which is also a proxy for vegetation. MaxEnt relied on most of topographic

variables for fossil detection (combined 15.04% contribution), while in BetaReg, slope is the only topographic feature of relevance (13.03%). By using a MaxEnt-derived threshold to filter the output of BetaReg, we generated a third model—PalaeoEnv—that effectively combines the strengths of both approaches (Figure 5.4 C). This resulted in significantly improved interpretability, as the model can now quickly and accurately remove areas with a low probability of containing fossils. The use of an ensemble approach, as demonstrated in Figure 5.4 C, provides a more reliable palaeoenvironmental reconstruction. This is because BetaReg alone would attempt to estimate any pixel it is presented with, whereas PalaeoEnv, the combination of BetaReg and MaxEnt, assesses only the palaeoecological conditions of cells representing exposed sediments likely to be fossiliferous.

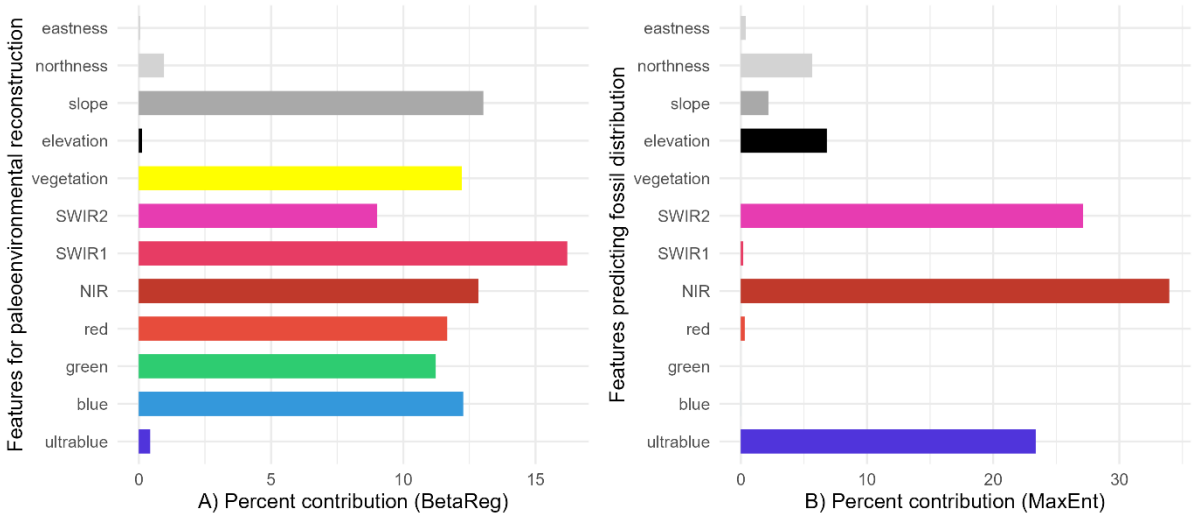


Figure 5.6 – **Comparison of variable importance metrics** for A) BetaReg and B) Maxent, as calculated by percent contribution, as defined in varImp() function from R (Liaw & Wiener, 2002).

5.3.4 Ileret

Research efforts in Ileret were conducted in areas 1A, 1, 8A, and 8B, resulting in a total of 16 bone walks in this region. Percentage of aquatic faunal input was calculated from the tallies and ranged from 11.61 to 70.83% with a mean of 35.12% (Figure 5.3 B). The Beta regression approach indicated the north, west, and southeast of Ileret as having a stronger spectral signal for wetter past environments compared to the rest of the region (Figure 5.7 A).

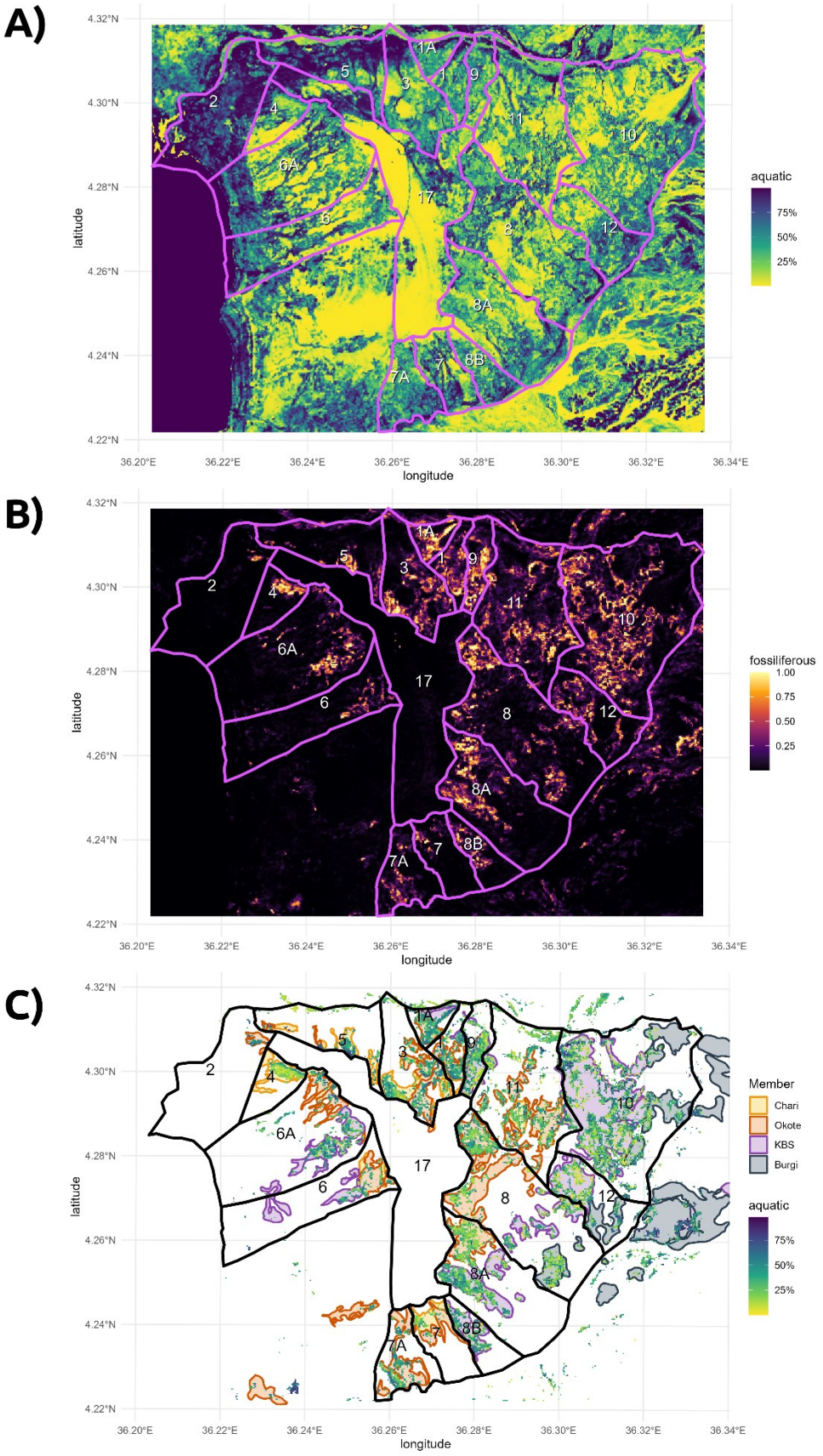


Figure 5.7 – **Predictive modelling of Ileret**: A) BetaReg with raw output before masking; B) MaxEnt model predicting exposure of fossiliferous deposits; C) PaleoEnv model overlapped by the geological members of the Koobi Fora Fm (Gathogo, 2003; Gathogo & Brown, 2006).

This is particularly true for areas 1A, 1, 2 and 5 that when filtered by the MaxEnt threshold, so that only densely fossiliferous predictions remain, provide a very clear aquatic signal (Table 5.2). MaxEnt also predicts Area 1A to be the densest area in terms of surface fossils in all East Turkana (Figure 5.7 B). The adjacent Area 3 is predicted to be palaeoecologically similar, but slightly drier and with a patchier distribution of fossils. Areas 6 and 6A are also reconstructed as well-watered habitats but are only fossil-bearing towards their easternmost sides, fossil density in Area 6 is expected to be notably low. Areas 1, 9, 10, and 11 are predicted to be overall patchier in terms of fossil finds, but with a relatively higher fossil density in their southern parts, although Area 10 also seems particularly fossiliferous in its northwest corner. Areas 8, 8A, and 8B show a mixed terrestrial-aquatic signal and are predicted to be particularly fossiliferous in their north-western sections. Area 12 seems to be particularly fossiliferous close to its southern border with Area 8, but also has some strong predictions of well-watered fossil sites in its east. To the east of Area 12, in Area 13 (only partially depicted), the PalaeoEnv model (Figure 5.7 C) also exhibits a patch expected to be particularly fossiliferous and wet. In the south, Area 7 exhibits an overall terrestrial trend, but MaxEnt indicates it to be very sparse in fossils, while Area 7A shows a wetter trend and a clearly higher fossil density extending towards its southernmost edge. The MaxEnt approach also estimates Area 17 to be completely unfossiliferous, and Area 2 to be almost entirely devoid of fossils (<1% density). Finally, there is a relatively large continuous patch on the northeast section of Area 4 estimated to be fossiliferous while having the driest exposed palaeoenvironments out of all Ileret according to the BetaReg and PalaeoEnv models (Table 5.2; Figure 5.7; Figure 5.8).

5.3.5 Karari

In Karari, we conducted all our sampling at Area 105, and we were able to sample more extreme aquatic environments. A total of 23 bonewalks resulted in ratios of aquatic faunal inputs ranging from 13.04–98.54% (mean = 50.64%). The Beta regression model predicts that a significant portion of the northwest of Area 105, as well as some patches in the southwest, have a very high likelihood of being aquatic, with most cells estimated as >75% aquatic (Figure

5.9 A). The central part of this region of the Karari ridge shows a very different pattern with an outer ring-like structure of mixed habitats (~50% aquatic), surrounding a drier core predicted to be mostly terrestrial (<25% aquatic).

Moreover, the MaxEnt model estimates that Karari is the most fossil-bearing of the three subregions analysed (Figure 5.9 B). With the exception of its eastern section, the northernmost rim, and a southwest corner, which were modelled as non-fossiliferous, the majority of Area 105 was predicted to have a high density of fossils (41.69% of its cells, Table 5.2). On the southeast corner of Area 105 there is a large U-shaped cluster of cells estimated to be highly fossiliferous mixed habitats (Figure 5.9 C). Additionally, Figure 5.9 also illustrate a significant portion of the eastern side of Area 116, located west of Area 105, which contains some sparse clusters of cells estimated by the models as highly fossiliferous and particularly aquatic. In fact, according to the PalaeoEnv model, Area 116 is by far the most aquatic in all of East Turkana (Figure 5.8), with a 59% (IQR: 40-77 %) predicted aquatic ratio (Table 5.2).

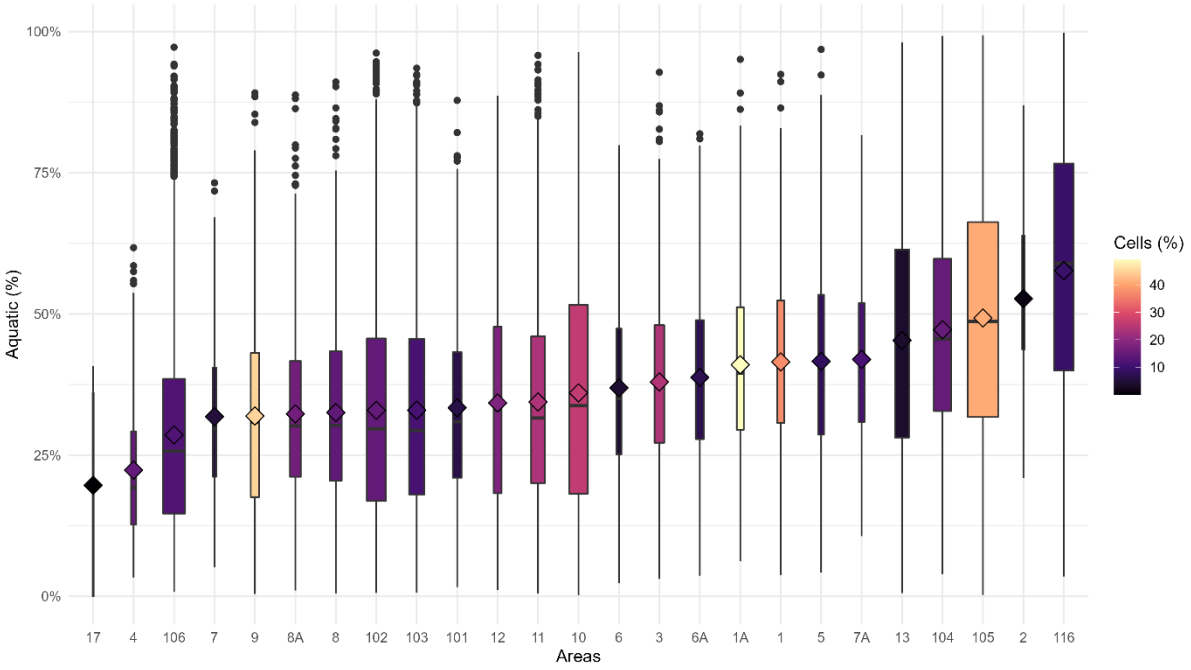


Figure 5.8 – **Boxplot of PaleoEnv model outputs** (BetaReg predictions after MaxEnt masking). Each box width is relative to the total number of cells after filtering (i.e., total fossiliferous pixels). Fill colour is the ratio of cells remaining by the total cells in each area (i.e., fossiliferous density). Diamonds are average means; and boxes are interquartile of aquatic ratio (25%; median; and 75%). Boxes are ordered from BetaReg's median prediction of most terrestrial to most aquatic (after filtering by MaxEnt).

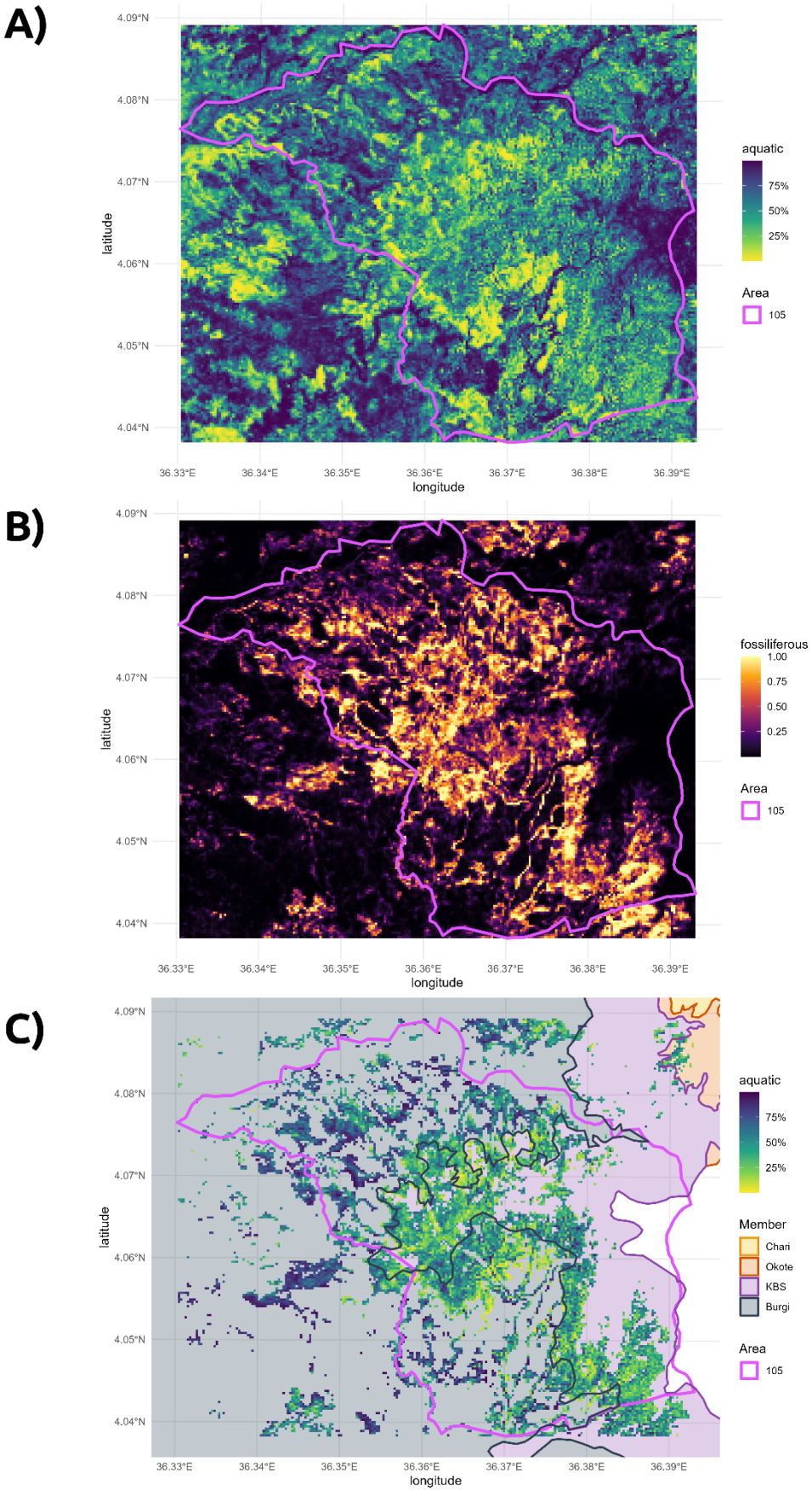


Figure 5.9 – **Predictive models of Karari's Area 105**. A) BetaReg output, before masking; B) MaxEnt model predicting exposure of fossiliferous deposits; C) PaleoEnv model with geological layers.

Table 5.2 – Descriptive statistics for the PalaeoEnv model, with Min to Max columns representing filtered BetaReg estimates of aquatic ratio; Empty is the total cells after MaxEnt masking; Total all the cells that exist in an area (without masking); Density is how many cells are fossiliferous using a MaxEnt predictive threshold of 25%.

Area	Min	LQ	Median	Mean	UQ	Max	Empty	Total	Density
1A	6.19	29.48	39.51	41	51.2	95.08	521	1028	49.32
9	0.42	17.57	30.81	31.92	43.12	89.14	869	1579	44.97
105	0.25	31.74	48.67	49.28	66.26	99.34	13728	23132	40.65
1	3.76	30.71	41.43	41.49	52.35	92.42	902	1436	37.19
10	0.15	18.18	33.76	36.01	51.58	96.39	10281	13894	26
3	3.07	27.19	37.92	37.95	48.01	92.79	3060	4019	23.86
11	0.52	20.04	31.57	34.41	46.02	95.79	6379	8335	23.47
12	1.12	18.24	32.97	34.22	47.74	88.62	2827	3452	18.11
8A	1.04	21.16	30.16	32.28	41.66	88.77	6192	7395	16.27
4	3.33	12.7	19.21	22.34	29.19	61.73	1526	1792	14.84
104	3.94	32.79	45.62	47.2	59.77	99.24	17745	20821	14.77
102	0.59	16.89	29.67	32.93	45.65	96.19	21182	24776	14.51
8	0.54	20.48	30.29	32.53	43.38	91.07	8805	10242	14.03
106	0.82	14.65	25.69	28.56	38.52	97.23	35754	40739	12.24
7A	10.66	30.84	40.98	41.95	51.94	81.64	2442	2756	11.39
103	0.64	18.03	29.38	32.95	45.57	93.52	18720	21076	11.18
116	3.5	40.01	58.95	57.68	76.62	99.79	38041	41947	9.31
5	4.2	28.62	40.98	41.61	53.39	96.84	3720	4058	8.33
6A	3.66	27.83	38.56	38.76	48.9	81.9	9080	9772	7.08
101	1.64	20.99	30.92	33.39	43.23	87.81	11643	12439	6.4
7	5.15	21.16	29.62	31.82	40.51	73.22	2330	2461	5.32
6	2.3	25.14	35.03	36.91	47.4	79.88	5949	6196	3.99
13	0.57	28.1	44.7	45.32	61.42	98.11	50662	52618	3.72
2	20.97	43.7	51.28	52.7	63.9	86.97	6456	6513	0.88
17	0	0	22.18	19.65	36.03	40.78	12485	12493	0.06

5.3.6 Koobi Fora

Close to Koobi Fora Base Camp, in Area 103, we collected a total of 6 bone walks (min = 20.00%; mean = 38.29%; max = 58.90%) over relatively fossiliferous POIs (Figure 5.3). BetaReg modelled a southwest-northeast gradient of aquatic to terrestrial palaeoenvironments (Figure 5.10 A), and it outputs an overall greater terrestrial signal (Figure 5.8) when compared to most areas analysed (Table 5.2). On the other hand, the MaxEnt model for high fossil density shows a smaller optimal prospection area relative to the other subregions analysed (Figure 5.10 B), with only 11.18% of the satellite cells in Area 103 predicted as rich in fossils.

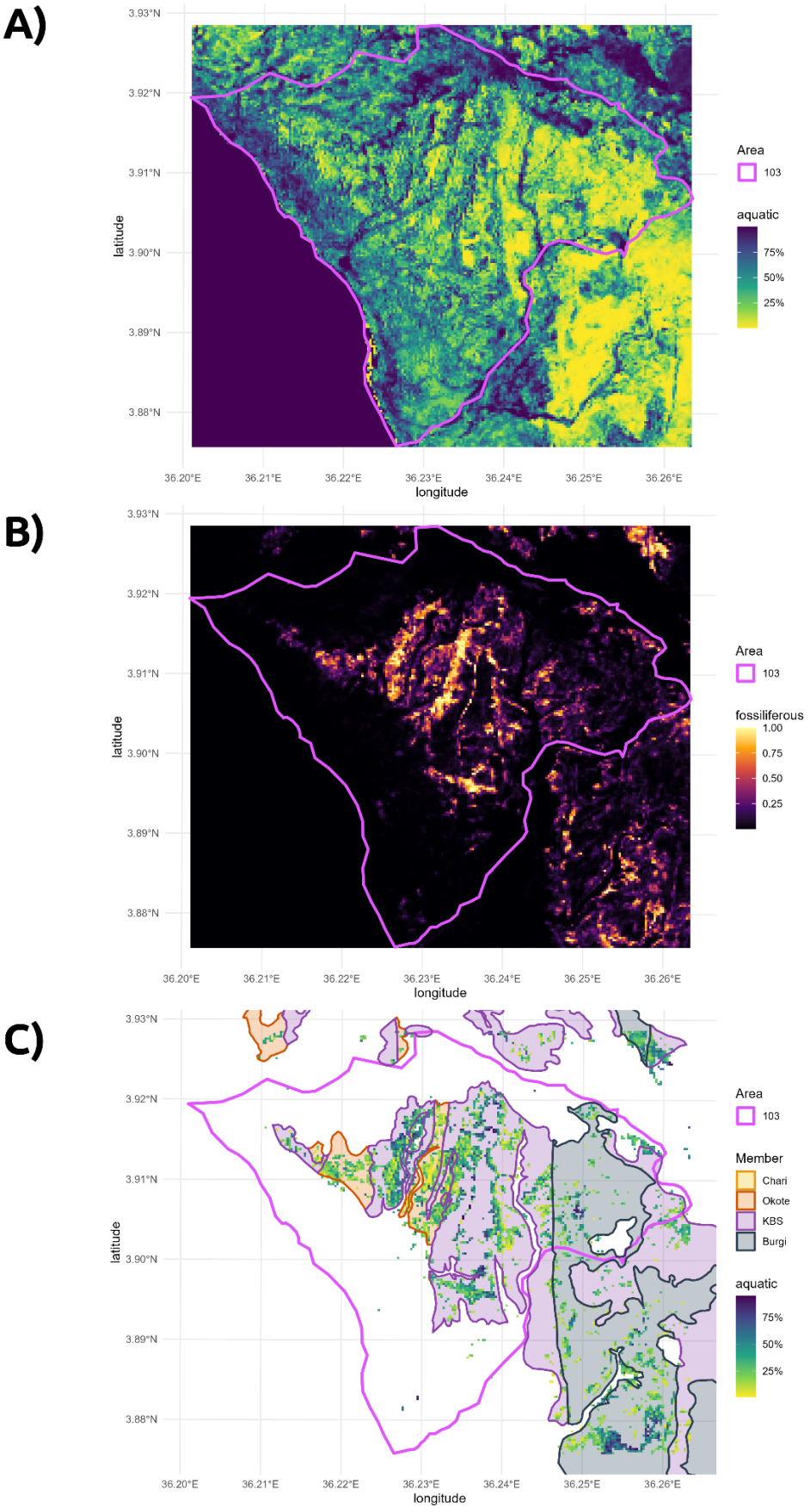


Figure 5.10 – **Predictive models of Koobi Fora's Area 103**. A) BetaReg with raw output, before masking; B) MaxEnt model predicting fossiliferous deposits; C) PaleoEnv with geological layers.

In the case of Area 103, its southern, western, and northern edges are predicted to be completely unfossiliferous (Figure 5.10 B). However, its central and (to a lesser degree) eastern portions are predicted to be rich in fossils. In the PalaeoEnv model a pattern of central corridors running SW-NE emerges (Figure 5.10 C). These were predicted to be rich in terrestrial fossil fauna, with the occasional scattered cells predicting very aquatic environments, particularly at the peripheries and terminations of the corridors.

In contrast to Ileret, where terrestrial predictions were more likely to be correlated with lower to zero fossil density, the results here indicate that in the Koobi Fora ridge subregion, it is instead the cells estimated to be aquatic that are more associated with non-fossiliferous surfaces. Area 106 is also partially illustrated to the southeast of Area 103 and shows some densely fossiliferous and aquatic predictions (Figure 5.10 C), possibly palaeo-lake shores or lacustrine deposits. However, the majority of Area 106 (non-depicted) is predicted to be sparsely fossiliferous and terrestrial (Figure 5.8; Table 5.2).

5.4. Discussion

5.4.1 Remote palaeoenvironmental reconstruction: spatiotemporal patterning

In this work we introduced the "aquatic-to-terrestrial ratio" concept which can be described as a quantitative palaeoenvironmental feature of the past landscape that reflects the relative abundance of open standing water bodies based on the composition of the palaeofauna. This ratio can be determined by analysing the fossil record and comparing the number of aquatic to terrestrial specimens. A high ratio of aquatic to terrestrial organisms would indicate that the landscape was dominated by habitats such as deltas and lakes, where standing water occurs during the majority of the year. On the other hand, a low ratio of aquatic to terrestrial organisms would indicate that the landscape was dominated by relatively drier habitats, such as shrublands and grassland floodplains. This means that intermediate values are likely indicative of intermediate ecologies, such as distributary channels, wetland forests, and riparian woodlands, among others. Surface water was a critical resource in past ecosystems, just as it is today

(Kihwele *et al.*, 2020), and understanding the water requirements of extinct fauna is essential for accurate palaeoenvironmental reconstructions (Maslin *et al.*, 2014; Quinn, 2015; Hopley *et al.*, 2023).

Variations in water dependence among different animal species have been studied to gain insight into the composition and dynamics of ancient ecosystems. Although our approach does not provide as fine a resolution as in ecomorphology (Barr, 2015, 2018; Forrest *et al.*, 2018), mammal community structure analysis (Kovarovic, Su & Lintulaakso, 2018; Du & Alemseged, 2018), or ecometrics (Fortelius *et al.*, 2016; Vermillion *et al.*, 2018; O'Brien *et al.*, 2020), it allows for automated estimate at a much larger scale of important traits of Pleistocene ecosystems and landscapes inhabited by hominins such as *Paranthropus boisei*, *Homo habilis*, *H. rudolfensis*, and *H. erectus*. Pontzer and colleagues (2021) have suggested that as *Homo* started engaging in hunting and gathering foraging in the Pleistocene, physiological adaptations to reduce its water demands evolved. Our palaeoenvironmental reconstructions for East Turkana are congruent with that scenario since they indicate an overall temporal gradient towards drier conditions.

The Ileret, Karari, and Koobi Fora subregions are predicted to have more abundance of water in the upper Burgi (1.98–1.87 Ma), when compared with the following drier periods. In terms of spatial patterning, Quinn et al. (2007) demonstrated a gradient of vegetation, based on isotopic composition of paedogenic carbonates, ranging from open savannas to woodland, with drier conditions observed at the Koobi Fora ridge, followed by the more vegetated Ileret, and finally, Karari had the most densely vegetated and closed habitats. This vegetation gradient suggests a corresponding gradient in water availability for each subregion, largely corresponding to our subregional palaeoenvironmental reconstructions, particularly for the Upper Burgi Mb. However, according to our models, the Karari ridge subregion gets substantially drier after the Upper Burgi, a result that is more in agreement with Patterson et al. (2017a) reconstruction of the subregions during the Okote. In the Karari ridge, the Okote Mb is marked by an absence of Reduncini, indicating very arid, likely shrubland, conditions at

the time. Relying solely on stable isotopes poses challenges in distinguishing between closed forest and shrubland, as both can yield a C3 signature (Negash & Barr, 2023). Therefore, emphasizing the importance of considering diverse lines of evidence in palaeoenvironmental reconstructions (Patterson *et al.*, 2017b, 2019; Villaseñor *et al.*, 2023).

Patterson et al. (2017a) showed that Ileret's habitats were heterogeneous during the Okote. Our palaeoenvironmental reconstructions suggest a high degree of landscape heterogeneity in Ileret across space *and time*. We found that the upper Burgi deposits preserved at Areas 8, 10, 12, and 13 had differential reconstructions. Areas 8 and 10 have a higher proportion of terrestrial predictions and are thus likely to have been deposited in a floodplain context. In contrast, Areas 12 and 13 were reconstructed as more water-rich environments. Because of the paucity of palaeoenvironmental reconstructions for Ileret's upper Burgi, it is challenging to confirm our predictions. Nevertheless, a recent study of a hominin site in Area 13 provides supporting evidence for our reconstruction as "multiple lines of evidence suggest that this locality was near a well-watered and open, grassy environment" (Hammond *et al.*, 2021, p. 10).

On the other hand, the Okote and KBS layers are well studied in Ileret, with several palaeoenvironmental reconstructions available in the literature. Our reconstruction indicates that in the western half of Ileret, at areas 6, 6A, 1A, and 1 the KBS deposits tend to be more aquatic than at its eastern counterpart in areas 8, 8A, 8B, 9, 10, 11 and 12, likely indicating a west-east gradient from lake margin and deltaic to channel and floodplain settings. A similar gradient can be observed for the Okote deposits, where the western areas in our reconstruction fit close to that of Isaac and Behrensmeyer (1997), while the eastern Ileret predictions match better the description of Patterson and colleagues (2017a) (Table 5.3). While not a primary focus of our study, our analysis also included the reconstruction of Chari deposits in Ileret. Our findings suggest an overall trend of aridity across Ileret during the Chari, with the most significant changes being observed in Areas 4 and 7. Despite the overall dry trend, it is worth noting that there is an exception, our reconstruction of Area 5 suggests the presence of a relatively large body of water during the Chari, possibly a river.

Table 5.3 – Summary of palaeoenvironmental reconstructions for the Ileret, Karari and Koobi Fora subregions in East Turkana.

Reference	Age	Ileret	Karari	Koobi Fora
Behrensmeyer, 1975	Okote	**Area 6, 8:** Floodplain with deltaic fan and closed habitats	**Area 105:** NA	**Area 103:** Distributary channel and beach complex
	KBS	**Area 6, 8:** Not described	**Area 105:** Fluvial channel complex with some gallery forest	**Area 103:** Deltaic mudflats with open grasslands
	Upper Burgi	**Area 6, 8:** NA	**Area 105:** Delta margin and lagoon	**Area 103**: Not described
Behrensmeyer, 1985	KOLM*	Delta with closed habitats and channels	Woodland, riverine forests, and bush	**Area 103:** Delta with open grasslands
Isaac and Behrensmeyer, 1997	Lower Okote	Delta with patches of woodland and forest	Dry bushland and riparian woodland	Open grasslands along lake margins
	KBS	Floodplain + large channel and tributaries	Proto-Ol Bakate River system; seasonal pools	Not described
	Upper Burgi	Not described	Lacustrine and lake margins	Not described
Lepre et al., 2007	KBS	Not described	Not described	Lacustrine, floodplain along lake margins
Quinn et al., 2007	2–1.5 Ma	Low-tree shrub with woodland and thicket	Woodland and thicket savannas	Low-tree shrub to grassland near lake
Patterson et al., 2017a	Okote	Well-watered grasslands near lake margins and deltas	Arid grassland to bushland setting, dominantly fluvial	Well-watered grasslands near lake margins and deltas

* - Roughly contemporaneous deposits from the 1.6 to 1.5 Ma interval (upper KBS and lower Okote).

In Karari, we obtained a pattern of increasing terrestrial settings from west to east across the ridge (particularly noticeable in Areas 116 and 105, see Figure 5.4 C). Such reconstruction is correlated to the age of the deposits, because the surface layers in Karari exhibit a west-east progression from older to younger strata (Isaac & Behrensmeyer, 1997). In Area 105, our

reconstruction for the upper Burgi Member shows a clear and strong aquatic signal, likely representing the Lorenyang palaeolake highstand (Feibel, 1997, 2011; Nutz *et al.*, 2020), whereas relatively drier mixed habitats were predicted for the KBS Member deposits to the east (see Figure 5.9 C). During the KBS period the lake level is known to have dropped considerably (Lepre, 2014). The Lorenyang Lake was the longest-lived palaeolake in the basin (2.14–1.5 Ma), it opened hydrological corridors facilitating the introduction of a new freshwater biota (Renaut & Owen, 2023). This period witnessed rapid evolution of endemic molluscs (Van Bocxlaer, 2011) and the appearance of the freshwater stingray *Dasyatis* sp., with the fauna persisting through subsequent lowstand phases during the KBS, indicating a significant impact on the palaeoecology of the region (Feibel, 1993). Shifts in the palaeolake level might be linked to orbital cycles and global climatic conditions (Trauth *et al.*, 2005, 2007; Joordens *et al.*, 2011; Maslin *et al.*, 2014; Nutz *et al.*, 2017), including increased aridification due to a stronger Pacific Walker circulation (Ravelo *et al.*, 2004; Trauth, Larrasoaña & Mudelsee, 2009). However, the Lorenyang lake highstand phase, centred around 2.1–1.9 Ma (upper Burgi), is attributed to the obstruction of the drainage pathway of the lake due to the eruption of Mt. Kulal at 2.1 Ma (Gathogo *et al.*, 2008; Bruhn *et al.*, 2011; Boës *et al.*, 2019), indicative of stronger tectonic and volcanic local influences on palaeolake level fluctuations in the region at this time (Feibel, 1988; Brown & Feibel, 1990; Lepre, 2014; Lupien *et al.*, 2018; Baldes, Raynolds & Feibel, 2023).

Our reconstructions align well with the available literature, as summarised in Table 5.3, especially with Behrensmeyer (1975a), which also focused on Area 105. Overall, the previous studies reconstructing the Karari ridge indicated a lacustrine to lake margin context during the upper Burgi, riverine forests and woodlands for the KBS, and an arid grassland to bushland setting with riparian woodlands in the Okote (Isaac & Behrensmeyer, 1997; Patterson *et al.*, 2017a). Our satellite-based reconstructions for this subregion exhibit a west-east gradient of aquatic to terrestrial settings, which is consistent with the age-constrained palaeoenvironmental reconstructions in the literature (Quinn *et al.*, 2007; Patterson *et al.*, 2017b; O'Brien *et al.*, 2020).

On a scale of terrestrial to aquatic settings, starting from floodplains, then distributary channels, and finally deltas and lakes, the floodplain represents the overall drier setting as sediment deposition occurs only at peak wet seasons when nearby streams, rivers, ponds, and lakes overflow (Behrensmeyer, 1975a). Our models indicate that the Koobi Fora Ridge subregion reflects a generally drier signal compared to Ileret or the Karari, as previously demonstrated by Quinn et al. (2007) analysis of paedogenic carbonates. In addition, our model reveals an interesting pattern of more aquatic reconstructions in the upper Burgi and the KBS than in the Okote for Area 103, which is consistent with the analysis of Area 103 by Behrensmeyer (1975a) (see Table 5.3). Lepre and colleagues (2007) reconstructed Koobi Fora during the KBS as lacustrine with floodplains near lake margins which would fit well with the heterogeneous output of PalaeoEnv for this member that also contains very aquatic cell clusters. Notice that Patterson and colleagues (2017a, p. 156) argue for "well-watered grasslands" during Koobi Fora's Okote, based on the abundance of reduncin bovids, similar to the present-day Urema floodplain at Gorongosa National Park (Stalmans *et al.*, 2019) which is currently dominated by a large waterbuck population with over 55000 individuals. For the same time period, Isaac and Behrensmeyer (1997) emphasised the presence of hippopotamids and alcelaphines as indicative of open grasslands along lake margins. Additionally, we reconstructed the upper Burgi for Area 103 and the adjacent Area 106, which is similar to the KBS in terms of heterogeneity and also contains some clusters of strong aquatic predictions, likely representing lake margins or deltaic deposits. The upper Burgi Member has been described as more mesic than the subsequent periods for all three subregions (O'Brien *et al.*, 2020), while our model is compatible overall with this interpretation, this difference is not as pronounced in Koobi Fora as it is in the other subregions.

5.4.2 Short-wave infrared: soil content and moisture

It is noteworthy that the short-wave infrared bands exhibit opposite effects in determining the aquatic ratio. For the BetaReg model, it was observed that higher values of SWIR1 tend to increase the estimations of terrestrial palaeoenvironments, while higher values of SWIR2

suggest aquatic palaeoenvironments. SWIR bands of the electromagnetic spectrum are known to be useful proxies for mapping soil composition and soil moisture (Pour & Hashim, 2015). In terms of their differences, SWIR1 is generally more sensitive to water content in soils (Hegazi *et al.*, 2023), while SWIR2 tends to be more sensitive to mineral content, particularly in arid contexts (Asner & Lobell, 2000). A class of topsoil minerals well known to show contrasting values in SWIR 1 and 2 are the clays (Osinowo, Gomy & Isseini, 2021). Clay minerals have reflectance features from 1.55 to 1.75 μm (SWIR1) and absorption from 2.1 to 2.4 μm (SWIR2), giving them a unique spectral signature in the medium-infrared regions (Watanabe & Matsuo, 2003). Therefore, a higher SWIR1/SWIR2 ratio (known informally as "ratio 6/7"; Ali & Pour, 2014) tends to indicate higher content of surface clays, which in our BetaReg model was generally associated with terrestrial predictions. Notice however, that in the masking performed by PalaeoEnv many of the most extreme terrestrial predictions by BetaReg were excluded (particularly in Ileret), since they are correlated with cells unlikely to be fossiliferous by MaxEnt. While clays can be associated with modern continental aquatic environments, and tend to be abundant in deltas, estuaries, rivers, and lakes (Hillier, 1995), they are overabundant in alluvial deposits and are also more commonly associated with younger sediments, as these are often less consolidated and more prone to contain unaltered clay minerals (Hanzawa & Adachi, 1983). Soil texture differs between erosional settings and depositional basins, with a higher prevalence of clays in the latter (Rosenbloom, Doney & Schimel, 2001). While fossils can certainly be very abundant in fine-grained sediments (Behrensmeyer, 1988), diminished erosion can inhibit exposure of outcrops and consequently fossil discovery (White, 2004). This interpretation is further supported by SWIR2 being among the most crucial variables in the MaxEnt model (27.14% contribution, and 37.54% permutation importance), and positively correlated with fossil sites. Thus, in East Turkana less clayey surfaces are generally indicative of more abundant fossils and of more well-watered palaeohabitats. On the other hand, SWIR1, a band highly correlated to soil moisture, was the most important variable for BetaReg. As the moisture content in the soil increases, the reflectance in the SWIR1 region tends to decrease (Zhang *et al.*, 2022). It is likely that this

variable is acting as a proxy for modern water erosion and therefore abundance of fossils exposed in these settings (i.e., more aquatic cells tended to be richer in fossils).

5.4.3 Near-infrared: a "fossil band"?

Based on our findings, NIR is the most important variable for identifying fossil sites, contributing 35.3% and showing a negative correlation with fossil presence in the final model (Extended Data Fig. S3). NIR is widely recognized as the best satellite-derived proxy for biomass (López-Serrano *et al.*, 2020), with higher values indicating abundant vegetation, foliage, and other kinds of organic material (Hu *et al.*, 2015; Viscarra Rossel & Hicks, 2015). Moreover, water absorbs a significant portion of the NIR spectrum (Mondejar & Tongco, 2019). Between the low values indicating water presence, and higher values associated with fresh soils with plants, occurs a very particular range of NIR values that indicate barren erosional surfaces. Erosion enhancing the probability of fossil discoverability is a well-documented phenomenon (Block *et al.*, 2016). Response curves indicate that if our MaxEnt model was generated using only the NIR variable, cells with NIR values in the range of 14000 to 15800 would have a 50% or higher chance of being fossiliferous, and specifically values around 14900 would have a 90% chance of containing fossils (Extended Data Fig. S2).

NIR is particularly useful because it can extract soil information by penetrating through forest canopy (Huete, Liu & van Leeuwen, 1997), and a previous study focused on remote fossil site detection in modern Miombo woodlands of central Mozambique also found near-infrared the most effective variable for modelling fossiliferous deposits (d'Oliveira Coelho *et al.*, 2021). Our study reinforces the foremost importance of NIR for identifying fossil sites, but in a far more arid region of the EARS with a limited number of trees (Mbaluka & Brown, 2016). Consequently, we tentatively hypothesise this might hold true throughout a larger range of modern continental ecosystems with fossil exposures. In light of our findings, emphasizing a possible distinct role of NIR in identifying fossil sites, we advocate for future investigations in geospatial palaeontology to employ variable importance metrics or other feature ranking techniques to allow for rigorous testing of this hypothesis.

5.4.4 The visible bands: RGB and ultrablue

The visible spectrum is the range of electromagnetic radiation that is visible to the human eye, and it is typically considered to extend from approximately 380 to 750 nanometers (nm) in wavelength. In Landsat 8, the visible spectrum is represented by the ultrablue (433–453 nm), blue (450–515 nm), green (525–600 nm) and red (630–680 nm) bands (Knight & Kvaran, 2014). Overall, while the RGB bands may not be optimal for detecting fossil sites using the MaxEnt model (combined contribution = 0.20%), they can still provide useful information for palaeoenvironmental reconstructions (combined contribution = 42.02%). It is difficult to determine the specific role of each band in the BetaReg model, but they are all commonly used in remote mineral detection, e.g., the red/blue bands ratio is particularly efficient at mapping soils rich in iron-oxide (Pour & Hashim, 2015), and these features are very likely to be correlated with differential environmental and depositional conditions at the time of soil formation, resulting in different chemical and textural soil patterns.

The ultrablue band is commonly referred to as the coastal/aerosol band due to its dual functionalities of shallow water body analysis (Pan, Xi & Wang, 2020), and monitoring the movement of small particles such as dust and smoke (Pahlevan *et al.*, 2014; Syam'ani, 2020). Ultrablue is also particularly optimised for chlorophyll detection (Flynn, Frazier & Admas, 2020). While ultrablue barely contributed to the BetaReg model (<0.5%), it was crucial for MaxEnt estimations (23.37% contribution, and 27.58% permutation importance), and it seems to be particularly efficient at detecting unsuitable conditions for fossil abundance. Water bodies and places like the Kokoi volcanic horst in Area 137, and other surface magmatic rock throughout East Turkana are mapped with low ultrablue values, which MaxEnt readily excluded as having 0% likelihood of being sedimentary deposits with fossil material, making it a particularly important feature to detected true negatives and increase the NPV ratio.

5.4.5 Modern environmental and topographic contexts

Vegetation was found to have a significant contribution to the BetaReg model, but it was not considered by the MaxEnt model. This discrepancy may be due to the vegetation index being negatively correlated with aquatic sites, since the locations we sampled with more aquatic fossils tended to be more fossil-rich and located in more arid regions, sometimes without any shrubs around. It is likely that vegetation did not make it into the final fossil-detection model, because the MaxEnt algorithm is relatively good at ignoring redundant information, and the most important variable in the MaxEnt model, NIR, already served as a proxy for vegetal biomass distribution (López-Serrano *et al.*, 2020), moreover, vegetation is calculated from NIR and the red bands, and contrary to regression models, MaxEnt excels at avoiding redundancy during weight calculation (Elith *et al.*, 2011). Vegetation Index would contribute more to MaxEnt in the absence of NIR, as demonstrated by its almost identical independent response curve (Extended Data Fig. S2).

Slopes are dynamic geomorphological features closely connected to the erosional and taphonomic processes underlying the increase or decrease in chance of fossil discovery (Reid & Frostick, 1985, 1986; White, 2004; Hubbard, MacEachern & Bann, 2012; Stetler, 2018). The role of slope in the BetaReg model is notable, with steeper slopes and hills associated with past wetter conditions, while flatter areas tend to support drier palaeohabitats. This might be due to the effects of differential erosion after deposition (Kidwell, 1986), as water erosion removes finer detritus from steeper areas, while wind deflation removes material from flatter and dryer areas (Makin, 1969). Slope did not contribute as much as expected to the MaxEnt model (2.18%), however, it is important to note that our methodology may have impacted the results, as we preferentially selected flatter areas for data collection due to the logistics of bone walks and safety concerns. Therefore, the quantitative determination of the role of slope in remote fossil detection requires further investigation with alternative sampling methods. But previous geospatial palaeontology, using other surveying protocols rather than bone walks, work attest to its importance (e.g., Egeland *et al.*, 2010; Anemone *et al.*, 2011b; Emerson *et*

al., 2015; Block *et al.*, 2016; Burk, 2021, 2023). While regions characterized by steep slopes might exhibit a profusion of exposed fossils, the same incline introduces the risk of accelerated transportation or destruction through erosive forces. This interplay can exert a substantial influence on the fossil record, shaping not only the quantity but also the quality of fossils that can be recovered (Behrensmeyer, 1975a; Kidwell & Flessa, 1995; White, 2004). An independent MaxEnt model using only the slope variable indicates optimal slope at ~ 7% for detecting fossiliferous deposits in East Turkana (Extended Data Fig. S2), but this model is likely to be biased towards a lower slope due to the sampling approach (i.e., bone walks) leading us to survey in relatively flat areas. Some authors have considered a cut-off of 5% slope minimum as useful for mapping likelihood of finding fossil sites (e.g., Anemone *et al.*, 2011b).

Elevation on the other hand, had a bigger contribution towards identification of fossil-bearing deposits, which conforms to the geomorphology of the Turkana Basin, since the lower regions tend to have modern water bodies, and the higher areas of East Turkana tend to be associated with basalts and not with sedimentary surfaces (see Appendix *in* Bobe *et al.*, 2022). Aspect has been previously demonstrated as a very useful feature in predictive modelling of fossil sites in mountainous regions (Burk, 2023), specially with satellite data of higher resolution (e.g., 5×5 m in Burk; 2021). In our protocol we opted to use northness and eastness instead of aspect, and it appears there is a slight tendency (~ 5.7% contribution to MaxEnt) for fossiliferous outcrops to align northwards. Although this observed pattern is not consistent (only 0.4% permutation importance) and could also be an artefact of our surveying protocol.

Ultimately whether we consider the mineralogical properties of the visible bands, or the ability to apply the infrared spectra as proxies for biomass, erosion, moisture, and soil granularity, or the modern environmental and the topographic features of the landscape, they are all connected through dynamic feedback loops with geological and taphonomic processes (Behrensmeyer, 1975a; D'Andrea, Gallotti & Piperno, 2002; Hlusko, 2018; Martínez *et al.*, 2019). The interplay between these requires further exploration in future geospatial palaeontology studies (Chew & Oheim, 2009; Anemone *et al.*, 2011a; Weihmüller *et al.*, 2022). Currently, understanding this

relationship is challenging due to the abstract nature of how remote sensing data interacts with taphonomy (Jennings & Hasiotis, 2006; Oostra *et al.*, 2020). Employing techniques for interpreting machine learning models, such as variable importance analyses, will be key in unlocking the black box and enhancing our comprehension.

5.4.6 Conclusion

In conclusion, this study successfully developed and tested models to predict fossil hotspots, and hydrological conditions of past landscapes in East Turkana, Kenya. The overall importance of the infrared spectrum for geospatial palaeontology has been confirmed by the contribution of near-infrared for fossil detection and short-wave infrared bands for palaeoenvironmental reconstruction. Previous studies demonstrated the high degree of correlation between NIR range and fossiliferous deposits (d'Oliveira Coelho *et al.*, 2021), and this consistency across EARS sites may mean NIR can act as a generalizable "fossil band", but further tests in other palaeontological settings are required to confirm this hypothesis. Additionally, the modelling of the terrestrial to aquatic ratio provides an innovative approach to palaeoecology that can be used in tandem with other palaeoecological methods to achieve a more detailed interpretation of landscape changes in the Turkana basin throughout time. Through the use of bone walks, remote sensing and machine learning techniques, we have gained new insights into the distribution of fossils in geological formations and the balance between water- and land-based palaeohabitats in East Turkana.

Our findings demonstrate that geospatial palaeontology methods, typically used for fossil site identification, can be adapted to effectively reconstruct palaeoecological features across large regions. The impressive predictive power of satellite imagery data indicates that these techniques can complement traditional fieldwork approaches in geology and palaeoanthropology. Our successful implementation of these methods suggests that they might be applicable to other palaeoecological research questions, such as predicting the distribution of specific land habitats or vegetation structure (Negash & Barr, 2023). The findings of this study are useful for advancing our understanding of the palaeoenvironmental conditions of past

landscapes and the interactions between hominins and their environment. Overall, our study highlights the promise of incorporating cutting-edge remote sensing and data science techniques to advance palaeoanthropological research.

Acknowledgments

We express our gratitude to the highly skilled field workers and fossil collectors in Kenya, whose valuable contributions are essential. Our sincere thanks extend to the National Museums of Kenya and the Koobi Fora Field School, including the numerous field school students who actively participated in the collection and processing of data. This research would not have been possible without their collaboration and dedication. This work owes its realization to the invaluable expertise of Frances Forrest, who provided crucial guidance in on-site taxonomy and species identification. Special acknowledgment goes to the diligent Elizabeth Dorans for her outstanding role as a hardworking mentee during J d'OC debut as Mentor Staff in the field school. Her valuable contributions to data collection and curation for this project are highly appreciated. The authors would like to give a special thanks to all the "bone walkers": Maryse Biernat, Tamara Capps, Bri Heisler, Maddie Kelly, Hannah Jacobson, Sharon Kuo, Deanna Maybee, Amanda McGrosky, Sahle Melaku, Leah Myerholtz, Georgia Oppenheim, Noelle Purcell, Mathilde Ribordy, Rowan Sherwood. We would also like to thank the people of Ileret and East Turkana who welcomed us to their lands. This research was supported by: Koobi Fora Research and Training Program, funded by NSF Archaeology Program #1624398 and REU #1930719; J d'OC was supported by FCT (SFRH/BD/122306/2016); and The Boise Trust Fund for fieldwork.

5.5 Supporting Info

5.5.1 SF1. A leave-one-out cross-validation (LOOCV) procedure for the beta regression model

To calculate model's accuracy, we created a metric of agreement that is calculated through R using the following code (Arlot & Celisse, 2010; Roberts *et al.*, 2017).

```
nobs <- nrow(betareg_dataset)
```

Obtains the number of observations in the betareg_dataset data frame.

```
predicted <- vector()
```

Creates an empty vector to store the predicted values for each iteration.

```
for (i in 1:nobs){

  # Fit a beta regression model on all observations except the ith observation

  betafit.test <-  betareg(aquatic_ratio ~ ., data = betareg_dataset[-i,], link
= "logit")

  # Predict the response value for the ith observation using the fitted model

  predicted[i] <- predict(betafit.test, betareg_dataset[i,])

}
```

Loops over each observation in the betareg_dataset data frame.

```
error.table <- cbind(betareg_dataset, predicted)

error.table$error <- abs(error.table$aquatic_ratio - error.table$predicted)
```

Combines the betareg_dataset data frame with the vector of predicted values and calculate the absolute error for each observation.

```
summary(error.table$error)
```

Print summary statistics of the absolute error measurements.

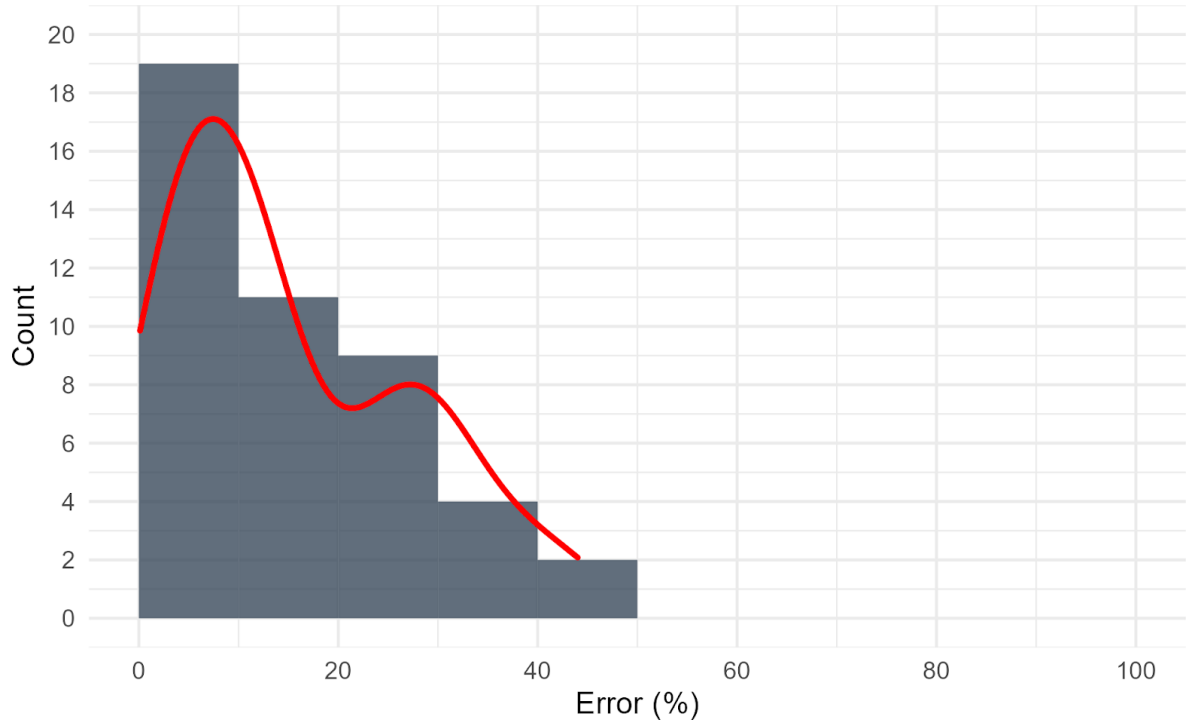
```
brk.loocv <- seq(0, 100, by = 10)
ggplot(error.table, aes(x = error * 100)) +
  geom_histogram(aes(y = ..count..),
                 fill = "#2c3e50", breaks = brk.loocv, alpha = 0.75) +
  geom_density(aes(y=..density..*nrow(error.table)*(brk.loocv[2]-brk.loocv[1])),
               color = "red", size = 1) +   # adds a density curve
  scale_x_continuous(breaks = brk.loocv[c(TRUE, FALSE)]) +
# removes every other idx
  scale_y_continuous(breaks = seq(0, 20, by = 2), limits = c(0, 20)) +
  xlab("Error (%)") + ylab("Count") + theme_minimal()
```

Creates a histogram of the absolute error LOOCV estimates using ggplot2.

It's worth noting that the area under the density curve is usually plotted as equal to 1, since the curve represents the probability density function of the distribution. This means that the height of the density curve at a given point represents the probability density of observing an error value near that point. The count scale shows the number of observations in each bin of the histogram, while the density scale shows the relative frequency of observations at each point along the x-axis. Therefore, the density scale is not directly comparable to the count scale on the y-axis of the histogram. We can fix this issue by adjusting the density. This scaling factor for the vertical axis is obtained by multiplying density by the total of observations, and then multiplying that by the bin width.

```
ggsave("Final_SF1_LOOCV.png", plot = last_plot(), width = 12, scale = 0.5,
       bg = 'white', dpi = 'retina')
```

Finally, save the plot as a .png Figure.



Supporting Figure 1 – Histogram and density curve of BetaReg model absolute errors as measured in a LOOCV architecture: models trained without the ith instance tested against that hold-out instance.

5.5.2 SF2. Calculating variable importance in Beta regression

After a deep search of the literature and of the R packages related to Beta regressions available in CRAN and GitHub (Ferrari & Cribari-Neto, 2004; Cribari-Neto & Zeileis, 2010), we were unable to find an implementation of a variable importance calculation for Beta regressions. Therefore, we created our own estimate variable importance via percent contribution using a jackknife procedure over log-likelihood, as follows: In each iteration of the loop, the model is fit without the i^{th} predictor variable, and the percent contribution of that variable is calculated as the difference in log-likelihoods between the full model and the reduced model, normalized by the log-likelihood of the full model. The resulting percent contribution for each variable is plotted using a bar chart. The percent contribution metric represents the amount of information gained or lost by including or excluding a predictor variable in the model, and might allow us to compare the two models (Support Table 1).

```
vars <- colnames(betareg_dataset)[-1]  # get variable names

pct_contrib <- numeric(length(vars))  # initialize percent contribution vector

for (i in seq_along(vars)) {

  # fit model without the ith variable

  formula_i <- as.formula(paste0("aquatic_ratio ~", paste(vars[-i], collapse =
"+")))

  betareg_i <- betareg(formula_i, data = betareg_dataset, link = "logit")



  # calculate percent contribution

  pct_contrib[i] <- 100 * (logLik(betafit) - logLik(betareg_i)) / logLik(betafit)

}

normalized_contrib <- 100 * pct_contrib / sum(pct_contrib)

BR.pct_contrib   <-   data.frame(Variable   =   vars,   PercentContribution   =
normalized_contrib)
```

Support Table 1 – Percent contribution for the aquatic-ratio and the fossil prediction models.

	Percent Contribution	
Variable	**BetaReg (%)**	**MaxEnt (%)**
ultrablue	0.4316	23.3731
blue	12.2669	0.0024
green	11.2268	0.0000
red	11.6606	0.3051
NIR	12.8430	33.9545
SWIR1	16.1999	0.1866
SWIR2	9.0096	27.1372
vegetation	12.2092	0.0000
elevation	0.1234	6.8204
slope	13.0260	2.1756
northness	0.9541	5.6573
eastness	0.0489	0.3877

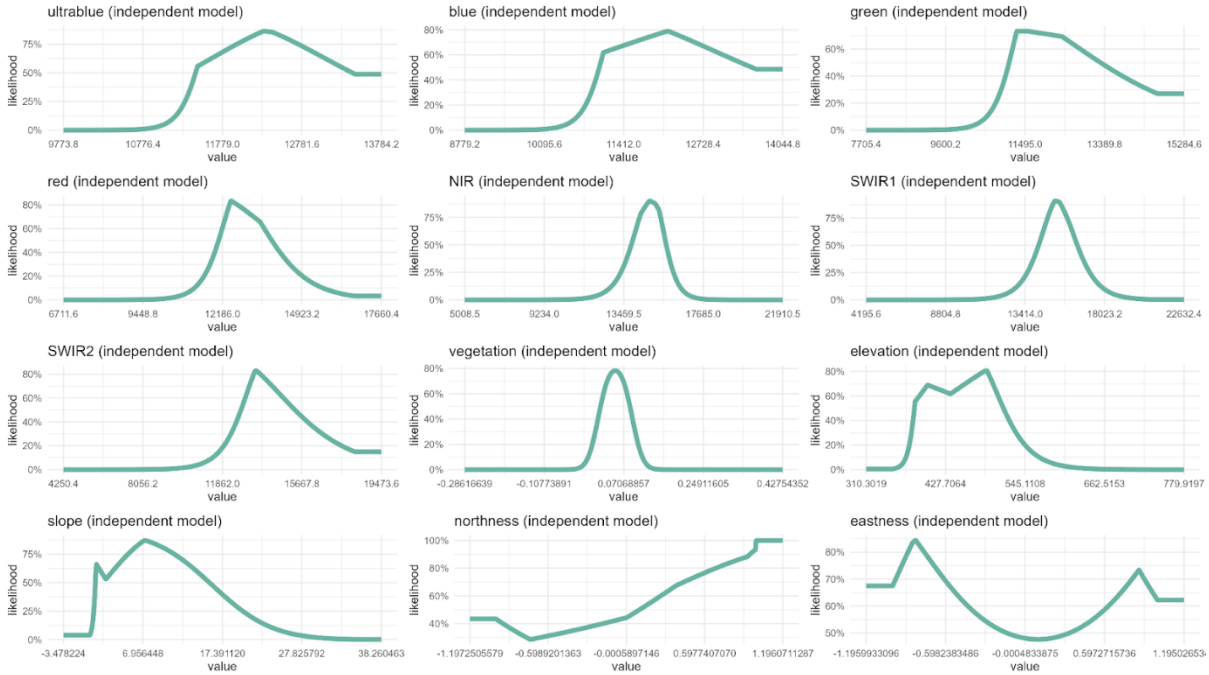
A high percent contribution value for a variable suggests that the variable has a strong influence on the response variable, while a low percent contribution value indicates that the variable may not be as important for predicting the response. Overall, this implementation provides a useful

tool for identifying the most important predictor variables in a betareg model, which can aid in model selection and interpretation. Also, it is a popular, frequently reported metric in MaxEnt implementations, therefore allowing for comparisons between the models (Support Table 1).

5.5.3 SF3. Response curves for single variable MaxEnt independent models

Response curve plots show the relationships between the bone walk cells with high density of fossils and the geospatial variables obtained from satellite images (Extended Data Fig. S2). In contrast to marginal response curves, each of the following curves represents a separate Maxent model created using only the corresponding variable.

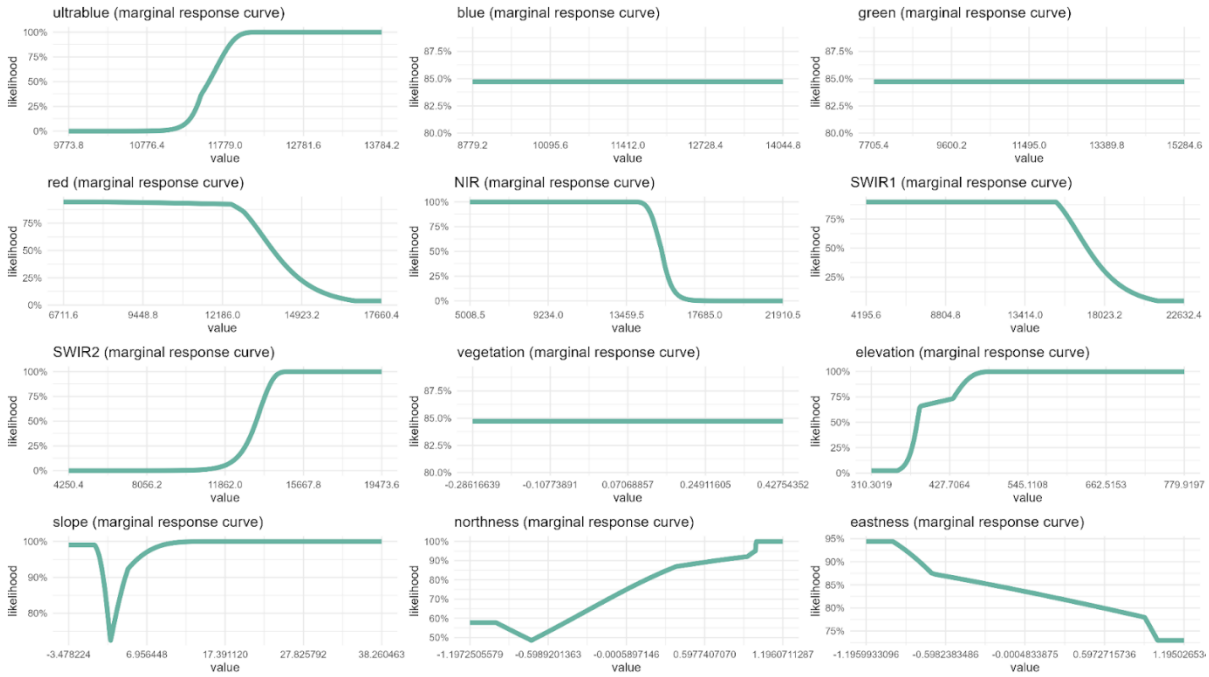
These curves illustrate the relationship between predicted suitability and the selected variable and any induced dependencies resulting from correlations between the chosen variable and other variables. They may be more straightforward to interpret in cases where there are strong correlations between variables (Hijmans *et al.*, 2022).



Extended Data Fig. S2 – Response curves as for independently generated MaxEnt models, using a single input feature.

5.5.4 SF4. *Response curves of the final MaxEnt model for remote detection of fossiliferous deposits*

To analyse the effect of each multispectral, environmental and topographic variable on the MaxEnt prediction, marginal response curves were generated (Extended Data Fig. S3). These curves display the change in the predicted probability of presence as each satellite-derived variable is altered while keeping all other variables at their average sample value. However, caution should be exercised when interpreting response curves with strongly correlated variables, as the model may exploit correlations in ways that are not evident in the curves. In other words, the curves show the impact of altering one variable only, whereas the final model may utilize sets of variables that change together (Phillips *et al.*, 2017). For example, we can see that vegetation was found to be redundant by the model, because it is calculated from NIR and red, and therefore it is highly correlated with both.



Extended Data Fig. S3 – Marginal response curves for the final MaxEnt models.

Code statement

The entirety of the code for reproducing this paper analyses, figures, and tables is available at https://github.com/Delvis/TURKAQUA

6

Discussion

6.1 Summary

The fossil record, a repository of invaluable clues about our evolutionary past, has long captivated the interest of palaeoanthropologists and other scholars. However, like a never-ending puzzle riddled with missing pieces, the study of hominins demands a nuanced understanding of the temporal and spatial biases associated with the fossil record. Weaving knowledge from palaeoecology, genetics, remote sensing, and machine learning provides valuable opportunities to address gaps in our understanding of evolution. The primary aim is to illuminate the spatiotemporal factors of hominin origins, enriching our comprehension of overlooked contexts that might have shaped our evolutionary trajectory.

In Chapter 1, the theoretical groundwork for the research conducted was introduced. The background is outlined, emphasising the biogeography and palaeoecology of Gorongosa, Mozambique. The chapter highlights the significance of Gorongosa as a testing ground for coastal models of ape evolution and hominin origins, but also the need for improving current geospatial palaeontology protocols so that they can eventually help us target palaeobiomes of interest. Chapter 2 presents an in-depth literature review, encompassing conventional techniques for surveying, and advanced approaches, such as the exploration of localities from

space. The review encompasses various aspects of geospatial applications in palaeontology, including its roots in 1970s archaeological predictive modelling in collaboration with NASA, to the continuous introduction of innovative GIS applications, culminating in the use of remote sensing combined with machine learning models. The chapter concludes by addressing new lines of research, including hybrid datasets, taxa-specific models, continental-wide approaches, and individual fossil targeting.

Chapter 3, provides a pioneering meta-analysis of molecular divergence estimates for the *Homo* and *Pan* clades, using fossil evidence to calibrate and improve the dating of this important evolutionary event. It concludes this split might have happened earlier than is usually considered, matching a period that has very few known palaeontological deposits in Africa. Chapter 4 details the application of a straightforward clustering technique for efficient partitioning of satellite spectral patterns, resulting in the discovery of new Miocene fossil sites in the eastern shoulder of the Urema Rift in Mozambique. It contains a simple geospatial protocol that does not require manual labelling of landcover classes, runs fast, and is straightforward to apply. This unsupervised approach can accurately identify fossil sites in the region, despite the challenging conditions characterised by limited exposure of potentially fossiliferous sedimentary deposits and the difficulty of conducting surveys in a densely vegetated area with a thick canopy. Chapter 5 focuses on *geospatial palaeoecology*, specifically evaluating the aquatic to terrestrial ratio of palaeoenvironments in East Lake Turkana. It also introduces one-class classification models as effective tools for fossil site detection and discusses their several advantages. This study aims to understand the preferential preservation of specific environments in the fossil record and explores the potential of modelling spectral differences in sediments to remotely and accurately reconstruct palaeoenvironments. Tested on the Koobi Fora formation in northern Kenya, which is known for its rich fossil record and the presence of multiple species of hominins, this novel approach provides a large-scale, remote method for palaeoecological reconstruction that is generalizable to other fossil-rich regions in the world and marks a significant step toward a scalable palaeoecology approach.

6.2 Key contributions

In this thesis, I propose the application of quantitative approaches to enhance the discovery and understanding of fossiliferous deposits that may contain ape and early hominin material dating from critical unknown time periods of African evolution. This discussion unfolds across three empirical chapters, each delineating its specific contributions to the overarching inquiry. These contributions encompass the alignment of molecular divergence estimates with the fossil record (Chapter 3), the utilisation of machine learning and satellite data for fossil site identification in less explored contexts (Chapter 4), and the innovative combination of geospatial and machine learning methods for large-scale palaeoenvironmental reconstruction (Chapter 5).

6.2.1 Through the hourglass: the double-helix and clocks

The inherent uncertainty in estimating divergence times from molecular genetic sequences naturally leads to discrepancies between molecular genetic inferences and palaeontological timescales (dos Reis, Donoghue & Yang, 2016; Brown & Smith, 2018). The timing of the split between *Homo* and *Pan* has been a subject of extensive debate within the field of palaeoanthropology for over a century (Keith, 1920). Chapter 3 delves into this contentious topic, focusing on a comprehensive review and meta-analysis of temporal estimates. By scrutinising the prevailing molecular evidence and fossil record, the primary objective is to shed light on the divergence timing and explore its compatibility with current scientific knowledge. Remarkably, the various analyses consistently indicate a divergence event occurring during the first half of the late Miocene epoch (i.e., the Tortonian, 11.6–7.25 Ma). Moreover, they illustrate the dilemma of bias toward younger estimates in molecular models (e.g., median of 6.4 Ma according to timetree.org, see also Figure 6.1), prompting a critical examination of how to integrate the contrasting strands of molecular and palaeontological evidence. Conclusively, Chapter 3 highlights a progressive convergence between the genetically estimated timing of the last common ancestor of *Pan* and *Homo*, and the timing inferred by the fossil record. By narrowing the gap, this research brings us closer to unravelling

the precise timing of the divergence of our last common ancestor (LCA) into the two lineages. Undoubtedly, this pivotal event carries profound implications for advancing our understanding of the evolutionary trajectory of our species. If we want to identify more putative fossils of earliest Homini and Panini, as well as Gorillini, and any other late Miocene African ape lineages that went extinct, it becomes imperative to find more fossiliferous deposits in Africa older than 7 million years. Additionally, the models strongly indicate that directing efforts toward deposits exceeding 8.5 million years in age could yield valuable fossil material potentially attributable to the LCA.

Remarkably, besides C'horora (Katoh *et al.*, 2016) and possibly Toros-Menalla (Lebatard *et al.*, 2008, 2010), there are presently no documented deposits spanning the 9 to 7 Ma period across the entire continent. This changed recently with the new radiometric dating of Gorongosa's fossil sites that has yielded promising results (Bobe *et al.*, 2023), indicating the presence of significant fossiliferous deposits in the region with potential to address and mitigate this and other significant temporal voids in a period of great interest for the diversification of the African great apes and hominin origins (Figure 6.1).

Chapter 3 presents the first meta-analysis of molecular phylogenetic divergences, building upon previous reviews of divergence dating methodologies. These reviews have often reached a consensus, epitomised by the assertion that "molecular clocks are not up to the job, but neither is the fossil record" (Donoghue & Benton, 2007, p. 429). This statement warrants a nuanced interpretation, as molecular clocks are becoming increasingly sophisticated, and the reliability of genetic versus fossil records can vary significantly across different taxa. For instance, in the case of orchid speciation, the scarcity of fossilised remains necessitates a predominant reliance on molecular data for phylogenetics (Givnish *et al.*, 2015). Conversely, for larger mammals, such as hominins, the fossil record has shown a propensity for growth and improvement (Wood & Smith, 2022). This is underscored by recent findings, including the identification of a second species of *Orrorin* that persisted into the Pliocene (Pickford *et al.*, 2022), and the discovery of the first *Homo erectus* from Atapuerca at 1.3 Ma (Herrero, 2023) or the many descriptions of new species of hominins just in the last decade, like *Australopithecus deyiremeda* (Haile-

Selassie *et al.*, 2015), *H. naledi* (Berger *et al.*, 2015), *H. luzonensis* (Détroit *et al.*, 2019) and *H. longi* (Ji *et al.*, 2021). These highlight the dynamic and improving nature of the fossil record in the hominin clade, suggesting that its utility in divergence dating is far from static and will continue to develop with each new pertinent fossil discovery in tandem with advancements in molecular divergence methods (Püschel *et al.*, 2021; Pugh, 2022).

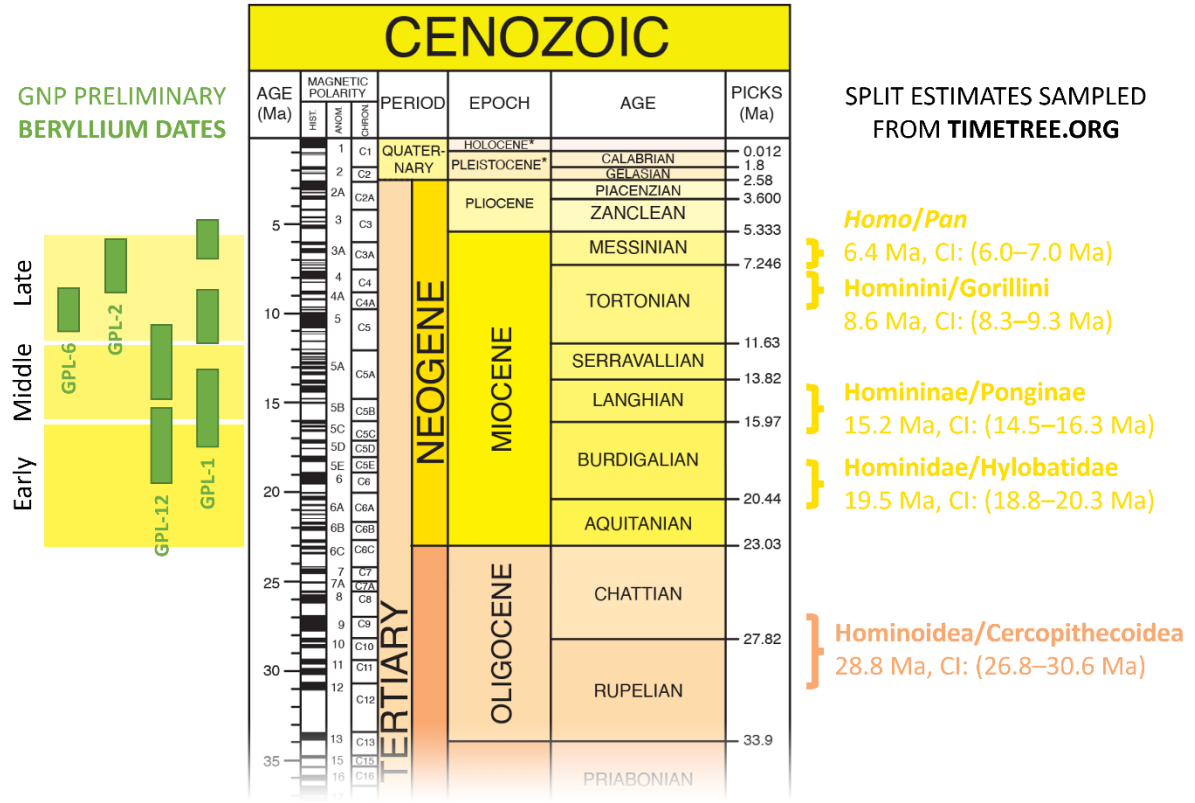


Figure 6.1 – **Preliminary temporal intervals for Gorongosa fossil sites** based on three-point estimates of $^{10}Be/^{9}Be$ dating using authigenic values based on different ecological assumptions (Appendix II), combined with the geological time scale from the Holocene to the Oligocene (GSA, 2022), and median divergence estimates of the literature, with respective confidence intervals, were obtained from timetree.org (Kumar *et al.*, 2022).

6.2.2 Filling gaps: the sands of time

Syria, 450 thousand years ago: a group of *Homo erectus* awaits in a desert oasis to hunt on a caravan of wild *Camelus* arriving to drink water (Reynaud Savioz & Morel, 2005; Al Khabour, 2022). However, it is not clear if Syrian camelid populations of this period belong to either the Asian Bactrian camel or the Arabian dromedary lineage, because fossils share mosaic skeletal

traits of both (Martini *et al.*, 2015). Adding to the complexity, biogeography fails to provide any further clues to their identity, as present-day Syria stands out as the main region where these two camelid species overlap (Dioli, 2020).

Geraads and colleagues (2020) reassessed the timing of camelid diversification using a new fossil record compilation and cutting-edge dating models based on the fossilised birth-death process (Didier & Laurin, 2020; Püschel *et al.*, 2021; Wright *et al.*, 2022). The study showed that the divergence between Bactrian camel and dromedary most likely occurred at 0.94 Ma, assigning a near-0% probability to the event occurring before 2 Ma. This finding contrasts markedly with all available molecular estimates for camels, which range widely from the early Pliocene to the late Miocene: 3.5 Ma (Hassanin *et al.*, 2012); 4.1 Ma (Wu *et al.*, 2014); 4.2 Ma (Heintzman *et al.*, 2015); 4.3 Ma (Toljagić *et al.*, 2018); 7.3 Ma (dos Reis *et al.*, 2012); c. 8 Ma (Cui *et al.*, 2007); and 10.4 Ma (Fritz, Bininda-Emonds & Purvis, 2009). The study suggests that the large discrepancy is attributable to inadequate calibration within molecular models, specifically due to the omission of palaeontological evidence or relying on outdated or low-resolution fossil records to constrain the phylogenetic distances in the molecular models (Geraads *et al.*, 2020). Another potential contributing factor is the variation in molecular evolution rates among species due to differences in life-history traits (Bromham, 2011, 2019). These differences can impact outcomes substantially, particularly since the calibration nodes often employed are from distantly related mammal lineages. A striking and extreme example of this phenomenon in the literature is a study by David and Alm (2011) using calibration nodes of Archaean bacteria, a lineage so far removed from mammals, that the *Homo*/*Pan* split was estimated at 139.7 Ma.

While camelids and Archaea provide good cases for the molecular overestimation bias, the problem of underestimating divergence dates is far more frequently acknowledged in the literature (Christin *et al.*, 2014; Marshall, 2019; Chen *et al.*, 2021). For instance, the first phylogenetic analysis of pine trees calibrated with a considerable number of fossils evenly distributed across all major clades, estimated that *Pinus* originated 30 million years earlier than indicated by any previous molecular study (Saladin *et al.*, 2017).

Similarly, a study on lizards found that undersampled clades had younger node age estimates than clades with more complete taxon sampling (Schulte II, 2013). The origination and diversification of birds have also been reassessed, revealing taphonomic biases that lead to underestimating the age of multiple avian lineages (Crouch, 2022). Likewise, Heads (2012) argued that most radiations related to the breakup of Gondwana, whether in flora or fauna, are likely underestimated by tens of millions of years. Therefore, suggesting that many of the major divergence events probably occurred much earlier in time, closer to the South Atlantic's formation at ~120 Ma (Scotese, 2021). This might apply to Atlantogenata, a proposed clade comprising the Afrotheria and Xenarthra cohorts of mammals native to Africa and South America, respectively (Waddell *et al.*, 1999).

In fact, there is a plethora of biogeography-inspired geneticists obtaining analogous results for other contexts (Ho *et al.*, 2015; Loeza-Quintana & Adamowicz, 2018). When the fossil record is sparse, these researchers prioritise geoclimatic and tectonic events for node calibrations (e.g., Irestedt *et al.*, 2009, on birds of paradise; Jønsson, Fabre & Irestedt, 2012, on crows; Wilf & Escapa, 2015, on Gondwana plants; Parks, Harrington & Thomson, 2022, on scaled lizards; Veličković *et al.*, 2023, on trout fish). In parallel, new statistical tools have been proposed to evaluate the reliability of molecular divergence dates, highlighting the need for empirical assessment of calibration approaches to avoid underestimating divergence times (Gunkel *et al.*, 2017; Wright *et al.*, 2022). Collectively, these studies and Chapter 3 underscore the complexity of accurately dating clade divergences and the necessity of integrating multiple lines of evidence to mitigate biases inherent to both molecular and fossil records.

The reconciliation of molecular divergence estimates with the fossil record is fraught with challenges (Ksepka, Ware & Lamm, 2014; Brown & Smith, 2018). Another significant issue is the underrepresentation of stem groups in the fossil record, which leads to discrepancies between molecular and fossil-based age estimates (Budd & Mann, 2020; Beavan, Pisani & Donoghue, 2021). To give an example, the recent discovery of a Devonian euthycarcinoid arthropod fossil with myriapod apomorphies (i.e., derived traits) has provided new insights to

close the 80–100 Ma gap between fossil data and molecular timing of Myriapoda origins, suggesting a much closer alignment than previously assumed (Edgecombe *et al.*, 2020).

The well-known Signor-Lipps effect postulates that the most recent fossil (=LAD) of an extinct clade always predates its extinction (Signor & Lipps, 1982). The reverse wordplay "Sppil–Rongis effect" has been coined in order to bring attention to the opposite phenomenon, that the oldest fossil (=FAD) of an extinct clade always postdate its origins (Dornburg *et al.*, 2011; Heads, 2012). This concept was, in fact, recognized considerably earlier by Jaanuson (1976), although it has not been as prominently featured in scholarly discourse, it has far greater consequences for divergence dating. The "Sppil–Rongis" or, Jaanuson effect, serves as a critical reminder of the inherent limitations of the fossil record in accurately capturing the emergence of new clades (Marshall, 1990, 2008, 2017, 2019).

It is noteworthy that the Signor-Lipps effect has gained prominence due to research trends and the dynamics of publication and citation, particularly as its recognition coincided with the intense debates of the 1980s surrounding the K/Pg impact (Alvarez *et al.*, 1980; Hildebrand *et al.*, 1991). Indeed, this effect serves as the main framework for understanding mass extinctions (Rampino & Adler, 1998; Alroy, 2014; Wang & Zhong, 2018; Nawrot *et al.*, 2018) as well as the popular, albeit problematic, concept of Lazarus taxa (Rickards & Wright, 2002). The coelacanths are the quintessential example of a Lazarus taxon, initially discovered as fossils (Agassiz, 1839), they were presumed to be extinct since the end of the Mesozoic Era, around 66 Ma (Toriño, Soto & Perea, 2021). However, exactly one century after their description, living populations were unexpectedly discovered in multiple localities (Smith, 1939, 1940, 1953), challenging previous extinction assumptions.

On the other hand, the Jaanusson effect was proposed in 1976, a period when the fields of palaeontology and taphonomy were not as integrated with molecular biology and computational phylogenetics as they are today (Ronquist *et al.*, 2012), limiting its initial exposure and integration into broader scientific paradigms (Heads, 2012). However, understanding the Jaanusson effect is crucial for devising appropriate calibration nodes, allowing more accurate phylogenetic reconstruction, and also for avoiding underestimation of

the true age of clades (Marshall, 1990; Dornburg *et al.*, 2011). It highlights the need for caution when using the fossil record to infer divergence times, as the oldest fossil found is not necessarily representative of the actual time of divergence (Ksepka & Clarke, 2015; Kimura, 2019; Dalmasso, Peláez-Campomanes & López-Antoñanzas, 2022). This has major implications for the calibration of molecular clocks and for dating the tree of life (Marshall, 2008; Brown & Smith, 2018).

The boarder limitations for the correct estimation of divergence time are: 1) proper identification of the lineage's FAD; 2) estimating the ΔT_{Gap} between a FAD accurately constrained in time and the moment when the first skeletal fossilizable derived character evolves; 3) estimating the $\Delta T_{Div\text{-}1stApo}$ between the first apomorphy likely to fossilise and the divergence event itself (Figure 6.2 A). The first and second intervals are complicated by the diminishing likelihood of finding fossils as we move further back into deep time (Figure 6.2 B), while the third interval is nearly impossible to determine as the clade would not be recognizable in the fossil record if skeletal derived traits have not evolved yet, and soft tissue traits are extremely unlikely to ever fossilise (Foote & Sepkoski, 1999; Marshall, 2019). Despite this, the $\Delta T_{Div\text{-}1stApo}$ interval is intrinsically linked to the completeness of a taxon's fossil record. A well-documented fossil record might suggest a narrow interval, potentially less than a million years. Conversely, a sparse fossil record could indicate a much broader interval (Tavaré *et al.*, 2002), and the Primate fossil record has been described as "frighteningly incomplete" (Fleagle, 2003, p. 22).

Extinct great ape species that are usually not attributed to any of the African ape lineages (Gorillini, Paninini, and Hominini), like *Nakalipithecus nakayamai*, dated to 9.9–9.8 Ma (Kunimatsu *et al.*, 2007), could still belong to one of them if they lived during this non-detectable $\Delta T_{Div\text{-}1stApo}$ interval that is an intrinsic aspect of the speciation process. In the same way that the 450 thousand years old camelid cranium described as intermediate by Martini et al. (2015) is not attributable to either lineage because it is likely in the $\Delta T_{Div\text{-}1stApo}$ time range of the Bactrian/Dromedary split, when "the phenotypes of both lineages should be markedly closer to each other than today" (Geraads *et al.*, 2020, p. 257).

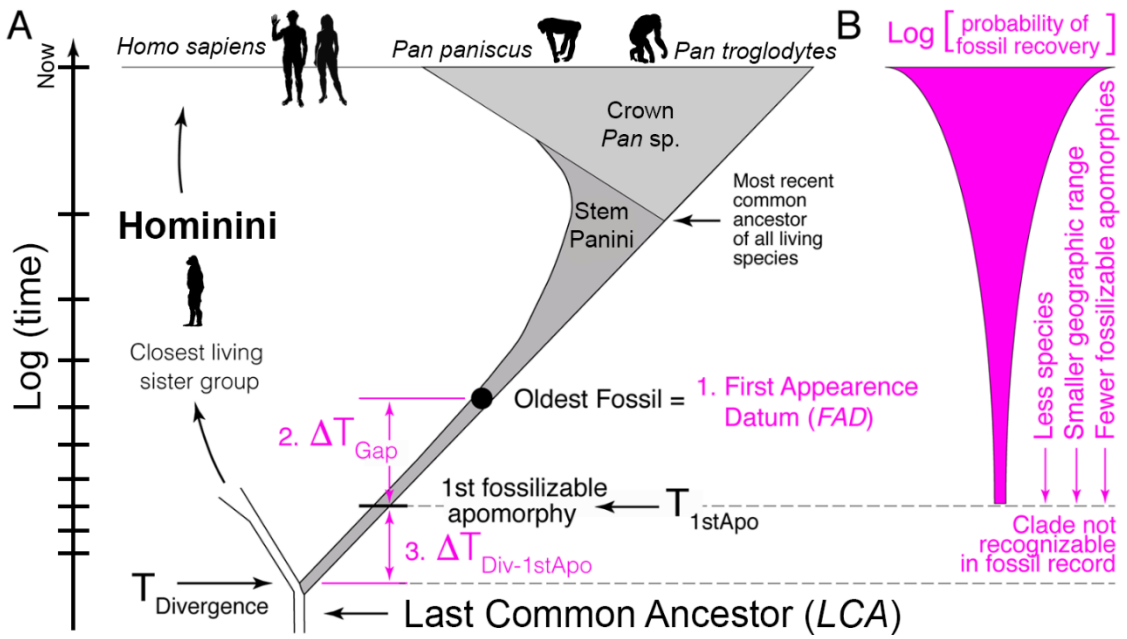


Figure 6.2 – **Challenges in deducing divergence times from the fossil record**. A) Primary obstacles in using palaeontological data to calibrate lineage splits: 1. Identifying and dating the clade's earliest known fossil (FAD); 2. Calculation of the temporal discrepancy ΔT_{Gap} between the FAD and the emergence of the lineage's initial fossilizable trait; 3. The interval $\Delta T_{Div\text{-}1stApo}$ between the clade's first fossilizable characteristics and the actual genetic point of divergence. The latter, $\Delta T_{Div\text{-}1stApo}$, cannot be known, as it pertains to a period for which the clade's fossils are indistinguishable and thus unidentifiable within the fossil record. B) The estimation of ΔT_{Gap} is complicated by the diminishing likelihood of fossil discovery near the lineage's origin, compounded by the inherently sporadic and fragmentary nature of fossils and stratigraphic records. Adapted from Marshall (2019) in order to illustrate the *Pan*/*Homo* split scenario.

The ΔT_{Gap}, however, should always be possible to target as new fossil sites of the relevant age are found. If such sites contain fossils of any ape lineage, their respective ΔT_{Gap} can be effectively reduced. Furthermore, it substantially facilitates proper estimation of the lineage origins using confidence intervals and other probabilistic methods (e.g., Du *et al.*, 2020; Bobe & Wood, 2022). Thus, the potential for narrowing the ΔT_{Gap} of *Pan*/*Homo* increases with the discovery of new fossil sites corresponding to critical time periods in the late Miocene (Chapter 3), such as those recently found in Gorongosa National Park, Mozambique (Chapter 4). Gorongosa, with its diverse palaeoenvironments and fossil-rich formations (Habermann *et al.*, 2019), offers a unique opportunity to explore this gap for multiple divergences of interest within hominoid radiations of the Miocene (Figure 6.1). Recent discoveries from the lower Mazamba formation in Gorongosa have unearthed fossils from multiple crucial time periods,

ranging from the early to the late Miocene (Bobe *et al.*, 2023). Finding fossils of either early hominins or other ape species during these periods will provide key insights into narrowing the ΔT_{Gap} and provide clearer dating for the origins of Hominini, Panini, Gorillini, and possibly other now-extinct lineages of Miocene African apes (Cote, 2004; Almécija *et al.*, 2021; Urciuoli & Alba, 2023).

6.2.3 The satellite's guide to Gorongosa's fossils

Chapter 4 introduces an efficient and scalable remote sensing protocol, enhancing our efforts to address an important temporal and geographic gap in our knowledge of the African Miocene. This approach resulted in the discovery of new fossil sites on sparsely sampled palaeobiomes, including coastal estuarine and deltaic forests and woodlands, potentially pivotal in the evolution of apes and hominins, as supported by recent behavioural ecology findings and long-standing evolutionary theories (Kingdon, 2003, 2023; Wrangham, 2005; Wrangham *et al.*, 2009; Head *et al.*, 2019; Nowak & Coles, 2019; Sponheimer *et al.*, 2019; Joordens *et al.*, 2019; Bobe *et al.*, 2020b, 2023).

By harnessing the power of satellite and machine learning, this chapter resulted in the discovery of four new fossil sites containing early to late Miocene fossil-bearing deposits in the densely vegetated landscapes of the EARS termination south of the Zambezi (Flores, 1973; Tinley, 1977; Ponte *et al.*, 2019). The study presents a simple yet effective solution for finding fossil sites based on clustering via unsupervised learning of satellite images (Conroy, 2014; Conroy *et al.*, 2018) with the *k*-means algorithm (Jain, 2010).

The objective was to identify additional outcrops and deposits from underexplored temporal intervals critical for understanding African ape and early hominin evolution, including the initial phase of the late Miocene (Chapter 3). This exploration was conducted in the Urema Rift, an overlooked region in southeastern Africa in terms of palaeontology (Böhme *et al.*, 2006; Fonseca *et al.*, 2014; Domingues *et al.*, 2016; Chirindja *et al.*, 2016). Preliminary beryllium dating results from selected sites (Bobe *et al.*, 2023) provide initial evidence supporting the hypothesis that these locations correspond to the targeted temporal intervals of

interest (Figure 6.1). Furthermore, owing to its geographical context and ecological characteristics, Mozambique has been posited as a region of potential strategic significance in the realms of human evolution (Wilson, 2014), early Pliocene hominins (Joordens *et al.*, 2019), and, intriguingly, the late Miocene LCA (Kingdon, 2023).

The clustering approach applied in Chapter 4 highlighted priority targets for prospecting that represented less than 4.5% of the total area analysed. Applying this method, four new fossil sites were discovered in the area, and results show an 85% accuracy in a binary classification. This indicates the high potential of a remote sensing tool for exploratory palaeontological surveys by enhancing the discovery of productive fossiliferous deposits. Notably, Chapter 4 shed light on the importance of longer wavelengths, particularly near-infrared, for enhancing visibility within dense vegetation cover—a critical revelation for palaeontological prospecting in such environments.

The journey of palaeontological discovery is often long and arduous, as exemplified by the decades-spanning efforts in southern and eastern Africa. The 44-year interruption of south African hominin discoveries, since *Paranthropus robustus* from Swartkrans (Broom, 1949), to the *Australopithecus* sp. at Gladysvale (Berger, Keyser & Tobias, 1993), and the Leakeys' 33-year dedication at Olduvai Gorge leading to the discovery of *P. boisei* (Leakey, 1959), illustrate the perseverance and resilience required in palaeoanthropological research. These examples serve as a testament to the necessity for continual exploration, but also indicate that there is a need for standardisation and adoption of quantitative protocols, such as geospatial surveying techniques, to enhance the probability of uncovering pivotal fossils (Njau & Hlusko, 2010; Emerson *et al.*, 2015; Emerson & Anemone, 2018).

Cutting-edge artificial intelligence algorithms, coupled with high-resolution satellite imagery and other GIS datasets, have enabled palaeontologists to pinpoint fossil-rich sites with unprecedented precision (Anemone *et al.*, 2011b; Conroy, 2014; Block *et al.*, 2016; Anemone & Conroy, 2018). Additionally, geospatial tools have facilitated the identification of potential new fossil localities and enhanced the efficiency of fieldwork (Chapter 4).

6.2.4 Searching for Kingdon's coastal ape

In Africa, all the living great African ape species can be found in the Congo Basin (Kingdon, 1990). Gorillas, chimpanzees, and bonobos are all known to use inundated areas for ranging, foraging, and sleeping, including swamp forest, swamp grassland, seasonally flooded forest, riparian forest, marsh grassland, among others (Yamagiwa *et al.*, 2019). Within tropical regions, as rivers approach the coastal areas, forests and woodlands undergo a transition, grading into mangrove ecosystems—littoral wooded habitats that harbour a diverse array of primate species. Notably, this includes *Pan troglodytes verus* communities at Cantanhez Forest, Guinea-Bissau, as well as *Gorilla gorilla gorilla* and *Pan troglodytes troglodytes* from Loango, Gabon, who exhibit a repertoire of foreshore behaviours that are yet to be formally described in long-term studies (Head *et al.*, 2019).

Only a single African ape fossil is known from palaeoecological coastal settings, more particularly at the early-to-mid Miocene deposits of the Ryskop mines in Namaqualand, South Africa (Pickford & Senut, 1997). Initially ascribed to cf. *Kenyapithecus*, Ryskop's Hominoidea is represented by a single fragmented molar dated to 16 Ma, and contemporary researchers assign it to Nyanzapithecidae indet. (Urciuoli & Alba, 2023).

Despite the current fragmentation of the coastal forests of eastern Africa (CFEA), which ran continuously from Somalia to South Africa up to the Pliocene (Joordens *et al.*, 2019), mangrove forests can still be observed up to 50 km inland in some areas of Mozambique (Head *et al.*, 2019). These coastal ecosystems meet riverine forests that can act as wooded and wet corridors from the CFEA to the lake basins of the EARS (Joordens *et al.*, 2019). In the mid-Miocene climatic optimum, when global temperature and humidity levels were higher, the core rainforest of the Congo basin extended continuously from the Guinean forests of west Africa all the way to the CFEA (Steinthorsdottir *et al.*, 2021; Kingdon, 2023). Aridification cycles intensified about 10.5 Ma, developing the arid corridor that would split western rainforests from the CFEA (Kingdon, 2003; Bobe *et al.*, 2023). This corridor generally correlates to the mountainous uplifts and subdued great lakes of the EARS that act as a dynamic biogeographic

border between west and east forest-dwelling African species (Morley & Kingdon, 2013). Curiously, the montane rainforest at Mount Gorongosa in the western shoulder of the Urema Rift is the only remnant of the larger ancient Congolese tropical forest in the southern EARS (Wilson, 2014; Tinley, 2020).

The discovery of new fossil sites in undersampled Miocene habitats (d'Oliveira Coelho *et al.*, 2021), such as the coastal estuarine forests and woodlands of Gorongosa (Habermann *et al.*, 2019), marks a pivotal step in our exploration of potential new early hominin and ape habitats (Bobe *et al.*, 2020b, 2023). In this advancing landscape of geospatial palaeontological research, the integration of scalable and generalizable computer vision approaches with ground-truthing promises to address long-standing limitations, from sample size constraints to geographic gaps and temporal biases. The recent discovery of four Primate fossils, including cf. Hominoidea teeth, in the PPPG 2022 field seasons (d'Oliveira Coelho *et al.*, 2023) set the stage for a more comprehensive and representative understanding of the intricate processes underpinning early Homininae evolution, guided by the potential of advanced computational methodologies and the rich promise of littoral wooded landscapes within the Miocene of the EARS (d'Oliveira Coelho, 2023).

6.2.5 Do orbiting machines dream of ancient environments?

In Behrensmeyer's landmark dissertation (1975a), it was concluded that in delta margin deposits, both aquatic and nonaquatic vertebrates (excluding fish) are equally abundant, while nonaquatic forms dominate fluvial deposits. Mammalian faunas, particularly hippos, suids, and bovids, show distinct abundance patterns, revealing habitat preferences. These insights from vertebrate occurrences laid the foundation for the palaeoecological framework in Turkana—and palaeoanthropology as a whole—by allowing the examination and reconstruction of hominin habitats. I expanded on these taphonomic and sedimentological insights by correlating them with readily available "big data" (i.e., large satellite datasets) encompassing spectral, environmental, and topographic information (Figure 6.3).

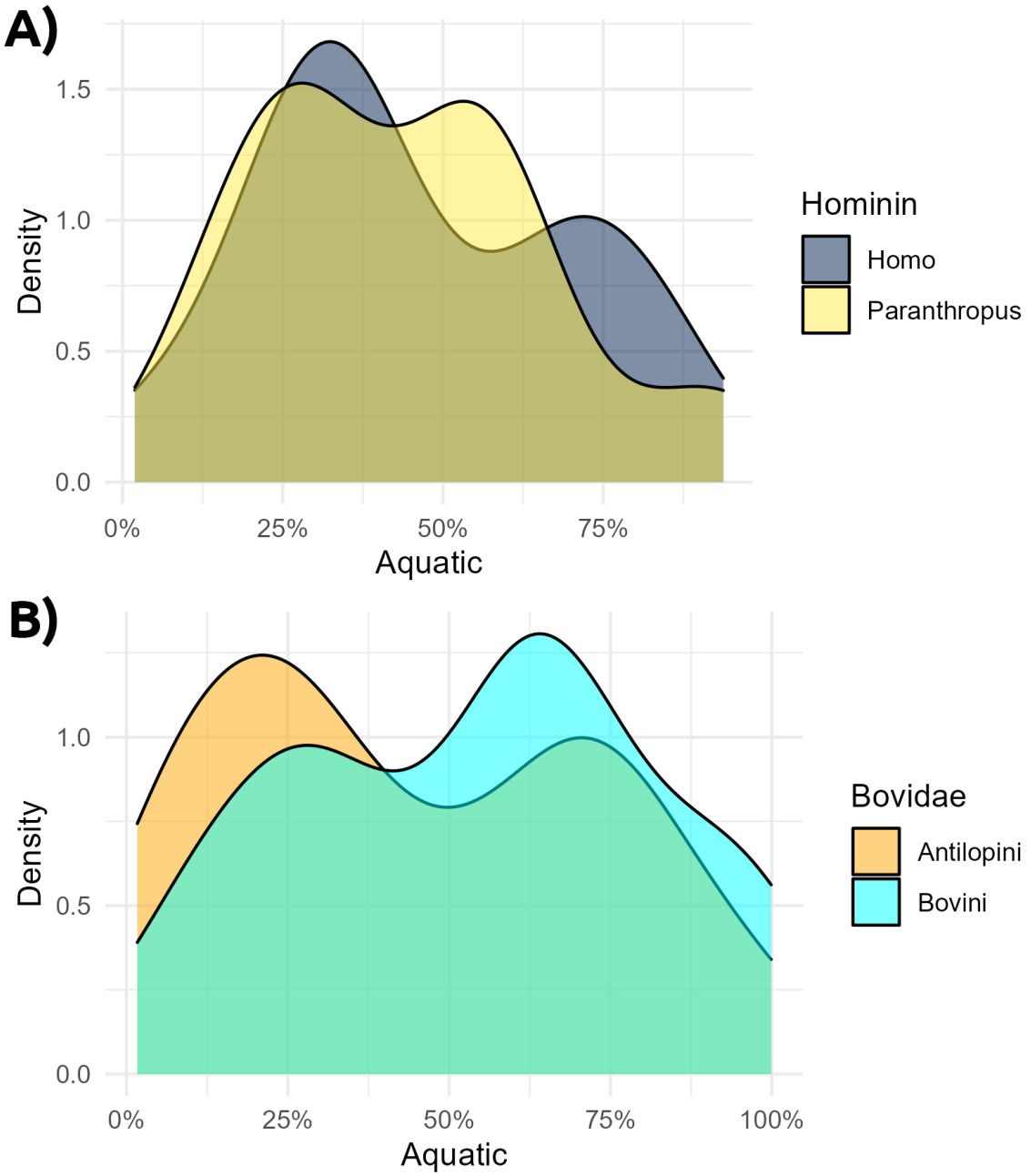


Figure 6.3 – **BetaReg predictions on grid cells** known to contain A) *Homo* and *Paranthropus*; B) Antilopini and Bovini. Geocoordinates sampled from the PaleoTurkana Database (Bobe et al., 2022).

Density kernel estimations can correlate fossil coordinates with BetaReg predictions. Notably, *Paranthropus* fossils cluster within a more limited range than *Homo*, indicating the latter are more generalist (Figure 6.3 A), although the sample size is relatively small (N = 60). Both species peak at relatively terrestrial environments like floodplains (~25%), but their second kernel density peaks differ, with *Paranthropus* at about 50% (river dominated environments)

and *Homo* at 75%, in a more aquatic setting. This mimics the well-known pattern of *Paranthropus* being more associated with rivers and *Homo* with lakes in east Turkana (Behrensmeyer, 1975a). However, this might be due to taphonomic processes, as robust molars tend to be more resistant to fluvial transportation (Behrensmeyer, 1975b). Additionally, using a far larger sample, at the two extremes of water-dependent bovids, a clearer pattern emerged (Figure 6.3 B), showing that the geospatial models of Chapter 5 allow us to infer behavioural ecology patterns, like habitat preference.

Why do certain environments exhibit a preferential preservation in the fossil record? In Chapter 5, efforts were made to advance geospatial palaeontology further by introducing the first protocols for remote reconstructing of ancient landscapes based on satellite data, expanding it into a new subdiscipline "geospatial palaeoecology". Machine learning models have proven successful in identifying optimal conditions for discovering fossil sites (Chapter 4) across diverse geographic and temporal contexts (Conroy *et al.*, 2012; Block *et al.*, 2016; Ghezzo *et al.*, 2023). The fossilisation process is expected to yield different sediments with distinct spectral signatures under various taphonomic and ecological conditions (Wills *et al.*, 2018). To investigate the disparate preservation of aquatic and terrestrial habitats, we present a pioneering effort to capture palaeoecological patterns through geospatial analysis of topographical, ecological, and spectral variables. This analysis aims to distinguish between aquatic and terrestrial faunal components within the palaeoenvironments of the Koobi Fora Formation. In this study, topographic variables were more important for habitat reconstruction than fossil site detection, showing that taphonomy plays a crucial role in differential preservation of the sediments.

Is it possible to model spectral variations in sediments for remote palaeoenvironmental reconstruction? As we delve into the nuances of spectral bands and their environmental correlates (Chapter 4), it becomes evident that our understanding of remote sensing and unsupervised learning in the context of fossil site detection has immense untapped potential (Chapter 5). Near-infrared (NIR), a recognized biomass proxy (Hu *et al.*, 2015), maps organic material in the soil (Viscarra Rossel & Hicks, 2015). We found that erosional surfaces within

a specific NIR range (14000 to 15800 in East Turkana) enhance fossil discoverability, while short-wave infrared (SWIR) bands were essential for environmental reconstructions through geospatial machine learning. NIR's penetrative capacity through forest canopy (Huete *et al.*, 1997) has also proved valuable in Gorongosa's miombo woodlands and riparian forests (Chapter 4). In the arid EARS region, NIR's effectiveness suggests it could be a useful and generalizable "fossil band" in varied ecosystems, urging further testing in palaeontological settings to confirm this hypothesis (Chapter 5).

6.3 Future directions

6.3.1 Dating the tree of life

While Chapter 3 focused on the divergence between *Homo* and *Pan*, it is essential to consider the broader context of human evolution by examining additional divergence events between hominins and other prominent ape lineages. By conducting a swift survey of the TimeTree database (Kumar *et al.*, 2022), we obtained preliminary estimates of split events between humans and various living ape lineages (Figure 6.1). The literature compiled by TimeTree indicates that *Homo* diverged from *Pan*, *Gorilla*, *Pongo*, and Hylobatidae at approximately 6.4, 8.6, 15.2, and 19.5 million years ago (Ma), respectively. However, as demonstrated in Chapter 3, our meta-analysis suggests that the *Homo*-*Pan* split may be more realistically situated within an interval of 8 to about 11 Ma, rather than the proposed 6.4 Ma. This conclusion was reached by significantly expanding the TimeTree dataset from 81 to 198 estimates and employing advanced data science techniques, such as Bayesian meta-analyses, to move beyond simple median averages.

Building upon these methodological advancements, it is worth investigating whether a similar bias toward more recent estimates exists in the other major divergence events within the Hominoidea radiation. Replicating our methodology for the divergences of *Gorilla*, *Pongo*, and hylobatids would be a promising future endeavour. By applying the same data science techniques to these additional divergence events, we can gain a more comprehensive

understanding of the temporal dynamics of Hominoidea radiations and speciation. Such an exploration would not only enhance our knowledge of the specific divergence events but also contribute to a broader understanding of the timeline and overall evolutionary history of the apes. In conclusion, the findings of our study provide a foundation for future investigations into the meta-science of temporal phylogenetics. The new methodological approaches contribute to the refinement of temporal estimates and deepen our understanding of the intricate tapestry of human evolutionary history within the Hominoidea (Pilbeam, 1996; Steiper *et al.*, 2004; Pugh, 2022)

6.3.2 Gorongosa's unfinished symphony: a work of decades

No time to sleep with a bonebed

While the exploration and surveying for new fossil sites in Gorongosa was paused partially due to the discovery of a highly fossiliferous bone bed in GPL-12, the ape fossil findings of the last two field seasons have made it worth it to concentrate all efforts on excavations. It is now urgent to investigate the Mazamba Fm in terms of bone bed genesis (Eberth, Rogers & Fiorillo, 2007). A possible explanation for the extensive bone beds would have to do with the frequent cyclones hitting the National Park area ~ 100 Km away from the coast. In average 1.2 cyclones make landfall in Mozambique per year (Walker *et al.*, 2023). In the Miocene epoch however Gorongosa was in the coast (Habermann *et al.*, 2019), but it is also relevant that then the nucleus of cyclone formation was not at the Indian to Pacific Ocean transition between Oceania and Southeast Asia as it stands today, but instead it was much closer to the Mozambican channel, just northeast of Madagascar (Yan *et al.*, 2019). Of course, that are many other possible explanations for bone bed formation (Behrensmeyer, 2007), yet according to the palaeoclimatic simulations, we can expect that the frequency and magnitude of cyclones in the area would be intensified, peaking in the late Oligocene to Early Miocene, and slowly declining to present day levels as worldwide temperatures decrease and the core area of cyclone formation moved significantly eastwards, by about 7000 Km, during the Pliocene (Yan *et al.*, 2019). This can be

tested using a multidisciplinary framework combining petrography, petrophysics, taphonomy, sedimentology, and geochemistry as demonstrated recently in a study of Atlantic tropical storms in the Miocene of Brazil (Aguilera *et al.*, 2023).

Anomaly detection: fossil sites as spectral outliers in the landscape

There were two main limitations slowing down surveying efforts at the Urema Rift for new fossil sites: 1) no field seasons on 2020 and 2021 during the worldwide pandemic; 2) the PPPG team focused exclusively in excavating GPL-12 to understand this fossil-rich site with three distinct fossiliferous layers, including a bonebed. However, new remote surveying models have been continuously worked on, and there is one innovative path of research demonstrating very promising results, that differ from the approach used in Chapter 4. Expanding on unsupervised learning of remote spectral data, particularly to approaches specialised in anomaly and outlier detection, could allow for the identification of previously unknown patterns in Gorongosa's landscape, potentially leading to the discovery of new fossil sites. A proof of principle using the dbscan algorithm (Ester *et al.*, 1996) and ensemble learning was implemented. It is more accurate than the previous *k*-means approach already described in detail (d'Oliveira Coelho *et al.*, 2021), when tested with the current set of known fossil sites in the region (d'Oliveira Coelho *et al.*, 2020). However new surveys should be carried out to ground-truth the never-before-surveyed spots suggested by the dbscan's anomaly detection approach to ensure its precision (Appendix III).

Taxonomy and Anatomy

After six field seasons, the number of fossils in Gorongosa now numbers in the thousands, and many of these are likely to be new species or even genera. This work has already started with several taxonomic groups, like the hyracoids and tiger sharks (Bobe et al., 2023). The discovery of fossil rich sites with advanced computational approaches inevitably has led to an abundance of new fossil material to describe, including the first Miocene primates from Mozambique.

There are two very promising incisors that are very likely to be the first Hominoidea fossils from Mozambique. PPG2022-P-091 is a left upper first incisor, and PPPG2023-P-232 is a right lower second incisor. Some preliminary work has already been done to address the upper

incisor from 2022, including geometric morphometrics (GMM) analysis (Figure 6.4). The protocol involved the analysis of landmark data to derive shape variables. Differences due to scale, translation, and rotation were minimised using the GPA (Generalised Procrustes Analysis) as implemented in 'geomorph' R package. Semi-landmarks were adjusted on the models' surfaces to minimise Procrustes distance, a process optimising their locations iteratively relative to the consensus shape configuration (Gunz & Mitteroecker, 2013). The resulting shape variables were then subjected to a Principal Component Analysis (PCA) as implemented in 'geomorph' to summarise shape variation (Adams & Otárola-Castillo, 2013).

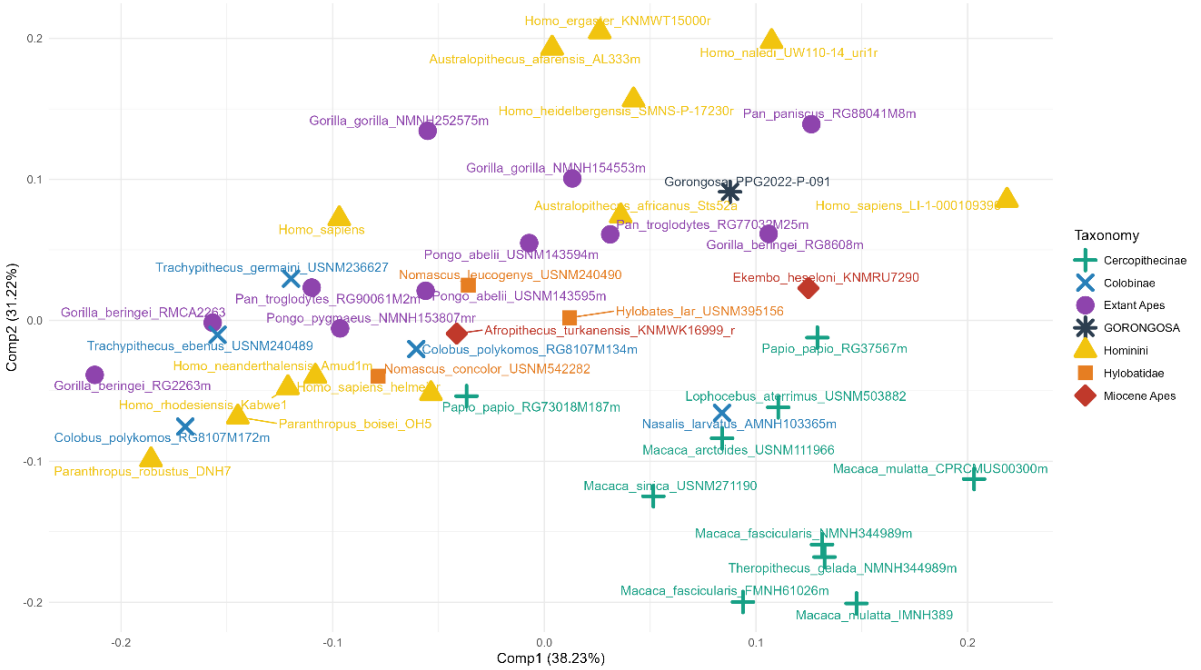


Figure 6.4 – **Morphospace for upper left first incisors**, a preliminary analysis to assess the phenetic affinities of the Gorongosa cf. Hominoidea UI1 PPG2022-P-091 to other Primates via PCA.

Overall, the upper incisor from Gorongosa clusters closely with gorillas, bonobos, chimpanzees and some sub-adult *Australopithecus* and *Homo*, supporting its tentative placement in Hominoidea. The upper right quadrant of the PCA morphospace is relevant not just in terms of taxonomy but of ontogenetic development because it is dominated by non-adults or sub-adults. However, this incisor is quite large for a non-adult, indicating it would then be close to *Gorilla* in terms of body size. What is intriguing is that this resemblance extends beyond size and encompasses shape as well, since the GMM analysis revealed that the closest shape match, in

both principal components, was with a *Gorilla beringei* individual. Note that these results are preliminary, and therefore might change.

6.3.3 Remote cave detection

The next frontier in geospatial palaeontology might be automating remote detection of fossiliferous caves like those found in the Cradle at South Africa (Figure 6.5 A). From a methodological perspective it should now be possible to implement a working protocol since the materials and methods are readily available. Notably, there are now two georeferenced databases for caves in Africa, the Cradle database of 597 caves, of which 81 are fossiliferous, available upon request (Dirks & Berger, 2013), and the PPPG Speleological Inventory, curated by the PPPG's Speleo Team, and at present containing 108 caves located in the eastern shoulder of the Urema Rift (Regala *et al.*, 2023). An optimal model would be one that would not just be able to learn spectral patterns but also the shape configurations and geometric patterns associated with fissures and entrances, and there is one candidate that stands out—convolutional neural networks—already shown to be extremely efficient at remote cave detection in China (Yan, Gu & Yan, 2022; Huang *et al.*, 2023).

In the long-term, the sparse fossil record associated with *Gorilla* and *Pan* stands to gain the most from fossil-rich cave prediction. From a biogeographic point of view, a more rational approach would be to seek their ancestors westward of the EARS, particularly in caves likely to preserve fossils better than open air sites with acidic and humid forest soils (Behrensmeyer, 1978; Vrba, 2007). Numerous unexplored areas, particularly from the palaeoanthropological perspective, are presently undergoing karstification or harbour cave systems across a vast expanse, spanning from Senegal to Cameroon, also from Gabon to central Angola, and from the DR Congo to northern Zimbabwe (Figure 6.5). Within the tropics alone, Africa spans 1.05 million km^2 of areas likely to be rich in cave systems. Furthermore, Africa has a total of 4.054 million km^2 of surface karst exposed, representing 13.5% of the continental landmass above sea level (Goldscheider *et al.*, 2020).

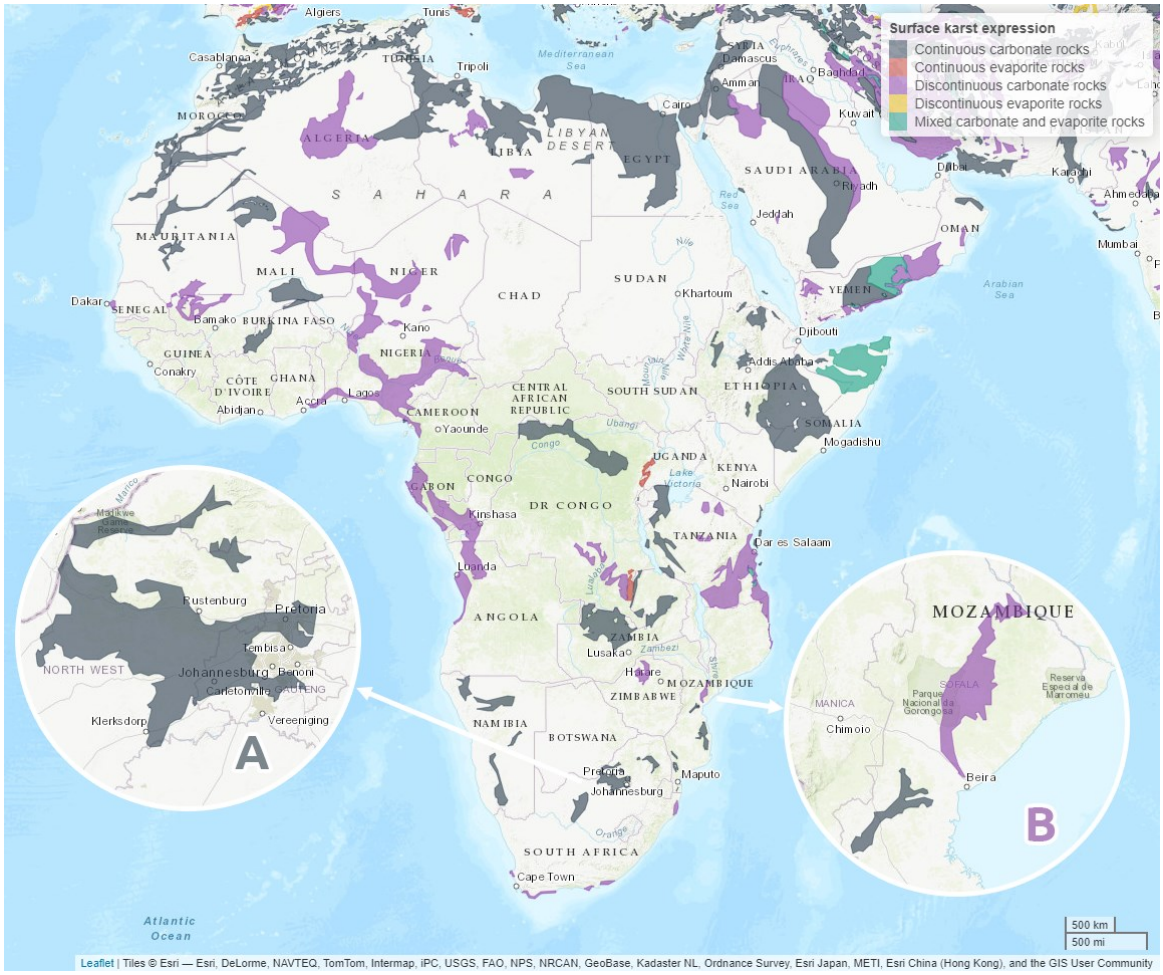


Figure 6.5 – **Karstic map of the Afro-Arabian continental landmass**. Vectorial dataset layer is the World Karst Aquifer Map (Goldscheider *et al.*, 2020), and the map was generated using the leaflet package for R (Cheng *et al.*, 2021). Zooming 10x: A) Total extension of cave systems in and around the Cradle of Humankind, South Africa; B) Gorongosa and associated limestone areas.

If a satellite-based computer vision model is trained, calibrated, and validated with either the Cradle of Humankind and/or the PPPG Cave Inventory, it could then be tested on karsts more likely to contain "Pancestors" or "Oldrillas". Particularly in regions overlapping the historical bounds of the Congo and the Guinean forests of western and central Africa (Kingdon, 2023). If successful, findings from any age would be of utmost interest considering the current incompleteness of the *Pan* and *Gorilla* fossil records.

On a short-term basis, this type of predictive model approach would also be essential to accelerate the rate of cave discovery at the Cheringoma limestones in Gorongosa (Figure 6.5 B) that are thought to contain deposits ranging throughout the Quaternary period (Laumanns,

2001). Hence, it is not impossible that these caves harbour *Homo* or *Paranthropus*, and possibly even late forms of *Australopithecus*, like *Au. africanus* or *Au. sediba*.

6.3.4 Geospatial palaeoecology: an emerging new discipline

In Chapter 5 we used the ratio of aquatic fauna present in bone walks to reconstruct water abundance of ancient landscapes. This type of protocol can be extended for other habitat reconstruction problems, by using compiled databases with geocoordinates of extinct fauna with ecological inclinations for certain types of biotas. An emblematic case is that of Bovidae, as it is well known that habitat preferences of bovid tribes have remained relatively constant over the last few million years (Bobe *et al.*, 2007b). For example, Alcelaphini are hypsodont grazers associated with open or wooded grasslands, while Tragelaphini are adapted to more heavy cover environments such as woodlands and forests (Kingdon, 2013).

Taking advantage of such well-known habitat-taxon associations, maximum entropy and one-class support vector machine algorithms could be trained with geolocated datasets like the PaleoTurkana database (Bobe *et al.*, 2022), to model environmentally constrained fossiliferous conditions. In this paradigm, a target concatenation of Acelaphini–Antilopini–Hippotragini geolocated data could be used to map new potential fossiliferous deposits containing fauna typical of open-dry environments (i.e. savanna grasslands, bushland, or woodland-grassland mosaics). A second model would use the abundant Reduncini tribe as an indicator of light cover wet grasslands. Another concatenation with Aepycerotini–Bovini could be used to determine moist/near-water grassland to woodland fossil sites. And finally, a Tragelaphini based-model could be implemented to map locations of heavy covered environments like forests (Bobe & Eck, 2001; Bobe *et al.*, 2007b).

Alternatively, a single classification model using neural networks, random forest, or any other type of supervised learning algorithm could be applied to a target variable with the four classes (open-dry, open-wet, woody-wet, and forest) trained using the geolocation of the same tribes of bovids described. All these predictions could be ground-truthed by visiting predicted cells and documenting and identifying every identifiable bovid fossil (e.g., horncores, tali, teeth,

mandibles, maxilla, etc.) to evaluate if the different competing models can accurately and efficiently model the palaeohabitats being surveying.

6.4 Conclusion

This discussion started by exploring the temporal biases and gaps, underscoring the ongoing improvements towards integrating the fossil record for divergence dating. Advancements in genetics and statistical methods, along with improved access to high-quality data such as full genomes, are noteworthy. However, all time-constrained phylogenetic trees ultimately rely on fossil-derived dates for node calibration and minimum ages of clades. To enhance the reliability of these advancements, better integration of data from sedimentology, geochronology, biogeography, and palaeontology is essential. A variety of examples from the tree of life were provided, spanning mammals, birds, reptiles, fish, invertebrates, plants, and even Archaea, demonstrating clearly that the biases in divergence timing are widely recognized and discussed across all living beings. There is no reason to assume that primates, including apes and hominins should be an exception. Chapter 3 takes a significant step towards rekindling constructive debates and fostering a continuous process of refinement in dating the origins of hominins. We must not forget that the *Pan-Homo* node itself is actually one of the most used to calibrate other divergences across all living taxa (Marshall, 2017; Hubisz, Williams & Siepel, 2020; Kumar *et al.*, 2022), and if it is underestimated significantly, this reinforces errors in estimations of other species through circularity i.e., one model result becomes an assumption in a next model for another taxonomic group, and as this process repeats, it creates a chain of assumptions biased by previous results.

The pioneering remote sensing protocols leveraging satellite imagery and machine learning to efficiently bridge temporal and geographic gaps in understanding the African Miocene were also discussed. This novel approach unearthed new fossil sites containing material likely to represent Hominoidea fossils in a littoral forest context. These exciting findings might allow palaeontologists to test for the time the biogeographic hypothesis of hominins deriving from

ground ape inhabiting the CFEA (Kingdon, 2003). Furthermore, Chapter 4 emphasised the significance of longer wavelengths, especially near-infrared, for enhanced visibility within dense vegetation and through the canopy, offering valuable insights for palaeontological prospecting in challenging environments that have been historically overlooked (Szymanski, 2018). This innovative approach aligns with the evolving landscape of palaeontological research, advocating for the adoption of quantitative open-source protocols to streamline the discovery of pivotal fossils (Block *et al.*, 2016).

Chapter 5 provides a groundbreaking step in bridging geospatial approaches to taphonomy by introducing original computational pipelines that reconstruct past environments based on satellite-derived data. By emphasising the crucial role of taphonomy in differential sediment preservation and how these hidden patterns can be recovered from topographical, ecological, and spectral variables, a new use case was found for geospatial palaeontology applications. Notably, the approach estimates aquatic to terrestrial conditions across the Koobi Fora Fm, and now that this protocol has been rigorously validated and tested in a fossiliferous basin studied for decades using multiple distinct lines of palaeoecological evidence and methods (Isaac & Behrensmeyer, 1997; Quinn *et al.*, 2013; Patterson *et al.*, 2019), it can be applied elsewhere. I also suggest how this protocol can be adapted and extended to reconstruct other kinds of palaeoecological features, such as gradients of open-to-close habitats or categories woody cover (Cerling *et al.*, 2011; Negash & Barr, 2023), by utilising the geolocations of fossil bovids and leveraging the modelling architecture on their known habitat preferences across time.

Lastly, the findings of each chapter have broader implications for future research and applications. The meta-dating of the *Pan-Homo* divergence (Chapter 3) contributes to refining our understanding of human evolution and guide us towards targeting deposits of more precise ages. The improved remote detection methods (Chapter 4) have implications for efficiently locating fossil sites, especially in undersampled regions and unexplored palaeoenvironmental contexts. The introduction of new tools for large-scale automated habitat predictions (Chapter 5) enhances our ability to reconstruct ancient landscapes and understand the ecological context of hominin and ape evolution.

Works Cited

ACHINO, K.F. & BARCELÓ, J.A. (2019) Spatial Prediction: Reconstructing the "Spatiality" of Social Activities at the Intra-Site Scale. *Journal of Archaeological Method and Theory* **26**, 112–134.

ADAMS, D.C. & OTÁROLA-CASTILLO, E. (2013) geomorph: an r package for the collection and analysis of geometric morphometric shape data. *Methods in Ecology and Evolution* **4**, 393–399.

AGASSIZ, L. (1839) *Recherches sur les poissons fossiles*. Imprimerie de Petitpierre, Neuchâtel.

AGUILERA, O., DE ARAUJO, O.M.O., LOPES, R.T., COHEN, M., SIERRA, D.A., GUIMARÃES, B.T., LINHARES, A.P., RODRIGUEZ, F., MOREIRA, M., DIAZ, R., GAMA FILHO, H.S., DOS ANJOS, M.J., LIMA, D., DOS SANTOS SILVA, J., GIRAUD-LOPEZ, M.J., ET AL. (2023) Miocene tropical storms: Carbonate framework approaches and geochemistry proxies in a reservoir model. *Marine and Petroleum Geology* **154**, 1–19.

AL KHABOUR, A. (2022) Insights from Central Syrian Desert on the migration routes of *Homo erectus* from Africa to Eurasia during the Paleolithic. *Anthropologica et Praehistoria*, 1–13.

ALEMSEGED, Z. (2003) An integrated approach to taphonomy and faunal change in the Shungura Formation (Ethiopia) and its implication for hominid evolution. *Journal of Human Evolution* **44**, 451–478.

ALI, A. & POUR, A. (2014) Lithological mapping and hydrothermal alteration using Landsat 8 data: a case study in ariab mining district, red sea hills, Sudan. *International Journal of Basic and Applied Sciences* **3**, 199–208.

ALLOGHANI, M., AL-JUMEILY, D., MUSTAFINA, J., HUSSAIN, A. & ALJAAF, A.J. (2020) A Systematic Review on Supervised and Unsupervised Machine Learning Algorithms for Data Science. In *Supervised and Unsupervised Learning for Data Science* (eds M.W. BERRY, A. MOHAMED & B.W. YAP), pp. 3–21. Springer International Publishing, Cham.

ALMÉCIJA, S., HAMMOND, A.S., THOMPSON, N.E., PUGH, K.D., MOYÀ-SOLÀ, S. & ALBA, D.M. (2021) Fossil apes and human evolution. *Science* **372**, eabb4363.

ALROY, J. (2014) Accurate and precise estimates of origination and extinction rates. *Paleobiology* **40**, 374–397.

ALVAREZ, L.W., ALVAREZ, W., ASARO, F. & MICHEL, H.V. (1980) Extraterrestrial Cause for the Cretaceous-Tertiary Extinction. *Science* **208**, 1095–1108.

ANDREWS, P. (2019) Last Common Ancestor of Apes and Humans: Morphology and Environment. *Folia Primatologica* **91**, 122–148.

ANDREWS, P., REYNOLDS, S.C. & BOBE, R. (2022) Approaches to the Study of Past Environments. In *African Paleoecology and Human Evolution* (eds S.C. REYNOLDS & R. BOBE), pp. 7–14. Cambridge University Press, Cambridge.

ANEMONE, R.L. & CONROY, G.C. (2018) Geospatial Anthropology: Integrating Remote Sensing and Geographic Information Sciences into Anthropological Fieldwork and Analysis. In *New Geospatial Approaches to the Anthropological Sciences* (eds R.L. ANEMONE & G.C. CONROY), pp. 1–20. New Mexico Press, Albuquerque, NM.

ANEMONE, R.L., CONROY, G.C. & EMERSON, C.W. (2011a) GIS and paleoanthropology: incorporating new approaches from the geospatial sciences in the analysis of primate and human evolution. *American Journal of Physical Anthropology* **146**, 19–46.

ANEMONE, R.L., EMERSON, C.W. & CONROY, G.C. (2011b) Finding fossils in new ways: an artificial neural network approach to predicting the location of productive fossil localities. *Evolutionary Anthropology: Issues, News, and Reviews* **20**, 169–180.

ARCHER, W., BRAUN, D.R., HARRIS, J.W.K., MCCOY, J.T. & RICHMOND, B.G. (2014) Early Pleistocene aquatic resource use in the Turkana Basin. *Journal of Human Evolution* **77**, 74–87.

ARLOT, S. & CELISSE, A. (2010) A survey of cross-validation procedures for model selection. *Statistics Surveys* **4**, 40–79.

ASFAW, B., BEYENE, Y., SEMAW, S., SUWA, G., WHITE, T. & WOLDEGABRIEL, G. (1991) Fejej: a new paleoanthropological research area in Ethiopia. *Journal of Human Evolution* **21**, 137–143.

ASFAW, B., EBINGER, C., HARDING, D., TD, W. & WOLDEGABRIEL, G. (1990) Space based imagery in paleoanthropological research: An Ethiopian example. *National Geographic Research* **6**, 418–434.

ASNER, G.P. & LOBELL, D.B. (2000) A biogeophysical approach for automated SWIR unmixing of soils and vegetation. *Remote sensing of environment* **74**, 99–112.

ÄYRÄMÖ, S. & KÄRKKÄINEN, T. (2006) Introduction to partitioning-based clustering methods with a robust example. *Reports of the Department of Mathematical Information Technology. Series C, Software engineering and computational intelligence* **C. 1/2006**, 1–34.

BAILEY, G. (2004) World prehistory from the margins: the role of coastlines in human evolution. *Journal of Interdisciplinary Studies in History and Archaeology*, 39–50.

BAILEY, G.N., REYNOLDS, S.C. & KING, G.C.P. (2011) Landscapes of human evolution: models and methods of tectonic geomorphology and the reconstruction of hominin landscapes. *Journal of Human Evolution* **60**, 257–280.

BALDES, M.J., RAYNOLDS, R.G.H. & FEIBEL, C.S. (2023) The Upper Burgi Unconformity: A major hiatus in the fossiliferous Koobi Fora formation identified in area 116, east Turkana, Kenya. *Journal of African Earth Sciences*, 105135.

BALL, G.H. & HALL, D.J. (1965) ISODATA, a novel method of data analysis and pattern classification. In pp. 1–61. Stanford Research Institute, Menlo Park CA.

BALLA, A., PAVLOGEORGATOS, G., TSIAFAKI, D. & PAVLIDIS, G. (2014) Recent advances in archaeological predictive modeling for archeological research and cultural heritage management. *Mediterranean Archaeology and Archaeometry* **14**, 143–153.

BAMFORD, M.K. (2017) Pleistocene fossil woods from the Okote Member, site FwJj 14 in the Ileret region, Koobi Fora Formation, northern Kenya. *Journal of Human Evolution* **112**, 134–147.

BARBA-MONTOYA, J., DOS REIS, M. & YANG, Z. (2017) Comparison of different strategies for using fossil calibrations to generate the time prior in Bayesian molecular clock dating. *Molecular Phylogenetics and Evolution* **114**, 386–400.

BARBONI, D., ASHLEY, G.M., BOUREL, B., ARRÁIZ, H. & MAZUR, J.-C. (2019) Springs, palm groves, and the record of early hominins in Africa. *Review of Palaeobotany and Palynology* **266**, 23–41.

BARR, A.W. (2018) Ecomorphology. In *Methods in Paleoecology: Reconstructing Cenozoic Terrestrial Environments and Ecological Communities* (eds D.A. CROFT, D.F. SU & S.W. SIMPSON), pp. 339–349. Springer, Cham, Switzerland.

BARR, W.A. (2015) Paleoenvironments of the Shungura Formation (Plio-Pleistocene: Ethiopia) based on ecomorphology of the bovid astragalus. *Journal of Human Evolution* **88**, 97–107.

BAUMGARTNER, A. & PEPPE, D.J. (2021) Paleoenvironmental changes in the Hiwegi Formation (lower Miocene) of Rusinga Island, Lake Victoria, Kenya. *Palaeogeography, Palaeoclimatology, Palaeoecology* **574**, 110458.

BEAVAN, A.J.S., PISANI, D. & DONOGHUE, P.C.J. (2021) Diversification dynamics of total-, stem-, and crown-groups are compatible with molecular clock estimates of divergence times. *Science Advances* **7**, eabf2257.

BEGUN, D.R. (2010) Miocene Hominids and the Origins of the African Apes and Humans. *Annual Review of Anthropology* **39**, 67–84.

BEGUN, D.R. (2018) *The Real Planet of the Apes: A New Story of Human Origins*, 2nd. edition. Princeton University Press, New Jersey, USA.

BEGUN, D.R. & NARGOLWALLA, M.C. (2004) Late Miocene hominid biogeography: Some recent perspectives. *Evolutionary Anthropology: Issues, News, and Reviews* **13**, 234–238.

BEHRENSMEYER, A.K. (1975a) The taphonomy and paleoecology of Plio-Pleistocene vertebrate assemblages east of Lake Rudolf, Kenya. *Bulletin of the Museum of Comparative Zoology at Harvard College.* **146**, 473–578.

BEHRENSMEYER, A.K. (1975b) Taphonomy and paleoecology in the hominid fossil record. *Yearbook of Physical Anthropology* **19**, 36–50.

BEHRENSMEYER, A.K. (1978) Taphonomic and ecologic information from bone weathering. *Paleobiology* **4**, 150–162.

BEHRENSMEYER, A.K. (1982) Time resolution in fluvial vertebrate assemblages. *Paleobiology* **8**, 211–227.

BEHRENSMEYER, A.K. (1985) Taphonomy and the paleoecologic reconstruction of hominid habitats in the Koobi Fora Formation. In *L'Environment des Hominides au Plio-Pleistocene* (ed Y. COPPENS), pp. 309–324. Masson, Paris.

BEHRENSMEYER, A.K. (1988) Vertebrate preservation in fluvial channels. *Palaeogeography, Palaeoclimatology, Palaeoecology* **63**, 183–199.

BEHRENSMEYER, A.K. (1992) Paleoenvironments Contexts and Taphonomic Modes. In *Terrestrial Ecosystem through Time, Evolutionary Paleoecology of Terrestrial Plants and Animals* (ed A.K. BEHRENSMEYER), pp. 15–138. The University of Chicago Press, Chicago.

BEHRENSMEYER, A.K. (2006) Climate Change and Human Evolution. *Science* **311**, 476–478.

BEHRENSMEYER, A.K. (2007) Bonebeds through time. In *Bonebeds: Genesis, Analysis, and Paleobiological Significance* (eds R.R. ROGERS, D.A. EBERTH & A.R. FIORILLO), pp. 65–102. University of Chicago Press, Chicago.

BEHRENSMEYER, A.K. & BARRY, J. (2005) Biostratigraphic surveys in the Siwaliks of Pakistan: A method for standardized surface sampling of the vertebrate fossil record. *Palaeontologia Electronica* **8**, 1–24.

BEHRENSMEYER, A.K., GORDON, K.D. & YANAGI, G.T. (1986) Trampling as a cause of bone surface damage and pseudo-cutmarks. *Nature* **319**, 768–771.

BEHRENSMEYER, A.K. & REED, K.E. (2013) Reconstructing the Habitats of *Australopithecus*: Paleoenvironments, Site Taphonomy, and Faunas. In *The Paleobiology of Australopithecus* (eds K.E. REED, J.G. FLEAGLE & R.E. LEAKEY), pp. 41–60. Springer Netherlands, Dordrecht.

BEN-DOR, E., PATKIN, K., BANIN, A. & KARNIELI, A. (2002) Mapping of several soil properties using DAIS-7915 hyperspectral scanner data—a case study over clayey soils in Israel. *International Journal of Remote Sensing* **23**, 1043–1062.

BENTON, M.J. & DONOGHUE, P.C.J. (2007) Paleontological evidence to date the tree of life. *Molecular Biology and Evolution* **24**, 26–53.

BERGER, L. (2020) Wits University OFFICIAL: How to Discover Your Own Fossil Site [Video Recording]. *YouTube* **https://youtu.be/hMQ1WFxd6E8**.

BERGER, L.R., HAWKS, J., RUITER, D.J. DE, CHURCHILL, S.E., SCHMID, P., DELEZENE, L.K., KIVELL, T.L., GARVIN, H.M., WILLIAMS, S.A., DESILVA, J.M., SKINNER, M.M., MUSIBA, C.M., CAMERON, N., HOLLIDAY, T.W., HARCOURT-SMITH, W., ET AL. (2015) *Homo naledi*, a new species of the genus *Homo* from the Dinaledi Chamber, South Africa. *eLife* **4**, e09560.

BERGER, L.R., KEYSER, A.W. & TOBIAS, P.V. (1993) Gladysvale: First early hominid site discovered in South Africa since 1948. *American Journal of Physical Anthropology* **92**, 107–111.

BERGER, L.R., DE RUITER, D.J., CHURCHILL, S.E., SCHMID, P., CARLSON, K.J., DIRKS, P.H.G.M. & KIBII, J.M. (2010) *Australopithecus sediba*: A New Species of *Homo*-Like Australopith from South Africa. *Science* **328**, 195–204.

BESENBACHER, S., HVILSOM, C., MARQUES-BONET, T., MAILUND, T. & SCHIERUP, M.H. (2019) Direct estimation of mutations in great apes reconciles phylogenetic dating. *Nature Ecology & Evolution* **3**, 286–292.

BLOCK, S., SALTRÉ, F., RODRÍGUEZ-REY, M., FORDHAM, D.A., UNKEL, I. & BRADSHAW, C.J.A. (2016) Where to Dig for Fossils: Combining Climate-Envelope, Taphonomy and Discovery Models. *PLOS ONE* **11**, e0151090.

BLUMENTHAL, S.A., CERLING, T.E., CHRITZ, K.L., BROMAGE, T.G., KOZDON, R. & VALLEY, J.W. (2014) Stable isotope time-series in mammalian teeth: *in situ* $\delta^{18}O$ from the innermost enamel layer. *Geochimica et Cosmochimica Acta* **124**, 223–236.

BLUMENTHAL, S.A., LEVIN, N.E., BROWN, F.H., BRUGAL, J.-P., CHRITZ, K.L., HARRIS, J.M., JEHLE, G.E. & CERLING, T.E. (2017) Aridity and hominin environments. *Proceedings of the National Academy of Sciences* **114**, 7331–7336.

BOBE, R. (2006) The evolution of arid ecosystems in eastern Africa. *Journal of Arid Environments* **66**, 564–584.

BOBE, R. (2011) Fossil mammals and paleoenvironments in the Omo-Turkana Basin. *Evolutionary Anthropology: Issues, News, and Reviews* **20**, 254–263.

BOBE, R., ALDEIAS, V., ALEMSEGED, Z., ANEMONE, R.L., ARCHER, W., AUMAÎTRE, G., BAMFORD, M.K., BIRO, D., BOURLÈS, D.L., BOYD, M.D., BRAUN, D.R., CAPELLI, C., D'OLIVEIRA COELHO, J., HABERMANN, J.M., HEAD, J.J., ET AL. (2023) The first Miocene fossils from coastal woodlands in the southern East African Rift. *iScience* **26**.

BOBE, R., ALEMSEGED, Z. & BEHRENSMEYER, A.K. (2007a) Approaches to the analysis of faunal change during the East African Pliocene. In *Hominin Environments in the East African Pliocene: An Assessment of the Faunal Evidence* (eds R. BOBE, Z. ALEMSEGED & A.K. BEHRENSMEYER), pp. 1–24. Springer Netherlands, Dordrecht.

BOBE, R., BEHRENSMEYER, A.K., ECK, G.G. & HARRIS, J.M. (2007b) Patterns of abundance and diversity in late Cenozoic bovids from the Turkana and Hadar Basins, Kenya and Ethiopia. In *Hominin Environments in the East African Pliocene: An Assessment of the Faunal Evidence* (eds R. BOBE, Z. ALEMSEGED & A.K. BEHRENSMEYER), pp. 129–157. Springer Netherlands. Springer.

BOBE, R., BEHRENSMEYER, A.K., LEAKEY, M.G. & MBUA, E. (2011) The Turkana Database: An archive of vertebrate evolution in East Africa. *Evolutionary Anthropology: Issues, News, and Reviews* **20**, 256.

BOBE, R. & CARVALHO, S. (2019a) Gorongosa National Park: A new window on the late Miocene at the southern end of the African Rift Valley. In *Proceedings of the European Society for the study of Human Evolution* p. 20.

BOBE, R. & CARVALHO, S. (2019b) Hominin diversity and high environmental variability in the Okote Member, Koobi Fora Formation, Kenya. *Journal of Human Evolution* **126**, 91–105.

BOBE, R. & CARVALHO, S. (2020) Late Miocene primates and the biogeography of hominin origins: a role for the unknown south? In *Folia Primatologica* p. 283.

BOBE, R., D'OLIVEIRA COELHO, J., CARVALHO, S. & LEAKEY, M. (2022) Early Hominins and Paleoecology of the Koobi Fora Formation, Lake Turkana Basin, Kenya. In *African Paleoecology and Human Evolution* (eds S.C. REYNOLDS & R. BOBE), pp. 311–331. Cambridge University Press, Cambridge.

BOBE, R. & ECK, G.G. (2001) Responses of African bovids to Pliocene climatic change. *Paleobiology* **27**, 1–47.

BOBE, R. & LEAKEY, M.G. (2009) Ecology of Plio-Pleistocene Mammals in the Omo—Turkana Basin and the Emergence of Homo. In *The First Humans – Origin and Early Evolution of the Genus Homo* (eds F.E. GRINE, J.G. FLEAGLE & R.E. LEAKEY), pp. 173–184. Springer Netherlands, Dordrecht.

BOBE, R., MANTHI, F.K., WARD, C.V., PLAVCAN, J.M. & CARVALHO, S. (2020a) The ecology of *Australopithecus anamensis* in the early Pliocene of Kanapoi, Kenya. *Journal of Human Evolution*, 102717.

BOBE, R., MARTÍNEZ, F.I. & CARVALHO, S. (2020b) Primate adaptations and evolution in the Southern African Rift Valley. *Evolutionary Anthropology: Issues, News, and Reviews* **29**, 94–101.

BOBE, R. & REYNOLDS, S.C. (2022) Hominid Paleoenvironments in Tropical Africa from the Late Miocene to the Early Pleistocene. In *African Paleoecology and Human Evolution* (eds S.C. REYNOLDS & R. BOBE), pp. 161–186. Cambridge University Press, Cambridge.

BOBE, R. & WOOD, B. (2022) Estimating origination times from the early hominin fossil record. *Evolutionary Anthropology: Issues, News, and Reviews* **31**, 92–102.

BOCK, H.-H. (2008) Origins and extensions of the *k*-means algorithm in cluster analysis. *Electronic Journal for History of Probability and Statistics* **4**, 1–18.

BOËS, X., PRAT, S., ARRIGHI, V., FEIBEL, C., HAILEAB, B., LEWIS, J. & HARMAND, S. (2019) Lake-level changes and hominin occupations in the arid Turkana basin during volcanic closure of the Omo River outflows to the Indian Ocean. *Quaternary Research* **91**, 892–909.

BÖHME, B., STEINBRUCH, F., GLOAGUEN, R., HEILMEIER, H. & MERKEL, B. (2006) Geomorphology, hydrology, and ecology of Lake Urema, central Mozambique, with focus on lake extent changes. *Physics and Chemistry of the Earth, Parts A/B/C* **31**, 745–752.

BÖHME, M., SPASSOV, N., FUSS, J., TRÖSCHER, A., DEANE, A.S., PRIETO, J., KIRSCHER, U., LECHNER, T. & BEGUN, D.R. (2019) A new Miocene ape and locomotion in the ancestor of great apes and humans. *Nature* **575**, 489–493.

BONNEFILLE, R., POTTS, R., CHALIÉ, F., JOLLY, D. & PEYRON, O. (2004) High-resolution vegetation and climate change associated with Pliocene *Australopithecus afarensis*. *Proceedings of the National Academy of Sciences of the United States of America* **101**, 12125–12129.

BOOM, A.F., MIGLIORE, J., KAYMAK, E., MEERTS, P. & HARDY, O.J. (2021) Plastid introgression and evolution of African miombo woodlands: New insights from the plastome-based phylogeny of *Brachystegia* trees. *Journal of Biogeography* **48**, 933–946.

BOWN, T.M., KRAUS, M.J., WING, S.L., FLEAGLE, J.G., TIFFNEY, B.H., SIMONS, E.L. & VONDRA, C.F. (1982) The fayum primate forest revisited. *Journal of Human Evolution* **11**, 603–632.

BOYD, R. & SILK, J.B. (2009) *How Humans Evolved*. Fifth Edition. W W Norton & Co Inc, New York.

BRADLEY, B.J. (2008) Reconstructing phylogenies and phenotypes: a molecular view of human evolution. *Journal of Anatomy* **212**, 337–353.

BRAIN, C.K. (1974) Some suggested procedures in the analysis of bone accumulations from southern African Quaternary sites. *Annals of the Transvaal Museum* **29**, 1–8.

BRAIN, C.K., BEHRENSMEYER, A.K. & HILL, A. (1980) Some criteria for the recognition of bone-collecting agencies in African caves. In *Fossils in the Making: Vertebrate Taphonomy and Paleoecology* pp. 107–130. University of Chicago Press, Chicago.

BRAUN, D.R., HARRIS, J.W.K., LEVIN, N.E., MCCOY, J.T., HERRIES, A.I.R., BAMFORD, M.K., BISHOP, L.C., RICHMOND, B.G. & KIBUNJIA, M. (2010) Early hominin diet included diverse terrestrial and aquatic animals 1.95 Ma in East Turkana, Kenya. *Proceedings of the National Academy of Sciences* **107**, 10002–10007.

BREIMAN, L. (2001) Random Forests. *Machine Learning* **45**, 5–32.

BROMHAM, L. (2011) The genome as a life-history character: why rate of molecular evolution varies between mammal species. *Philosophical Transactions of the Royal Society B: Biological Sciences* **366**, 2503–2513.

BROMHAM, L. (2019) Six Impossible Things before Breakfast: Assumptions, Models, and Belief in Molecular Dating. *Trends in Ecology & Evolution* **34**, 474–486.

BROOM, R. (1938) The pleistocene anthropoid apes of South Africa. *Nature* **142**, 377–379.

BROOM, R. (1949) Another New Type of Fossil Ape-man. *Nature* **163**, 57.

BROOM, R. & ROBINSON, J.T. (1949) A New Type of Fossil Man. *Nature* **164**, 322–323.

BROOM, R., ROBINSON, J.T. & SCHEPERS, G.W.H. (1950) *Sterkfontein Ape-man Plesianthropus*. Transvaal Museum, Pretoria.

BROWN, F.H. & FEIBEL, C.S. (1986) Revision of lithostratigraphic nomenclature in the Koobi Fora region, Kenya. *Journal of the Geological Society* **143**, 297–310.

BROWN, F.H. & FEIBEL, C.S. (1990) Stratigraphy, Depositional Environments, and Palaeogeography of the Koobi Fora Formation. In *Koobi Fora Research Project, Volume 3: The Fossil Ungulates: Geology, Fossil Artiodactyls, and Paleoenvironments* (ed J.M. HARRIS), pp. 1–30. Clarendon Press, Oxford.

BROWN, J.W. & SMITH, S.A. (2018) The Past Sure is Tense: On Interpreting Phylogenetic Divergence Time Estimates. *Systematic Biology* **67**, 340–353.

BROYDEN, C.G. (1970) The Convergence of a Class of Double-rank Minimization Algorithms 1. General Considerations. *IMA Journal of Applied Mathematics* **6**, 76–90.

BRUHN, R.L., BROWN, F.H., GATHOGO, P.N. & HAILEAB, B. (2011) Pliocene volcano-tectonics and paleogeography of the Turkana Basin, Kenya and Ethiopia. *Journal of African Earth Sciences* **59**, 295–312.

BRUNET, M., GUY, F., PILBEAM, D., LIEBERMAN, D.E., LIKIUS, A., MACKAYE, H.T., PONCE DE LEÓN, M.S., ZOLLIKOFER, C.P.E. & VIGNAUD, P. (2005) New material of the earliest hominid from the Upper Miocene of Chad. *Nature* **434**, 752–755.

BRUNET, M., GUY, F., PILBEAM, D., MACKAYE, H.T., LIKIUS, A., AHOUNTA, D., BEAUVILAIN, A., BLONDEL, C., BOCHERENS, H., BOISSERIE, J.-R., BONIS, L.D., COPPENS, Y., DEJAX, J., DENYS, C., DURINGER, P., ET AL. (2002) A new hominid from the Upper Miocene of Chad, Central Africa. *Nature* **418**, 145–151.

BUDD, G.E. & MANN, R.P. (2020) The dynamics of stem and crown groups. *Science Advances* **6**, eaaz1626.

BURK, D. (2021) Slope and aspect as predictors of surface fossil abundance in the Uinta Basin, Utah. *Academia Letters* **4474**.

BURK, D. (2023) A fossil locality predictive model using weighted suitability analysis for the Early Cretaceous Cedar Mountain Formation, Utah, USA. *Palaeontologia Electronica* **26**, a43.

BÜRKNER, P.-C. (2017) **brms**: An *R* Package for Bayesian Multilevel Models Using *Stan*. *Journal of Statistical Software* **80**, 1–28.

BÜRKNER, P.-C. (2018) Advanced Bayesian Multilevel Modeling with the R Package brms. *The R Journal* **10**, 395.

CALDER, J., COIL, R., MELTON, J.A., OLVER, P.J., TOSTEVIN, G. & YEZZI-WOODLEY, K. (2022) Use and Misuse of Machine Learning in Anthropology. *IEEE BITS the Information Theory Magazine* **2**, 102–115.

CERLING, T.E., ANDANJE, S.A., BLUMENTHAL, S.A., BROWN, F.H., CHRITZ, K.L., HARRIS, J.M., HART, J.A., KIRERA, F.M., KALEME, P., LEAKEY, L.N., LEAKEY, M.G., LEVIN, N.E.,

MANTHI, F.K., PASSEY, B.H. & UNO, K.T. (2015) Dietary changes of large herbivores in the Turkana Basin, Kenya from 4 to 1 Ma. *Proceedings of the National Academy of Sciences* **112**, 11467–11472.

CERLING, T.E., BOWMAN, J.R. & O'NEIL, J.R. (1988) An isotopic study of a fluvial-lacustrine sequence: The Plio-Pleistocene Koobi Fora sequence, East Africa. *Palaeogeography, Palaeoclimatology, Palaeoecology* **63**, 335–356.

CERLING, T.E., HARRIS, J.M. & PASSEY, B.H. (2003) Diets of east African Bovidae based on stable isotope analysis. *Journal of Mammalogy* **84**, 456–470.

CERLING, T.E., MANTHI, F.K., MBUA, E.N., LEAKEY, L.N., LEAKEY, M.G., LEAKEY, R.E., BROWN, F.H., GRINE, F.E., HART, J.A., KALEME, P., ROCHE, H., UNO, K.T. & WOOD, B.A. (2013) Stable isotope-based diet reconstructions of Turkana Basin hominins. *Proceedings of the National Academy of Sciences* **110**, 10501–10506.

CERLING, T.E., WYNN, J.G., ANDANJE, S.A., BIRD, M.I., KORIR, D.K., LEVIN, N.E., MACE, W., MACHARIA, A.N., QUADE, J. & REMIEN, C.H. (2011) Woody cover and hominin environments in the past 6 million years. *Nature* **476**, 51–56.

CHEN, Y., WANG, Y., LI, J., WANG, W., FENG, D. & MAO, K. (2021) Principles, error sources and application suggestions of prevailing molecular dating methods. *Biodiversity Science* **29**, 629–646.

CHENG, J., KARAMBELKAR, B. & XIE, Y. (2021) leaflet: Create interactive web maps with the JavaScript 'leaflet' library.

CHEW, A. & OHEIM, K. (2009) Using GIS to Determine the Effects of Two Common Taphonomic Biases on Vertebrate Fossil Assemblages. *PALAIOS* **24**, 367–376.

CHIRINDJA, F.J., DAHLIN, T., PERTTU, N., STEINBRUCH, F. & OWEN, R. (2016) Combined electrical resistivity tomography and magnetic resonance sounding investigation of the surface-water/groundwater interaction in the Urema Graben, Mozambique. *Hydrogeology Journal* **24**, 1583–1592.

CHRISTIN, P.-A., SPRIGGS, E., OSBORNE, C.P., STROMBERG, C.A.E., SALAMIN, N. & EDWARDS, E.J. (2014) Molecular Dating, Evolutionary Rates, and the Age of the Grasses. *Systematic Biology* **63**, 153–165.

CLARK, J.D., ASFAW, B., ASSEFA, G., HARRIS, J.W.K., KURASHINA, H., WALTER, R.C., WHITE, T.D. & WILLIAMS, M. A. J. (1984) Palaeoanthropological discoveries in the Middle Awash Valley, Ethiopia. *Nature* **307**, 423–428.

CLARKE, R.J. & HOWELL, F.C. (1972) Affinities of the Swartkrans 847 hominid cranium. *American Journal of Physical Anthropology* **37**, 319–325.

COBLENTZ, W.W. (1906) Radiometric Investigations of Infra-red Absorption and Reflection Spectra. *Bulletin of the Bureau of Standards* **2**, 457–478.

D'OLIVEIRA COELHO, J. (2023) Searching for Kingdon's Coastal Ape in Miocene Estuarine Forests of Gorongosa. In *Joint Meeting of the International Primatological Society and the Malaysian Primatological Society.* p. 2023. Kuching, Malaysia.

D'OLIVEIRA COELHO, J., ANEMONE, R.L. & CARVALHO, S. (2020) Filling Gaps in Primate Evolution: Machine Learning Approaches for Automated Fossil Site Discovery in Gorongosa, Mozambique. In *Folia Primatologica* pp. 251–252.

D'OLIVEIRA COELHO, J., ANEMONE, R.L. & CARVALHO, S. (2021) Unsupervised learning of satellite images enhances discovery of late Miocene fossil sites in the Urema Rift, Gorongosa, Mozambique. *PeerJ* **9**, e11573.

D'OLIVEIRA COELHO, J. & CURATE, F. (2019) CADOES: An interactive machine-learning approach for sex estimation with the pelvis. *Forensic Science International* **302**, 109873.

D'OLIVEIRA COELHO, J., PÜSCHEL, T.A., BOBE, R. & CARVALHO, S. (2023) Taxonomic Identification of Lower Mazamba Formation Fossils Collected in 2022: A Preliminary Study. *Paleo-Primate Project Gorongosa – 2022 Field Reports* **Unpublished**, 133–207.

COLONESE, A.C., MANNINO, M.A., BAR-YOSEF MAYER, D.E., FA, D.A., FINLAYSON, J.C., LUBELL, D. & STINER, M.C. (2011) Marine mollusc exploitation in Mediterranean prehistory: An overview. *Quaternary International* **239**, 86–103.

CONROY, G.C. (2006) Creating, displaying, and querying interactive paleoanthropological maps using GIS: An example from the Uinta Basin, Utah. *Evolutionary Anthropology: Issues, News, and Reviews* **15**, 217–223.

CONROY, G.C. (2014) Walking back the cat: Unsupervised classification as an aid in "remote" fossil prospecting. *Evolutionary Anthropology: Issues, News, and Reviews* **23**, 172–176.

CONROY, G.C., ANEMONE, R.L., VAN REGENMORTER, J. & ADDISON, A. (2008) Google Earth, GIS, and the Great Divide: A new and simple method for sharing paleontological data. *Journal of Human Evolution* **55**, 751–755.

CONROY, G.C., CHEW, A., ROSE, K.D., BOWN, T.M., ANEMONE, R.L. & GUNNELL, G.F. (2018) Assessing Unsupervised Image Classification as an Aid in Paleoanthropological Explorations. In *New Geospatial Approaches to the Anthropological Sciences* (eds R.L. ANEMONE & G.C. CONROY), pp. 59–80. New Mexico Press, Albuquerque, NM.

CONROY, G.C., EMERSON, C.W., ANEMONE, R.L. & TOWNSEND, K.E.B. (2012) Let your fingers do the walking: A simple spectral signature model for 'remote' fossil prospecting. *Journal of Human Evolution* **63**, 79–84.

CORTÉS-SÁNCHEZ, M., MORALES-MUÑIZ, A., SIMÓN-VALLEJO, M.D., LOZANO-FRANCISCO, M.C., VERA-PELÁEZ, J.L., FINLAYSON, C., RODRÍGUEZ-VIDAL, J., DELGADO-HUERTAS, A., JIMÉNEZ-ESPEJO, F.J., MARTÍNEZ-RUIZ, F., MARTÍNEZ-AGUIRRE, M.A., PASCUAL-GRANGED, A.J., BERGADÀ-ZAPATA, M.M., GIBAJA-BAO, J.F., RIQUELME-CANTAL, J.A., ET AL. (2011) Earliest Known Use of Marine Resources by Neanderthals. *PLoS ONE* **6**, e24026.

COTE, S.M. (2004) Origins of the African hominoids: an assessment of the palaeobiogeographical evidence. *Comptes Rendus Palevol* **3**, 323–340.

COTE, S.M. (2018) Savannah savvy. *Nature Ecology & Evolution* **2**, 210–211.

CRAWFORD, M.A. (2002) Cerebral evolution. *Nutrition and Health* **16**, 29–34.

CRAWFORD, M.A. & BROADHURST, C.L. (2012) The role of docosahexaenoic and the marine food web as determinants of evolution and hominid brain development: the challenge for human sustainability. *Nutrition and Health* **21**, 17–39.

CRIBARI-NETO, F. & ZEILEIS, A. (2010) Beta regression in R. *Journal of statistical software* **34**, 1–24.

CROMPTON, R.H., SELLERS, W.I. & THORPE, S.K.S. (2010) Arboreality, terrestriality and bipedalism. *Philosophical Transactions of the Royal Society B: Biological Sciences* **365**, 3301–3314.

CROUCH, N.M.A. (2022) Interpreting the fossil record and the origination of birds. *bioArxiv*.

CUI, P., JI, R., DING, F., QI, D., GAO, H., MENG, H., YU, J., HU, S. & ZHANG, H. (2007) A complete mitochondrial genome sequence of the wild two-humped camel (*Camelus bactrianus ferus*): an evolutionary history of camelidae. *BMC Genomics* **8**, 241.

CUMMING, G. (2013) *Understanding the new statistics: Effect sizes, confidence intervals, and meta-analysis*. Routledge, London, UK.

CUNNANE, S.C. & CRAWFORD, M.A. (2014) Energetic and nutritional constraints on infant brain development: Implications for brain expansion during human evolution. *Journal of Human Evolution* **77**, 88–98.

CUNNANE, S.C., PLOURDE, M., STEWART, K. & CRAWFORD, M.A. (2007) Docosahexaenoic acid and shore-based diets in hominin encephalization: a rebuttal. *American Journal of Human Biology* **19**, 578–581.

CUSTER, J.F., EVELEIGH, T. & KLEMAS, V. (1983) A LANDSAT-Generated Predictive Model for Prehistoric Archaeological Sites in Delaware's Coastal Plain. *Bulletin of Archeological Society of Delaware* **14**, 19–38.

CUSTER, J.F., EVELEIGH, T., KLEMAS, V. & WELLS, I. (1986) Application of Landsat Data and Synoptic Remote Sensing to Predictive Models for Prehistoric Archaeological Sites: An Example from the Delaware Coastal Plain. *American Antiquity* **51**, 572–588.

DALMASSO, A., PELÁEZ-CAMPOMANES, P. & LÓPEZ-ANTOÑANZAS, R. (2022) Relative performance of Bayesian morphological clock and parsimony methods for phylogenetic reconstructions: Insights from the case of Myomiminae and Dryomyinae glirid rodents. *Cladistics* **38**, 702–710.

D'ANDREA, A., GALLOTTI, R. & PIPERNO, M. (2002) Taphonomic interpretation of the Developed Oldowan site of Garba IV (Melka Kunture, Ethiopia) through a GIS application. *Antiquity* **76**, 991–1001.

DART, R. (1925) *Australopithecus africanus*. The man-ape of South Africa. *Nature* **115**, 195–199.

DART, R.A. (1948) The Makapansgat proto-human *Australopithecus prometheus*. *American Journal of Physical Anthropology* **6**, 259–284.

DARWIN, C. (1871) *The Descent of Man and Selection in Relation to Sex*. John Murray, London.

DAVER, G., GUY, F., MACKAYE, H.T., LIKIUS, A., BOISSERIE, J.-R., MOUSSA, A., PALLAS, L., VIGNAUD, P. & CLARISSE, N.D. (2022) Postcranial evidence of late Miocene hominin bipedalism in Chad. *Nature* **609**, 94–100.

DAVID, L.A. & ALM, E.J. (2011) Rapid evolutionary innovation during an Archaean genetic expansion. *Nature* **469**, 93–96.

DEBLIEUX, D.D., SMITH, J.A., MCGUIRE, J.L., SANTUCCI, V.L., KIRKLAND, J.L. & BUTLER, M. (2003) A Paleontological Inventory of Zion National Park, Utah, and the Use of GIS Technology to Create Paleontological Sensitivity Maps for Use in Resource Management. *Journal of Vertebrate Paleontology* **23**, 45A-45A.

DEMIGUEL, D., BRILHA, J., ALEGRET, L., ARENILLAS, I., ARZ, J.A., GILABERT, V., STRANI, F., VALENCIANO, A., VILLAS, E. & AZANZA, B. (2021) Linking geological heritage and geoethics with a particular emphasis on palaeontological heritage: the new concept of 'palaeontoethics'. *Geoheritage* **13**, 69.

DÉTROIT, F., MIJARES, A.S., CORNY, J., DAVER, G., ZANOLLI, C., DIZON, E., ROBLES, E., GRÜN, R. & PIPER, P.J. (2019) A new species of *Homo* from the Late Pleistocene of the Philippines. *Nature* **568**, 181–186.

DIDIER, G. & LAURIN, M. (2020) Exact Distribution of Divergence Times from Fossil Ages and Tree Topologies. *Systematic Biology* **69**, 1068–1087.

DIOLI, M. (2020) Dromedary (*Camelus dromedarius*) and Bactrian camel (*Camelus bactrianus*) crossbreeding husbandry practices in Turkey and Kazakhstan: An in-depth review. *Pastoralism* **10**, 6.

DIRKS, P.H.G.M. & BERGER, L.R. (2013) Hominin-bearing caves and landscape dynamics in the Cradle of Humankind, South Africa. *Journal of African Earth Sciences* **78**, 109–131.

DIRKS, P.H.G.M., KIBII, J.M., KUHN, B.F., STEININGER, C., CHURCHILL, S.E., KRAMERS, J.D., PICKERING, R., FARBER, D.L., MÉRIAUX, A.-S., HERRIES, A.I.R., KING, G.C.P. & BERGER, L.R. (2010) Geological Setting and Age of *Australopithecus sediba* from Southern Africa. *Science* **328**, 205–208.

DOMINGUES, A., SILVEIRA, G., FERREIRA, A.M.G., CHANG, S.-J., CUSTÓDIO, S. & FONSECA, J.F.B.D. (2016) Ambient noise tomography of the East African Rift in Mozambique. *Geophysical Journal International* **204**, 1565–1578.

DONOGHUE, P.C.J. & BENTON, M.J. (2007) Rocks and clocks: calibrating the Tree of Life using fossils and molecules. *Trends in Ecology & Evolution* **22**, 424–431.

DORANS, E.R., D'OLIVEIRA COELHO, J., ANEMONE, R.L., BOBE, R., CARVALHO, S., FORREST, F. & BRAUN, D.R. (2020) Using remote sensing and machine learning to reconstruct

paleoenvironmental features in the Koobi Fora Formation. *American Journal of Physical Anthropology* **171 (S69)**, 73–74.

DORNBURG, A., BEAULIEU, J.M., OLIVER, J.C. & NEAR, T.J. (2011) Integrating Fossil Preservation Biases in the Selection of Calibrations for Molecular Divergence Time Estimation. *Systematic Biology* **60**, 519–527.

DRAKE, N.A., BLENCH, R.M., ARMITAGE, S.J., BRISTOW, C.S. & WHITE, K.H. (2011) Ancient watercourses and biogeography of the Sahara explain the peopling of the desert. *Proceedings of the National Academy of Sciences of the United States of America* **108**, 458–462.

DRUMMOND-CLARKE, R.C., KIVELL, T.L., SARRINGHAUS, L., STEWART, F.A., HUMLE, T. & PIEL, A.K. (2022) Wild chimpanzee behavior suggests that a savanna-mosaic habitat did not support the emergence of hominin terrestrial bipedalism. *Science Advances* **8**, eadd9752.

DU, A. & ALEMSEGED, Z. (2018) Diversity analysis of Plio-Pleistocene large mammal communities in the Omo-Turkana Basin, eastern Africa. *Journal of Human Evolution* **124**, 25–39.

DU, A., ROWAN, J., WANG, S.C., WOOD, B.A. & ALEMSEGED, Z. (2020) Statistical estimates of hominin origination and extinction dates: A case study examining the *Australopithecus anamensis–afarensis* lineage. *Journal of Human Evolution* **138**, 102688.

DU, A., ZIPKIN, A.M., HATALA, K.G., RENNER, E., BAKER, J.L., BIANCHI, S., BERNAL, K.H. & WOOD, B.A. (2018) Pattern and process in hominin brain size evolution are scale-dependent. *Proceedings of the Royal Society B: Biological Sciences* **285**, 20172738.

DUMOUCHEL, L., BOBE, R., WYNN, J.G. & BARR, W.A. (2021) The environments of *Australopithecus anamensis* at Allia Bay, Kenya: A multiproxy analysis of early Pliocene Bovidae. *Journal of Human Evolution* **151**, 102928.

EBERT, D. & SINGER, M. (2004) Modelling Erosion and Archaeological Potential Using GIS. *Assemblage: The Sheffield Graduate Journal of Archaeology* **8**.

EBERT, J.I. (1999) The state of the art in 'inductive' predictive modeling: Seven big mistakes (and lots of smaller ones). In *Practical Applications of GIS for Archaeologists: A Predictive Modeling Toolkit* (eds K.L. WESCOTT & R.J. BRANDON), pp. 129–134. Taylor and Francis, Philadelphia.

EBERTH, D.A., ROGERS, R.R. & FIORILLO, A.R. (2007) A practical approach to the study of bonebeds. In *Bonebeds: Genesis, Analysis, and Paleobiological Significance* (eds R.R. ROGERS, D.A. EBERTH & A.R. FIORILLO), pp. 265–332. University of Chicago Press, Chicago.

EDGECOMBE, G.D., STRULLU-DERRIEN, C., GÓRAL, T., HETHERINGTON, A.J., THOMPSON, C. & KOCH, M. (2020) Aquatic stem group myriapods close a gap between molecular divergence dates and the terrestrial fossil record. *Proceedings of the National Academy of Sciences* **117**, 8966–8972.

EGELAND, C., NICHOLSON, C. & GASPARIAN, B. (2010) Using GIS and Ecological Variables to Identify High Potential Areas for Paleoanthropological Survey: An Example from Northern Armenia. *Journal of Ecological Anthropology* **14**, 89–98.

ELANGO, N., THOMAS, J.W., NISC COMPARATIVE SEQUENCING PROGRAM & YI, S.V. (2006) Variable molecular clocks in hominoids. *Proceedings of the National Academy of Sciences* **103**, 1370–1375. Proceedings of the National Academy of Sciences.

ELITH, J., PHILLIPS, S.J., HASTIE, T., DUDÍK, M., CHEE, Y.E. & YATES, C.J. (2011) A statistical explanation of MaxEnt for ecologists. *Diversity and Distributions* **17**, 43–57.

EMERSON, C.W. & ANEMONE, R.L. (2012) An artificial neural network-based approach to identifying mammalian fossil localities in the Great Divide Basin, Wyoming. *Remote Sensing Letters* **3**, 453–460.

EMERSON, C.W. & ANEMONE, R.L. (2018) Ongoing Developments in Geospatial Data, Software, and Hardware with Prospects for Anthropological Applications. In *New Geospatial Approaches to the Anthropological Sciences* (eds R.L. ANEMONE & G.C. CONROY), pp. 21–38. New Mexico Press, Albuquerque, NM.

EMERSON, C.W., BOMMERSBACH, B., NACHMAN, B. & ANEMONE, R.L. (2015) An Object-Oriented Approach to Extracting Productive Fossil Localities from Remotely Sensed Imagery. *Remote Sensing* **7**, 16555–16570.

ENDERLE, D. & WEIH, R. (2005) Integrating Supervised and Unsupervised Classification Methods to Develop a More Accurate Land Cover Classification. *Journal of the Arkansas Academy of Science* **59**, 65–73.

ESTER, M., KRIEGEL, H.-P., SANDER, J. & XU, X. (1996) A density-based algorithm for discovering clusters in large spatial databases with noise. *KDD96: Proceedings of the second international conference on Knowledge, Discovery and Data Mining* **34**, 226–231.

FEIBEL, C.S. (1988) Paleoenvironments of the Koobi Fora Formation, Turkana Basin, Northern Kenya. Ph.D. Dissertation, University of Utah, Salt Lake City.

FEIBEL, C.S. (1993) Freshwater stingrays from the Plio-Pleistocene of the Turkana Basin, Kenya and Ethiopia. *Lethaia* **26**, 359–366.

FEIBEL, C.S. (1997) A terrestrial auxiliary stratotype point and section for the Plio-Pleistocene boundary in the Turkana Basin, East Africa. *Quaternary International* **40**, 73–79.

FEIBEL, C.S. (1999) Basin evolution, sedimentary dynamics and hominid habitats in East Africa: an ecosystem approach. *African Biogeography, Climate Change, and Human Evolution. Oxford University Press, Oxford*, 276–281.

FEIBEL, C.S. (2011) A Geological History of the Turkana Basin. *Evolutionary Anthropology: Issues, News, and Reviews* **20**, 206–216.

FEIBEL, C.S., BROWN, F.H. & MCDOUGALL, I. (1989) Stratigraphic context of fossil hominids from the Omo group deposits: Northern Turkana Basin, Kenya and Ethiopia. *American Journal of Physical Anthropology* **78**, 595–622.

FEIBEL, C.S., HARRIS, J.M. & BROWN, F.H. (1990) Palaeoenvironmental context for the late Neogene of the Turkana Basin. In *Koobi Fora Research Project, Volume 3: The Fossil Ungulates: Geology, Fossil Artiodactyls, and Paleoenvironments* (ed J.M. HARRIS), pp. 321–370. Clarendon Press, Oxford.

FERGUSON, C.A., BODENBENDER, B.E., HONES, J.L. & AHMED, K. (2000) Recording the fossil record: a GIS database of Middle Devonian fossils in the Michigan Basin. In *Geological Society of America Annual Meeting, 2000, Abstracts with Programs* p. A131.

FERRARI, S. & CRIBARI-NETO, F. (2004) Beta Regression for Modelling Rates and Proportions. *Journal of Applied Statistics* **31**, 799–815.

FEYZIYEV, F., BABAYEV, M., PRIORI, S. & L'ABATE, G. (2016) Using Visible-Near Infrared Spectroscopy to Predict Soil Properties of Mugan Plain, Azerbaijan. *Open Journal of Soil Science* **6**, 52–58.

FIELD, J.S., PETRAGLIA, M.D. & LAHR, M.M. (2007) The southern dispersal hypothesis and the South Asian archaeological record: Examination of dispersal routes through GIS analysis. *Journal of Anthropological Archaeology* **26**, 88–108.

FILLION, E.N. & HARRISON, T. (2023) Mixed models elucidate local- and regional-scale drivers of paleoenvironmental change in eastern Africa during the emergence of *Paranthropus* and *Homo*. *Palaeogeography, Palaeoclimatology, Palaeoecology* **616**, 111479.

FITZGIBBON, A., PISUT, D. & FLEISHER, D. (2022) Evaluation of Maximum Entropy (Maxent) Machine Learning Model to Assess Relationships between Climate and Corn Suitability. *Land* **11**, 1382.

FLEAGLE, J.G. (2003) The primate fossil record. *Evolutionary Anthropology: Issues, News, and Reviews* **11**, 20–23.

FLEMING, M.D. & HOFFER, R.M. (1979) Machine processing of Landsat MSS data and DMA topographic data for forest cover type mapping. In *LARS Symposia* p. 302.

FLETCHER, R. (1970) A new approach to variable metric algorithms. *The Computer Journal* **13**, 317–322.

FLORES, G. (1973) The Cretaceous and Tertiary sedimentary basins of Mozambique and Zululand. In *Sedimentary basins of the African coasts* (ed G. BRANT), pp. 81–111. International Union of Geological Sciences (IUGS).

FLYNN, K.C., FRAZIER, A.E. & ADMAS, S. (2020) Performance of chlorophyll prediction indices for Eragrostis tef at Sentinel-2 MSI and Landsat-8 OLI spectral resolutions. *Precision Agriculture* **21**, 1057–1071.

FOLEY, R. & LAHR, M.M. (2014) The role of "the aquatic" in human evolution: Constraining the Aquatic Ape Hypothesis. *Evolutionary Anthropology: Issues, News, and Reviews* **23**, 56–59.

FOLEY, R.A. (2018) Evolutionary Geography and the Afrotropical Model of Hominin Evolution. *Bulletins et Mémoires de la Société d'Anthropologie de Paris* **30**, 17–31.

FOLEY, R.A. & LEWIN, R. (2013) *Principles of Human Evolution*. Third Edition. Wiley-Blackwell, Malden, MA.

FONSECA, J.F.B.D., CHAMUSSA, J., DOMINGUES, A., HELFFRICH, G., ANTUNES, E., ASWEGEN, G. VAN, PINTO, L.V., CUSTÓDIO, S. & MANHIÇA, V.J. (2014) MOZART: A Seismological Investigation of the East African Rift in Central Mozambique. *Seismological Research Letters* **85**, 108–116.

FOOTE, M. & SEPKOSKI, J.J. (1999) Absolute measures of the completeness of the fossil record. *Nature* **398**, 415–417.

FORGY, E.W. (1965) Cluster analysis of multivariate data: efficiency versus interpretability of classifications. *Biometrics* **21**, 768–769.

FORREST, F.L., PLUMMER, T.W. & RAAUM, R.L. (2018) Ecomorphological analysis of bovid mandibles from Laetoli Tanzania using 3D geometric morphometrics: Implications for hominin paleoenvironmental reconstruction. *Journal of Human Evolution* **114**, 20–34.

FORTELIUS, M., ŽLIOBAITĖ, I., KAYA, F., BIBI, F., BOBE, R., LEAKEY, L., LEAKEY, M., PATTERSON, D., RANNIKKO, J. & WERDELIN, L. (2016) An ecometric analysis of the fossil mammal record of the Turkana Basin. *Philosophical Transactions of the Royal Society B: Biological Sciences* **371**, 20150232.

FRITZ, S.A., BININDA-EMONDS, O.R.P. & PURVIS, A. (2009) Geographical variation in predictors of mammalian extinction risk: big is bad, but only in the tropics. *Ecology Letters* **12**, 538–549.

GAFFNEY, V. & VAN LEUSEN, P.M. (1995) Postscript - GIS, environmental determinism and archaeology. In *Archaeology and Geographical Information Systems: A European Perspective* (eds G. LOCK & Z. STANČIČ), pp. 367–382. Taylor and Francis, London.

GATHOGO, P.N. (2003) Stratigraphy and paleoenvironments of the Koobi Fora Formation of the Ileret Area, Northern Kenya. Unpublished M.Sc. thesis, University of Utah.

GATHOGO, P.N. & BROWN, F.H. (2006) Stratigraphy of the Koobi Fora Formation (Pliocene and Pleistocene) in the Ileret region of northern Kenya. *Journal of African Earth Sciences* **45**, 369–390.

GATHOGO, P.N., BROWN, F.H. & MCDOUGALL, I. (2008) Stratigraphy of the Koobi Fora Formation (Pliocene and Pleistocene) in the Loiyangalani region of northern Kenya. *Journal of African Earth Sciences* **51**, 277–297.

GERAADS, D., DIDIER, G., BARR, A., REED, D. & LAURIN, M. (2020) The fossil record of camelids demonstrates a late divergence between Bactrian camel and dromedary. *Acta Palaeontologica Polonica* **65.2**, 251–260.

GHAFFAR, A. (2010) GIS and paleontology of Dhok Bun Ameer Khatoon fossil site, Pakistan. *Pakistan Journal of Science* **62**, 163–167.

GHEZZO, E., MASSIRONI, M. & DAVIS, E.B. (2023) Multispectral satellite imaging improves detection of large individual fossils. *Geological Magazine* **160**, 535–544.

GIARDINO, M.J. (2011) A history of NASA remote sensing contributions to archaeology. *Journal of Archaeological Science* **38**, 2003–2009.

GIVNISH, T.J., SPALINK, D., AMES, M., LYON, S.P., HUNTER, S.J., ZULUAGA, A., ILES, W.J.D., CLEMENTS, M.A., ARROYO, M.T.K., LEEBENS-MACK, J., ENDARA, L., KRIEBEL, R., NEUBIG, K.M., WHITTEN, W.M., WILLIAMS, N.H., ET AL. (2015) Orchid phylogenomics and multiple drivers of their extraordinary diversification. *Proceedings of the Royal Society B: Biological Sciences* **282**, 20151553.

GOLDFARB, D. (1970) A family of variable-metric methods derived by variational means. *Mathematics of Computation* **24**, 23–26.

GOLDSCHEIDER, N., CHEN, Z., AULER, A.S., BAKALOWICZ, M., BRODA, S., DREW, D., HARTMANN, J., JIANG, G., MOOSDORF, N., STEVANOVIC, Z. & VENI, G. (2020) Global distribution of carbonate rocks and karst water resources. *Hydrogeology Journal* **28**, 1661–1677.

GONÇALVES, C., RAJA, M., MADIME, O., CASCALHEIRA, J., HAWS, J., MATOS, D. & BICHO, N. (2016) Mapping the Stone Age of Mozambique. *African Archaeological Review* **33**, 1–12.

GOODMAN, M. (1961) The role of immunochemical differences in the phyletic development of human behavior. *Human Biology* **33**, 131–162.

GOODMAN, M. (1963) Serological analysis of the systematics of recent hominoids. *Human Biology* **35**, 377–436.

GOODMAN, M. (1981) Decoding the pattern of protein evolution. *Progress in Biophysics and Molecular Biology* **38**, 105–164.

GOSWAMI, A. (2012) A dating success story: genomes and fossils converge on placental mammal origins. *EvoDevo* **3**, 18.

GRAHAM, R.W. (2000) FAUNMAP database: Filter effects from field to literature to database to analysis to interpretation. In *Geological Society of America Annual Meeting, 2000, Abstracts with Programs* p. A131.

GRAHAM, R.W., LUNDELIUS, E.L., GRAHAM, M.A., SCHROEDER, E.K., TOOMEY, R.S., ANDERSON, E., BARNOSKY, A.D., BURNS, J.A., CHURCHER, C.S., GRAYSON, D.K., GUTHRIE, R.D., HARINGTON, C.R., JEFFERSON, G.T., MARTIN, L.D., MCDONALD, H.G., ET AL. (1996) Spatial Response of Mammals to Late Quaternary Environmental Fluctuations. *Science* **272**, 1601–1606.

GRANTHAM, G.H., MARQUES, J.M., WILSON, M.G.C., MANHIÇA, V. & HARTZER, F.J. (2011) *Explanation of the Geological Map of Mozambique, 1:1,000,000*. National Directorate of Geology, Maputo.

GRIFFIN, D.L. (2002) Aridity and humidity: two aspects of the late Miocene climate of North Africa and the Mediterranean. *Palaeogeography, Palaeoclimatology, Palaeoecology* **182**, 65–91.

GROSS, L. (2005) Wild Gorillas Handy with a Stick. *PLoS Biology* **3**, e385.

GRÜN, B., KOSMIDIS, I. & ZEILEIS, A. (2012) Extended Beta Regression in *R* : Shaken, Stirred, Mixed, and Partitioned. *Journal of Statistical Software* **48**, 1–25.

GSA (2022) GSA geologic time scale v6.0. Geological Society of America. https://www.geosociety.org/GSA/GSA/timescale/home.aspx.

GUISAN, A. & THUILLER, W. (2005) Predicting species distribution: offering more than simple habitat models. *Ecology Letters* **8**, 993–1009.

GUNKEL, S., RUST, J., WAPPLER, T., MAYER, C., NIEHUIS, O. & MISOF, B. (2017) A posteriori evaluation of molecular divergence dates using empirical estimates of time-heterogeneous fossilization rates. Preprint, Paleontology.

GUNTER, C. & DHAND, R. (2005) The chimpanzee genome. *Nature* **437**, 47.

GUNZ, P. & MITTEROECKER, P. (2013) Semilandmarks: A Method for Quantifying Curves and Surfaces. *Hystrix, the Italian Journal of Mammalogy* **24**, 103–109.

HABERMANN, J.M., ALBERTI, M., ALDEIAS, V., ALEMSEGED, Z., ARCHER, W., BAMFORD, M., BIRO, D., BRAUN, D.R., CAPELLI, C., CUNHA, E., DA SILVA, M.F., LÜDECKE, T., MADIQUIDA, H., MARTINEZ, F.I., MATHE, J., ET AL. (2019) Gorongosa by the sea: First Miocene fossil sites from the Urema Rift, central Mozambique, and their coastal paleoenvironmental and paleoecological contexts. *Palaeogeography, Palaeoclimatology, Palaeoecology* **514**, 723–738.

HAILE-SELASSIE, Y. (2001) Late Miocene hominids from the Middle Awash, Ethiopia. *Nature* **412**, 178–181.

HAILE-SELASSIE, Y., DEINO, A., SAYLOR, B., UMER, M. & LATIMER, B. (2007) Preliminary geology and paleontology of new hominid-bearing Pliocene localities in the central Afar region of Ethiopia. *Anthropological Science* **115**, 215–222.

HAILE-SELASSIE, Y., GIBERT, L., MELILLO, S.M., RYAN, T.M., ALENE, M., DEINO, A., LEVIN, N.E., SCOTT, G. & SAYLOR, B.Z. (2015) New species from Ethiopia further expands Middle Pliocene hominin diversity. *Nature* **521**, 483–488.

HAILE-SELASSIE, Y., MELILLO, S.M. & SU, D.F. (2016) The Pliocene hominin diversity conundrum: Do more fossils mean less clarity? *Proceedings of the National Academy of Sciences* **113**, 6364–6371.

HAILE-SELASSIE, Y., SUWA, G. & WHITE, T. (2009) 7. Hominidae. In Ardipithecus kadabba*: late Miocene evidence from the Middle Awash, Ethiopia* (eds Y. HAILE-SELASSIE & G. WOLDEGABRIEL), pp. 159–236. University of California Press, Berkeley.

HAILE-SELASSIE, Y., SUWA, G. & WHITE, T.D. (2004) Late Miocene teeth from Middle Awash, Ethiopia, and early hominid dental evolution. *Science* **303**, 1503–1505.

HALSEY, L.G., TYLER, C.J. & KULIUKAS, A.V. (2014) The energy costs of wading in water. *Biology Open* **3**, 571–574.

HAMILTON, W.J. & TILSON, R.L. (1985) Fishing baboons at desert waterholes. *American Journal of Primatology* **8**, 255–257.

HAMMOND, A.S., MAVUSO, S.S., BIERNAT, M., BRAUN, D.R., JINNAH, Z., KUO, S., MELAKU, S., WEMANYA, S.N., NDIEMA, E.K., PATTERSON, D.B., UNO, K.T. & PALCU, D.V. (2021) New hominin remains and revised context from the earliest Homo erectus locality in East Turkana, Kenya. *Nature Communications* **12**, 1–12.

HAMMOND, A.S., ROOK, L., ANAYA, A.D., CIOPPI, E., COSTEUR, L., MOYÀ-SOLÀ, S. & ALMÉCIJA, S. (2020) Insights into the lower torso in late Miocene hominoid *Oreopithecus bambolii*. *Proceedings of the National Academy of Sciences* **117**, 278–284.

HAMMOND, P., LEWIS-BEVAN, L., BIRO, D. & CARVALHO, S. (2022) Risk perception and terrestriality in primates: A quasi-experiment through habituation of chacma baboons (*Papio ursinus*) in Gorongosa National Park, Mozambique. *American Journal of Biological Anthropology* **179**, 48–59.

HANZAWA, H. & ADACHI, K. (1983) Overconsolidation of Alluvial Clays. *Soils and Foundations* **23**, 106–118.

HARRISON, T. (2010) Dendropithecoidea, Proconsuloidea, and Hominoidea. In *Cenozoic Mammals of Africa* (ed L. WERDELIN), pp. 429–469. University of California Press, Berkeley.

HARRISON, T.S. & HARRISON, T. (1989) Palynology of the late Miocene *Oreopithecus*-bearing lignite from Baccinello, Italy. *Palaeogeography, Palaeoclimatology, Palaeoecology* **76**, 45–65.

HASEGAWA, M., KISHINO, H. & YANO, T. (1985) Dating of the human-ape splitting by a molecular clock of mitochondrial DNA. *Journal of Molecular Evolution* **22**, 160–174.

HASSANIN, A., DELSUC, F., ROPIQUET, A., HAMMER, C., JANSEN VAN VUUREN, B., MATTHEE, C., RUIZ-GARCIA, M., CATZEFLIS, F., ARESKOUG, V., NGUYEN, T.T. & COULOUX, A. (2012) Pattern and timing of diversification of Cetartiodactyla (Mammalia, Laurasiatheria), as revealed by a comprehensive analysis of mitochondrial genomes. *Comptes Rendus Biologies* **335**, 32–50.

HASTIE, T., TIBSHIRANI, R. & FRIEDMAN, J. (2009) *The Elements of Statistical Learning*. 2nd Ed. Springer, New York.

HAWKS, J., ELLIOTT, M., SCHMID, P., CHURCHILL, S.E., RUITER, D.J. DE, ROBERTS, E.M., HILBERT-WOLF, H., GARVIN, H.M., WILLIAMS, S.A., DELEZENE, L.K., FEUERRIEGEL, E.M., RANDOLPH-QUINNEY, P., KIVELL, T.L., LAIRD, M.F., TAWANE, G., ET AL. (2017) New fossil remains of *Homo naledi* from the Lesedi Chamber, South Africa. *eLife* **6**, e24232.

HAY, G.J. & CASTILLA, G. (2008) Geographic Object-Based Image Analysis (GEOBIA): A new name for a new discipline. In *Object-Based Image Analysis* pp. 75–89. Springer, Berlin, Heidelberg.

HAYASHI, T., YAMANAKA, T., HIKASA, Y., SATO, M., KUWAHARA, Y. & OHNO, M. (2020) Latest Pliocene Northern Hemisphere glaciation amplified by intensified Atlantic meridional overturning circulation. *Communications Earth & Environment* **1 (25)**, 1–10.

HEAD, J., HEALY, A. & NOWAK, K. (2019) Primates of African Mangroves. In *Primates in Flooded Habitats: Ecology and Conservation* (eds A.A. BARNETT, I. MATSUDA & K. NOWAK), pp. 77–88. Cambridge University Press, Cambridge.

HEADS, M. (2012) Bayesian transmogrification of clade divergence dates: a critique. *Journal of Biogeography* **39**, 1749–1756.

HEGAZI, E.H., SAMAK, A.A., YANG, L., HUANG, R. & HUANG, J. (2023) Prediction of Soil Moisture Content from Sentinel-2 Images Using Convolutional Neural Network (CNN). *Agronomy* **13**, 656.

HEINTZMAN, P.D., ZAZULA, G.D., CAHILL, J.A., REYES, A.V., MACPHEE, R.D.E. & SHAPIRO, B. (2015) Genomic Data from Extinct North American *Camelops* Revise Camel Evolutionary History. *Molecular Biology and Evolution* **32**, 2433–2440.

HENKE, W. (2015) Historical Overview of Paleoanthropological Research. In *Handbook of Paleoanthropology* pp. 3–95. Springer, Berlin, Heidelberg.

HERRERO, J. (2023) Atapuerca completa el puzle con el 'Homo erectus': 'Es seguro, no hay dudas'. *La Razón*.

HIGGINS, J.P.T., THOMPSON, S.G. & SPIEGELHALTER, D.J. (2009) A re-evaluation of random-effects meta-analysis. *Journal of the Royal Statistical Society: Series A (Statistics in Society)* **172**, 137–159.

HIJMANS, R.J. (2022) raster: Geographic data analysis and modeling.

HIJMANS, R.J. (2023) terra: Spatial data analysis.

HIJMANS, R.J., PHILLIPS, S., LEATHWICK, J. & ELITH, J. (2022) dismo: Species distribution modeling.

HILDEBRAND, A.R., PENFIELD, G.T., KRING, D.A., PILKINGTON, M., CAMARGO Z., A., JACOBSEN, S.B. & BOYNTON, W.V. (1991) Chicxulub Crater: A possible Cretaceous/Tertiary boundary impact crater on the Yucatán Peninsula, Mexico. *Geology* **19**, 867.

HILLIER, S. (1995) Erosion, Sedimentation and Sedimentary Origin of Clays. In *Origin and Mineralogy of Clays: Clays and the Environment* (ed B. VELDE), pp. 162–219. Springer, Berlin, Heidelberg.

HLUSKO, L.J. (2018) Geospatial Approaches to Hominid Paleontology in Africa. In *New Geospatial Approaches to the Anthropological Sciences* (eds R.L. ANEMONE & G.C. CONROY), pp. 39–58. New Mexico Press, Albuquerque, NM.

HO, S.Y.W., TONG, K.J., FOSTER, C.S.P., RITCHIE, A.M., LO, N. & CRISP, M.D. (2015) Biogeographic calibrations for the molecular clock. *Biology Letters* **11**, 20150194.

HOFFECKER, J.F. (2017) *Modern humans: Their african origin and global dispersal*. First Edition. Columbia University Press, New York.

HOHMANN, G., ORTMANN, S., REMER, T. & FRUTH, B. (2019) Fishing for iodine: what aquatic foraging by bonobos tells us about human evolution. *BMC Zoology* **4**, 1–5.

HOLDEN, P.B., EDWARDS, N.R., RANGEL, T.F., PEREIRA, E.B., TRAN, G.T. & WILKINSON, R.D. (2019) PALEO-PGEM v1.0: a statistical emulator of Pliocene–Pleistocene climate. *Geoscientific Model Development* **12**, 5137–5155. Copernicus GmbH.

HOPLEY, P.J., CERLING, T.E., CRÉTÉ, L., WERDELIN, L., MWEBI, O., MANTHI, F.K. & LEAKEY, L.N. (2023) Stable isotope analysis of carnivores from the Turkana Basin, Kenya: Evidence for temporally-mixed fossil assemblages. *Quaternary International* **650**, 12–27.

HORNING, N., ROBINSON, J.A., STERLING, E.J., TURNER, W. & SPECTOR, S. (2010) Measuring and Monitoring Land Cover, Land use, and Vegetation Characteristics. In *Remote Sensing for Ecology and Conservation: A Handbook of Techniques* (eds N. HORNING, J.A. ROBINSON, E.J. STERLING, W. TURNER & S. SPECTOR), p. Oxford University Press, Oxford.

HOWELL, F.C., HAESAERTS, P. & DE HEINZELIN, J. (1987) Depositional environments, archeological occurrences and hominids from Members E and F of the Shungura Formation (Omo basin, Ethiopia). *Journal of Human Evolution* **16**, 665–700.

HU, W., CHAU, H.W. & SI, B.C. (2015) Vis-Near IR Reflectance Spectroscopy for Soil Organic Carbon Content Measurement in the Canadian Prairies. *CLEAN – Soil, Air, Water* **43**, 1215–1223.

HUANG, J., HUANG, Y., MA, Y. & LIU, B. (2023) Automatic karst cave detection from seismic images via a convolutional neural network and transfer learning. *Frontiers in Earth Science* **10**, 1043218.

HUANG, S., TANG, L., HUPY, J.P., WANG, Y. & SHAO, G. (2021) A commentary review on the use of normalized difference vegetation index (NDVI) in the era of popular remote sensing. *Journal of Forestry Research* **32**, 1–6.

HUBBARD, S.M., MACEACHERN, J.A. & BANN, K.L. (2012) Chapter 20 - Slopes. In *Developments in Sedimentology* (eds D. KNAUST & R.G. BROMLEY), pp. 607–642. Elsevier, Oxford.

HUBISZ, M.J., WILLIAMS, A.L. & SIEPEL, A. (2020) Mapping gene flow between ancient hominins through demography-aware inference of the ancestral recombination graph. *PLoS genetics* **16**, e1008895.

HUETE, A.R., LIU, H. & VAN LEEUWEN, W.J.D. (1997) The use of vegetation indices in forested regions: issues of linearity and saturation. In *IGARSS'97. 1997 IEEE International Geoscience and Remote Sensing Symposium Proceedings. Remote Sensing - A Scientific Vision for Sustainable Development* pp. 1966–1968 vol.4.

HUXLEY, T.H. (1863) *Evidence as to Man's Place in Nature*. Williams and Norgate, London, UK.

ILICH, A.R., MISIUK, B., LECOURS, V. & MURAWSKI, S.A. (2023) MULTISCALEDTM : An open-source R package for multiscale geomorphometric analysis. *Transactions in GIS* **27**, 1164–1204.

IRESTEDT, M., JØNSSON, K.A., FJELDSÅ, J., CHRISTIDIS, L. & ERICSON, P.G. (2009) An unexpectedly long history of sexual selection in birds-of-paradise. *BMC Evolutionary Biology* **9**, 235.

ISAAC, G.L. & BEHRENSMEYER, A.K. (1997) Chapter 2: Geological context and palaeoenvironments. In *Koobi Fora Research Project Volume 5: Plio-Pleistocene Archaeology* (eds G.L. ISAAC & B. ISAAC), pp. 12–70. Clarendon Press, Oxford.

ISHIDA, H. & PICKFORD, M. (1997) A new Late Miocene hominoid from Kenya: *Samburupithecus kiptalami* gen. et sp. nov. *Comptes Rendus de l'Académie des Sciences - Series IIA - Earth and Planetary Science* **325**, 823–829.

JAANUSSON, V. (1976) Faunal dynamics in the middle Ordovician (Viruan) of Balto-Scandia. In *The Ordovician System: Proceedings of a Palaeontological Association Symposium* (ed M.G. BASSET), pp. 301–326. University of Wales Press and National Museum of Wales, Cardiff.

JAIN, A.K. (2010) Data clustering: 50 years beyond K-means. *Pattern Recognition Letters* **31**, 651–666.

JAMES, G., WITTEN, D., HASTIE, T. & TIBSHIRANI, R. (eds) (2013) *An introduction to statistical learning: with applications in R*. Springer, New York.

JAPKOWICZ, N. (1999) Concept-learning in the absence of counter-examples: An autoassociation-based approach to classification. Ph.D. Dissertation, New Brunswick Rutgers, The State University of New Jersey.

JENNINGS, D.S. & HASIOTIS, S.T. (2006) Taphonomic analysis of a dinosaur feeding site using Geographic Information Systems (GIS), Morrison Formation, Southern Bighorn Basin, Wyoming, USA. *PALAIOS* **21**, 480–492.

JENSEN-SEAMAN, M.I. & HOOPER-BOYD, K.A. (2008) Molecular Clocks: Determining the Age of the Human–Chimpanzee Divergence. In *Encyclopedia of Life Sciences (ELS)* p. John Wiley & Sons, Ltd, Chichester.

JI, Q., WU, W., JI, Y., LI, Q. & NI, X. (2021) Late Middle Pleistocene Harbin cranium represents a new *Homo* species. *The Innovation* **2**, 100132.

JOHANSON, D.C., MASAO, F.T., ECK, G.G., WHITE, T.D., WALTER, R.C., KIMBEL, W.H., ASFAW, B., MANEGA, P., NDESSOKIA, P. & SUWA, G. (1987) New partial skeleton of *Homo habilis* from Olduvai Gorge, Tanzania. *Nature* **327**, 205–209.

JOHANSON, D.C. & TAIEB, M. (1976) Plio—Pleistocene hominid discoveries in Hadar, Ethiopia. *Nature* **260**, 293–297.

JOLLY, C.J. (1970) The Seed-Eaters: A New Model of Hominid Differentiation Based on a Baboon Analogy. *Man* **5**, 5–26.

JOLLY, C.J. (2001) A proper study for mankind: Analogies from the Papionin monkeys and their implications for human evolution. *American Journal of Physical Anthropology* **116**, 177–204.

JONES, K.H. (1998) A comparison of algorithms used to compute hill slope as a property of the DEM. *Computers and Geosciences* **24**, 315–323.

JØNSSON, K.A., FABRE, P.-H. & IRESTEDT, M. (2012) Brains, tools, innovation and biogeography in crows and ravens. *BMC Evolutionary Biology* **12**, 72.

JOORDENS, J.C.A. (2011) The power of place: climate change as driver of hominin evolution and dispersal over the past five million years. PhD, Vrije Universiteit Amsterdam.

JOORDENS, J.C.A., D'ERRICO, F., WESSELINGH, F.P., MUNRO, S., VOS, J. DE, WALLINGA, J., ANKJÆRGAARD, C., REIMANN, T., WIJBRANS, J.R., KUIPER, K.F., MÜCHER, H.J., COQUEUGNIOT, H., PRIÉ, V., JOOSTEN, I., OS, B. VAN, ET AL. (2015) *Homo erectus* at Trinil on Java used shells for tool production and engraving. *Nature* **518**, 228–231.

JOORDENS, J.C.A., FEIBEL, C.S., VONHOF, H.B., SCHULP, A.S. & KROON, D. (2019) Relevance of the eastern African coastal forest for early hominin biogeography. *Journal of Human Evolution* **131**, 176–202.

JOORDENS, J.C.A., KUIPERS, R.S., WANINK, J.H. & MUSKIET, F.A.J. (2014) A fish is not a fish: Patterns in fatty acid composition of aquatic food may have had implications for hominin evolution. *Journal of Human Evolution* **77**, 107–116.

JOORDENS, J.C.A., VONHOF, H.B., FEIBEL, C.S., LOURENS, L.J., DUPONT-NIVET, G., VAN DER LUBBE, J.H.J.L., SIER, M.J., DAVIES, G.R. & KROON, D. (2011) An astronomically-tuned climate framework for hominins in the Turkana Basin. *Earth and Planetary Science Letters* **307**, 1–8.

JOORDENS, J.C.A., WESSELINGH, F.P., DE VOS, J., VONHOF, H.B. & KROON, D. (2009) Relevance of aquatic environments for hominins: a case study from Trinil (Java, Indonesia). *Journal of Human Evolution* **57**, 656–671.

JURESTOVSKY, D. & JOYNER, T.A. (2017) Applications of species distribution modeling for palaeontological fossil detection: late Pleistocene models of Saiga (Artiodactyla: Bovidae, *Saiga tatarica*). *Palaeobiodiversity and Palaeoenvironments*, 1–9.

KALB, J.E., WOOD, C.B., SMART, C., OSWALD, E.B., MABRETE, A., TEBEDGE, S. & WHITEHEAD, P. (1980) Preliminary geology and palaeontology of the Bodo D'ar hominid Site, Afar, Ethiopia. *Palaeogeography, Palaeoclimatology, Palaeoecology* **30**, 107–120.

KATOH, S., BEYENE, Y., ITAYA, T., HYODO, H., HYODO, M., YAGI, K., GOUZU, C., WOLDEGABRIEL, G., HART, W.K., AMBROSE, S.H., NAKAYA, H., BERNOR, R.L., BOISSERIE, J.-R., BIBI, F., SAEGUSA, H., ET AL. (2016) New geological and palaeontological age constraint for the gorilla–human lineage split. *Nature* **530**, 215–218.

KAYA, F., BIBI, F., ŽLIOBAITĖ, I., ERONEN, J.T., HUI, T. & FORTELIUS, M. (2018) The rise and fall of the Old World savannah fauna and the origins of the African savannah biome. *Nature Ecology & Evolution* **2**, 241–246.

KEITH, A. (1920) *The antiquity of man*. J.B. Lippincott Company; Williams & Norgate, Philadelphia, London.

KEMPF, E. (2009) Patterns of Water Use in Primates. *Folia Primatologica* **80**, 275–294.

KHAN, S.S. & MADDEN, M.G. (2010) A Survey of Recent Trends in One Class Classification. In *Artificial Intelligence and Cognitive Science* (eds L. COYLE & J. FREYNE), pp. 188–197. Springer, Berlin, Heidelberg.

KIDWELL, S.M. (1986) Models for fossil concentrations: paleobiologic implications. *Paleobiology* **12**, 6–24.

KIDWELL, S.M. & FLESSA, K.W. (1995) The Quality of the Fossil Record: Populations, Species, and Communities. *Annual Review of Ecology and Systematics* **26**, 269–299.

KIHWELE, E.S., MCHOMVU, V., OWEN-SMITH, N., HETEM, R.S., HUTCHINSON, M.C., POTTER, A.B., OLFF, H. & VELDHUIS, M.P. (2020) Quantifying water requirements of African ungulates through a combination of functional traits. *Ecological Monographs* **90**, e01404.

KIMURA, T. (2019) How did humans acquire erect bipedal walking? *Anthropological Science* **127**, 1–12.

KINGDON, J. (1990) *Island Africa: the evolution of Africa's rare animals and plants*. Collins, London.

KINGDON, J. (2003) *Lowly Origin: Where, When, and why Our Ancestors First Stood Up*. Princeton University Press.

KINGDON, J. (2019) *The Kingdon Field Guide to African Mammals*. Second Edition. Bloomsbury Wildlife.

KINGDON, J. (2023) Origin Africa: Safaris in Deep Time. In *Origin Africa* p. 472. British Edition. William Collins, London, UK.

KISSEL, M. & HAWKS, J. (2015) What are the Lothagam and Tabarin Mandibles? *PaleoAnthropology*, 37−43.

KNIGHT, E. & KVARAN, G. (2014) Landsat-8 Operational Land Imager Design, Characterization and Performance. *Remote Sensing* **6**, 10286–10305.

KOHLER, T.A. & PARKER, S.C. (1986) Predictive Models for Archaeological Resource Location. *Advances in Archaeological Method and Theory* **9**, 397–452.

KOOPS, K., WRANGHAM, R.W., CUMBERLIDGE, N., FITZGERALD, M.A., VAN LEEUWEN, K.L., ROTHMAN, J.M. & MATSUZAWA, T. (2019) Crab-fishing by chimpanzees in the Nimba Mountains, Guinea. *Journal of Human Evolution* **133**, 230–241.

KOVAROVIC, K., SU, D.F. & LINTULAAKSO, K. (2018) Mammal community structure analysis. In *Methods in Paleoecology: Reconstructing Cenozoic Terrestrial Environments and Ecological Communities* (eds D.A. CROFT, D.F. SU & S.W. SIMPSON), pp. 351–372. Springer, Cham, Switzerland.

KSEPKA, D. & CLARKE, J. (2015) Phylogenetically vetted and stratigraphically constrained fossil calibrations within Aves. *Palaeontologia Electronica* **18**, 1–25.

KSEPKA, D.T., WARE, J.L. & LAMM, K.S. (2014) Flying rocks and flying clocks: disparity in fossil and molecular dates for birds. *Proceedings of the Royal Society B: Biological Sciences* **281**, 20140677.

KUDERNA, L.F.K., GAO, H., JANIAK, M.C., KUHLWILM, M., ORKIN, J.D., BATAILLON, T., MANU, S., VALENZUELA, A., BERGMAN, J., ROUSSELLE, M., SILVA, F.E., AGUEDA, L., BLANC, J., GUT, M., DE VRIES, D., ET AL. (2023) A global catalog of whole-genome diversity from 233 primate species. *Science* **380**, 906–913.

KUMAR, S., STECHER, G., SULESKI, M. & HEDGES, S.B. (2017) TimeTree: A Resource for Timelines, Timetrees, and Divergence Times. *Molecular Biology and Evolution* **34**, 1812–1819.

KUMAR, S., SULESKI, M., CRAIG, J.M., KASPROWICZ, A.E., SANDERFORD, M., LI, M., STECHER, G. & HEDGES, S.B. (2022) TimeTree 5: An Expanded Resource for Species Divergence Times. *Molecular Biology and Evolution*, msac174.

KUNIMATSU, Y., NAKATSUKASA, M., SAWADA, Y., SAKAI, T., HYODO, M., HYODO, H., ITAYA, T., NAKAYA, H., SAEGUSA, H., MAZURIER, A., SANEYOSHI, M., TSUJIKAWA, H., YAMAMOTO, A. & MBUA, E. (2007) A new Late Miocene great ape from Kenya and its implications for the origins of African great apes and humans. *Proceedings of the National Academy of Sciences* **104**, 19220–19225.

KUNIMATSU, Y., NAKATSUKASA, M., SAWADA, Y., SAKAI, T., SANEYOSHI, M., NAKAYA, H., YAMAMOTO, A. & MBUA, E. (2016) A second hominoid species in the early Late Miocene fauna of Nakali (Kenya). *Anthropological Science* **124**, 75–83.

KUTZBACH, J.E., GUAN, J., HE, F., COHEN, A.S., ORLAND, I.J. & CHEN, G. (2020) African climate response to orbital and glacial forcing in 140,000-y simulation with implications for early modern human environments. *Proceedings of the National Academy of Sciences* **117**, 2255–2264.

KVAMME, K.L. (1983) Computer processing techniques for regional modeling of archaeological site locations. *Advances in computer archaeology* **1**, 26–52.

KVAMME, K.L. (1999) Recent Directions and Developments in Geographical Information Systems. *Journal of Archaeological Research* **7**, 153–201.

KVAMME, K.L. (2005) There and Back Again: Revisiting Archaeological Locational Modeling. In *GIS and Archaeological Site Location Modeling* (eds M.W. MEHRER & K.L. WESCOTT), pp. 3–38. Taylor and Francis, Florida.

KVAMME, K.L. & JOCHIM, M.A. (1989) The Environmental Basis of Mesolithic Settlement In Bonsall. In *The Mesolithic in Europe: Papers Presented at the Third International*

Symposium, Edinburgh 1985 (ed C. BONSALL), pp. 1–12. John Donald Publishers Ltd., Edinburgh.

LAHR, M.M. (2010) Saharan Corridors and Their Role in the Evolutionary Geography of 'Out of Africa I'. In *Out of Africa I* (eds J.G. FLEAGLE, J.J. SHEA, F.E. GRINE, A.L. BADEN & R.E. LEAKEY), pp. 27–46. Springer Netherlands, Dordrecht.

LAHR, M.M. (2016) The shaping of human diversity: filters, boundaries and transitions. *Philosophical Transactions of the Royal Society B: Biological Sciences* **371**, 20150241.

LARSEN, C.S. (2009) *Essentials of Physical Anthropology: Discovering Our Origins*. First Edition. W. W. Norton & Company, New York.

LAUMANNS, M. (2001) *Mozambique 1998: Report on the European Speleological Project 'Cheringoma 1998'*. Speläoclub, Berlin.

LE FUR, S., FARA, E., MACKAYE, H.T., VIGNAUD, P. & BRUNET, M. (2009) The mammal assemblage of the hominid site TM266 (Late Miocene, Chad Basin): ecological structure and paleoenvironmental implications. *Naturwissenschaften* **96**, 565–574.

LEAKEY, L.S. (1961) New finds at Olduvai Gorge. *Nature* **189**, 649.

LEAKEY, L.S., TOBIAS, P.V. & NAPIER, J.R. (1964) A new species of the genus *Homo* from Olduvai Gorge. *Nature* **202**, 7–9.

LEAKEY, L.S.B. (1958) Recent discoveries at Olduvai Gorge, Tanganyika. *Nature* **181**, 1099.

LEAKEY, L.S.B. (1959) A New Fossil Skull From Olduvai. *Nature* **184**, 491–493.

LEAKEY, L.S.B. (1960) Recent Discoveries at Olduvai Gorge. *Nature* **188**, 1050–1052.

LEAKEY, L.S.B., EVERNDEN, J.F. & CURTIS, G.H. (1961) Age of Bed I, Olduvai Gorge, Tanganyika. *Nature* **191**, 478–479.

LEAKEY, M.D. (1969) Recent Discoveries of Hominid Remains at Olduvai Gorge, Tanzania. *Nature* **223**, 756.

LEAKEY, M.D. & HAY, R.L. (1979) Pliocene footprints in the Laetolil Beds at Laetoli, northern Tanzania. *Nature* **278**, 317–323.

LEAKEY, M.G., FEIBEL, C.S., MCDOUGALL, I. & WALKER, A. (1995) New four-million-year-old hominid species from Kanapoi and Allia Bay, Kenya. *Nature* **376**, 565–571.

LEAKEY, M.G. & WALKER, A.C. (2003) 6.2. The Lothagam Hominids. In *Lothagam: The Dawn of Humanity in Eastern Africa* (eds M.G. LEAKEY & J.M. HARRIS), pp. 249–257. Columbia University Press, New York Chichester, West Sussex.

LEAKEY, R.E.F. & WALKER, A.C. (1985) Further hominids from the Plio-Pleistocene of Koobi Fora, Kenya. *American Journal of Physical Anthropology* **67**, 135–163.

LEBATARD, A.-E., BOURLÈS, D.L., BRAUCHER, R., ARNOLD, M., DURINGER, P., JOLIVET, M., MOUSSA, A., DESCHAMPS, P., ROQUIN, C., CARCAILLET, J., SCHUSTER, M., LIHOREAU,

F., LIKIUS, A., MACKAYE, H.T., VIGNAUD, P., ET AL. (2010) Application of the authigenic 10Be/9Be dating method to continental sediments: Reconstruction of the Mio-Pleistocene sedimentary sequence in the early hominid fossiliferous areas of the northern Chad Basin. *Earth and Planetary Science Letters* **297**, 57–70.

LEBATARD, A.-E., BOURLÈS, D.L., DURINGER, P., JOLIVET, M., BRAUCHER, R., CARCAILLET, J., SCHUSTER, M., ARNAUD, N., MONIÉ, P., LIHOREAU, F., LIKIUS, A., MACKAYE, H.T., VIGNAUD, P. & BRUNET, M. (2008) Cosmogenic nuclide dating of *Sahelanthropus tchadensis* and *Australopithecus bahrelghazali*: Mio-Pliocene hominids from Chad. *Proceedings of the National Academy of Sciences of the United States of America* **105**, 3226–3231.

LEPRE, C.J. (2014) Early Pleistocene lake formation and hominin origins in the Turkana–Omo rift. *Quaternary Science Reviews* **102**, 181–191.

LEPRE, C.J., QUINN, R.L., JOORDENS, J.C.A., SWISHER, C.C. & FEIBEL, C.S. (2007) Plio-Pleistocene facies environments from the KBS Member, Koobi Fora Formation: implications for climate controls on the development of lake-margin hominin habitats in the northeast Turkana Basin (northwest Kenya). *Journal of Human Evolution* **53**, 504–514.

LEVIN, N.E. (2015) Environment and Climate of Early Human Evolution. *Annual Review of Earth and Planetary Sciences* **43**, 405–429.

LEVIN, N.E., BROWN, F.H., BEHRENSMEYER, A.K., BOBE, R. & CERLING, T.E. (2011) Paleosol carbonates from the Omo Group: Isotopic records of local and regional environmental change in East Africa. *Palaeogeography, Palaeoclimatology, Palaeoecology* **307**, 75–89.

LEWIS, M.C. & O'RIAIN, M.J. (2017) Foraging Profile, Activity Budget and Spatial Ecology of Exclusively Natural-Foraging Chacma Baboons (*Papio ursinus*) on the Cape Peninsula, South Africa. *International Journal of Primatology* **38**, 751–779.

LI, W. & GUO, Q. (2010) A maximum entropy approach to one-class classification of remote sensing imagery. *International Journal of Remote Sensing* **31**, 2227–2235.

LIAW, A. & WIENER, M. (2002) Classification and Regression by randomForest. *R News* **2**, 18–22.

LIMP, W. (1989) *The Use of Multispectral Digital Imagery in Archaeological Applications*. Arkansas Archaeological Survey, Research Series No. 34, Arkansas, USA.

LLOYD, S. (1982) Least squares quantization in PCM. *IEEE Transactions on Information Theory* **28**, 129–137.

LOEZA-QUINTANA, T. & ADAMOWICZ, S.J. (2018) Iterative Calibration: A Novel Approach for Calibrating the Molecular Clock Using Complex Geological Events. *Journal of Molecular Evolution* **86**, 118–137.

LÓPEZ-SERRANO, P.M., CÁRDENAS DOMÍNGUEZ, J.L., CORRAL-RIVAS, J.J., JIMÉNEZ, E., LÓPEZ-SÁNCHEZ, C.A. & VEGA-NIEVA, D.J. (2020) Modeling of Aboveground

Biomass with Landsat 8 OLI and Machine Learning in Temperate Forests. *Forests* **11**, 1–11.

LOVEJOY, C.O., LATIMER, B., SUWA, G., ASFAW, B. & WHITE, T.D. (2009a) Combining Prehension and Propulsion: The Foot of *Ardipithecus ramidus*. *Science* **326**, 72-72e8.

LOVEJOY, C.O., SUWA, G., SIMPSON, S.W., MATTERNES, J.H. & WHITE, T.D. (2009b) The Great Divides: *Ardipithecus ramidus* Reveals the Postcrania of Our Last Common Ancestors with African Apes. *Science* **326**, 73–106.

LÜDECKE, T., LEICHLITER, J.N., ALDEIAS, V., BAMFORD, M.K., BIRO, D., BRAUN, D.R., CAPELLI, C., CYBULSKI, J.D., DUPREY, N.N., FERREIRA DA SILVA, M.J., FOREMAN, A.D., HABERMANN, J.M., HAUG, G.H., MARTÍNEZ, F.I., MATHE, J., ET AL. (2022) Carbon, nitrogen, and oxygen stable isotopes in modern tooth enamel: A case study from Gorongosa National Park, central Mozambique. *Frontiers in Ecology and Evolution* **10**, 958032.

LUNCZ, L.V., TAN, A., HASLAM, M., KULIK, L., PROFFITT, T., MALAIVIJITNOND, S. & GUMERT, M. (2017) Resource depletion through primate stone technology. *eLife* **6**, e23647.

LUPIEN, R.L., RUSSELL, J.M., FEIBEL, C., BECK, C., CASTAÑEDA, I., DEINO, A. & COHEN, A.S. (2018) A leaf wax biomarker record of early Pleistocene hydroclimate from West Turkana, Kenya. *Quaternary Science Reviews* **186**, 225–235.

LYON, R.J.P. & BURNS, E.A. (1963) Analysis of rocks and minerals by reflected infrared radiation. *Economic Geology* **58**, 274–284.

LYONS, T.R. & AVERY, T.E. (1977) *Remote sensing: a handbook for archeologists and cultural resource managers*. Cultural Resources Management Division, National Park Service, US Department of the Interior., Washington, DC.

MACCHIARELLI, R., BERGERET-MEDINA, A., MARCHI, D. & WOOD, B. (2020) Nature and relationships of *Sahelanthropus tchadensis*. *Journal of Human Evolution* **149**, 102898.

MACGREGOR, D. (2015) History of the development of the East African Rift System: A series of interpreted maps through time. *Journal of African Earth Sciences* **101**, 232–252.

MACK, B. & WASKE, B. (2017) In-depth comparisons of MaxEnt, biased SVM and one-class SVM for one-class classification of remote sensing data. *Remote Sensing Letters* **8**, 290–299.

MACQUEEN, J. (1967) Some methods for classification and analysis of multivariate observations. *Proceedings of the Fifth Berkeley Symposium on Mathematical Statistics and Probability* **Volume 1: Statistics, No. 14**, 281–297.

MAIER, G. (2003) *African Dinosaurs Unearthed: The Tendaguru Expeditions*. Indiana University Press, Indiana.

MAKIN, J. (1969) Soil Formation in the Turkana Desert. *East African Agricultural and Forestry Journal* **34**, 493–496.

MALAKHOV, D.V., DYKE, G.J. & KING, C. (2009) Remote sensing applied to paleontology: exploration of Upper Cretaceous sediments in Kazakhstan for potential fossil sites. *Palaeontologica Electronica* **12**, 12–13.

MALAPERDAS, G.D. & PANAGIOTIDIS, V.V. (2018) The aspects of Aspect: Understanding land exposure and its part in geographic information systems analysis. *Energy & Environment* **29**, 1022–1037.

MANTHI, F.K., CERLING, T.E., CHRITZ, K.L. & BLUMENTHAL, S.A. (2020) Diets of mammalian fossil fauna from Kanapoi, northwestern Kenya. *Journal of Human Evolution* **140**, 102338.

MAREAN, C.W. (2014) The origins and significance of coastal resource use in Africa and Western Eurasia. *Journal of Human Evolution* **77**, 17–40.

MARSHALL, C.R. (1990) The fossil record and estimating divergence times between lineages: Maximum divergence times and the importance of reliable phylogenies. *Journal of Molecular Evolution* **30**, 400–408.

MARSHALL, C.R. (2008) A Simple Method for Bracketing Absolute Divergence Times on Molecular Phylogenies Using Multiple Fossil Calibration Points. *The American Naturalist* **171**, 726–742.

MARSHALL, C.R. (2017) Five palaeobiological laws needed to understand the evolution of the living biota. *Nature Ecology & Evolution* **1**, 1–6.

MARSHALL, C.R. (2019) Using the Fossil Record to Evaluate Timetree Timescales. *Frontiers in Genetics* **10**, 1–20.

MARTINEZ, F.I., CAPELLI, C., FERREIRA DA SILVA, M.J., ALDEIAS, V., ALEMSEGED, Z., ARCHER, W., BAMFORD, M., BIRO, D., BOBE, R., BRAUN, D.R., HABERMANN, J.M., LÜDECKE, T., MADIQUIDA, H., MATHE, J., NEGASH, E., ET AL. (2019) A missing piece of the *Papio* puzzle: Gorongosa baboon phenostructure and intrageneric relationships. *Journal of Human Evolution* **130**, 1–20.

MARTÍNEZ, G.A., MARTÍNEZ, G., ALCARÁZ, A.P. & STOESSEL, L. (2019) Geoarchaeology and taphonomy: Deciphering site formation processes for late Holocene archaeological settings in the eastern Pampa-Patagonian transition, Argentina. *Quaternary International* **511**, 94–106.

MARTINI, P., COSTEUR, L., LE TENSORER, J.-M. & SCHMID, P. (2015) Pleistocene camelids from the Syrian Desert: The diversity in El Kowm. *L'Anthropologie* **119**, 687–693.

MASEK, J.G., WULDER, M.A., MARKHAM, B., MCCORKEL, J., CRAWFORD, C.J., STOREY, J. & JENSTROM, D.T. (2020) Landsat 9: Empowering open science and applications through continuity. *Remote Sensing of Environment* **248**, 111968.

MASLIN, M.A., BRIERLEY, C.M., MILNER, A.M., SHULTZ, S., TRAUTH, M.H. & WILSON, K.E. (2014) East African climate pulses and early human evolution. *Quaternary Science Reviews* **101**, 1–17.

MATSUDA, I., NAKABAYASHI, M., OTANI, Y., WAI, Y.S., TUUGA, A., WONG, A., BERNARD, H., WICH, S.A. & KUBO, T. (2019) Comparison of Plant Diversity and Phenology of Riverine and Mangrove Forests with Those of the Dryland Forest in Sabah, Borneo, Malaysia. In *Primates in Flooded Habitats: Ecology and Conservation* (eds A.A. BARNETT, I. MATSUDA & K. NOWAK), pp. 15–28. Cambridge University Press, Cambridge.

MBALUKA, J.K. & BROWN, F.H. (2016) Vegetation of the Koobi fora region northeast of Lake Turkana, Marsabit County, northern Kenya. *Journal of East African Natural History* **105**, 21–50.

MCBREARTY, S. & JABLONSKI, N.G. (2005) First fossil chimpanzee. *Nature* **437**, 105–108.

MCCOY, M.D. & LADEFOGED, T.N. (2009) New Developments in the Use of Spatial Technology in Archaeology. *Journal of Archaeological Research* **17**, 263–295.

MCDOUGALL, I. & FEIBEL, C.S. (2003) 2.3. Numerical Age Control for the Miocene-Pliocene Succession at Lothagam, a Hominoid-bearing Sequence in the Northern Kenya Rift. In *Lothagam: The Dawn of Humanity in Eastern Africa* (eds M. LEAKEY & J. HARRIS), pp. 43–64. Columbia University Press, New York Chichester, West Sussex.

MCELREATH, R. (2020) *Statistical Rethinking: A Bayesian course with examples in R and Stan*. CRC press, Boca Raton, FL.

MERCADER, J. & SILLÉN, P. (2012) Preliminary Archaeological Survey of Gorongosa National Park: The Cheringoma plateau. *Field Reports, Gorongosa National Park* **Unpublished**, 1–21.

MERCADER, J. & SILLÉN, P. (2013) Middle and Later Stone Age Sites from Sofala, Gorongosa (Central Mozambique). *Nyame akuma*, 3–13.

MEYER, M.R., JUNG, J.P., SPEAR, J.K., ARAIZA, I.FX., GALWAY-WITHAM, J. & WILLIAMS, S.A. (2023) Knuckle-walking in *Sahelanthropus*? Locomotor inferences from the ulnae of fossil hominins and other hominoids. *Journal of Human Evolution* **179**, 103355.

MILLER, G., MAGEE, J., SMITH, M., SPOONER, N., BAYNES, A., LEHMAN, S., FOGEL, M., JOHNSTON, H., WILLIAMS, D., CLARK, P., FLORIAN, C., HOLST, R. & DEVOGEL, S. (2016) Human predation contributed to the extinction of the Australian megafaunal bird *Genyornis newtoni* ~47 ka. *Nature Communications* **7**, 10496.

MOHAMED, E.S., ALI, A.M., EL SHIRBENY, M.A., ABD EL RAZEK, A.A. & SAVIN, I.YU. (2016) Near infrared spectroscopy techniques for soil contamination assessment in the Nile Delta. *Eurasian Soil Science* **49**, 632–639.

MOHAMED, E.S., SALEH, A.M., BELAL, A.B. & GAD, A. (2018) Application of near-infrared reflectance for quantitative assessment of soil properties. *The Egyptian Journal of Remote Sensing and Space Science* **21**, 1–14.

MOLINARO, A.M., SIMON, R. & PFEIFFER, R.M. (2005) Prediction error estimation: a comparison of resampling methods. *Bioinformatics* **21**, 3301–3307.

MONDEJAR, J.P. & TONGCO, A.F. (2019) Near infrared band of Landsat 8 as water index: a case study around Cordova and Lapu-Lapu City, Cebu, Philippines. *Sustainable Environment Research* **29**, 16.

MONGLE, C.S., STRAIT, D.S. & GRINE, F.E. (2019) Expanded character sampling underscores phylogenetic stability of *Ardipithecus ramidus* as a basal hominin. *Journal of Human Evolution* **131**, 28–39.

MONTAGNON, D. (2013) Strepsirhine Divergence Dates Estimated from Mitochondrial Gene Sequences, and the Status of *Daubentonia madagascariensis*. In *Leaping Ahead: Advances in Prosimian Biology* (eds J. MASTERS, M. GAMBA & F. GÉNIN), pp. 21–32. Springer, New York, NY.

MOORJANI, P., AMORIM, C.E.G., ARNDT, P.F. & PRZEWORSKI, M. (2016) Variation in the molecular clock of primates. *Proceedings of the National Academy of Sciences* **113**, 10607–10612.

MORLEY, R. & KINGDON, J. (2013) Africa's environmental and climatic past. *Mammals of Africa* **1**, 43–56.

MOYA, M.M., KOCH, M.W. & HOSTETLER, L.D. (1993) One-class classifier networks for target recognition applications. Sandia National Labs., Albuquerque, NM (United States).

MOYÀ-SOLÀ, S., KÖHLER, M. & ROOK, L. (2005) The *Oreopithecus* thumb: a strange case in hominoid evolution. *Journal of Human Evolution* **49**, 395–404.

NAVEGA, D., VICENTE, R., VIEIRA, D.N., ROSS, A.H. & CUNHA, E. (2015) Sex estimation from the tarsal bones in a Portuguese sample: a machine learning approach. *International Journal of Legal Medicine* **129**, 651–659.

NAWROT, R., SCARPONI, D., AZZARONE, M., DEXTER, T.A., KUSNERIK, K.M., WITTMER, J.M., AMOROSI, A. & KOWALEWSKI, M. (2018) Stratigraphic signatures of mass extinctions: ecological and sedimentary determinants. *Proceedings of the Royal Society B: Biological Sciences* **285**, 20181191.

NEGASH, E.W., ALEMSEGED, Z., BOBE, R., GRINE, F., SPONHEIMER, M. & WYNN, J.G. (2020) Dietary trends in herbivores from the Shungura Formation, southwestern Ethiopia. *Proceedings of the National Academy of Sciences* **117**, 21921–21927.

NEGASH, E.W., ALEMSEGED, Z., WYNN, J.G. & BEDASO, Z.K. (2015) Paleodietary reconstruction using stable isotopes and abundance analysis of bovids from the Shungura Formation of South Omo, Ethiopia. *Journal of Human Evolution* **88**, 127–136.

NEGASH, E.W. & BARR, W.A. (2023) Relative abundance of grazing and browsing herbivores is not a direct reflection of vegetation structure: Implications for hominin paleoenvironmental reconstruction. *Journal of Human Evolution* **177**, 1–11.

NIGRO, J.D., UNGAR, P.S., DE RUITER, D.J. & BERGER, L.R. (2003) Developing a Geographic Information System (GIS) for Mapping and Analysing Fossil Deposits at Swartkrans, Gauteng Province, South Africa. *Journal of Archaeological Science* **30**, 317–324.

NJAU, J.K. & HLUSKO, L.J. (2010) Fine-tuning paleoanthropological reconnaissance with high-resolution satellite imagery: the discovery of 28 new sites in Tanzania. *Journal of Human Evolution* **59**, 680–684.

NOWAK, K., BARNETT, A.A. & MATSUDA, I. (eds) (2019) *Primates in Flooded Habitats: Ecology and Conservation*, 1st. edition. Cambridge University Press, Cambridge.

NOWAK, K. & COLES, R. (2019) Worldwide Patterns in the Ecology of Mangrove-living Monkeys and Apes. In *Primates in Flooded Habitats: Ecology and Conservation* (eds A.A. BARNETT, I. MATSUDA & K. NOWAK), pp. 45–53. Cambridge University Press, Cambridge.

NUTZ, A., SCHUSTER, M., BARBONI, D., GASSIER, G., VAN BOCXLAER, B., ROBIN, C., RAGON, T., GHIENNE, J.-F. & RUBINO, J.-L. (2020) Plio-Pleistocene sedimentation in West Turkana (Turkana Depression, Kenya, East African Rift System): Paleolake fluctuations, paleolandscapes and controlling factors. *Earth-Science Reviews* **211**, 103415.

NUTZ, A., SCHUSTER, M., BOËS, X. & RUBINO, J.-L. (2017) Orbitally-driven evolution of Lake Turkana (Turkana Depression, Kenya, EARS) between 1.95 and 1.72 Ma: A sequence stratigraphy perspective. *Journal of African Earth Sciences* **125**, 230–243.

O'BRIEN, K., PATTERSON, D.B., BIERNAT, M.D., BRAUN, D.R., CERLING, T.E., MCGROSKY, A. & FAITH, J.T. (2020) Ungulate turnover in the Koobi Fora Formation: Spatial and temporal variation in the Early Pleistocene. *Journal of African Earth Sciences* **161**, 103658.

OHEIM, K.B. (2007) Fossil site prediction using geographic information systems (GIS) and suitability analysis: The Two Medicine Formation, MT, a test case. *Palaeogeography, Palaeoclimatology, Palaeoecology* **251**, 354–365.

OOSTRA, R.-J., GELDERMAN, T., GROEN, W.J.M., UITERDIJK, H.G., CAMMERAAT, E.L.H., KRAP, T., WILK, L.S., LÜSCHEN, M., MORRIËN, W.E., WOBBEN, F., DUIJST, W.L.J.M. & AALDERS, M.C.G. (2020) Amsterdam Research Initiative for Sub-surface Taphonomy and Anthropology (ARISTA) - A taphonomic research facility in the Netherlands for the study of human remains. *Forensic Science International* **317**, 110483.

OPENTOPOGRAPHY (2013) Shuttle Radar Topography Mission (SRTM) Global. OpenTopography.

OSINOWO, O.O., GOMY, A. & ISSEINI, M. (2021) Mapping hydrothermal alteration mineral deposits from Landsat 8 satellite data in Pala, Mayo Kebbi Region, Southwestern Chad. *Scientific African* **11**, e00687.

OWEN, R.B., POTTS, R., BEHRENSMEYER, A.K. & DITCHFIELD, P. (2008) Diatomaceous sediments and environmental change in the Pleistocene Olorgesailie Formation, southern Kenya Rift Valley. *Palaeogeography, Palaeoclimatology, Palaeoecology* **269**, 17–37.

OWEN, R.B., RENAUT, R.W., POTTS, R. & BEHRENSMEYER, A.K. (2011) Geochemical trends through time and lateral variability of diatom floras in the Pleistocene Olorgesailie Formation, southern Kenya Rift Valley. *Quaternary Research* **76**, 167–179.

OWEN, R.B., RENAUT, R.W., SCOTT, J.J., POTTS, R. & BEHRENSMEYER, A.K. (2009) Wetland sedimentation and associated diatoms in the Pleistocene Olorgesailie Basin, southern Kenya Rift Valley. *Sedimentary Geology* **222**, 124–137.

PAHLEVAN, N., LEE, Z., WEI, J., SCHAAF, C.B., SCHOTT, J.R. & BERK, A. (2014) On-orbit radiometric characterization of OLI (Landsat-8) for applications in aquatic remote sensing. *Remote Sensing of Environment* **154**, 272–284.

PAN, F., XI, X. & WANG, C. (2020) A Comparative Study of Water Indices and Image Classification Algorithms for Mapping Inland Surface Water Bodies Using Landsat Imagery. *Remote Sensing* **12**, 1611.

PARKER, W.G. & MARTZ, J.W. (2017) Building Local Biostratigraphic Models for the Upper Triassic of Western North America: Methods and Considerations. In *Terrestrial Depositional Systems: Deciphering Complexities through Multiple Stratigraphic Methods* (eds K.E. ZEIGLER & W.G. PARKER), pp. 39–125. Elsevier, Amsterdam.

PARKS, R., HARRINGTON, S.M. & THOMSON, R.C. (2022) Divergence Dating and Biogeography of Xenosauridae Including Fossils as Terminal Taxa. *Journal of Herpetology* **56**, 349–354.

PATTERSON, D.B., BRAUN, D.R., ALLEN, K., BARR, W.A., BEHRENSMEYER, A.K., BIERNAT, M., LEHMANN, S.B., MADDOX, T., MANTHI, F.K., MERRITT, S.R., MORRIS, S.E., O'BRIEN, K., REEVES, J.S., WOOD, B.A. & BOBE, R. (2019) Comparative isotopic evidence from East Turkana supports a dietary shift within the genus *Homo*. *Nature Ecology & Evolution* **3**, 1048–1056.

PATTERSON, D.B., BRAUN, D.R., BEHRENSMEYER, A.K., LEHMANN, S.B., MERRITT, S.R., REEVES, J.S., WOOD, B.A. & BOBE, R. (2017a) Landscape scale heterogeneity in the East Turkana ecosystem during the Okote Member (1.56–1.38 Ma). *Journal of Human Evolution* **112**, 148–161.

PATTERSON, D.B., BRAUN, D.R., BEHRENSMEYER, A.K., MERRITT, S., ZLIOBAITE, I., REEVES, J.S., WOOD, B.A., FORTELIUS, M. & BOBE, R. (2017b) Ecosystem evolution and hominin paleobiology at East Turkana, northern Kenya between 2.0 and 1.4 Ma. *Palaeogeography, Palaeoclimatology, Palaeoecology* **481**, 1–13.

PATTERSON, D.B., FAITH, J.T., BOBE, R. & WOOD, B. (2014) Regional diversity patterns in African bovids, hyaenids, and felids during the past 3 million years: the role of taphonomic bias and implications for the evolution of Paranthropus. *Quaternary Science Reviews* **96**, 9–22.

PERAKIS, K.G. & MOYSIADIS, A.K. (2011) Geospatial predictive modelling of the Neolithic archaeological sites of Magnesia in Greece. *International Journal of Digital Earth* **4**, 421–433.

PETRAGLIA, M.D., BREEZE, P.S. & GROUCUTT, H.S. (2019) Blue Arabia, Green Arabia: Examining Human Colonisation and Dispersal Models. In *Geological Setting,*

Palaeoenvironment and Archaeology of the Red Sea (eds N.M.A. RASUL & I.C.F. STEWART), pp. 675–683. Springer International Publishing, Cham.

PHILLIPS, S.J., ANDERSON, R.P., DUDÍK, M., SCHAPIRE, R.E. & BLAIR, M.E. (2017) Opening the black box: an open-source release of Maxent. *Ecography* **40**, 887–893.

PHILLIPS, S.J., ANDERSON, R.P. & SCHAPIRE, R.E. (2006) Maximum entropy modeling of species geographic distributions. *Ecological Modelling* **190**, 231–259.

PHILLIPS, S.J., DUDÍK, M., ELITH, J., GRAHAM, C.H., LEHMANN, A., LEATHWICK, J. & FERRIER, S. (2009) Sample selection bias and presence-only distribution models: implications for background and pseudo-absence data. *Ecological Applications: A Publication of the Ecological Society of America* **19**, 181–197.

PHILLIPS, S.J., DUDÍK, M. & SCHAPIRE, R.E. (2004) A maximum entropy approach to species distribution modeling. In *Proceedings of the twenty-first international conference on Machine learning* p. 83. Association for Computing Machinery, New York, NY, USA.

PICKFORD, M. (2005) Orientation of the Foramen Magnum in Late Miocene to Extant African Apes and Hominids. *Anthropologie (1962-)* **43**, 103–110. Moravian Museum.

PICKFORD, M. (2012) Mozambique Paleontology Reconnaissance - November 2012. In p. 22. Field Reports, Gorongosa National Park.

PICKFORD, M. (2013) Gorongosa Palaeontology Survey - November, 2013. In p. 13. Field Reports, Gorongosa National Park.

PICKFORD, M., COPPENS, Y., SENUT, B., MORALES, J. & BRAGA, J. (2009) Late Miocene hominoid from Niger. *Comptes Rendus Palevol* **8**, 413–425.

PICKFORD, M. & SENUT, B. (1997) Cainozoic mammals from coastal Namaqualand, South Africa. *Paleontologia Africana* **34**, 199–217.

PICKFORD, M. & SENUT, B. (2001) The geological and faunal context of Late Miocene hominid remains from Lukeino, Kenya. *Comptes Rendus de l'Académie des Sciences - Series IIA - Earth and Planetary Science* **332**, 145–152.

PICKFORD, M. & SENUT, B. (2005) Hominoid teeth with chimpanzee-and gorilla-like features from the Miocene of Kenya: implications for the chronology of ape-human divergence and biogeography of Miocene hominoids. *Anthropological Science* **113**, 95–102.

PICKFORD, M., SENUT, B., GOMMERY, D. & KIPKECH, J. (2022) New Pliocene hominid fossils from Baringo County, Kenya. *Fossil Imprint* **78**, 451–488.

PICKFORD, M., SENUT, B., MORALES, J. & BRAGA, J. (2008) First hominoid from the Late Miocene of Niger. *South African Journal of Science* **104**, 337–339.

PICKFORD, M., SENUT, B., SSEMMANDA, I., ELEPU, D. & OBWONA, P. (1988) Premiers resultats de la mission de l'Uganda palaeontology expedition a Nkondo (Pliocene du bassin du lac Albert, Ouganda). *Comptes rendus de l'Académie des sciences. Série 2, Mécanique, Physique, Chimie, Sciences de l'univers, Sciences de la Terre* **306**, 315–320.

PILBEAM, D. (1996) Genetic and Morphological Records of the Hominoidea and Hominid Origins: A Synthesis. *Molecular Phylogenetics and Evolution* **5**, 155–168.

PILBEAM, D.R. (1967) Man's earliest ancestors. *Science journal* **3**, 47–53.

PONTE, J.-P., ROBIN, C., GUILLOCHEAU, F., POPESCU, S., SUC, J.-P., DALL'ASTA, M., MELINTE-DOBRINESCU, M.C., BUBIK, M., DUPONT, G. & GAILLOT, J. (2019) The Zambezi delta (Mozambique channel, East Africa): High resolution dating combining bio- orbital and seismic stratigraphies to determine climate (palaeoprecipitation) and tectonic controls on a passive margin. *Marine and Petroleum Geology* **105**, 293–312.

PONTZER, H., BROWN, M.H., WOOD, B.M., RAICHLEN, D.A., MABULLA, A.Z.P., HARRIS, J.A., DUNSWORTH, H., HARE, B., WALKER, K., LUKE, A., DUGAS, L.R., SCHOELLER, D., PLANGE-RHULE, J., BOVET, P., FORRESTER, T.E., ET AL. (2021) Evolution of water conservation in humans. *Current Biology* **31**, 1804-1810.e5.

POUR, A.B. & HASHIM, M. (2015) Hydrothermal alteration mapping from Landsat-8 data, Sar Cheshmeh copper mining district, south-eastern Islamic Republic of Iran. *Journal of Taibah University for Science* **9**, 155–166.

POWERS, D. (2011) Evaluation: From precision, recall and f-measure to ROC, informedness, markedness & correlation. *Journal of Machine Learning Technologies* **2**, 37–63.

PUGH, K.D. (2022) Phylogenetic analysis of Middle-Late Miocene apes. *Journal of Human Evolution* **165**, 103140.

PÜSCHEL, H.P., BERTRAND, O.C., O'REILLY, J.E., BOBE, R. & PÜSCHEL, T.A. (2021) Divergence-time estimates for hominins provide insight into encephalization and body mass trends in human evolution. *Nature Ecology & Evolution* **5**, 808–819.

QUINN, R.L. (2015) Influence of Plio-Pleistocene basin hydrology on the Turkana hominin enamel carbonate δ 18 O values. *Journal of Human Evolution* **86**, 13–31.

QUINN, R.L., LEPRE, C.J., FEIBEL, C.S., WRIGHT, J.D., MORTLOCK, R.A., HARMAND, S., BRUGAL, J.-P. & ROCHE, H. (2013) Pedogenic carbonate stable isotopic evidence for wooded habitat preference of early Pleistocene tool makers in the Turkana Basin. *Journal of Human Evolution* **65**, 65–78.

QUINN, R.L., LEPRE, C.J., WRIGHT, J.D. & FEIBEL, C.S. (2007) Paleogeographic variations of pedogenic carbonate δ13C values from Koobi Fora, Kenya: implications for floral compositions of Plio-Pleistocene hominin environments. *Journal of Human Evolution* **53**, 560–573.

R CORE TEAM (2023) *R: A Language and Environment for Statistical Computing*. R Foundation for Statistical Computing, Vienna, Austria.

RAMPINO, M.R. & ADLER, A.C. (1998) Evidence for abrupt latest Permian mass extinction of foraminifera: Results of tests for the Signor-Lipps effect. *Geology* **26**, 415.

RAVELO, A.C., ANDREASEN, D.H., LYLE, M., OLIVAREZ LYLE, A. & WARA, M.W. (2004) Regional climate shifts caused by gradual global cooling in the Pliocene epoch. *Nature* **429**, 263–267.

RAYFIELD, E.J., BARRETT, P.M., MCDONNELL, R.A. & WILLIS, K.J. (2005) A Geographical Information System (GIS) study of Triassic vertebrate biochronology. *Geological Magazine* **142**, 327–354.

REAL, F. (1966) *Geologia da bacia do rio Zambeze (Moçambique): características geológico-mineiras da bacia do rio Zambeze, em território Moçambicano.* Junta de Investigações do Ultramar, Lisboa, Portugal.

REED, D., BARR, W.A., MCPHERRON, S.P., BOBE, R., GERAADS, D., WYNN, J.G. & ALEMSEGED, Z. (2015) Digital data collection in paleoanthropology. *Evolutionary Anthropology: Issues, News, and Reviews* **24**, 238–249.

REED, D.N., BARR, W.A. & KAPPELMAN, J. (2018) PaleoCore: An Open-Source Platform for Geospatial Data Integration in Paleoanthropology. In *New Geospatial Approaches to the Anthropological Sciences* (eds R.L. ANEMONE & G.C. CONROY), pp. 211–224. New Mexico Press, Albuquerque, NM.

REED, K.E. (1997) Early hominid evolution and ecological change through the African Plio-Pleistocene. *Journal of Human Evolution* **32**, 289–322.

REGALA, F.T., PINTO, M.J. & PAULO, L.M. (2023) Speleology Field Report 2022. *Paleo-Primate Project Gorongosa – 2022 Field Reports* **Unpublished**, 1–68.

REGALA, F.T., PINTO, M.J., PAULO, L.M., BOBE, R., ALDEIAS, V., BRAUN, D.R., MATHE, J., MACAMO, S., BAMFORD, M., STALMANS, M. & CARVALHO, S. (2022) The caves of Gorongosa National Park, Mozambique. In *Explorations & History: Proceedings of the 18th International Congress of Speleology* pp. 165–168. Association française de karstologie, Savoie Mont Blanc, Nîmes.

REID, I. & FROSTICK, L., E. (1985) Arid Zone Slopes and their Archaeological Materials. In *Themes in Geomorphology* (ed A. PITTY), pp. 141–157. Routledge, London.

REID, I. & FROSTICK, L.E. (1986) Slope processes, sediment derivation and landform evolution in a rift valley basin, northern Kenya. *Geological Society, London, Special Publications* **25**, 99–111.

DOS REIS, M., DONOGHUE, P.C.J. & YANG, Z. (2016) Bayesian molecular clock dating of species divergences in the genomics era. *Nature Reviews Genetics* **17**, 71–80.

DOS REIS, M., GUNNELL, G.F., BARBA-MONTOYA, J., WILKINS, A., YANG, Z. & YODER, A.D. (2018) Using Phylogenomic Data to Explore the Effects of Relaxed Clocks and Calibration Strategies on Divergence Time Estimation: Primates as a Test Case. *Systematic Biology* **67**, 594–615.

DOS REIS, M., INOUE, J., HASEGAWA, M., ASHER, R.J., DONOGHUE, P.C.J. & YANG, Z. (2012) Phylogenomic datasets provide both precision and accuracy in estimating the timescale of placental mammal phylogeny. *Proceedings of the Royal Society B: Biological Sciences* **279**, 3491–3500.

DOS REIS, M. & YANG, Z. (2019) Bayesian Molecular Clock Dating Using Genome-Scale Datasets. In *Evolutionary Genomics: Statistical and Computational Methods* (ed M. ANISIMOVA), pp. 309–330. Springer, New York, NY.

RENAUT, R.W. & OWEN, R.B. (2023) The Turkana Basin. In *The Kenya Rift Lakes: Modern and Ancient: Limnology and Limnogeology of Tropical Lakes in a Continental Rift* (eds R.W. RENAUT & R.B. OWEN), pp. 631–691. Springer, Berlin, Heidelberg.

RENNE, P.R., WOLDEGABRIEL, G., HART, W.K., HEIKEN, G. & WHITE, T.D. (1999) Chronostratigraphy of the Miocene–Pliocene Sagantole Formation, Middle Awash Valley, Afar rift, Ethiopia. *GSA Bulletin* **111**, 869–885.

REYNAUD SAVIOZ, N. & MOREL, P. (2005) La faune de Nadaouiyeh Aïn Askar (Syrie centrale, Pléistocène moyen): aperçu et perspectives. *Revue de Paléobiologie* **10**, 31–35.

RICKARDS, R.B. & WRIGHT, A.J. (2002) Lazarus taxa, refugia and relict faunas: evidence from graptolites. *Journal of the Geological Society* **159**, 1–4.

RIGHTMIRE, G.P., MARGVELASHVILI, A. & LORDKIPANIDZE, D. (2019) Variation among the Dmanisi hominins: Multiple taxa or one species? *American Journal of Physical Anthropology* **168**, 481–495.

RITTER, P. (1987) A vector-based slope and aspect generation algorithm. *Photogrammetric Engineering and Remote Sensing* **53**, 1109–1111.

RIVAS-GONZÁLEZ, I., ROUSSELLE, M., LI, F., ZHOU, L., DUTHEIL, J.Y., MUNCH, K., SHAO, Y., WU, D., SCHIERUP, M.H. & ZHANG, G. (2023) Pervasive incomplete lineage sorting illuminates speciation and selection in primates. *Science* **380**, eabn4409.

ROACH, N.T., HATALA, K.G., OSTROFSKY, K.R., VILLMOARE, B., REEVES, J.S., DU, A., BRAUN, D.R., HARRIS, J.W.K., BEHRENSMEYER, A.K. & RICHMOND, B.G. (2016) Pleistocene footprints show intensive use of lake margin habitats by *Homo erectus* groups. *Scientific Reports* **6**, 26374.

ROBERTS, D.R., BAHN, V., CIUTI, S., BOYCE, M.S., ELITH, J., GUILLERA-ARROITA, G., HAUENSTEIN, S., LAHOZ-MONFORT, J.J., SCHRÖDER, B., THUILLER, W., WARTON, D.I., WINTLE, B.A., HARTIG, F. & DORMANN, C.F. (2017) Cross-validation strategies for data with temporal, spatial, hierarchical, or phylogenetic structure. *Ecography* **40**, 913–929.

ROBINSON, J.T. (1963) Adaptive Radiation in The Australopithecines and The Origin of Man. In *African Ecology and Human Evolution* (eds F.C. HOWELL & F. BOURLIÈRE), pp. 385–416. Routledge, London.

ROCHE, D., SÉGALEN, L., SENUT, B. & PICKFORD, M. (2013) Stable isotope analyses of tooth enamel carbonate of large herbivores from the Tugen Hills deposits: Palaeoenvironmental context of the earliest Kenyan hominids. *Earth and Planetary Science Letters* **381**, 39–51.

RODE, A.L. & LIEBERMAN, B.S. (2004) Using GIS to unlock the interactions between biogeography, environment, and evolution in Middle and Late Devonian brachiopods and bivalves. *Palaeogeography, Palaeoclimatology, Palaeoecology* **211**, 345–359.

RODE, A.L. & LIEBERMAN, B.S. (2005) Integrating evolution and biogeography: a case study involving Devonian Crustaceans. *Journal of Paleontology* **79**, 267–276.

ROMERO, A., GATTA, C. & CAMPS-VALLS, G. (2016) Unsupervised Deep Feature Extraction for Remote Sensing Image Classification. *IEEE Transactions on Geoscience and Remote Sensing* **54**, 1349–1362.

ROMERO-HERRERA, A.E., LEHMANN, H., JOYSEY, K.A. & FRIDAY, A.E. (1973) Molecular Evolution of Myoglobin and the Fossil Record: a Phylogenetic Synthesis. *Nature* **246**, 389–395.

RONQUIST, F., KLOPFSTEIN, S., VILHELMSEN, L., SCHULMEISTER, S., MURRAY, D.L. & RASNITSYN, A.P. (2012) A Total-Evidence Approach to Dating with Fossils, Applied to the Early Radiation of the Hymenoptera. *Systematic Biology* **61**, 973–999.

ROOK, L., BONDIOLI, L., KÖHLER, M., MOYÀ-SOLÀ, S. & MACCHIARELLI, R. (1999) *Oreopithecus* was a bipedal ape after all: Evidence from the iliac cancellous architecture. *Proceedings of the National Academy of Sciences* **96**, 8795–8799.

ROSENBLOOM, N.A., DONEY, S.C. & SCHIMEL, D.S. (2001) Geomorphic evolution of soil texture and organic matter in eroding landscapes. *Global Biogeochemical Cycles* **15**, 365–381.

RÖVER, C. (2020) Bayesian Random-Effects Meta-Analysis Using the **bayesmeta** *R* Package. *Journal of Statistical Software* **93**, 1–51.

RÖVER, C., BENDER, R., DIAS, S., SCHMID, C.H., SCHMIDLI, H., STURTZ, S., WEBER, S. & FRIEDE, T. (2021) On weakly informative prior distributions for the heterogeneity parameter in Bayesian random-effects meta-analysis. *Research Synthesis Methods* **12**, 448–474.

ROWAN, J. & REED, K.E. (2015) The Paleoclimatic Record and Plio-Pleistocene Paleoenvironments. In *Handbook of Paleoanthropology* (eds W. HENKE & I. TATTERSALL), pp. 465–491. Springer Berlin Heidelberg, Berlin, Heidelberg.

ROY, D.P., WULDER, M.A., LOVELAND, T.R., C.E., W., ALLEN, R.G., ANDERSON, M.C., HELDER, D., IRONS, J.R., JOHNSON, D.M., KENNEDY, R., SCAMBOS, T.A., SCHAAF, C.B., SCHOTT, J.R., SHENG, Y., VERMOTE, E.F., ET AL. (2014) Landsat-8: Science and product vision for terrestrial global change research. *Remote Sensing of Environment* **145**, 154–172.

RUSSO, G.A. & SHAPIRO, L.J. (2013) Reevaluation of the lumbosacral region of *Oreopithecus bambolii*. *Journal of Human Evolution* **65**, 253–265.

RUSSON, A.E., COMPOST, A., KUNCORO, P. & FERISA, A. (2014) Orangutan fish eating, primate aquatic fauna eating, and their implications for the origins of ancestral hominin fish eating. *Journal of Human Evolution* **77**, 50–63.

RUVOLO, M. (1997) Molecular phylogeny of the hominoids: inferences from multiple independent DNA sequence data sets. *Molecular Biology and Evolution* **14**, 248–265.

SALADIN, B., LESLIE, A.B., WÜEST, R.O., LITSIOS, G., CONTI, E., SALAMIN, N. & ZIMMERMANN, N.E. (2017) Fossils matter: improved estimates of divergence times in *Pinus* reveal older diversification. *BMC Evolutionary Biology* **17**, 95.

SALEH, A.M., BELAL, A.B. & ARAFAT, S.M. (2013) Identification and mapping of some soil types using field spectrometry and spectral mixture analyses: a case study of North Sinai, Egypt. *Arabian Journal of Geosciences* **6**, 1799–1806.

SANCHEZ GOÑI, M.F. (2024) Pollen: A Key Tool for Understanding Climate, Vegetation, and Human Evolution. In *Progress in Botany Vol. 84* (eds U. LÜTTGE, F.M. CÁNOVAS, M.-C. RISUEÑO, C. LEUSCHNER & H. PRETZSCH), pp. 395–434. Springer Nature Switzerland, Cham.

SARICH, V.M. (1971) A molecular approach to the question of human origins. In *Background for Man: Readings in Physical Anthropology* (eds P. DOHLINOW & V.M. SARICH), pp. 60–81. Little Brown, Boston.

SARICH, V.M. & WILSON, A.C. (1967) Immunological time scale for hominid evolution. *Science* **158**, 1200–1203.

SAWADA, Y., PICKFORD, M., SENUT, B., ITAYA, T., HYODO, M., MIURA, T., KASHINE, C., CHUJO, T. & FUJII, H. (2002) The age of *Orrorin tugenensis*, an early hominid from the Tugen Hills, Kenya. *Comptes Rendus Palevol* **1**, 293–303.

SCERRI, E.M.L., THOMAS, M.G., MANICA, A., GUNZ, P., STOCK, J.T., STRINGER, C., GROVE, M., GROUCUTT, H.S., TIMMERMANN, A., RIGHTMIRE, G.P., D'ERRICO, F., TRYON, C.A., DRAKE, N.A., BROOKS, A.S., DENNELL, R.W., ET AL. (2018) Did Our Species Evolve in Subdivided Populations across Africa, and Why Does It Matter? *Trends in Ecology & Evolution* **33**, 582–594.

SCHEFUß, E. & DUPONT, L.M. (2020) Multiple drivers of Miocene C4 ecosystem expansions. *Nature Geoscience* **13**, 463–464.

SCHOENINGER, M.J., REESER, H. & HALLIN, K. (2003) Paleoenvironment of *Australopithecus anamensis* at Allia Bay, East Turkana, Kenya: evidence from mammalian herbivore enamel stable isotopes. *Journal of Anthropological Archaeology* **22**, 200–207.

SCHRAGO, C.G. & VOLOCH, C.M. (2013) The precision of the hominid timescale estimated by relaxed clock methods. *Journal of Evolutionary Biology* **26**, 746–755.

SCHUBERT, E., SANDER, J., ESTER, M., KRIEGEL, H.P. & XU, X. (2017) DBSCAN Revisited, Revisited: Why and How You Should (Still) Use DBSCAN. *ACM Transactions on Database Systems* **42**, 1–21.

SCHULTE II, J.A. (2013) Undersampling Taxa Will Underestimate Molecular Divergence Dates: An Example from the South American Lizard Clade Liolaemini. *International Journal of Evolutionary Biology* **2013**, 1–12.

SCOTESE, C.R. (2021) An Atlas of Phanerozoic Paleogeographic Maps: The Seas Come In and the Seas Go Out. *Annual Review of Earth and Planetary Sciences* **49**, 679–728.

SCOTT, R.S., UNGAR, P.S., BERGSTROM, T.S., BROWN, C.A., GRINE, F.E., TEAFORD, M.F. & WALKER, A. (2005) Dental microwear texture analysis shows within-species diet variability in fossil hominins. *Nature* **436**, 693–695.

SELIYA, N., ABDOLLAH ZADEH, A. & KHOSHGOFTAAR, T.M. (2021) A literature review on one-class classification and its potential applications in big data. *Journal of Big Data* **8**, 122.

SENUT, B. (2010) Upper Miocene hominoid distribution and the origin of hominids revisited. *Historical Biology* **22**, 260–267.

SENUT, B. (2015) The Miocene Hominoids and the Earliest Putative Hominids. In *Handbook of Paleoanthropology* (eds W. HENKE & I. TATTERSALL), pp. 2043–2069. Springer, Berlin, Heidelberg.

SENUT, B. & PICKFORD, M. (2001) 'Millennium Ancestor', a 6-million-year-old bipedal hominid from Kenya. *South African Journal of Science* **97**, 22.

SENUT, B. & PICKFORD, M. (2004) La dichotomie grands singes–homme revisitée. *Comptes Rendus Palevol* **3**, 265–276.

SENUT, B., PICKFORD, M. & GOMMERY, D. (2018a) Dental anatomy of the early hominid, *Orrorin tugenensis*, from the Lukeino Formation, Tugen Hills, Kenya. *Revue de Paléobiologie* **37**, 577–591.

SENUT, B., PICKFORD, M., GOMMERY, D., MEIN, P., CHEBOI, K. & COPPENS, Y. (2001) First hominid from the Miocene (Lukeino Formation, Kenya). *Comptes Rendus de l'Académie des Sciences - Series IIA - Earth and Planetary Science* **332**, 137–144.

SENUT, B., PICKFORD, M., GOMMERY, D. & SÉGALEN, L. (2018b) Palaeoenvironments and the origin of hominid bipedalism. *Historical Biology* **30**, 284–296.

SHANNO, D.F. (1970) Conditioning of quasi-Newton methods for function minimization. *Mathematics of Computation* **24**, 647–656.

SHAO, Y., ZHOU, L., LI, F., ZHAO, L., ZHANG, B.-L., SHAO, F., CHEN, J.-W., CHEN, C.-Y., BI, X., ZHUANG, X.-L., ZHU, H.-L., HU, J., SUN, Z., LI, X., WANG, D., ET AL. (2023) Phylogenomic analyses provide insights into primate evolution. *Science* **380**, 913–924.

SIGNOR, P.W. & LIPPS, J.H. (1982) Sampling bias, gradual extinction patterns, and catastrophes in the fossil record. *Geological implications of impacts of large asteroids and comets on the Earth* **190**, 291–296.

SILVA, E.B., TEN CATEN, A., DALMOLIN, R.S.D., DOTTO, A.C., SILVA, W.C. & GIASSON, E. (2016) Estimating Soil Texture from a Limited Region of the Visible/Near-Infrared Spectrum. In *Digital Soil Morphometrics* (eds A.E. HARTEMINK & B. MINASNY), pp. 73–87. Springer International Publishing, Cham.

SIMAS, A.B., BARRETO-SOUZA, W. & ROCHA, A.V. (2010) Improved estimators for a general class of beta regression models. *Computational Statistics & Data Analysis* **54**, 348–366.

SIMPSON, G.G. (1959) The Nature and Origin of Supraspecific Taxa. *Cold Spring Harbor Symposia on Quantitative Biology* **24**, 255–271.

SIMPSON, S.W., KLEINSASSER, L., QUADE, J., LEVIN, N.E., MCINTOSH, W.C., DUNBAR, N., SEMAW, S. & ROGERS, M.J. (2015) Late Miocene hominin teeth from the Gona

Paleoanthropological Research Project area, Afar, Ethiopia. *Journal of Human Evolution* **81**, 68–82.

SIMPSON, S.W., LEVIN, N.E., QUADE, J., ROGERS, M.J. & SEMAW, S. (2019) *Ardipithecus ramidus* postcrania from the Gona Project area, Afar Regional State, Ethiopia. *Journal of Human Evolution* **129**, 1–45.

SMITH, J.L.B. (1939) A Living Fish of Mesozoic Type. *Nature* **143**, 455–456.

SMITH, J.L.B. (1940) A living coelacanthid fish from South Africa. *Transactions of the Royal Society of South Africa* **28**, 1–106.

SMITH, J.L.B. (1953) The Second Cœlacanth. *Nature* **171**, 99–101.

SMITH, R.J. (2005) Species Recognition in Paleoanthropology: Implications of Small Sample Sizes. In *Interpreting the Past* (eds D. LIEBERMAN, R.W. SMITH & J. KELLEY), pp. 207–219. Brill Academic Publishers, Boston, MA.

SPONHEIMER, M., ALEMSEGED, Z., CERLING, T.E., GRINE, F.E., KIMBEL, W.H., LEAKEY, M.G., LEE-THORP, J.A., MANTHI, F.K., REED, K.E., WOOD, B.A. & WYNN, J.G. (2013) Isotopic evidence of early hominin diets. *Proceedings of the National Academy of Sciences* **110**, 10513–10518.

SPONHEIMER, M., LOUDON, J.E. & HOWELLS, M.E. (2019) Fossil Primates from Flooded Habitats: The Antiquity of an Association. In *Primates in Flooded Habitats: Ecology and Conservation* (eds A.A. BARNETT, I. MATSUDA & K. NOWAK), pp. 10–14. Cambridge University Press, Cambridge.

STALMANS, M.E., MASSAD, T.J., PEEL, M.J.S., TARNITA, C.E. & PRINGLE, R.M. (2019) War-induced collapse and asymmetric recovery of large-mammal populations in Gorongosa National Park, Mozambique. *PLOS ONE* **14**, e0212864.

STEINBRUCH, F. (2010) Geology and geomorphology of the Urema Graben with emphasis on the evolution of Lake Urema. *Journal of African Earth Sciences* **58**, 272–284.

STEINHAUS, H. (1956) Sur la division des corp materiels en parties. *Bulletin de l'Académie Polonaise des Sciences* **C1. III vol IV**, 801–804.

STEINTHORSDOTTIR, M., COXALL, H.K., DE BOER, A.M., HUBER, M., BARBOLINI, N., BRADSHAW, C.D., BURLS, N.J., FEAKINS, S.J., GASSON, E., HENDERIKS, J., HOLBOURN, A.E., KIEL, S., KOHN, M.J., KNORR, G., KÜRSCHNER, W.M., ET AL. (2021) The Miocene: The Future of the Past. *Paleoceanography and Paleoclimatology* **36**, e2020PA004037.

STEIPER, M.E. & SEIFFERT, E.R. (2012) Evidence for a convergent slowdown in primate molecular rates and its implications for the timing of early primate evolution. *Proceedings of the National Academy of Sciences* **109**, 6006–6011.

STEIPER, M.E. & YOUNG, N.M. (2006) Primate molecular divergence dates. *Molecular Phylogenetics and Evolution* **41**, 384–394.

STEIPER, M.E., YOUNG, N.M. & SUKARNA, T.Y. (2004) Genomic data support the hominoid slowdown and an Early Oligocene estimate for the hominoid–cercopithecoid

divergence. *Proceedings of the National Academy of Sciences of the United States of America* **101**, 17021–17026.

STETLER, L. (2018) Impacts of Material Engineering Properties on Slope Wash and Stability in Fine-Grained Bedrock Slopes at Fossil-Bearing Sites, Badlands National Park, South Dakota, USA. *Geosciences* **8**, 267.

STEWART, K.M. (1994) Early hominid utilisation of fish resources and implications for seasonality and behaviour. *Journal of Human Evolution* **27**, 229–245.

STEWART, K.M. (2010) The Case for Exploitation of Wetlands Environments and Foods by Pre-Sapiens Hominins. In *Human Brain Evolution: the influence of freshwater and marine food resources* (eds S.C. CUNNANE & K.M. STEWART), pp. 137–171, 1st. edition. John Wiley & Sons, Inc., Hoboken, NJ, USA.

STEWART, K.M. (2014) Environmental change and hominin exploitation of C4-based resources in wetland/savanna mosaics. *Journal of Human Evolution* **77**, 1–16.

STIGALL, A.L. & LIEBERMAN, B.S. (2006) Quantitative palaeobiogeography: GIS, phylogenetic biogeographical analysis, and conservation insights. *Journal of Biogeography* **33**, 2051–2060.

STIGALL-RODE, A.L. (2005) The Application of Geographic Information Systems to Paleobiogeography: Implications for the Study of Invasions and Mass Extinctions. *The Paleontological Society Papers* **11**, 77–88.

STONE, M. (1974) Cross-Validatory Choice and Assessment of Statistical Predictions. *Journal of the Royal Statistical Society: Series B (Methodological)* **36**, 111–133.

STRINGER, C.B., FINLAYSON, J.C., BARTON, R.N.E., FERNÁNDEZ-JALVO, Y., CÁCERES, I., SABIN, R.C., RHODES, E.J., CURRANT, A.P., RODRÍGUEZ-VIDAL, J., GILES-PACHECO, F. & RIQUELME-CANTAL, J.A. (2008) Neanderthal exploitation of marine mammals in Gibraltar. *Proceedings of the National Academy of Sciences* **105**, 14319–14324.

STRINGER, W.J. & COOK, J.P. (1974) Feasibility study for locating archaeological village sites by satellite remote sensing techniques. Contract: NAS5-21833. Task 110-N, National Aeronautics and Space Administration.

SU, D. & HARRISON, T. (2008) Ecological implications of the relative rarity of fossil hominins at Laetoli. *Journal of Human Evolution* **55**, 672–681.

SU, D.F., AMBROSE, S.H., DEGUSTA, D. & HAILE-SELASSIE, Y. (2009) 17. Paleoenvironment. In Ardipithecus kadabba*: late Miocene evidence from the Middle Awash, Ethiopia* (eds Y. HAILE-SELASSIE & G. WOLDEGABRIEL), pp. 521–548. University of California Press, Berkeley.

SURECH, G.J., SREENIVAS, K. & SIVASAMY, R. (2014) Hyperspectral analysis of clay minerals. *ISPRS - International Archives of the Photogrammetry, Remote Sensing and Spatial Information Sciences* **XL–8**, 443–446.

SUSMAN, R.L. (2004) *Oreopithecus bambolii*: an unlikely case of hominid-like grip capability in a Miocene ape. *Journal of Human Evolution* **46**, 105–117.

SUWA, G., ASFAW, B., KONO, R.T., KUBO, D., LOVEJOY, C.O. & WHITE, T.D. (2009) The *Ardipithecus ramidus* Skull and Its Implications for Hominid Origins. *Science* **326**, 68-68e7.

SUWA, G., KONO, R.T., KATOH, S., ASFAW, B. & BEYENE, Y. (2007) A new species of great ape from the late Miocene epoch in Ethiopia. *Nature* **448**, 921–924.

SYAM'ANI (2020) Radiometric Enhancement of Landsat 8 OLI Imagery Using Coastal/Aerosol Band. In *2020 IEEE Asia-Pacific Conference on Geoscience, Electronics and Remote Sensing Technology (AGERS)* pp. 148–157.

SZYMANSKI, R.M. (2018) Middle Holocene Environmental Change at Mtwapa Creek, Kenya: Distinguishing Human Activity from Regional Ecological Processes. In *Plants and People in the African Past* (eds A.M. MERCURI, A.C. D'ANDREA, R. FORNACIARI & A. HÖHN), pp. 194–214. Springer International Publishing, Cham.

TAKENAKA, M., HAYASHI, K., YAMADA, G., OGURA, T., ITO, M., MILNER, A.M. & TOJO, K. (2022) Behavior of snow monkeys hunting fish to survive winter. *Scientific Reports* **12**, 20324.

TALUKDAR, S., SINGHA, P., MAHATO, S., SHAHFAHAD, PAL, S., LIOU, Y.-A. & RAHMAN, A. (2020) Land-Use Land-Cover Classification by Machine Learning Classifiers for Satellite Observations—A Review. *Remote Sensing* **12**, 1135.

TAPPEN, M., BUKHSIANIDZE, M., FERRING, R., COIL, R. & LORDKIPANIDZE, D. (2022) Life and death at Dmanisi, Georgia: Taphonomic signals from the fossil mammals. *Journal of Human Evolution* **171**, 103249.

TAVARÉ, S., MARSHALL, C.R., WILL, O., SOLIGO, C. & MARTIN, R.D. (2002) Using the fossil record to estimate the age of the last common ancestor of extant primates. *Nature* **416**, 726–729.

TAX, D.M.J. (2001) One-class classification: Concept-learning in the absence of counterexamples. Ph.D. Dissertation, Delft University of Technology, Delft, Netherlands.

TAX, D.M.J. & DUIN, R.P. (2001) Uniform object generation for optimizing one-class classifiers. *Journal of Machine Learning Research* **2**, 155–173.

THORPE, S.K.S., HOLDER, R.L. & CROMPTON, R.H. (2007) Origin of human bipedalism as an adaptation for locomotion on flexible branches. *Science* **316**, 1328–1331.

THORPE, S.K.S., MCCLYMONT, J.M. & CROMPTON, R.H. (2014) The arboreal origins of human bipedalism. *Antiquity* **88**, 906–914.

TINLEY, K.L. (1977) Framework of Gorongosa Ecosystem. Unpublished DSc thesis, University of Pretoria, South Africa.

TINLEY, K.L. (2020) *Montane to mangrove: framework of the Gorongosa ecosystem, Mozambique*. PhD thesis (1977) re-edition. Hamilton-Fynch, Nelspruit.

TOLJAGIĆ, O., VOJE, K.L., MATSCHINER, M., LIOW, L.H. & HANSEN, T.F. (2018) Millions of Years Behind: Slow Adaptation of Ruminants to Grasslands. *Systematic Biology* **67**, 145–157.

TORIÑO, P., SOTO, M. & PEREA, D. (2021) A comprehensive phylogenetic analysis of coelacanth fishes (Sarcopterygii, Actinistia) with comments on the composition of the Mawsoniidae and Latimeriidae: evaluating old and new methodological challenges and constraints. *Historical Biology* **33**, 3423–3443.

TRAUTH, M.H., LARRASOAÑA, J.C. & MUDELSEE, M. (2009) Trends, rhythms and events in Plio-Pleistocene African climate. *Quaternary Science Reviews* **28**, 399–411.

TRAUTH, M.H., MASLIN, M.A., DEINO, A. & STRECKER, M.R. (2005) Late Cenozoic moisture history of East Africa. *Science* **309**, 2051–2053.

TRAUTH, M.H., MASLIN, M.A., DEINO, A.L., STRECKER, M.R., BERGNER, A.G.N. & DÜHNFORTH, M. (2007) High- and low-latitude forcing of Plio-Pleistocene East African climate and human evolution. *Journal of Human Evolution* **53**, 475–486.

TUCKER, C.J. (1979) Red and photographic infrared linear combinations for monitoring vegetation. *Remote sensing of Environment* **8**, 127–150.

UNGAR, P. (2004) Dental topography and diets of *Australopithecus afarensis* and early *Homo*. *Journal of Human Evolution* **46**, 605–622.

URCIUOLI, A. & ALBA, D.M. (2023) Systematics of Miocene apes: State of the art of a neverending controversy. *Journal of Human Evolution* **175**, 103309.

VAN BOCXLAER, B. (2011) Palaeobiology and evolution of the late Cenozoic freshwater molluscs of the Turkana Basin: Unionidae Rafinesque, 1820, *partim Coelatura* (Bivalvia: Unionoidea). *Journal of Systematic Palaeontology* **9**, 523–550.

VARELA, S., LOBO, J.M. & HORTAL, J. (2011) Using species distribution models in paleobiogeography: A matter of data, predictors and concepts. *Palaeogeography, Palaeoclimatology, Palaeoecology* **310**, 451–463.

VELIČKOVIĆ, T., SNOJ, A., SIMIĆ, V., ŠANDA, R., VUKIĆ, J., BARCYTĖ, D., STANKOVIĆ, D. & MARIĆ, S. (2023) A new perspective on the molecular dating of the brown trout complex with an extended phylogeographic information on the species in Serbia. *Contributions to Zoology*, 1–28.

VENN, O., TURNER, I., MATHIESON, I., DE GROOT, N., BONTROP, R. & MCVEAN, G. (2014) Strong male bias drives germline mutation in chimpanzees. *Science* **344**, 1272–1275.

VERHAGEN, P., NUNINGER, L., BERTONCELLO, F., TOURNEUX, F.-P. & JENESON, K. (2012) Introducing the human factor in predictive modelling: a work in progress. In *CAA2012 Proceedings of the 40th Conference in Computer Applications and Quantitative Methods in Archaeology, Southampton, United Kingdom, 26-30 March 2012* pp. 379–388. Pallas Publication, Amsterdam.

VERMILLION, W., POLLY, P.D., HEAD, J., ERONEN, J. & LAWING, A.M. (2018) Ecometrics: A trait-based approach to paleoclimate and paleoenvironmental reconstruction. In

Methods in Paleoecology: Reconstructing Cenozoic Terrestrial Environments and Ecological Communities (eds D.A. CROFT, D.F. SU & S.W. SIMPSON), pp. 373–394. Springer, Cham, Switzerland.

VIGLIETTI, P.A., SMITH, R.M.H., ANGIELCZYK, K.D., KAMMERER, C.F., FRÖBISCH, J. & RUBIDGE, B.S. (2016) The Daptocephalus Assemblage Zone (Lopingian), South Africa: A proposed biostratigraphy based on a new compilation of stratigraphic ranges. *Journal of African Earth Sciences* **113**, 153–164.

VIGNAUD, P., DURINGER, P., MACKAYE, H.T., LIKIUS, A., BLONDEL, C., BOISSERIE, J.-R., BONIS, L. DE, EISENMANN, V., ETIENNE, M.-E., GERAADS, D., GUY, F., LEHMANN, T., LIHOREAU, F., LOPEZ-MARTINEZ, N., MOURER-CHAUVIRÉ, C., ET AL. (2002) Geology and palaeontology of the Upper Miocene Toros-Menalla hominid locality, Chad. *Nature* **418**, 152–155.

VILLASEÑOR, A., BOBE, R. & BEHRENSMEYER, A.K. (2020) Middle Pliocene hominin distribution patterns in Eastern Africa. *Journal of Human Evolution* **147**, 102856.

VILLASEÑOR, A., UNO, K.T., KINYANJUI, R.N., BEHRENSMEYER, A.K., BOBE, R., ADVOKAAT, E.L., BAMFORD, M., CARVALHO, S.C., HAMMOND, A.S., PALCU, D.V., SIER, M.J., WARD, C.V. & BRAUN, D.R. (2023) Pliocene hominins from East Turkana were associated with mesic environments in a semiarid basin. *Journal of Human Evolution* **180**, 103385.

VISCARRA ROSSEL, R.A. & HICKS, W.S. (2015) Soil organic carbon and its fractions estimated by visible–near infrared transfer functions. *European Journal of Soil Science* **66**, 438–450.

VRBA, E.S. (2007) Role of environmental stimuli in hominid origins. In *Handbook of Paleoanthropology Volume III, Phylogeny of Hominids* (eds W. HENKE & I. TATTERSALL), pp. 1441–1482. Springer-Verlag.

WADDELL, P.J., CAO, Y., HASEGAWA, M. & MINDELL, D.P. (1999) Assessing the Cretaceous Superordinal Divergence Times within Birds and Placental Mammals by Using Whole Mitochondrial Protein Sequences and an Extended Statistical Framework. *Systematic Biology* **48**, 119–137.

WALKER, R.H., HUTCHINSON, M.C., BECKER, J.A., DASKIN, J.H., GAYNOR, K.M., PALMER, M.S., GONÇALVES, D.D., STALMANS, M.E., DENLINGER, J., BOULEY, P., ANGELA, M., PAULO, A., POTTER, A.B., ARUMOOGUM, N., PARRINI, F., ET AL. (2023) Trait-based sensitivity of large mammals to a catastrophic tropical cyclone. *Nature* **623**, 757–764.

WANG, S.C. & ZHONG, L. (2018) Estimating the number of pulses in a mass extinction. *Paleobiology* **44**, 199–218.

WARD, C.V. (2014) Taxonomic affinity of the Pliocene hominin fossils from Fejej, Ethiopia. *Journal of Human Evolution* **73**, 98–102.

WARD, C.V., PLAVCAN, J.M. & MANTHI, F.K. (2020) New fossils of *Australopithecus anamensis* from Kanapoi, West Turkana, Kenya (2012–2015). *Journal of Human Evolution* **140**, 102368.

WATANABE, H. & MATSUO, K. (2003) Rock type classification by multi-band TIR of ASTER. *Geosciences Journal* **7**, 347–358.

WEIHMÜLLER, M.P., BRIZUELA, C., MIGNINO, J. & ROBLEDO, A.I. (2022) Bones, carnivores, and grassland fires. Actualistic taphonomy of faunal assemblages from two caves in Central Argentina and its implication for the fossil record. *Historical Biology* **34**, 2273–2286.

WESTOVER, K.S., STONE, J.R., YOST, C.L., SCOTT, J.J., COHEN, A.S., RABIDEAUX, N.M., STOCKHECKE, M. & KINGSTON, J.D. (2021) Diatom paleolimnology of late Pliocene Baringo Basin (Kenya) paleolakes. *Palaeogeography, Palaeoclimatology, Palaeoecology* **570**, 109382.

WHEATLEY, D. (2004) Making space for an archaeology of place. *Internet Archaeology*.

WHEELER, P.E. (1984) The evolution of bipedality and loss of functional body hair in hominids. *Journal of Human Evolution* **13**, 91–98.

WHITE, T.D. (2004) Managing paleoanthropology's nonrenewable resources: a view from Afar. *Comptes Rendus Palevol* **3**, 341–351.

WHITE, T.D., ASFAW, B., BEYENE, Y., HAILE-SELASSIE, Y., LOVEJOY, C.O., SUWA, G. & WOLDEGABRIEL, G. (2009) *Ardipithecus ramidus* and the Paleobiology of Early Hominids. *Science* **326**, 64–86.

WHITE, T.D., LOVEJOY, C.O., ASFAW, B., CARLSON, J.P. & SUWA, G. (2015) Neither chimpanzee nor human, Ardipithecus reveals the surprising ancestry of both. *Proceedings of the National Academy of Sciences* **112**, 4877–4884.

WHITE, T.D., SUWA, G. & ASFAW, B. (1994) *Australopithecus ramidus*, a new species of early hominid from Aramis, Ethiopia. *Nature* **371**, 306–312.

WHITING, M.L., LI, L. & USTIN, S.L. (2004) Predicting water content using Gaussian model on soil spectra. *Remote Sensing of Environment* **89**, 535–552.

WILF, P. & ESCAPA, I.H. (2015) Green Web or megabiased clock? Plant fossils from Gondwanan Patagonia speak on evolutionary radiations. *New Phytologist* **207**, 283–290.

WILKINSON, R.D., STEIPER, M.E., SOLIGO, C., MARTIN, R.D., YANG, Z. & TAVARÉ, S. (2011) Dating Primate Divergences through an Integrated Analysis of Palaeontological and Molecular Data. *Systematic Biology* **60**, 16–31.

WILLEY, G.R. (1953) *Prehistoric settlement patterns in the Viru; Valley, Peru*. Smithsonian Institution, Washington, DC.

WILLIAMS, D.R., RAST, P. & BÜRKNER, P.-C. (2018) Bayesian Meta-Analysis with Weakly Informative Prior Distributions. Preprint, PsyArXiv.

WILLIAMS, S. (1956) Settlement patterns in the lower Mississippi valley. In *Prehistoric Settlement Patterns in the New World* (ed G.R. WILLEY), pp. 52–62. Wenner-Gren Foundation For Anthropological Research, Inc. New York.

WILLIAMS, S.A., GARCÍA-MARTÍNEZ, D., BASTIR, M., MEYER, M.R., NALLA, S., HAWKS, J., SCHMID, P., CHURCHILL, S.E. & BERGER, L.R. (2017) The vertebrae and ribs of *Homo naledi*. *Journal of Human Evolution* **104**, 136–154.

WILLS, S., CHOINIERE, J.N. & BARRETT, P.M. (2018) Predictive modelling of fossil-bearing locality distributions in the Elliot Formation (Upper Triassic–Lower Jurassic), South Africa, using a combined multivariate and spatial statistical analyses of present-day environmental data. *Palaeogeography, Palaeoclimatology, Palaeoecology* **489**, 186–197.

WILSON, A.C. & SARICH, V.M. (1969) A molecular time scale for human evolution. *Proceedings of the National Academy of Sciences* **63**, 1088–1093. National Acad Sciences.

WILSON, E.O. (1998) *Consilience: the unity of knowledge*. 1st ed. Knopf : Distributed by Random House, New York.

WILSON, E.O. (2014) *A Window on Eternity: A Biologist's Walk Through Gorongosa National Park*. Simon & Schuster Children's Publishing, New York.

WOLDEGABRIEL, G., HAILE-SELASSIE, Y., RENNE, P.R., HART, W.K., AMBROSE, S.H., ASFAW, B., HEIKEN, G. & WHITE, T. (2001) Geology and palaeontology of the Late Miocene Middle Awash valley, Afar rift, Ethiopia. *Nature* **412**, 175–178.

WOLDEGABRIEL, G., WHITE, T., SUWA, G., SEMAW, S., BEYENE, Y., ASFAW, B. & WALTER, R. (1992) Kesem-Kebena: A Newly Discovered Paleoanthropological Research Area in Ethiopia. *Journal of Field Archaeology* **19**, 471–493.

WOŁODŹKO, T. (2020) extraDistr: Additional univariate and multivariate distributions.

WOLPOFF, M.H., HAWKS, J., SENUT, B., PICKFORD, M. & AHERN, J. (2006) An ape or the ape: is the Toumaï cranium TM 266 a hominid. *PaleoAnthropology* **2006**, 36–50.

WOLPOFF, M.H., SENUT, B., PICKFORD, M. & HAWKS, J. (2002) *Sahelanthropus* or 'Sahelpithecus'? *Nature* **419**, 581–582.

WOOD, B. (1991) *Koobi Fora Research Project, Volume 4. Hominid Cranial Remains*. Clarendon Press, Oxford.

WOOD, B. (1992) Palaeoanthropology. A remote sense for fossils. *Nature* **355**, 397–398.

WOOD, B. & LEAKEY, M. (2011) The Omo-Turkana Basin fossil hominins and their contribution to our understanding of human evolution in Africa. *Evolutionary Anthropology: Issues, News, and Reviews* **20**, 264–292.

WOOD, B. & SMITH, R.J. (2022) Towards a more realistic interpretation of the human fossil record. *Quaternary Science Reviews* **295**, 107722.

WRANGHAM, R., CHENEY, D., SEYFARTH, R. & SARMIENTO, E. (2009) Shallow-water habitats as sources of fallback foods for hominins. *American Journal of Physical Anthropology* **140**, 630–642.

WRANGHAM, R.W. (2005) The delta hypothesis: hominoid ecology and hominin origins. In *Interpreting the Past: Essays on Human, Primate, and Mammal Evolution in Honor of David Pilbeam* (eds D.E. LIEBERMAN, R.J. SMITH & J. KELLEY), pp. 231–242. Brill Academic Publishers, Boston, MA.

WRIGHT, A.M., BAPST, D.W., BARIDO-SOTTANI, J. & WARNOCK, R.C.M. (2022) Integrating Fossil Observations Into Phylogenetics Using the Fossilized Birth–Death Model. *Annual Review of Ecology, Evolution, and Systematics* **53**, 251–273.

WU, H., GUANG, X., AL-FAGEEH, M.B., CAO, J., PAN, S., ZHOU, H., ZHANG, L., ABUTARBOUSH, M.H., XING, Y., XIE, Z., ALSHANQEETI, A.S., ZHANG, Y., YAO, Q., AL-SHOMRANI, B.M., ZHANG, D., ET AL. (2014) Camelid genomes reveal evolution and adaptation to desert environments. *Nature Communications* **5**, 5188.

WU, X., KUMAR, V., ROSS QUINLAN, J., GHOSH, J., YANG, Q., MOTODA, H., MCLACHLAN, G.J., NG, A., LIU, B., YU, P.S., ZHOU, Z.-H., STEINBACH, M., HAND, D.J. & STEINBERG, D. (2008) Top 10 algorithms in data mining. *Knowledge and Information Systems* **14**, 1–37.

WULDER, M.A., COOPS, N.C., ROY, D.P., WHITE, J.C. & HERMOSILLA, T. (2018) Land cover 2.0. *International Journal of Remote Sensing* **39**, 4254–4284.

WYNN, J.G., ALEMSEGED, Z., BOBE, R., GRINE, F.E., NEGASH, E.W. & SPONHEIMER, M. (2020) Isotopic evidence for the timing of the dietary shift toward C $_4$ foods in eastern African *Paranthropus*. *Proceedings of the National Academy of Sciences* **117**, 21978–21984.

YAMAGIWA, J., IWATA, Y., ANDO, C. & BASABOSE, A.K. (2019) Use of swamp and riverside forest by eastern and western gorillas. In *Primates in flooded habitats: Ecology and conservation* (eds K. NOWAK, A.A. BARNETT & I. MATSUDA), pp. 184–194. Cambridge University Press, Cambridge.

YAN, Q., KORTY, R., ZHANG, Z. & WANG, H. (2019) Evolution of tropical cyclone genesis regions during the Cenozoic era. *Nature Communications* **10**, 3076.

YAN, X., GU, H. & YAN, Y. (2022) Karst cave detection and prediction by using two fully convolutional neural networks. In *SEG 2021 Workshop: 4th International Workshop on Mathematical Geophysics: Traditional & Learning, Virtual, 17–19 December 2021* pp. 90–93. Society of Exploration Geophysicists, Virtual.

YANG, Z. & RANNALA, B. (2006) Bayesian estimation of species divergence times under a molecular clock using multiple fossil calibrations with soft bounds. *Molecular Biology and Evolution* **23**, 212–226.

YI, S.V. (2013) Morris Goodman's hominoid rate slowdown: The importance of being neutral. *Molecular Phylogenetics and Evolution* **66**, 569–574.

YOST, C.L., LUPIEN, R.L., BECK, C., FEIBEL, C.S., ARCHER, S.R. & COHEN, A.S. (2021) Orbital Influence on Precipitation, Fire, and Grass Community Composition From 1.87 to 1.38 Ma in the Turkana Basin, Kenya. *Frontiers in Earth Science* **9**, 568646.

ZACHOS, J., PAGANI, M., SLOAN, L., THOMAS, E. & BILLUPS, K. (2001) Trends, Rhythms, and Aberrations in Global Climate 65 Ma to Present. *Science* **292**, 686–693.

ZHANG, Y., LIANG, S., ZHU, Z., MA, H. & HE, T. (2022) Soil moisture content retrieval from Landsat 8 data using ensemble learning. *ISPRS Journal of Photogrammetry and Remote Sensing* **185**, 32–47.

ZHANG, Z., RAMSTEIN, G., SCHUSTER, M., LI, C., CONTOUX, C. & YAN, Q. (2014) Aridification of the Sahara desert caused by Tethys Sea shrinkage during the Late Miocene. *Nature* **513**, 401–404.

ZHAO, W., MA, H. & HE, Q. (2009) Parallel K-Means Clustering Based on MapReduce. In *Cloud Computing* (eds M.G. JAATUN, G. ZHAO & C. RONG), pp. 674–679. Springer, Berlin, Heidelberg.

ZOLLIKOFER, C.P.E., LEÓN, M.S.P. DE, LIEBERMAN, D.E., GUY, F., PILBEAM, D., LIKIUS, A., MACKAYE, H.T., VIGNAUD, P. & BRUNET, M. (2005) Virtual cranial reconstruction of *Sahelanthropus tchadensis*. *Nature* **434**, 755–759.

ZUCCOTTI, L.F., WILLIAMSON, M.D., LIMP, W.F. & UNGAR, P.S. (1998) Technical note: Modeling primate occlusal topography using geographic information systems technology. *American Journal of Physical Anthropology* **107**, 137–142.

ZUCKERKANDL, E. & PAULING, L. (1965) Evolutionary Divergence and Convergence in Proteins. In *Evolving Genes and Proteins* (eds V. BRYSON & H.J. VOGEL), pp. 97–166. Academic Press, Rutgers University.